Tail-anchored proteins at peroxisomes: identification of MIRO1 as a novel peroxisomal motility factor

Submitted by Inês Gomes Oliveira Castro to the University of Exeter
as a thesis for the degree of
Doctor of Philosophy in Biological Sciences
in July 2016

I certify that all material in this thesis which is not my own work has been identified and that no material has previously been submitted and approved for the award of a degree by this or any other University.

Signature: ……..

Abstract

Peroxisomes are dynamic and multifunctional organelles, which are essential for human health and development. They are remarkably diverse, with functions that vary significantly between cells and organisms, and can dramatically change their size, shape and dynamics in response to cellular cues. In the past few years, several studies have significantly increased our understanding of the basic principles that enable peroxisome biogenesis and degradation, as well as their pivotal role in cellular signalling and homeostasis. However, several of these processes are still poorly understood. In this thesis we initially studied the peroxisome targeting mechanism of a group of C-terminally anchored membrane proteins, known as tail-anchored (TA) proteins. In order to investigate the molecular signals that enable TA protein targeting to cellular organelles, we analysed the physicochemical properties of a cohort of TA proteins both *in silico* and *in vivo*, and show that a combination of transmembrane domain (TMD) hydrophobicity and C-terminal tail charge determines organelle-specific targeting. Focusing on peroxisomes, we demonstrate that a balance between TMD hydrophobicity and high positive tail charge directs TA proteins to this organelle, and enables binding to the peroxisomal chaperone PEX19. These results allowed us to create a bioinformatical tool to predict the targeting of uncharacterised TA proteins and further develop our understanding of the molecular mechanisms involved in the targeting of this protein group. From our initial TA protein screen, we identified the TA protein MIRO1 at peroxisomes and looked at its role in the regulation of peroxisome motility. We show that endogenous MIRO1 localises to mitochondria and peroxisomes, and that dual targeting depends on the C-terminal tail. MIRO1 expression significantly increased peroxisome motility in several cell lines, and revealed a role for motility in peroxisome dynamics, by inducing organelle proliferation and elongation. These results reveal a new molecular complex at peroxisomes and provide us with a tool to further dissect the role of motility on peroxisome function.

Acknowledgments

I would first like to thank my supervisor Dr. Michael Schrader for the opportunity to develop this project and for supporting me all these years, all the way from sunny Portugal to the rainy UK, and I'm sure in the future to come.

I would like to thank everyone in lab 211 over the last 4 years for their support and for making this a great experience. In particular, I would like to thank all of the members of the Schrader lab with whom I've shared so many hours, days, and months of my life: Sandra, Tina, Joe, Afsoon, Sofia, Luís, and even our undergraduate and master students.

I would particularly like to thank Joe for his invaluable scientific support, friendship and for convincing me to try climbing, and Afsoon for being the sweetest friend and always there to laugh with me (night time, day time!). I would also like to thank Jeremy for teaching me more about the matrix and for all our philosophical discussions, and Citlali, the most energetic woman on Earth, for her constant enthusiasm and support when I really needed.

I would also like to thank Dr. Imogen Sparkes for all her scientific feedback and for giving me the opportunity to work with her.

I would like to thank all the friends who have supported me through these years, who have taught me so many new things and helped me grow as a person and a scientist. In particular, to my greatest friend Sofy, who was always there to talk about science, life, and random crazy ideas, even if we were ~1,400 km apart (yes, I checked!).

I would like to thank Patrick for coming into my life and making everyday a better day. For sharing my love of knowledge and life, for being kind and honest, and for making me happy.

Finally, I would like to thank my family for always excitingly asking when I was going to get a noble prize! In particular, I would like to thank my sister Bárbara who makes sure I can always be the little sister, and my mother, who after all these years, has never stopped being my role model. She has made me into who I am today and has always believed in me!

Table of contents

List of figures

List of tables

List of accompanying materials

The attached CD contains:

Supplementary movies from chapter 4

Movie S1 – Peroxisome motility in a COS-7 cell expressing GFP-SKL (10x original speed).

Movie S2 – Peroxisome motility in a COS-7 cell expressing GFP-SKL and myc-MIRO1V13-Pex (10x original speed).

Movie S3 – Dynamics of peroxisome accumulations at the cell periphery (COS-7 cells expressing GFP-SKL and myc-MIRO1V13-Pex, 10x original speed).

Movie S4 – Peroxisome motility in a control mouse embryonic fibroblast (MEF) expressing GFP-SKL (10x original speed).

Movie S5 – Peroxisome motility in a MIRO1 knockout (KO) MEF expressing GFP-SKL (10x original speed).

Movie S6 – Peroxisome motility in a C109 fibroblast expressing GFP-ACBD5^{TMT-T} (10x original speed).

Movie S7 – Peroxisome motility in a C109 fibroblast expressing GFP-ACBD5^{TMT-T} and myc-MIRO1WT-Pex (10x original speed).

Movie S8 – Peroxisome motility in a ΔPEX5 fibroblast expressing GFP-ACBD5^{TMT-T} (10x original speed).

Movie S9 – Peroxisome motility in a ΔPEX5 fibroblast expressing GFP-ACBD5^{TMT-T} and myc-MIRO1WT-Pex (10x original speed).

Movie S10 – Peroxisome motility in a ΔPEX14 fibroblast expressing GFP-ACBD5^{TMT-T} (10x original speed).

Movie S11 – Peroxisome motility in a ΔPEX14 fibroblast expressing GFP-ACBD5^{TMT-T} and myc-MIRO1WT-Pex (10x original speed).

Movie S12 – Peroxisome motility in a ΔPEX5 fibroblast expressing GFP-ACBD5^{TMT-T} and myc-MIRO1WT-Pex, with several small peroxisomes and peroxisome elongations (10x original speed).

Movie S13 – Peroxisome elongation in a ΔPEX5 fibroblast expressing GFP-ACBD5^{TMT-T} and myc-MIRO1WT-Pex (10x original speed).

Author's declaration

This work was performed with the help of co-workers:

Chapter 3

Dr. Joseph Costello performed the immunoprecipitations (IP) and western blots (WB) presented in figure 3.2C and figure 3.6A and B, and expressed/ imaged the proteins tested in figure 3.7B.

Dr. Nina Bonekamp performed the experiments with BCL2 family proteins in figure 3.1

Dr. Markus Islinger purified the organelle fractions used in figure 3.2C

Dr. Doug McNeall created the TA protein classifier presented in figure 3.7A

Dr. Michael Schrader and Mrs Tina Schrader performed the cells counts presented in figure 3.4C and figure 3.5C.

Chapter 4

Dr. Markus Islinger purified the organelle fractions used in figure 4.1B

Ms. Ana Gouveia cloned myc-MIRO1V13-Pex and myc-MIRO1N18-Pex, and performed de cells counts for these two plasmids presented in figure 4.3E

Dr. Jeremy Metz created the tracking algorithm used to identify and track peroxisome motility throughout the chapter, and created the CDF graphs shown in figure 4.4B and F, and figure 4.5C.

This project was initiated as part of my Master's degree. As so, some of the results presented were previously used for my Master's thesis dissertation. The following results were previously used: endogenous localisation of MIRO1 in rat liver purified peroxisomes, expression and quantification of myc-MIRO1WT and mutants, cloning of myc-MIRO1WT-Pex and myc-MIRO1KK-Pex and expression in COS-7 cells. These results are shown in chapter 4 to present a coherent story and, in some cases, new and improved images were obtained to show these results.

I would like to thank all of the co-authors for their support and help.

Abbreviations

ACBD5 – acyl-CoA binding domain protein 5

Acyl-CoA – acetyl coenzyme A

ALDP – adrenoleukodystrophy protein

ALS – amyotrophic lateral sclerosis

ATAD1 – ATPase family, AAA domain containing 1

ATM – ataxia telangiectasia mutated protein

ATP – adenosine-5’-triphosphate

BAG6 – BCL2 associated athanogene 6

BAX – BCL2 associated X

BSA – bovine serum albumin

CDF – cumulative distribution function

CENP-F – centromeric protein F

DLP1 – dynamin-like protein 1

DMEM – Dulbecco’s modified eagle medium

DMSO – dimethyl sulfoxide

ECL – enhanced chemiluminescence

EDTA – 2-Amino-2-(hydroxymethyl)-1,3-propanediol

E.coli – *Escherischia coli*

ER – endoplasmic reticulum

ERAD – ER-associated protein degradation machinery

ERMES – ER-mitochondria encountering structure

FALDH – fatty aldehyde dehydrogenase

FBS – fetal bovine serum

FIS1 – mitochondrial fission 1 protein

GABAA – γ-aminobutyric acid type A receptor

GAP – GTPase activating protein

GDAP1 – Ganglioside-induced differentiation-associated protein 1

GEF – guanine nucleotide exchange factor

GET – guided entry of TA proteins

GFP – green fluorescence protein

GTP – Guanosine-5'-triphosphate

GRAVY – grand average of hydropathy

H_2O_2 – hydrogen peroxide

HAP1 – huntingtin-associated protein 1

HRP – horseradish peroxidase

HSC – heat shock protein

HUMMR – hypoxia up-regulate mitochondria movement regulator

IMF – immunofluorescence

IMM – inner mitochondrial membrane

KD – knockdown

KHC – kinesin heavy chain

KIF – kinesin family member

KO – knockout

LCFA – long-chain fatty acids

MAVS – mitochondrial anti-viral signalling protein

MDV – mitochondria-derived vesicle

MEF – mouse embryonic fibroblasts

MFF – mitochondrial fission factor

MFN – mitofusin

MIRO – mitochondrial Rho GTPase

MITO – mitochondria

mPTS – membrane peroxisome targeting signal

NO• – nitric oxide

NCBI – National Centre for Biotechnology Information

$O_2^{\bullet -}$ – oxygen superoxide

OGT – N-acetylglucosamine transferase

OMP25 – outer membrane protein 25

PAGE – polyacrylamide gel electrophoresis

PBS – phosphate buffer saline

PCR – polymerase chain reaction

PEI – polyethylenimine

PEX - peroxin

PINK1 – PTEN-induced putative kinase

PMP – peroxisomal membrane protein

PO – peroxisome

PPAR – peroxisome proliferator-activated receptor

PPRE – peroxisome proliferator response elements

PTS – peroxisomal targeting signal

RIG-I – retinoic acid-inducible gene I

ROS – reactive oxygen species

RNS – reactive nitrogen species

S. cerevisiae – *Saccharomyces cerevisiae*

SDS – sodium dodecyl sulphate

SPP – signal peptide peptidase

SRP – signal recognition particle

TA – tail-anchored

TAE – tris-acetate-EDTA

TMD – transmembrane domain

TOM – translocase of the mitochondrial outer membrane

TRAK – trafficking kinesin protein

TRC – transmembrane domain recognition complex

Tris – 2-Amino-2-(hydroxymethyl)-1,3-propanediol

TSC – tuberous sclerosis complex

UBL – ubiquitin like protein

UV - ultraviolet

VAPB – VAMP associated protein B

VLCFA – very-long-chain fatty acids

WB – western blot

WT – wild type

Chapter 1 – Introduction

1.1. Peroxisomes

Peroxisomes are dynamic and multifunctional organelles present in virtually all eukaryotic cells. They were initially described by Rhodin in 1954 as spherical and oval microbodies (Rhodin, 1954) and later characterized and renamed by Christian de Duve and his group, who identified several enzymes responsible for hydrogen peroxide metabolism (Baudhuin et al., 1964; De Duve and Baudhuin, 1966). Peroxisomes are bound by a single membrane and are usually found as spherical or rod-like shapes (0.1 to 0.5 µm in diameter), but can also form elongated tubular structures and networks (Figure 1.1) (Schrader et al., 2000). Their number can range from just a few organelles in yeast cells to several hundred in mammalian hepatocytes (Yan et al., 2005).

Peroxisomes are involved in numerous essential cellular processes, such as lipid and reactive oxygen species (ROS) metabolism (see below). Consequently, defects in genes coding for peroxisomal proteins lead to several peroxisomal disorders with varying degrees of severity (reviewed in Waterham et al., 2016). Although the severity of the pathology can in some cases be associated to defects in specific proteins, patients with different mutations in the same protein can present very different phenotypes. For example, mutations in PEX16, an essential protein for peroxisome biogenesis, tipically lead to the development of Zellwegger syndrome and premature death within the first year after birth. However, several patients with mutations in this protein have been recently identified which present milder phenotypes, surviving for several years (Ebberink et al., 2010).

Patients born with peroxisomal disorders generally present mild to very severe neurodevelopmental defects, organ specific pathologies particularly affecting the liver and kidneys, as well as sight and hearing impairments (Berger et al., 2016; Braverman et al., 2013; Waterham et al., 2016). Due to the genetic component of these disorders, to this date no cure has been identified for any of the peroxisome spectrum disorders. However, symptom management and controlled diets (particularly regarding the ingestion of lipids) have enabled improvements in the quality of life of these patients (Klouwer et a., 2015).

Additionally, due to their roles in cellular metabolism and redox status, peroxisomal dysfunction contributes to aging, cancer and several

neurodegenerative disorders, such as Alzheimer's and Parkinson's disease (Fransen et al., 2013; Lizard et al., 2012; Titorenko and Terlecky, 2011).

1.1.1. Peroxisomal functions

Peroxisomes harbour a vast array of metabolic functions that vary according to species, cell type, developmental stage and environmental conditions (Hu et al., 2012; Islinger et al., 2010; Pieuchot and Jedd, 2012; Smith and Aitchison, 2013). In most organisms peroxisomes play an essential role in lipid and ROS metabolism (Smith and Aitchison, 2013). In mammals, peroxisomes are responsible for three key pathways in lipid metabolism: fatty acid α-oxidation,

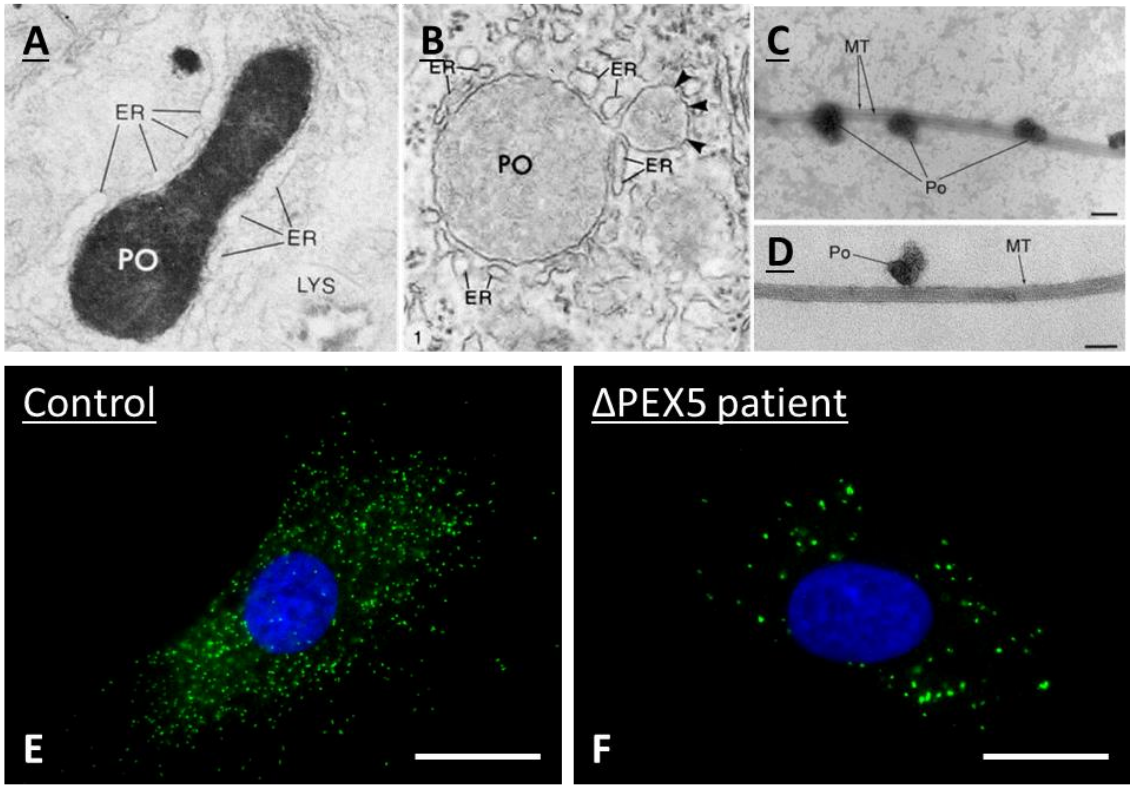

Figure 1.1 – Microscopic views of peroxisomes. (A-B) Electron micrographs of peroxisomes from regenerating rat liver. (A) Tubular peroxisome next to a lysosome (LYS) and in close association with the ER. Magnification: x85,000. (B) Regular spherical peroxisome with attached smaller one (arrows), and in close association with the ER. Magnification: x135,000. (C-D) Highly purified rat liver peroxisomes (Po) associating with taxol-stabilised microtubules (MT) from bovine brain (MT). Bars: 0.2 µm (C), 0.5 µm (D). (E-F) Human skin fibroblasts stained against PEX14 (peroxisomal marker) and Hoechst (DNA/nucleus). (E) Control fibroblast; (F) ΔPEX5 patient fibroblast with membrane ghosts. Scale bar 20 µm. ((A-B) from (Fahimi et al., 1993), (C-D) from (Schrader et al., 2003).

β-oxidation and ether phospholipid biosynthesis (Lodhi and Semenkovich, 2014; Wanders et al., 2010). These processes are performed in close association with mitochondria and the ER, which are responsible for later steps in these pathways (Wanders et al., 2016). As a result of these and other peroxisomal metabolic functions, several types of reactive oxygen and nitrogen species (ROS/RNS) are produced (e.g. H_2O_2, $O_2^{\bullet -}$ and NO•) (Bonekamp et al., 2009; Fransen et al., 2012; Nordgren and Fransen, 2014). To balance out the production of ROS/RNS, and help maintain the cellular redox state, peroxisomes also possess several antioxidant enzymes, such as catalase, peroxiredoxin 5 and superoxide dismutase 1 (Antonenkov et al., 2010; Fransen et al., 2012). Additionally, mammalian peroxisomes are also responsible for other anabolic and catabolic reactions such as glyoxylate detoxification, purine catabolism, bile acid and docosahexaenoic acid synthesis, and amino acid degradation (Wanders and Waterham, 2006).

Recently, peroxisomes have been identified as essential signalling platforms, playing key roles in antiviral signalling and ROS-dependent regulation of mTORC1 signalling (reviewed in Mast et al., 2015; Tripathi and Walker, 2016). In a breakthrough study, Dixit and colleagues reported the dual targeting of the mitochondrial antiviral signalling (MAVS) protein to peroxisomes and mitochondria, and its ability to induce different signalling cascades at each organelle in response to viral RNA recognition by RIG-I-like receptors (Dixit et al., 2010; Odendall et al., 2014). The peroxisomal targeting of MAVS was recently confirmed by other groups. However, the authors were unable to find any differences in the signalling cascades activated at each organelle (Bender et al., 2015). Additionally, the ataxia telangiectasia mutated (ATM) protein and the tuberous sclerosis complex (TSC) have been found at the peroxisomal membrane, where they can upregulate autophagy (and pexophagy) by repressing mTORC1 signalling, in response to increases in ROS (Zhang et al., 2013, 2015b). Despite the novelty and potential impact of these studies on our understanding of peroxisome function, further studies will be needed to confirm these results, in particular due to the contradicting nature of some of the published data. For example, whereas the authors point to an increase in peroxisome degradation in response to ROS, other studies have shown the opposite effect, with the same stimulus leading to peroxisome proliferation (Delmaghani et al., 2015). Furthermore, the mechanism by which TSC proteins

and ATM are targeted to peroxisomes was poorly characterised and should be further investigated.

1.1.2. Peroxisomal biogenesis

Peroxisome formation and maintenance are dependent on a unique set of proteins known as peroxins (Just and Kunau, 2014). Several of these proteins are conserved from yeast to plants and mammals (Smith and Aitchison, 2013), and mutations in their genes lead to peroxisome biogenesis disorders, such as Zellweger syndrome (Waterham and Ebberink, 2012). Peroxins are involved in targeting, membrane insertion and import of peroxisomal proteins, membrane biogenesis and regulation of peroxisome proliferation. Mutation or deletion of a single peroxin can lead to the complete absence of peroxisomes (i.e. *PEX3*, *PEX16* and *PEX19*) (Ghaedi et al., 2000; Honsho et al., 1998; Matsuzono et al., 1999; Muntau et al., 2000), or to the formation of empty organelles known as membrane “ghosts” (e.g. *PEX5*, *PEX6*, *PEX14*) (Figure 1.1 F) (Dodt et al., 1995; Fukuda et al., 1996; Shimozawa et al., 2004).

1.1.2.1. Matrix protein import

Peroxisomal matrix proteins are synthesised in the cytosol and transported to the organelle by the shuttling receptors PEX5 and PEX7 (Braverman et al., 1998; Dodt and Gould, 1996; Otera et al., 1998), which recognize peroxisomal targeting signal 1 and 2 (PTS1/PTS2) sequences in matrix proteins (Rehling et al., 1996; Terlecky et al., 1995). These receptors and bound proteins are transported across the peroxisomal membrane by interacting with membrane peroxins (PEX14 and PEX13) to form import channels (Emmanouilidis et al., 2016; Gould et al., 1996; Meinecke et al., 2016; Schliebs et al., 1999). Interestingly, these channels are capable of importing completely folded, co-factor bound and even oligomeric proteins (Erdmann and Schliebs, 2005; Léon et al., 2006; McNew and Goodman, 1994). This characteristics enable the import of peroxisomal matrix proteins that lack PTS signals, by a process known as piggybacking (reviewed in Thoms, 2015). For example, the cytosolic protein

SOD1 lacks a PTS sequence, but by forming a hetero-oligomer with CCS (PTS1-bearing protein), it can be imported to peroxisomes.

Following cargo release, PEX5 and PEX7 are recycled back to the cytosol for further rounds of import, via an ubiquitin-dependent pathway which relies on PEX2, PEX10 and PEX12 for receptor ubiquitination, and the AAA ATPases PEX1 and PEX6, in association with PEX26 for receptor export (reviewed in Francisco et al., 2014; Platta et al., 2016).

1.1.2.2. Membrane protein import

Peroxisome membrane proteins (PMPs) can be synthesised in the cytosol and inserted directly into peroxisomes, or travel to this organelle via the ER (reviewed in Giannopoulou et al 2016). These proteins contain one or more membrane peroxisome targeting signals (mPTS), formed by a PEX19 binding motif and a transmembrane domain (TMD) (Halbach et al., 2006; Jones et al., 2001). PMPs are recognised and targeted to peroxisomes by the cytosolic chaperone PEX19, which maintains them in a stable and import competent conformation, and keeps them from aggregating (Fang et al., 2004; Shibata et al., 2004). The PMP-PEX19 complex docks at the peroxisomal membrane by interacting with PEX3 to insert newly formed proteins (Figure 1.4) (Fang et al., 2004; Fujiki et al., 2006; Giannopoulou et al., 2016). An additional membrane protein, PEX16, has been shown to regulate the insertion of PEX3 into peroxisomal (and ER) membranes and might play a similar role for other PMPs (Kim and Mullen, 2013; Kim et al., 2006; Matsuzaki and Fujiki, 2008), but its functions in mammalian peroxisomes are still poorly understood.

Interestingly, in mammalian cells both PEX3 and PEX16 have been shown to target peroxisomes either directly (Jones et al., 2004; Matsuzaki and Fujiki, 2008), or indirectly via the ER (Kim et al., 2006; Toro et al., 2009). The latter pathway has been strongly associated with the *de novo* formation of peroxisomes from ER-derived pre-peroxisomal vesicles (see below). Several other PMPs have been detected in the ER in different organisms (reviewed in Mayerhofer, 2016), but the physiological role of this targeting is still poorly understood.

1.1.2.3. Theories of peroxisome biogenesis

In comparison to other organelles, the mechanism of peroxisome biogenesis is still a matter of debate, confronting a classical view of peroxisome generation by growth and division and the more recent *de novo* formation from the ER. In brief, according to the growth and division model, peroxisomes form by importing newly synthesized proteins from the cytosol and lipids from other organelles such as the ER and lipid droplets, in a multistep pathway that leads to their elongation, constriction and fission (Figure 1.2) (Fujiki et al., 2014; Schrader et al., 2016). In contrast, the *de novo* synthesis model states that several peroxins, in particular PEX3 and PEX16, are initially inserted in the ER, and subsequently segregate to specialized ER exit sites, leading to the formation of pre-peroxisomal vesicles (Agrawal and Subramani, 2013; Dimitrov et al., 2013). These vesicles have been suggested to i) mature into functional peroxisomes, ii) fuse into pre-existing peroxisomes, and iii) fuse with other pre-peroxisomal vesicles to form mature peroxisomes (Agrawal et al., 2011; Kim et al., 2006; Toro et al., 2009; van der Zand et al., 2012).

Despite the lack of evidence for peroxisome (or pre-peroxisomal) membrane fusion, several groups have been able to show that PEX3, an essential protein for peroxisome biogenesis, is targeted to the ER. Understanding the role of this protein in the ER should further help us comprehend peroxisome formation and establish a clear model for organelle biogenesis. Furthermore, understanding how peroxisomes receive lipids for membrane formation (vesicles and/or membrane tethering) should further clarify the events leading to their formation. In view of this, a combined model where both pathways operate simultaneously serving complementary purposes, with different contributions depending on the cellular state and organism, is the most current view of peroxisome biogenesis (Agrawal and Subramani, 2016; Hettema et al., 2014; Hua and Kim, 2016).

1.1.3. Peroxisome dynamics

Peroxisomes respond to fluctuations in the cellular nutritional and environmental states by changing their number, position, morphology and function (Figure 1.2) (Kaur and Hu, 2009; Schrader et al., 2012b). To do so, several signalling pathways are activated which fine tune the expression of specific peroxisomal

proteins or that activate/inhibit peroxisome associated proteins (Mast et al., 2015; Schrader et al., 2012b, 2016).

1.1.3.1. Proliferation

In mammalian cells, peroxisome proliferation can be upregulated by several nutritional and environmental cues, such as increases in free fatty acids and growth factors, hypoxia and cold exposure (Figure 1.2) (Bagattin et al., 2010; Delmaghani et al., 2015; Laurenti et al., 2011; Schrader et al., 1998a). These stimuli induce an increase in the number and size of peroxisomes, and alterations in the expression of several peroxisomal proteins, in order to increase their metabolic activity (Bagattin et al., 2010; Diano et al., 2011; Gurvitz and Rottensteiner, 2006). Potentially, an increase in peroxisome number/size could also facilitate interactions with other organelles by increasing the available surface area and facilitate metabolism.

The most studied pathway of peroxisome proliferation in mammals is mediated by a family of ligand-activated transcription factors known as peroxisome proliferator activated receptors (PPARs) (Rakhshandehroo et al., 2010; Schrader et al., 2012b; Wang, 2010). These transcription factors are typically activated by lipid-ligands and regulate the expression of genes associated with lipid metabolism and adipocyte differentiation (Kliewer et al., 1992; Reddy et al., 1986). Additional pathways independent of PPARs have also been described and it is likely that yet unknown mechanisms contribute to the regulation of peroxisome proliferation (Gondcaille et al., 2005; Li and Gould, 2002; Sexton et al., 2010).

1.1.3.2. Division

Peroxisome division allows cells to balance the formation of new peroxisomes with the degradation of damaged or excessive organelles. Peroxisomes divide in a multistep process that involves membrane elongation, constriction and final membrane fission to form new organelles (Figure 1.2) (reviewed in Honsho et al., 2016; Schrader et al., 2016). Interestingly, several of the proteins involved in peroxisomal division are also targeted to mitochondria and regulate

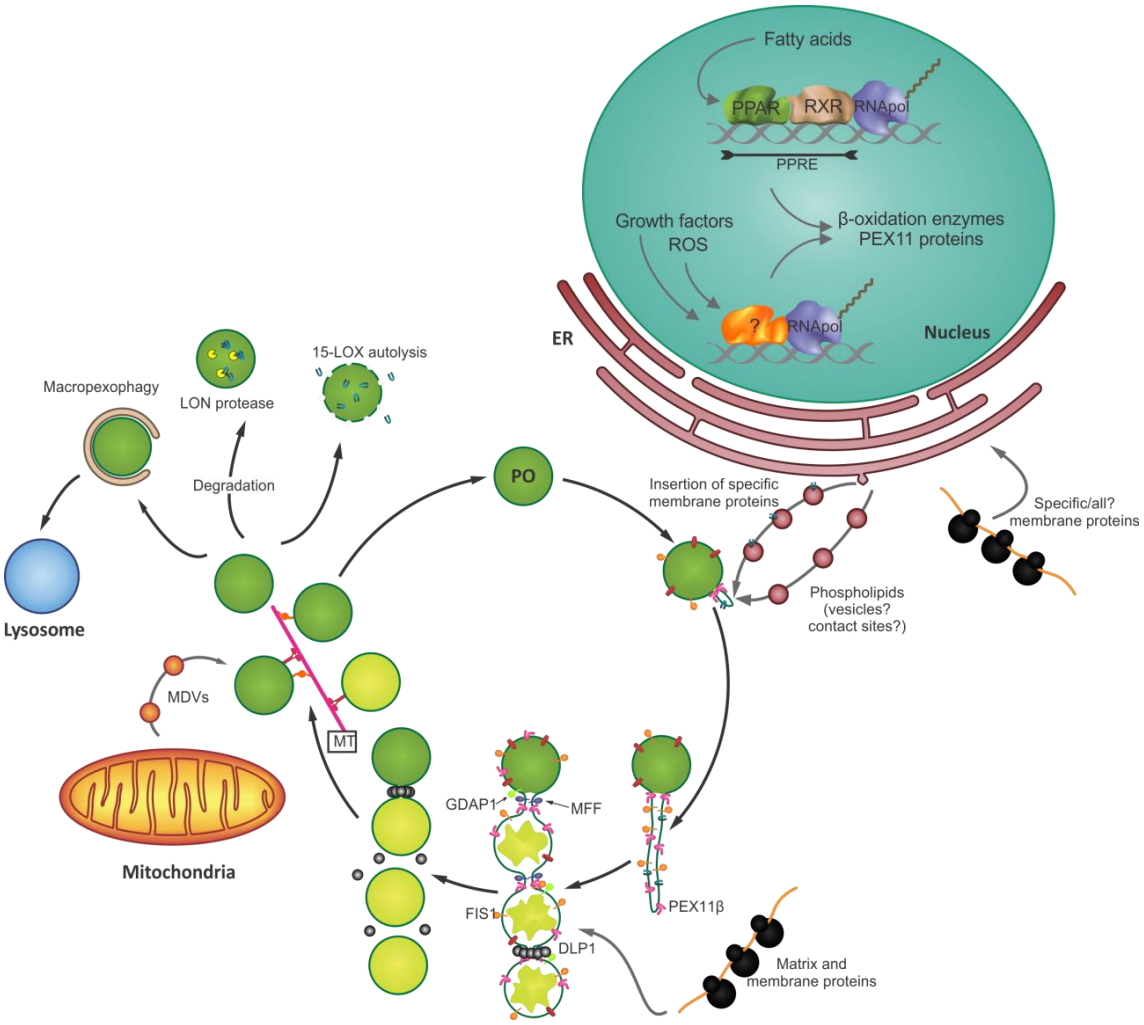

Figure 1.2 – Model of peroxisome dynamics and interactions in mammalian cells. Intra- and extracellular signals such as free fatty acids, growth factors and ROS can induce peroxisomal proliferation by activating and/or inducing the nuclear targeting of transcription factors. For example, free fatty acids induce targeting of PPARs and their binding partner retinoid-X-receptor (RXR) to the nucleus, where they bind peroxisome proliferator response elements (PPRE). These elements are present on peroxisomal genes encoding proteins involved in β-oxidation and peroxisome proliferation. New peroxisomes form by growth and division in a multi-step pathway that starts with the import of membrane lipids, likely from the ER and lipid droplets, and newly synthesized proteins from the cytosol and the ER (presumably by vesicular transport). Peroxisome membrane elongation and remodelling is regulated by PEX11 proteins, in particular PEX11β. Following elongation, membranes are constricted by a mechanism still unknown, and divide in a process mediated by DLP1, FIS1 and MFF, and likely regulated by GDAP1. In order to maintain a homogenous population, peroxisomes move through the microtubule cytoskeleton, and excess peroxisomes (or damaged) are removed by macropexophagy. Other pathways such as 15-LOX-mediated autolysis and LON-protease mediated degradation of matrix proteins have also been

described. Peroxisomes share close functional relationship with mitochondria and the ER, but have also been shown to interact with lipid droplets, lysosomes and other peroxisomes (Schrader et al., 2015b). Recently, a vesicular mitochondria-to-peroxisome trafficking route has been described, but the role of these mitochondria-derived vesicles (MDVs) in peroxisome function remains unknown. Adapted from (Islinger et al., 2012b).

mitochondrial division (Figure 1.3) (Gandre-Babbe and van der Bliek, 2008; Huber et al., 2013; Koch et al., 2003, 2005).

Peroxisome elongation is regulated by the Pex11 family of proteins across several species (Koch et al., 2010; Williams and van der Klei, 2014), with three proteins present in mammals: PEX11α, PEX11β and PEX11γ (Schrader et al., 1998b; Tanaka et al., 2003). The best characterised of these, PEX11β, has been shown to induce membrane deformation due to its strong affinity to membrane lipids (Itoyama et al., 2012; Schrader et al., 2012a) and its N-terminal amphipathic helix (Opaliński et al., 2011; Yoshida et al., 2015). Additionally, PEX11β dimerization might contribute to maintain membrane tubulation by creating a stable curvature, similarly to BAR domain proteins (Daumke et al., 2014), and play a role in membrane constriction (Yoshida et al., 2015).

Peroxisomal fission is mediated by the dynamin-like protein DLP1, a large cytosolic GTPase which forms oligomeric helixes around constriction sites and induces fission (Bui and Shaw, 2013; Li and Gould, 2003; Mears et al., 2011). DLP1 is recruited to peroxisomes by the tail-anchored (TA) proteins FIS1 and MFF, which facilitate oligomerisation of DLP1 (Otera et al., 2010; Yoon et al., 2003). Recently, the mitochondrial TA protein GDAP1 has also been shown to dually target peroxisomes and mitochondria, and to regulate organelle division (Huber et al., 2013). Interestingly, PEX11β interacts with FIS1 and MFF on the membrane (Kobayashi et al., 2007; Koch and Brocard, 2012), and is able to activate DLP1 due to its GTPase activating protein (GAP) activity (Williams et al., 2015).

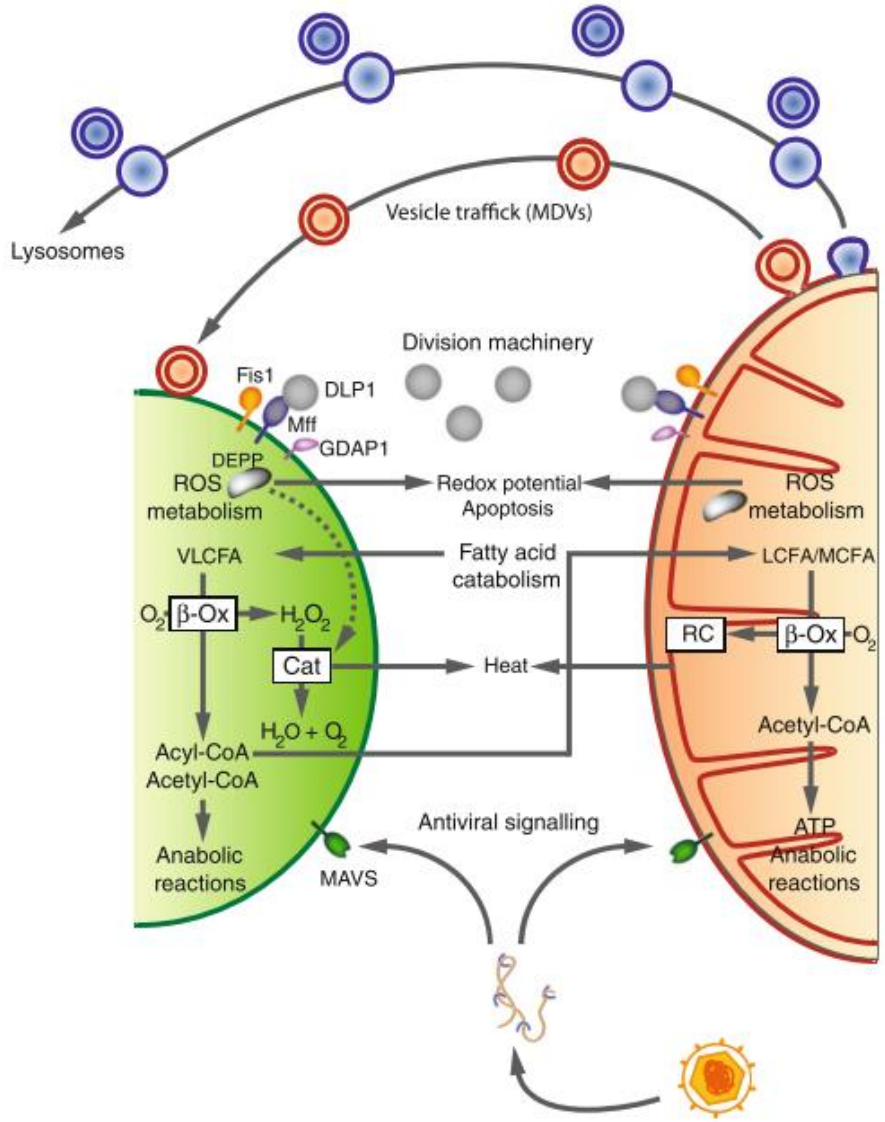

Figure 1.3 – Schematic view of peroxisomal and mitochondrial cooperation and cross-talk. Peroxisomes (left) and mitochondria (right) in mammals share several functions such as fatty acid β-oxidation (β-Ox), ROS metabolism and heat production. As a result, altered homeostasis in either organelle affects the other. Peroxisome and mitochondria share several proteins of their division machinery (e.g., DLP1, MFF, FIS1, GDAP1), as well as MAVS, a protein required for antiviral signalling. Furthermore, a novel trafficking pathways from mitochondria to peroxisomes (and lysosomes) involving mitochondria-derived vesicles (MDVs) has been reported. Cat - catalase; VLCFA, LCFA, MCFA, very long-chain, long-chain and medium-chain fatty acids; RC, respiratory chain. From (Schrader et al., 2015a).

1.1.3.3. Degradation

The major process for peroxisome degradation in mammalian cells is pexophagy, a form of autophagy that selectively targets peroxisomes (Figure 1.2) (reviewed in Honsho et al., 2016; Nordgren et al., 2013). Additional mechanisms include LON-protease dependent degradation of matrix proteins and 15-lipoxygenase-mediated autolysis (Yokota et al., 2001, 2008).

Pexophagy allows cells to remove excessive or damaged peroxisomes to maintain organelle homeostasis, and can be induced by cellular stresses such as altered redox state and hypoxia (Iwata et al., 2006; Walter et al., 2014; Zhang et al., 2015b). The majority of peroxisomes in mammalian cells are degraded by macropexophagy, a process in which a double membrane structure, the autophagosome, grows and engulfs the target peroxisome and delivers it to lysosomes for recycling (Iwata et al., 2006; Mizushima and Komatsu, 2011). Organelles tagged for degradation are recognised by specific autophagy adaptors that form a bridge between the organelle and the growing autophagosomal membrane (Behrends and Fulda, 2012). Two of these adaptors, NBR1 and p62, can recognize ubiquitinated proteins at the peroxisomal membrane, but their physiological targets are still unknown (Deosaran et al., 2013; Kim et al., 2008).

Recently, two groups have reported the ubiquitination of PEX5 as a trigger for pexophagy. Nordgren and colleagues showed that by expressing an export-incompetent version of PEX5 (EGFP-tagged), this protein became mono-ubiquitinated at the membrane and triggered pexophagy (Nordgren et al., 2015). The second group reported a role for ATM kinase in the phosphorylation of PEX5 in response to intracellular ROS. This phosphorylation induced the mono-ubiquitination of PEX5 (at a different residue from the previous group), and its recognition by p62, triggering pexophagy (Zhang et al., 2015b). However, further studies will be necessary to confirm these results, has other groups have shown that increases in intracellular ROS induce peroxisome proliferation instead of degradation (Delmaghani et al., 2015, Diano et al. 2011). Additionally, the TA protein ACBD5 has also been suggested to induce pexophagy in mammalian cells but its role is less well characterised (Nazarko et al., 2014).

1.1.3.4. Motility

Eukaryotic cells strictly regulate the movement and distribution of their organelles in order to guarantee their optimal activity and inheritance during the cell cycle (Jongsma et al., 2015). Whereas in yeast and plant cells peroxisomes predominantly move along actin filaments by interacting with myosin motors (Fagarasanu et al., 2010; Sparkes and Gao, 2014), in mammalian cells they have been shown to move along microtubules via kinesin and dynein motors (Figure 1.1, 1.2) (Neuhaus et al., 2016; Schrader et al., 2003).

In mammalian cells, two main populations of peroxisomes can be observed by live-cell imaging: the majority of peroxisomes (85-95%) exhibit slow oscillatory movement, whereas the remaining 5-15% display fast, directional, and microtubule-dependent movement (Bharti et al., 2011; Rapp et al., 1996; Schrader et al., 2000; Wiemer et al., 1997). This low percentage of directed movement appears to be sufficient to maintain a homogeneous peroxisomal distribution at minimum energy expenditure, as calculated using modelling approaches (Bonekamp et al., 2012).

Earlier studies analysed peroxisome motility after treatment with several microtubule and actin depolymerising drugs such as nocodazole, vinblastine and cytochalasins (Huber et al., 1997; Schrader et al., 1996; Wiemer et al., 1997). Whereas nocodazole and vinblastine completely abrogated fast and directed peroxisome motility, actin depolymerising drugs had no clear effects on this organelle. Interestingly, in cells treated with nocodazole, peroxisomes were still able to elongate, suggesting that peroxisome motility is not essential for organelle division (Schrader et al., 1996, 1998b). Additional treatments such as ATP and GTP depletion, or changes in the intracellular calcium pool, showed that long-range peroxisome movement is a regulated and energy dependent process (Huber et al., 1997).

Peroxisomes move both towards and away from the cell centre, in a dynein and kinesin dependent manner (Dietrich et al., 2013; Kural et al., 2005; Schrader et al., 2003). Strikingly, little is known about the recruiting factors for these motors in mammalian cells. Recently, Bharti et al. proposed a new role for PEX14 in the regulation of peroxisome motility by binding directly to tubulin (Bharti et al., 2011). The authors suggest that this interaction is necessary to regulate

peroxisome motility and that this protein anchors peroxisomes to microtubules. Similarly, Dietrich and co-workers propose an interaction between the AAA ATPase PEX1 and the unconventional kinesin KIFC3, which may function in the tethering of peroxisomes to microtubules (Dietrich et al., 2013). The authors also suggest that this minus-end directed motor might regulate or disrupt the activity of the dynein complex in peroxisome motility. Additional roles for peroxins in motility regulation have also been described in yeast, where PEX3 and PEX19 interact with myosin motors (Chang et al., 2009; Otzen et al., 2012).

So far, the correlation between peroxisome motility and function in mammalian cells remains elusive. Mammalian peroxisomes are generally homogeneously distributed in the cytosol, which might facilitate interaction with other organelles and distribution during the cell cylcle. However, peroxisomal disorder patients with larger and less abundant peroxisomes, present clustering of this organelle close to the nucleus (Nguyen et al., 2006). This suggestes a connection between peroxisome metabolism and/or biogenesis with organelle motility.

1.1.4. Interactions with other organelles

Peroxisomes exert their functions as part of an intracellular network that enables their communication with other organelles such as mitochondria, ER and lipid droplets (Schrader et al., 2013, 2015b; Shai et al., 2015). These connections can form through contact sites for protein-protein and lipid interactions, by exchange of vesicles between organelles (e.g. mitochondria derived vesicles), and through signalling pathways and metabolite diffusion (Ivashchenko et al., 2011; Neuspiel et al., 2008; Raychaudhuri and Prinz, 2008).

Peroxisomes share a particularly close connection with mitochondria, cooperating in β-oxidation and ROS degradation, coordinating the cellular antiviral responses, and sharing several membrane proteins (Figure 1.3) (reviewed in Schrader et al., 2015a). Interestingly, several of these proteins are TA proteins (e.g. FIS1, MFF, GDAP1 and MAVS) (Dixit et al., 2010; Gandre-Babbe and van der Bliek, 2008; Huber et al., 2013; Koch et al., 2005) (see 1.2). As a result of this close interaction, homeostatic changes in either organelle can closely affect the other, and mutations in shared proteins are the foundation of a

new group of mitochondrial-peroxisomal disorders (Koch et al., 2016; López-Erauskin et al., 2013; Schrader et al., 2014; Shamseldin et al., 2012; Waterham et al., 2007).

1.2. Tail-anchored (TA) membrane proteins

TA proteins are a heterogeneous group of integral membrane proteins found in all intracellular organelles which are characterised by their topology. TA proteins have a single hydrophobic TMD located near the C-terminus, that anchors them to the lipid bilayer, and a short C-terminal polar tail that protrudes into the organelle matrix (Borgese et al., 2003). The N-terminal part of the protein faces the cytosol and includes the functional domains, which can be involved in several functions such as vesicular trafficking, apoptosis, signal transduction and redox reactions (Borgese and Fasana, 2011). TA proteins are found across all three domains of life (Borgese and Righi, 2010), and several screening approaches have shown their abundance in animals, plants and fungi (Beilharz et al., 2003; Kalbfleisch et al., 2007; Kriechbaumer et al., 2009).

Because of their structure, the TMD of TA proteins only emerges from the ribosome at the end of translation. As a result, TA proteins require post-translational mechanisms for sorting and membrane insertion (Borgese and Fasana, 2011; Kutay et al., 1993). Additionally, TA proteins lack traditional signal sequences that allow the recognition and sorting by cytosolic chaperones. Instead, the physicochemical properties of their TMD, such as length and hydrophobicity, and the charge of flanking amino acids, appear to regulate targeting to each organelle (Beilharz et al., 2003; Borgese et al., 2007; Kuroda et al., 1998; Marty et al., 2014). Furthermore, some of these proteins are targeted to more than one organelle, raising the possibility of competitive binding pathways for TA proteins (Borgese and Fasana, 2011).

1.2.1. Targeting and insertion of TA proteins

Post-translational sorting and insertion of TA proteins to each organelle requires distinct mechanisms (Figure 1.4) (reviewed in Borgese and Fasana, 2011). Although some TA proteins have the ability to spontaneously integrate into the

ER and outer mitochondrial membrane (Brambillasca et al., 2005; Kemper et al., 2008; Setoguchi et al., 2006), most TA proteins are recognized by cytosolic chaperones and form complexes with membrane receptors.

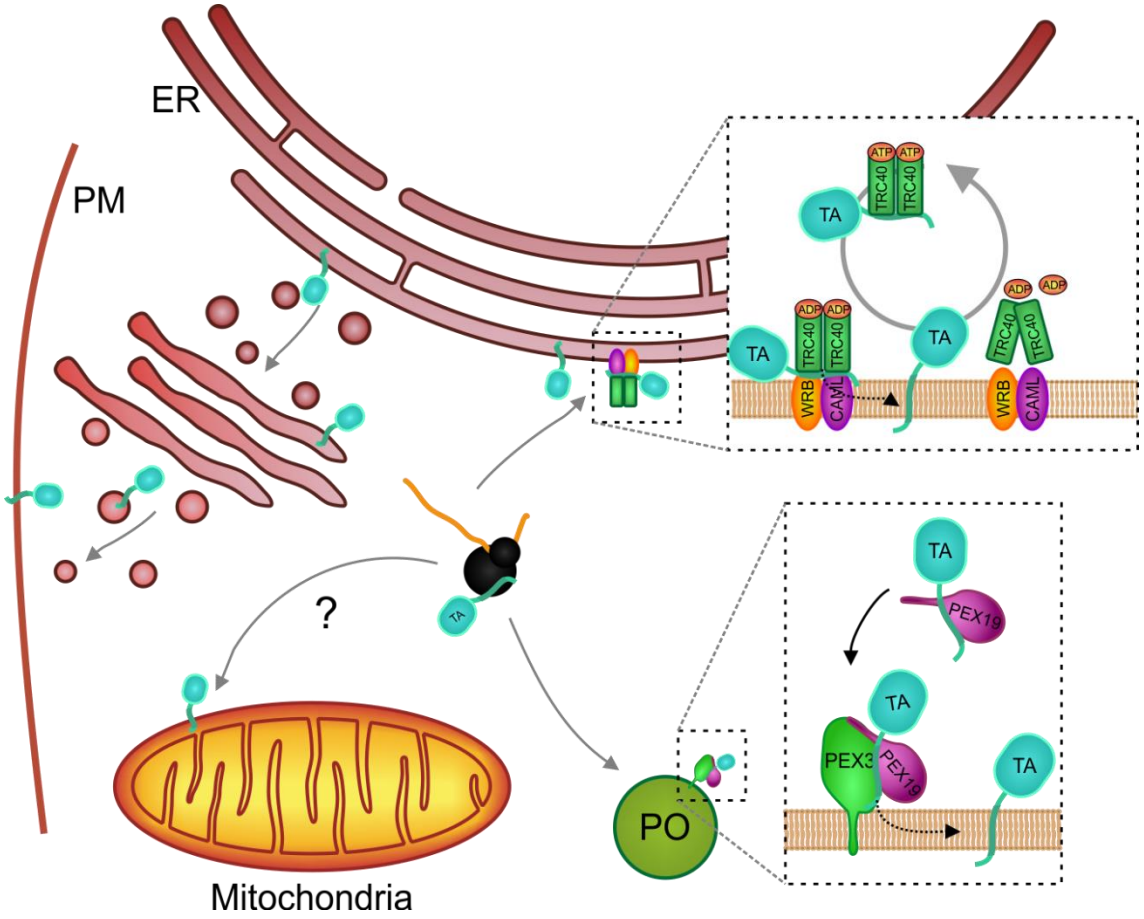

Figure 1.4 – Trafficking and membrane insertion of TA proteins. After translation, TA proteins are initially targeted to peroxisomes, mitochondria or the ER. Golgi and plasma membrane (PM) proteins are first inserted in the ER and reach their final destination by a vesicular pathway. ER TA proteins are targeted and inserted by the TRC pathway. The BAG6/TRC35/UBL4A sorting complex (not shown) delivers ER TA proteins to dimeric, ATP bound TRC40. TRC40 interacts with WRB and CAML at the ER membrane, and releases its substrate after ATP hydrolysis. ATP binding recycles TRC40 back to the cytosol for another round of import. Peroxisomal TA proteins are bound by the cytosolic chaperone PEX19 and delivered to peroxisomes by its interaction with PEX3, in an ATP-independent manner (Yagita et al, 2013).

1.2.1.1. ER and the TRC/GET pathway

Several pathways have been implicated in the targeting and insertion of ER TA proteins, including the SRP-mediated co-translational pathway and a HSC70/HSP40-mediated mechanism (Rabu et al., 2009). However, the majority of ER TA proteins appear to be sorted by the TMD-recognition complex (TRC) pathway in mammals, which has been extensively characterised for the past few years (Figure 1.4) (reviewed in Denic et al., 2013; Hegde and Keenan, 2011). Numerous insights into this pathway have been obtained from the study of the homologous mechanism in yeast (GET pathway) where the crystal structure of several components has been characterised (Chartron et al., 2012).

In this pathway, a TMD recognition complex composed by BAG6, UBL4A and TRC35 binds newly translated proteins at the ribosome and delivers them to the cytosolic ATPase TRC40 (yeast Get3) (Leznicki et al., 2010; Mariappan et al., 2010; Stefanovic and Hegde, 2007). ER TA proteins are characterised by highly hydrophobic TMDs which enable their interaction with BAG6 and TRC40 (Borgese et al., 2007; Brodsky, 2010). TRC40 forms homodimers that cycle between open and closed conformations, depending on their bound nucleotide. In its ATP-bound state, TRC40 acquires a closed conformation which enables the formation of a hydrophobic groove that interacts with substrate TMDs. (Favaloro et al., 2008; Mariappan et al., 2011; Mateja et al., 2009; Schuldiner et al., 2008; Stefanovic and Hegde, 2007). ATP hydrolysis appears to promote binding of TRC40 to the ER membrane receptors WRB and CAML, which tether and mediate the insertion of the TMD in the membrane (Vilardi and Lorenz, 2011; Yamamoto and Sakisaka, 2012).

Interestingly, the TMD recognition complex could be playing additional roles in the sorting of TA proteins, namely in the degradation of misfolded proteins or the sorting of TA proteins to other organelles by interacting with different chaperones (Hegde and Keenan, 2011; Kawahara et al., 2013).

1.2.1.2. Mitochondria

Despite the numerous mitochondrial TA proteins identified, their targeting and membrane insertion is still poorly understood (Borgese and Fasana, 2011).

Mitochondrial TA proteins have moderately hydrophobic TMDs in comparison with ER proteins, and are usually flanked by positive charges on one or both sides (Borgese et al., 2001, 2003; Horie et al., 2002).

Due to the moderate hydrophobicity of their TMD, some mitochondrial proteins spontaneously translocate across membranes *in vitro*, in the absence of both cytosolic and membrane proteins (e.g. cytochrome b5) (Brambillasca et al., 2005; Colombo et al., 2009; Kemper et al., 2008). Owing to their propensity to aggregate in the cytosol, it is unlikely that many proteins follow this pathway. However, no cytosolic chaperones have yet been shown to interact with and stabilise these proteins.

A role for the translocase of the outer mitochondrial membrane (TOM) complex has been proposed for the membrane insertion of BCL2 and BAX (Bellot et al., 2007; Motz et al., 2002). Conversely, insertion of BAK, BCL-XL and OMP25 is independent of this pathway (Setoguchi et al., 2006), suggesting that multiple pathways might be involved in the insertion of mitochondrial TA proteins.

Lastly, a role for the membrane lipid composition has also been proposed both in yeast and mammals, with changes in ergosterol and cholesterol content, respectively, affecting the ability of some proteins to translocate the membrane (Brambillasca et al., 2005; Kemper et al., 2008; Krumpe et al., 2012).

1.2.1.3. Peroxisomes and the PEX19 pathway

Similarly to mitochondria, peroxisomal TA proteins possess moderately hydrophobic TMDs and have a positively charged C-terminal polar region (Chen et al., 2014a; Delille and Schrader, 2008; Yagita et al., 2013). However, studies on this system have been hampered by the lack of described peroxisomal TA proteins, and have focused mainly on PEX26 and its yeast counterpart Pex15, which are responsible for the anchoring of Pex1 and Pex6 to the peroxisomal membrane (Birschmann et al., 2003; Matsumoto et al., 2003). Whereas yeast Pex15 appears to be indirectly targeted to peroxisomes via the ER (Buentzel et al., 2015; Elgersma et al., 1997; Schuldiner et al., 2008; van der Zand et al., 2010), human PEX26 follows a direct pathway relying on PEX19 and PEX3 for targeting and membrane insertion (Figure 1.4) (Buentzel et al., 2015; Halbach

et al., 2006; Yagita et al., 2013) (see 1.1.2.2). Two recent publications have further characterized this targeting by using semi-permeabilized cells (Yagita et al., 2013) and a cell-free system (Chen et al., 2014a), in human and *Neurospora crassa* cells, respectively. In both, PEX26 is bound and stabilized by PEX19, and delivered to the peroxisomal membrane where it forms a ternary complex with PEX3. This process is TRC40/GET3 independent in both systems. Furthermore, Chen and co-workers have also shed some light on the mechanistic functions of PEX19 and PEX3 in the filamentous fungus *N. crassa*, describing a new amphipathic domain in PEX19 that is required for TA protein TMD insertion, and a hydrophobic surface on PEX3 that is also required for the insertion of cargo protein TMDs (Chen et al., 2014a). Additionally, dually targeted TA proteins FIS1 and GDAP1 have also been shown to interact with PEX19 and are likely to follow the same direct pathway for peroxisomal insertion (Delille and Schrader, 2008; Huber et al., 2013).

1.2.2. Mistargeting and degradation

In addition to specific targeting pathways for TA proteins, new machinery has been described for the degradation of mistargeted proteins. Two pathways have recently been proposed, one for ER proteins and a second for mitochondrial proteins (Boname et al., 2014; Chen et al., 2014b; Okreglak and Walter, 2014).

The signal peptide peptidase (SPP) protein is an aspartyl protease that cleaves the TMD of ER-resident proteins, releasing the cytosolic fragment of the substrate for proteasomal degradation (Golde et al., 2009; Loureiro et al., 2006). This type of protease can only cleave ER proteins with cytosolic N-terminal domains, such as TA proteins. By altering the availability of SPP, Boname and colleagues were able to show that HMOX1, CYTB5, RAMP4 and RAMP4-2 are specifically cleaved by this protein (Boname et al., 2014). An additional TA protein, UBE2J1, was not cleaved by SPP, pointing to the presence of multiple degradation pathways for ER TA proteins.

A second pathway is mediated by the AAA ATPase ATAD1 (Msp1 in yeast), a membrane-bound protein which is dually targeted to mitochondria and peroxisomes (Chen et al., 2014b; Okreglak and Walter, 2014). In two concurrent publications, Msp1 was shown to bind Pex15 and promote its

degradation when mistargeted to mitochondria. This interaction was particularly evident when an ATPase mutant of Msp1 was expressed, which locked target proteins at the membrane and inhibited their turnover. Similar results were obtained with the human homolog ATAD1, suggesting that this function is conserved (Chen et al., 2014b). Additionally, Msp1/ATAD1 were also shown to bind and degrade mitochondrially mistargeted Gos1/GOS28 (homologous Golgi resident TA proteins) (Chen et al., 2014b). However, how these proteins are recognised and removed is still unknown. A possible pathway would be through the ubiquitination of residues that are otherwise shielded by interacting partners at the correct membrane. This ubiquitination would then allow the recognition of target proteins, similarly to the mechanism of p97 (Cdc48 in yeast) AAA ATPase (Stolz et al., 2011; Tanaka et al., 2010). Lastly, a role for these proteins on peroxisomes is still unknown, as no mistargeted TA proteins were analysed in this organelle.

1.3. MIRO proteins

Miro proteins are TA proteins localized on the outer mitochondrial membrane and highly conserved across eukaryotes (Reis et al., 2009; Vlahou et al., 2011). The human proteins, MIRO1 and MIRO2, have a similar structure and share 60% similarity (Figure 1.5 A) (Fransson et al., 2003). Due to their structure and GTPase domain sequence, these proteins have been identified as a new family within the superfamily of small Ras GTPases (Reis et al., 2009; Wennerberg and Der, 2004). Unlike other Ras GTPases, Miro proteins are anchored to the membrane by a TMD instead of post-translational lipid moieties, and possess two GTPase domains, making these proteins significantly bigger than other members of this family (Wennerberg and Der, 2004). The first GTPase domain has sequence similarities to Rho GTPases, which lead to their original classification within the Rho family (Fransson et al., 2003), but the absence of an insert domain and a CAAX-motif (which are typical of Rho GTPases) lead to their re-classification as a distinct family. The second GTPase domain is only distantly related to the Ras superfamily (Klosowiak et al., 2013).

Ras GTPases regulate several cellular processes such as cell proliferation, morphology and apoptosis (Goitre et al., 2014). These molecular switches

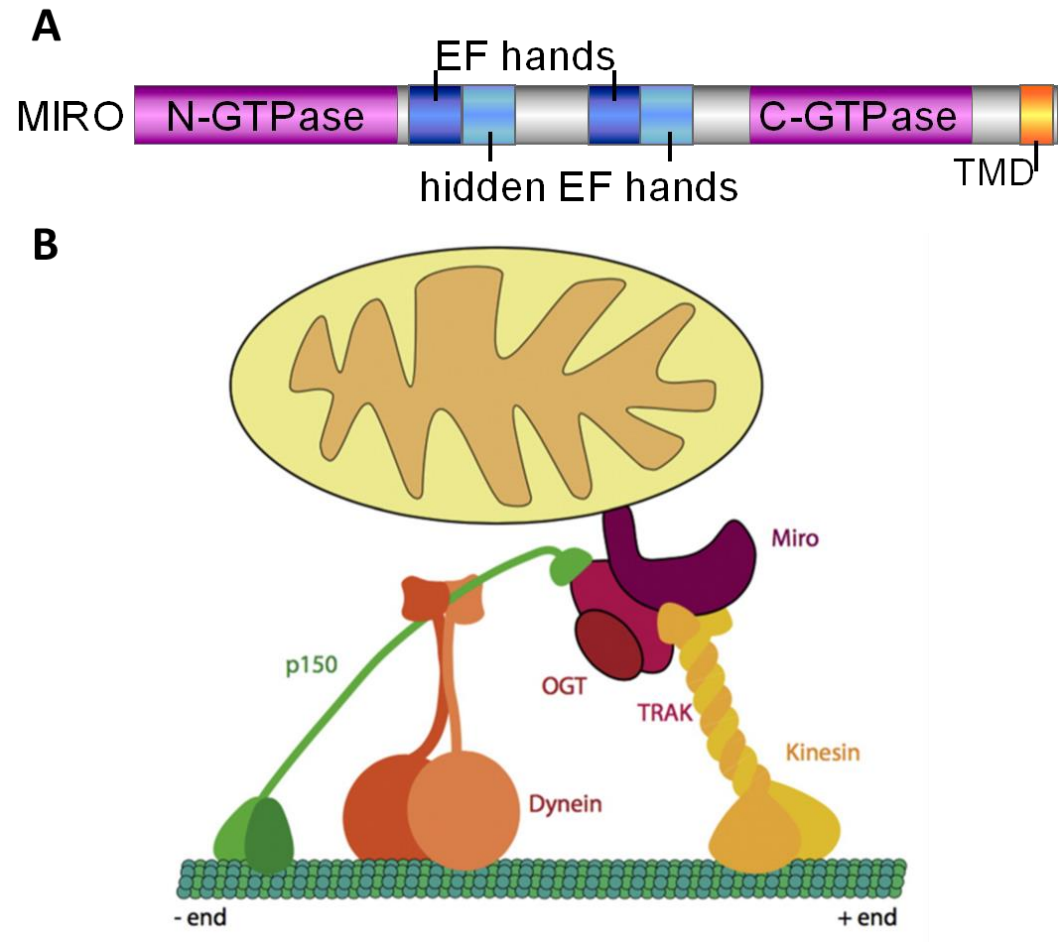

Figure 1.5 – Schematic representation of mammalian MIRO and the mitochondrial trafficking complex. (A) Structure of mammalian MIRO protein, with two GTPase domains flanking two calcium binding EF-hand motifs, and two "hidden" EF-motifs. (B) The TA proteins MIRO1 and MIRO2 enable mitochondrial motility by forming a motility complex. MIRO binds directly with Kinesin-1 (also known as kinesin heavy chain or KIF5) and TRAK1/TRAK2 to promote anterograde motility, and with dynein via the interaction of p150 with TRAK proteins. TRAK proteins interact and can be post-translationally modified by OGT. ((B) adapted from (Devine et al., 2016).

change from on/off states depending on their binding to GTP/GDP, respectively. Additionally, Ras GTPases are strictly regulated by guanine nucleotide exchange factors (GEFs) and GTPase activating proteins (GAPs), which exchange GDP for GTP (GEF) or induce GTP hydrolysis (GAP). Despite Miro's classification within this superfamily, little is known about its GTP hydrolysis activity and protein regulation. Thus far, a study on the yeast orthologue, Gem1, has shown that both GTPase domains are capable of GTP hydrolysis, and that this activity is not affected by the calcium binding capacity of the EF-hand motifs

(Koshiba et al., 2011). Furthermore, the *Vibrio cholera* protein VopE has been shown to interact with human MIRO1 and MIRO2, and increase the hydrolytic activity of the GTPase domains, switching the proteins to an off state due to its GAP activity (Suzuki et al., 2014). This inhibits mitochondrial clustering near the nucleus during bacterial infection and is proposed to inhibit MAVS-dependent signalling, delaying an immune response.

1.3.1. Genes and functions

As previously mentioned, Miro genes are conserved in almost all eukaryotic genomes (Vlahou et al., 2011), suggesting their presence in early eukaryotic evolution. Miro's domain architecture is mostly conserved across species, with a few exceptions present in trypanosomatid flagellates and ciliates (Vlahou et al., 2011), and it typically contains two GTPase domains separated by two calcium-binding EF-hand motifs, and a C-terminal TMD and short tail. Two additional hidden EF-hand motifs were identified by structural analysis of the *Drosophila* orthologue dMiro (Figure 1.5 A) (Klosowiak et al., 2013), forming a pair with the canonical domains. Yet, these hidden motifs are unlikely to bind Ca^{2+} due their altered loop structure and lack of negatively charged residues. Miro proteins are targeted to mitochondria in all studied species and play roles in mitochondrial dynamics and homeostasis (reviewed in Yamaoka and Hara-Nishimura, 2014). However, specific functions have evolved for different organisms, adding layers of complexity to the understanding of the function of these proteins.

1.3.1.1. Mitochondrial motility

Human MIRO1 and MIRO2 were initially described by Fransson and colleagues as new Rho GTPases involved in mitochondrial homeostasis and apoptosis (Fransson et al., 2003). Expression of these proteins severely altered mitochondrial distribution in COS-7 cells, leading to several phenotypes such as mitochondrial elongation and collapse of the mitochondrial network, as well as an increase in cell death with the expression of mutated proteins (Fransson et al., 2003, 2006). Concurrently, studies on the *Drosophila* orthologue, dMiro, showed that the absence of this protein lead to mitochondrial accumulation in

neuronal cell bodies, whereas protein expression induced an accumulation of mitochondria in synapses, pointing to a role of dMiro in anterograde mitochondrial movement (Guo et al., 2005). Subsequent studies showed that the kinesin-interacting protein Milton forms a complex with dMiro, and that this complex is responsible for mitochondrial anterograde and retrograde transport in *Drosophila* (Glater et al., 2006).

The homologous complex was later described in mammalian cells, where MIRO1 interacts with TRAK1 and TRAK2 (orthologues of Milton) and both kinesin and dynein motors (Figure 1.5 B) (Fransson et al., 2006; MacAskill et al., 2009b; Saotome et al., 2008; van Spronsen et al., 2013; Wang and Schwarz, 2009). Additionally, due to its calcium binding motifs, MIRO1 has been proposed to inhibit mitochondrial motility in active synapses, where glutamate signalling induces high intracellular calcium concentrations (MacAskill et al., 2009b; Wang and Schwarz, 2009), and to regulate mitochondrial Ca^{2+} storage in response to cytosolic fluctuations (Chang et al., 2011). In contrast, experiments performed using a MIRO1 knockout (KO) mouse model challenged the role of this protein in calcium sensing (Nguyen et al., 2014). In this study, the authors did not observe changes in mitochondrial calcium uptake between control and KO cells (unlike what had been proposed in (Chang et al., 2011)). Additionally, mitochondria motility in mouse embryonic fibroblasts (MEFs) and cortical neurons of wild-type (WT) and KO mice was similarly affected by changes in intracellular calcium, arguing against a role for this protein in calcium-dependent motility control. A similar result using WT and a calcium mutant of MIRO1 had been previously shown in cardiomyocytes (Saotome et al., 2008). Interestingly, Nguyen and colleagues also observed changes in the mitochondrial retrograde motility instead of the expected effects in anterograde motility. Whereas this is in conflict with evidence obtained from protein silencing and overexpression experiments, it should be noted that several studies have also shown a role for MIRO1 in retrograde movement (Morlino et al., 2014; Russo et al., 2009; van Spronsen et al., 2013).

Interestingly, the regulation of mitochondrial motility by the MIRO1/TRAK complex is in contrast with the frequently suggested model of organelle motility – the tug-of-war. According to this model, membrane bound opposition motors push the organelle in both directions, with the resulting speed and direction

relaying on the strength and number of attached motors. In the absence of one motor, a shift towards the opposite direction should be observed (Hendricks et al., 2010). When considering the existing data on MIRO1-regulated motility, a more complex system emerges. Here, MIRO1 functions as a regulator of both plus and minus end directed motility in response to cellular cues such as calcium concentration and GTP/GDP availability. As both kinesin and dynein motors are part of the same complex, a system where different signals can activate/inhibit one or both motors should be considered (Hancock, 2014).

Additionally, due to its role in mitochondrial motility, MIRO1 has been implicated in the transport of mitochondria via tunnelling nanotubes (Ahmad et al., 2014). Using both an *in vitro* model of rotenone-induce mitochondrial damage, and *in vivo* models of asthma and airway injury, Ahmad et al. showed that high levels of MIRO1 improve mitochondrial transfer from healthy mesenchymal stem cells to epithelial cells containing damaged mitochondria. This process lead to a decrease in epithelial cell apoptosis and decreased the inflammatory response to airway damage, suggesting that MIRO1 could be targeted for therapeutic approaches.

1.3.1.2. Gem1 and mitochondrial dynamics

Whereas mammalian MIRO proteins seem to play a key role in mitochondrial microtubule-dependent motility, a reciprocal function in yeast was not expected, as mitochondria move through the actin cytoskeleton in this organism (Boldogh and Pon, 2007). Initial studies on the yeast orthologue Gem1 revealed changes in the mitochondrial network in *gem1*Δ cells, with an increase in the number of cells presenting globular or collapsed tubular mitochondria (Frederick et al., 2004). As these changes were not a result of defects in mitochondrial fission or fusion, Gem1 was proposed to regulate a new pathway in mitochondrial signalling and dynamics (Frederick et al., 2004). Double mutants of Gem1 and Mmr1, a yeast protein involved in mitochondrial inheritance, showed synthetic growth defects pointing to a possible role of Gem1 in mitochondrial inheritance (Frederick et al., 2008). In agreement with this, mutations in Gem1 GTPase domains strongly affected mitochondrial inheritance in budding yeast (Koshiba et al., 2011).

Recently, a role for Gem1 has been proposed in the regulation of the ER-mitochondria tethering (ERMES) complex (Kornmann et al., 2009, 2011; Stroud et al., 2011). This structure has been suggested to regulate several processes such as mitochondrial division, inheritance, mitochondrial DNA replication and lipid transfer (Boldogh et al., 2004; Kornmann et al., 2011; Murley et al., 2013; Youngman et al., 2004). However, contradictory results suggest that Gem1 is not necessary for ERMES function and formation, and that this complex is not involved in lipid transfer nor mitochondrial inheritance (Nguyen et al., 2012).

1.3.2. Interacting partners

In order to regulate mitochondrial motility and function, MIRO1 and MIRO2 interact with several other cytosolic and mitochondrial proteins, namely TRAK1 and TRAK2 (Fransson et al., 2006), KIF5 (MacAskill et al., 2009b), Dynein complex (Morlino et al., 2014), PINK1 and PARKIN (Weihofen et al., 2009), MFN1 and MFN2 (Misko et al., 2010), HUMMR (Li et al., 2009), ARMC3 (López-Doménech et al., 2012), VopE (Suzuki et al., 2014) and CENP-F (Kanfer et al., 2015). Some of these interactions have been well characterised and are described below.

1.3.2.1. TRAK proteins and the motility complex

As previously mentioned, TRAK1 and TRAK2, also known as OIP106 and GRIF-1/OIP98 respectively, form a complex with MIRO and motor proteins, enabling mitochondrial motility along microtubules (reviewed in Devine et al., 2016). Both TRAK proteins were initially shown to interact directly with kinesin-1 family proteins (KIF5A-C, also known as kinesin heavy chain (KHC)) (Brickley et al., 2005; Smith et al., 2006), and their overexpression in mammalian cells lead to similar phenotypes to that of MIRO proteins – elongated and collapsed mitochondrial networks in COS-7 cells, and reduced mitochondrial motility in cultured neurons (Brickley and Stephenson, 2011; Koutsopoulos et al., 2010; Wang and Schwarz, 2009). Their function is particularly well characterised in neuronal cells where these proteins appear to play complementary roles in axonal and dendritic mitochondrial motility (van Spronsen et al., 2013). TRAK1

is mostly axonal and interacts with both kinesin and dynein motors, whereas TRAK2 shows a more dendritic localisation and interacts preferentially with dynein motors. Both TRAK proteins also interact and are modified by the β O-linked N-acetylglucosamine transferase (OGT) enzyme, which attaches monosaccharides to serine and threonine residues (Brickley et al., 2011; Iyer et al., 2003). Recently, Pekkurnaz et al. were able to show that OGT activity increases in response to higher glucose levels, leading to TRAK1 O-glycosylation and consequent mitochondrial arrest, suggesting that neuronal mitochondrial motility is regulated in response to changes in nutrient availability (Pekkurnaz et al., 2014).

The MIRO/TRAK complex also interacts with mitofusin 1 and 2 (MFN1/MFN2), two dynamin related GTPases that regulate mitochondrial fusion (Misko et al., 2010). Although the function of this interaction is unknown, it should be noted that MFN2 has been shown to tether mitochondria to the ER (de Brito and Scorrano, 2008), and so, its interaction with MIRO could mimic the role of the ERMES complex in yeast.

Lastly, some proteins have been shown to regulate mitochondrial motility by interacting with the MIRO-TRAK complex. For example, the hypoxia up-regulated mitochondrial movement regulator (HUMMR) protein, which is up-regulated by HIF-1α during hypoxic conditions, interacts with MIRO and TRAK proteins, increasing anterograde mitochondrial motility in neurons (Li et al., 2009). Two other proteins, ALEX3 and ARMC10, interact with MIRO1-2, TRAK2 and KIF5C and regulated mitochondrial motility in neurons (López-Doménech et al., 2012; Serrat et al., 2014). Despite the unknown function of these proteins, they belong to the Armcx family of proteins which is exclusive to Eutherian mammals, adding an extra layer of complexity to the regulation of mitochondrial motility in mammals.

1.3.2.2. PINK1/PARKIN and mitochondrial degradation

The PTEN-induced putative kinase (PINK1) and the ubiquitin ligase PARKIN are core regulators of the mitochondrial quality-control system, and are involved in the selective degradation of damaged mitochondria. PINK1 has been shown to phosphorylate PARKIN, recruiting it to the membrane of damaged

mitochondria, and increasing its ubiquitin ligase activity (Deas et al., 2011). Both PINK1 and PARKIN have been shown to interact with MIRO proteins (Wang et al., 2011; Weihofen et al., 2009). While PINK1 has been proposed to phosphorylate dMiro (Wang et al., 2011), ubiquitination by PARKIN appears to be more important for MIRO regulation, leading to its proteasomal degradation and consequent mitochondrial arrest (Birsa et al., 2014; Liu et al., 2012; Wang et al., 2011). This process may facilitate mitochondrial degradation by mitophagy by inhibiting mitochondrial motility and may be implicated in the pathology of familial Parkinson's disease.

1.3.2.3. CENP-F and cell cycle

Recently, Kanfer et al. described a role for MIRO1 in mitochondrial distribution during the cell cycle (Kanfer et al., 2015). The authors show that MIRO1 interacts with the centromeric protein F (CENP-F), a large microtubule binding protein which is recruited to mitochondria during cytokinesis, and that this interaction links mitochondria to microtubule growing tips, allowing their distribution to the cell periphery at the end of mitosis. How CENP-F drags mitochondria along growing microtubule tips is still unknown, but this interaction sheds some light on the regulation of mitochondrial distribution during the cell cycle. In another study, Lawrence and colleagues showed that disruption of MIRO1 and KIF5B using dominant negative mutants altered mitochondrial positioning during cytokinesis, pointing to a role for kinesin motors in this process (Lawrence et al., 2016). Further studies will be necessary to understand this process and to reveal the protein complexes responsible for mitochondrial distribution during the cell cycle.

1.3.3. Miro and its role in disease

Mitochondria play essential roles in energy production and calcium buffering. As a result, defects in their motility or in the maintenance of a healthy mitochondrial population are common hallmarks of several neurodegenerative disorders such as Alzheimer's and Parkinson's disease, amyotrophic lateral sclerosis (ALS) and spastic paraplegia (Mattson et al., 2008). Since MIRO proteins play an

essential role in mitochondrial motility and are involved in their ability to sense intracellular calcium shifts, defects in these proteins have been linked to ALS (Mórotz et al., 2012; Zhang et al., 2015a) and Parkinson's disease (Liu et al., 2012; Wang et al., 2011).

Evidence of Miro's role in neurodevelopment is particularly evident in animal models. *Drosophila* mutants expressing truncated versions of dMiro die prematurely and present movement defects during the larvae phase, with weak muscular capacity leading to paralysis (Guo et al., 2005). In neurons, mitochondria were shown to accumulate in the cell soma, and to be reduced or completely absent in axons and neuromuscular junctions, showing impaired anterograde mitochondrial transport. Curiously, mitochondria in these cells had no observable changes in structure and function (Guo et al., 2005). Absence of MIRO1 in mice is lethal at birth, as these animals are unable to breathe due to degeneration of specific motor neuron axons (Nguyen et al., 2014). *Ex vivo* analysis of neurons from these animals showed defects in retrograde axonal mitochondrial transport, without affecting respiratory and calcium buffering functions. A conditional KO mouse lacking neuronal MIRO1 was alive at birth but showed progressive symptoms of a motor neuron disorder similar to spastic paraplegia (Nguyen et al., 2014). Interestingly, the results from both animal models suggest that the pathology is caused by defects in mitochondrial motility (not function), and that this can be the primary cause of some neurological disorders.

In line with these results, a link between MIRO and ALS has been recently proposed. Mórotz and colleagues have shown that expression of a mutated variant of VAPB (VAMP associated protein B), which is known to cause a familial form of ALS, alters mitochondrial anterograde motility by decreasing the ability of MIRO1 to interact with tubulin via kinesin motors (Mórotz et al., 2012). Additionally, analysis of patient and mouse model cells of ALS showed a significant reduction in MIRO1 expression (Zhang et al., 2015a). Interestingly, this reduction could also be induced by increasing glutamate levels both *in vitro* and *in vivo*, as glutamate toxicity is believed to strongly contribute to the pathology of ALS (Zhang et al., 2015a).

1.4. Objectives

Peroxisomes play an essential role in human health and development. As such, the study of their functions, biogenesis and dynamics is essential to understand how cells and organisms work, and how to repair them in pathological conditions.

This thesis aims to further develop our knowledge of the basic regulation of peroxisomes by addressing two main distinct points: how are tail-anchored proteins recognized and targeted to peroxisomes, and what's the molecular machinery responsible for peroxisomal motility?

In chapter 3, the targeting of TA proteins to peroxisomes is analysed. To do this, a bioinformatics approach was used to identify several physicochemical parameters that define the targeting signals of TA proteins. The two main factors identified, TMD hydrophobicity and tail charge, were then tested by mutating model TA proteins and analysing their localisation and ability to bind the peroxisomal chaperone PEX19. As a result, a bioinformatical tool was developed that allows us to predict the targeting of uncharacterised TA proteins and further develop our understanding of the molecular mechanisms involved in the targeting of this protein group.

In chapter 4, the targeting and function of a specific TA protein, MIRO1, was characterised. To do so, the cellular localisation of MIRO1 was established using imaging and biochemical methods. As MIRO1 was identified on peroxisomes, its function at this organelle was investigated using several MIRO1 mutants, as well as live-cell imaging techniques coupled with a bioimaging analysis of whole cell motility data. As a result, MIRO1 was shown to regulate peroxisomal motility, allowing us to use it as a tool to further dissect the role of motility on peroxisome dynamics. Subsequently, we demonstrated that the application of a directed motor force may play a role in the formation of new peroxisomes.

In chapter 5, the localisation and function of the MIRO1 interacting partner TRAK1 was briefly analysed. This was performed by expressing this protein in conjunction with MIRO1, and by analysing the effects of its mutation in a patient cell line. As a result, TRAK1 presented no clear effects on peroxisomes and appears to play specific roles in mitochondrial distribution.

Chapter 2 – Materials and Methods

2.1. Chemicals

All chemicals were purchased from Sigma-Aldrich (St Louis, USA), GE Healthcare (Buckinghamshire, UK), Merck Millipore (Darmstadt, Germany), ThermoFisher Scientific (Waltham, USA), and Roche (Basel, Switzerland). Restriction enzymes and other cloning reagents were from New England Biolabs (Ipswich, USA). Cell culture medium and additives were from Gibco, as part of ThermoFisher Scientific (Waltham, USA).

2.2. Buffers and solutions

General buffers and solutions are present in table 2.1. All buffers and solutions used for cell culture were sterilised by autoclaving or filtration prior to use.

Table 2.1 – Buffers and solutions

Buffers and solutions	Recipe
Blocking solution for IMF	1% (w/v) BSA in PBS
Blocking solution for WB	5% (w/v) low-fat milk powder in TBS-T
Chloroquine solution	60 mg/ml in deionized H_2O
Cross-linker solution	1 mM DSP
DEAE-dextran solution	25 mg/ml in deionized H_2O
Fixative for IMF, pH 7.4	4% (w/v) Paraformaldehyde in PBS
LB medium	2.5% (w/v) LB-Broth Miller
LB plates	2.5% (w/v) LB-Broth Miller 1% (w/v) Agar
Lysis buffer pH 7.5	25 mM TrisHCl 150 mM NaCl 0,5 mM EDTA Add fresh: 0.5% (w/v) Triton X-100, 1 mM PMSF, 1 mini protease inhibitor cocktail (Roche)
Mounting medium for IMF	3 volumes Mowiol stock 1 volume Propyl gallate stock

Mowiol stock	12 g Mowiol 4-88 40 ml PBS, stir over night + 20 ml Glycerol, stir over night Centrifuge 1 hour, 15,000 rpm, 4°C Add sodium azide to the supernatant
Phosphate buffered saline (PBS) pH 7.35	140 mM NaCl 2.5 mM KCl 6.5 mM Na_2HPO_4 1.5 mM K_2HPO_4
Permeabilisation for IMF	0.2% (v/v) Triton X-100 in PBS
Permeabilisation for IMF	1 mg/ml Digitonin stock solution 1:400 diluted in PBS
Propyl gallate stock	2.5% (w/v) Propyl gallate in PBS 50% (v/v) Glycerol
Laemmli loading buffer	60 mM Tris, pH 6.8 2% (w/v) SDS 10% (v/v) Glycerol 0.005% (w/v) Bromophenol blue 20 mM DTT 5% (v/v) β-Mercaptoethanol (fresh)
SDS running buffer	25 mM Tris 190 mM Glycine 0.1% (w/v) SDS
Semidry blotting buffer	48 mm Tris 39 mM Glycine 0.4% (w/v) SDS 20% (v/v) Methanol
50x TAE – Tris-Acetate-EDTA pH 8.0	40 mM Tris 20 mM Acetic acid 1 mM EDTA
TBS-T	50 mM Tris, pH 7.5 150 mM Sodium chloride 0,05% Tween20
Tris buffer separation gel, pH 8.8	2 M Tris in water
Tris buffer stacking gel, pH 6.8	1 M Tris in water

2.3. Cloning

All expression plasmids were designed using Clone Manager 9 (Sci-Ed Software, USA) (Table 2.2), or kind offers from collaborators (Table 2.3). Primer synthesis (Table 2.4) and DNA sequencing were from Eurofins MWG Operon

(Ebersberg, Germany). Gene synthesis (Table 2.5) was performed by Genscript (Genscript, Piscataway, USA) or Eurofins (Eurofins Genomics, Ebersberg, Germany).

Genes of interest were amplified by PCR from previously cloned plasmids or human cDNA obtained from cultured HepG2 cells. The latter was obtained by extracting total RNA from HepG2 cells using TRIZOL reagent and reverse transcribing it into cDNA. PCR conditions were adapted for each primer pair and optimized for KOD DNA polymerase activity, according to the manufacture's protocol.

DNA products from PCR and digestion reactions were run in agarose gels prior to purification. DNA electrophoresis was routinely performed in an agarose gel (1% agarose in 1x TAE buffer) stained with ethidium bromide (0.5 µg/ml). Separation was performed at 75 V for 45 to 60 minutes in TAE 1x buffer. DNA samples were mixed with 6x purple loading dye buffer and loaded to individual wells. A DNA ladder was also loaded to one well to compare band sizes. Digital images were taken using the BioDoc-It Imaging System (UVP, USA). Specific DNA bands were excised with a scalpel under UV light and purified using the NucleoSpin Extract II kit (Macherey-Nagel, Germany), following the manufacturer's protocol

DNA and vectors were digested with restriction enzymes (Table 2.2) following the manufacturer's suggested buffers and additives (e.g. BSA) at 37°C, for 4h or overnight. Enzyme inactivation was performed at 65°C for 20 minutes. Upon digestion, samples were run in an agarose gel to remove unwanted DNA fragments. Vector DNA was dephosphorylated with antarctic phosphatase for 40 minutes at 37°C, followed by enzyme inactivation for 20 minutes at 65°C. DNA concentration was determined using the Qubit2.0 fluorometer (Invitrogen, USA).

For ligation, the molecule ratios between vector and insert were 1:3 and 1:5. To calculate the exact amount of DNA to be used, the following formula was used:

$$insert\ (ng) = \frac{vector\ (ng) \times insert\ (kb)}{vector\ (kb)} \times ratio$$

Ligation was performed with T4 ligase at 4 or 16°C overnight, and control ligations were performed in parallel with the dephosphorylated vector.

Plasmid amplification was performed in competent DH5α *Escherichia coli* following a standard heat shock protocol. For each plasmid, 50 µl of competent *E.coli* bacteria were mixed with 2 µl of ligation mixture and incubated for 30 minutes on ice, followed by a 90 seconds heat shock at 42°C, and a short incubation on ice. For recovery, bacteria were incubated with 950 µl of LB medium for 45 minutes at 37°C with low agitation. Cells were centrifuged for 3 minutes at 3000 rpm and the pellets were resuspended in 100 µl of LB medium. Cells were spread with the aid of glass beads on LB agar plates containing kanamycin (30 µg/ml) or ampicillin (100 µg/ml). Plates were incubated overnight at 37°C.

Colonies were tested by DNA digestion following plasmid DNA isolation using the NucleoSpin Plasmid Miniprep kit (Macherey-Nagel, Germany). A single positive clone for each plasmid was selected and sequenced. For positive clones, DNA yield was increased by performing midi preparations using the NucleoBond Xtra Midi kit (Macherey-Nagel, Germany) according to the manufacturer's protocol.

Table 2.2 – Plasmids generated

Name	Template	Primers	Enzymes	Vector
Myc-FALDH-PO	HepG2 cDNA	Myc-FALDH-XhoI-Fw Myc-FALDH-PO-BamHI-Rv	XhoI BamHI	pCMV-3b
Myc-FALDH-ER	HepG2 cDNA	Myc-FALDH-XhoI-Fw Myc-FALDH-ER-BamHI-Rv	XhoI BamHI	pCMV-3b
GFP-FALDH-PO	myc-FALDH-PO	GFP-FALDH-PO-XhoI-Fw GFP-FALDH-PO-BamHI-Rv	XhoI BamHI	pEGFP-C1
GFP-FALDH-ER	myc-FALDH-ER	GFP-FALDH-ER-XhoI-Fw GFP-FALDH-ER-BamHI-Rv	XhoI BamHI	pEGFP-C1
Myc-ACBD4 isoform2	HepG2 cDNA	Myc-ACBD4 isoform 1 For Myc-ACBD4 isoform 2 Rev	XhoI BamHI	pCMV-3b
Myc-ACBD5 isoform1	HepG2 cDNA	Myc-ACBD5 For Myc-ACBD5 Rev	EcoRV XhoI	pCMV-3b
GFP-ACBD5 isoform1	myc-rACBD5.1	GFP-ACBD5.1-XhoI-Fw GFP-ACBD5.1-EcoRI-Rv	XhoI EcoRI	pEGFP-C1

GFP-ACBD5 $^{TMD+T}$ WT	Gene synthesis	-	EcoRI SacII	pEGFP-C1
GFP-ACBD5 $^{TMD+T}$ Mut1	Gene synthesis	-	EcoRI SacII	pEGFP-C1
GFP-ACBD5 $^{TMD+T}$ Mut2	Gene synthesis	-	EcoRI SacII	pEGFP-C1
GFP-ACBD5 $^{TMD+T}$ Mut3	Gene synthesis	-	EcoRI SacII	pEGFP-C1
Myc-ATP5J2	Gene synthesis	-	BamHI XhoI	pcDNA3.1 N-Myc
Myc-PPP1R3F	Gene synthesis	-	EcoRI XhoI	pcDNA3.1 N-Myc
Myc-Miro1-Pex	Myc-Miro1	Myc-Miro1_AgeI_F Miro1_dTM_R	AgeI BglII	pAH26
Myc-Miro1-PO	Myc-Miro1	Myc-Miro1_AgeI_F Miro1_EcoRI-R	AgeI EcoRI	pEGFP-ACBD5 $^{TMD+T}$ WT

Table 2.3 – Plasmids used

Plasmid	Source
GFP-BCL2	Kindly provided by R. Youle, NIH, Bethesda, USA
GFP-BCL-XL	Kindly provided by R. Youle, NIH, Bethesda, USA
GFP-BAX	Kindly provided by R. Youle, NIH, Bethesda, USA
GFP-BAK	Kindly provided by R. Youle, NIH, Bethesda, USA
Myc-MIRO1 WT, V13, N18, KK, ΔTM	Kindly provided by P. Aspenström, Karolinska Institute, Sweden
Myc-MIRO2 WT	kindly provided by P. Aspenström, Karolinska Institute, Sweden
Myc-OMP25	Kindly provided by P. DeCamilli, Yale University, USA
GFP-SEC61β	Kindly provided by W.A. Prinz, NIH, Bethesda, USA
Myc-VAPB	Kindly provided by C. Miller, King's College London, UK
Myc-rACBD5.1	(Islinger et al., 2007)
Flag-FIS1-WT and SR	Kindly provided by N. Ishihara, Kurume University, Japan
GFP-SKL	(Koch et al., 2005)
HA-Pex19	(Delille and Schrader, 2008)
pAH26	(Halbach et al., 2006)

Table 2.4 – Primers for cloning and sequencing

Name	Sequence (5' to 3')
GFP-ACBD5.1-XhoI-Fw	5' CCGCTCGAGAAATGGCGGACACACGATCAG 3'
GFP-ACBD5.1-EcoRI-Rv	5' CCGGAATTCCGTCAATTTAGTTTTCTTCTCCTTC 3'
Myc-FALDH-XhoI-Fw	5' AATAAGGATCCATGGAGCTCGAAGTCCG 3'
Myc-FALDH-PO-BamHI-Rv	5' AATAACTCGAGCAGACAGGGCTGGGTTTTGA 3'
Myc-FALDH-ER-BamHI-Rv	5'AATAACTCGAGGCACTAGGAGGTTGAACAGGA 3'
GFP-FALDH-PO-XhoI-Fw	5' CCGCTCGAGAAATGGAGCTCGAAGTCCGGC 3'
GFP-FALDH-PO-BamHI-Rv	5' CGGGATCCCGTCATCTCTGCTTACTGGACC 3'
GFP-FALDH-ER-XhoI-Fw	5' CCGCTCGAGAAATGGAGCTCGAAGTCCGGC 3'
GFP-FALDH-ER-BamHI-Rv	5' CGGGATCCCGTCAGTAATATTCTGCCTTGACAA 3'
Myc-ACBD4 For	5' AAGGATCCATGGGCACCGAGAAAGAAAGCCCAGAGCC CGAC 3'
Myc-ACBD4 Rev	5' CTCTCGAGTCACCTCTTTTGGGTCCGAAACATTCGGAA GAGCC 3'
Myc-ACBD5 For	5' AAAGGATCCATGCTCTTCCTCTCGTTTCATG 3'
Myc-ACBD5 Rev	5' GTTCTCGAGTTATCAGTTCAGTTTTCTTCTCCTTCTTTG 3'
Myc-Miro1_AgeI_F	5' GGAACCGGTCACCATGGAGCAGAAGCTGATC 3'
Miro1-dTM_R	5' GGAAGATCTAAACGTGGAGCTCTTGGGGTC 3'
Miro1_EcoRI-R	5' GCGGAATTCGAAAACGTGGAGCTCTTGAGGTC 3'
Miro1seqmid1	5' CGCACAGAAAGCTGTTCTTCATCC 3'
Miro1seqmid2	5' GACTGAGCAAGAGTCTCAAG 3'
pEGFPC1for	5' GATCACTCTCGGCATGGAC 3'
pEGFPC1rev	5' CATTTTATGTTTCAGGTTCAGGG 3'
pShuttleCMV-f	5' GGTCTATATAAGCAGAGCTG 3'
CMVfor	5' CGCAAATGGGCGGTAGGCGTG 3'

Table 2.5 – Gene synthesis

Gene	Sequence
ACBD5 $^{TMD+T}$ WT	GCGGCGAATTCTCCTGGTGTGCTAACGTTTGCTATTATATGG CCTTTTATTGCTCAGTGGTTGGTGCATTTGTATTATCAAAGA AGGAGAAGAAAACTGAACTGAACCGCGGGC
ACBD5 $^{TMD+T}$ Mut1	GCGGCGAATTCCCCTGGTGCATTAGCTTTTGCTATTATATGG CCTTTTATTGCTCAGTGGTTGGTGCATTTGTATTATCAAAGA **GCC**AGA**GCC**AAACTAAATTGAACCGCGGGC
ACBD5 $^{TMD+T}$ Mut2	GCGGCGAATTCCCCTGGTGCATTAGCTTTTGCTATTATATGG CCTTTTATTGCTCAGTGGTTGGTGCATTTGTATTATCAA**GCC GCCGCCGCC**AAACTAAATTGAACCGCGGGC
ACBD5 $^{TMD+T}$ Mut3	GCGGCGAATTCCCCTGGT**CTG**TTA**CTG**TTT**CTG**ATTATA**CTG CTG**TTTATT**CTGCTGCTG**TTGGTG**CTG**TTGTATTATCAAAGA AGGAGAAGAAAACTAAATTGAACCGCGGGC

2.4. Cell culture and transfection

Cell lines (Table 2.6) were routinely cultured in Dulbecco's modified Eagle medium (DMEM) high glucose (4.5 g/L) supplemented with 10% FBS, 100 U/ml penicillin and 100 µg/ml streptomycin at 37°C with 5% CO_2 and 95% humidity. HepG2 cells were cultured in similar conditions but with MEM medium. Mouse embryonic fibroblast (MEF) media was supplemented with β-mercaptoethanol at a final concentration of 50 µM to prevent the accumulation of oxygen radicals.

Immortalised cells were maintained in culture for 30-40 passages and rimary cell lines for 10-15 passages. Cells were regularly monitored for alterations in cell shape and proliferation.

Cell passage was performed twice a week, after the cells reached confluence. Cells were washed once with PBS 1x and incubated for 5 minutes with 1.5 ml TrypLE Express at 37°C. Upon resuspension in medium, cells were centrifuged for 3 minutes at 1000 rpm to remove debris. Cell pellets were resuspended in 10 ml of fresh medium and seeded at 1:10 to 1:5 dilution. Cells were routinely grown on 10ø cm dishes. For immunofluorescence, cells were seeded on round 19ø mm glass coverslips 24 hours prior to transfection. When using HepG2 cells, coverslips were coated with collagen prior to seeding. To ensure reproducibility between experiments, cell number was determined using a Neubauer counting chamber or a TC20™ Automated Cell Counter (Bio-Rad, USA).

Table 2.6 – Cell lines

Cell line	Organism	Tissue	Cell type	Morphology	Source
COS7	*Cercopithecus aethiops*	Kidney	SV40 transformed	Fibroblast-like	ATCC (CRL-1651)
HepG2	*Homo sapiens*	Liver	carcinoma	Epithelial	ATCC (HB-8065)
C109	*Homo sapiens*	Skin	primary	Fibroblast	H. Waterham (University of Amsterdan, Netherlands)
ΔPEX5	*Homo sapiens*	Skin	primary	Fibroblast	H. Waterham (University of Amsterdan, Netherlands)

ΔPEX14	*Homo sapiens*	Skin	primary	Fibroblast	M. Fransen (KU Leuven, Belgium)
ΔPEX19	*Homo sapiens*	Skin	primary	Fibroblast	G. Dodt (University of Tübingen, Germany)
MEF MIRO1 +/+ and -/-	*Mus musculus*	Embryo	SV40 transformed	Fibroblast	J. Shaw (University of Utah, USA)
TRAK1	*Homo sapiens*	Skin	primary	Fibroblast	Yair Anikster (Sheba Medical Center, Israel)

2.4.1. Cell freezing and thawing

Stocks for each cell line were kept through cryopreservation in liquid nitrogen. Cell pellets from confluent dishes were prepared as described above and resuspended in freezing medium (DMEM supplemented with 20% FBS and 10% DMSO). 1 ml aliquots were prepared in cryovials and frozen overnight at -80°C, before being stored in a liquid nitrogen tank. For thawing, cells were quickly resuspended with pre-warmed culture medium and seeded in a 10ø cm dish. The culture medium was changed after a few hours (after cell adhesion) to remove debris and DMSO.

2.4.2. Transfection methods

Several transfection methods were used, depending on the cell line and experimental objective. COS-7 cells were routinely transfected with TurboFect for IMF and live-cell imaging, and with (DEAE)-dextran for WB and IPs. HepG2 cells were transfected using Lipofectamine® 3000. Human skin fibroblasts and mouse embryonic fibroblasts were transfected by microporation. Transfection efficiency varied with method and cell line, and was optimised by adjusting cell number, plasmid concentration and transfection time. For each experiment, controls were performed with non-transfected cells and cells transfected without plasmid. For all transfection methods used, except microporation, cells were seeded in dishes or 19ø mm glass coverslips 24 hours prior to transfection.

2.4.2.1. TurboFect™ (ThermoFisher Scientific)

For transfection, 4 µg of DNA and 6 µl of TurboFect were diluted in 400 µl of DMEM medium without FBS and antibiotics and incubated for 20 minutes. During incubation, the culture dish was washed once with PBS and fresh media (without FBS or antibiotics) was added. The DNA/TurboFect mixture was added drop-wise to the dish and incubated for 3 to 6 hours at 37 °C after which the cells were washed with PBS and incubated in fresh complete medium for 24/48 hours.

2.4.2.2. DEAE-dextran (Sigma-Aldrich)

For transfection of 10ø cm dishes, 10 µg of DNA and 18 µl of DEAE-dextran were diluted in 1.5 ml of complete medium, and incubated at room temperature for 20 minutes. Cells were washed twice with PBS and incubated with the DNA-DEAE-dextran mixture for 90 minutes, at 37ºC and 5% CO_2. During incubation, the dishes were shaken every 15 minutes. After 90 minutes, the DNA-DEAE-dextran mixture was removed and 10 ml of complete medium supplemented with 10 µl of chloroquine were added to the dishes for 3 hours. Lastly, the cells were washed 3 times with PBS and incubated with fresh medium for 24/48 hours. To control the level of transfection, one coverslip was added to the dishes before seeding and prepared for immunofluorescence before cell lysis and collection.

2.4.2.3. Lipofectamine® 3000 (ThermoFisher Scientific)

Transfection protocols for lipofectamine were optimized for DNA and siRNA following the manufacturer's protocol, and scaled up or down as necessary. For DNA transfection in a 6ø cm dish, one tube was prepared with 16.5 µl of lipofectamine diluted in 250 µl of Opti-MEM medium, and another with 11 µg of DNA and 22 µl of P3000 reagent in 250 µl of Opti-MEM medium, and mixed well. The DNA-P3000 mix was added to the diluted lipofectamine and incubated for 5 minutes. Lastly, the DNA-lipid mixture was added to the previously seeded cells and incubated for 24/48 hours. For silencing experiments (Table 2.7), 166

pmol or 332 pmol of siRNA was used instead of DNA, the P3000 reagent was excluded, and the cells were incubated for 72 hours.

Table 2.7 – siRNA pools (Dharmacon, GE Healthcare)

Gene	Sequence
siGENOME non-targeting pool D-001206	5’ UAAGGCUAUGAAGAGAUAC 3’ 5’ AUGUAUUGGCCUGUAUUAG 3’ 5’ AUGAACGUGAAUUGCUCAA 3’ 5’ UGGUUUACAUGUCGACUAA 3’
SiGENOME MIRO1 pool M-010365	5’ GAACUCAACUUCUUUCAGA 3’ 5’ GAACCAGUAUACAGAAAUA 3’ 5’ GAACAUAUCAGAGCUCUUU 3’ 5’ CAGAAUACCUUGCUUAAUC 3’
ON-TARGETplus MIRO1 pool L-010365	5’ GCUUAAUCGUAGCUGCAAA 3’ 5’ CCAGAGAGGGAGACACGAA 3’ 5’ GCAAUUAGCAGAGGCGUUA 3’ 5’ UGUGGAGUGUUCAGCGAAA 3’

2.4.2.4. Microporation

Human and mouse fibroblasts were transfected using the Neon® Transfection System (ThermoFisher Scientific) following the manufacturer’s protocol. In short, cells dishes at 70-90% confluency were washed once with PBS and trypsinized using TrypLE Express as above. Trypsinized cells were resuspended in normal medium without antibiotics, and counted to determine cell density. The required amount of cells was centrifuged for 3 minutes at 1000 rpm and the pellet washed with PBS. The cells were once again centrifuged and carefully resuspended in Buffer R. For each condition, the required number of cells was pre-mixed with the plasmid of interest and microporated using the 10 or 100 µl Neon tip. Microporated cells were immediately seeded into plates with pre-warmed media without antibiotics and incubated for 24/48 hours.

For each cell line, an optimization protocol was performed to select the most effective conditions (pulse voltage, pulse width, and pulse number). The following conditions were used:

- C109, ΔPEX5, ΔPEX14 and TRAK1 patient fibroblasts: 1700 v, 20 ms, 1 pulse
- ΔPEX19 patient fibroblasts: 850 v, 30 ms, 2 pulse

- MEF MIRO1 +/+ and -/-: 1350 v, 30 ms, 1 pulse

Cell number and plasmid concentration was optimized for each experimental set up, taking into consideration the dish/well size and time of incubation after transfection.

2.4.3. Treatments

To analyse the effects of microtubule depolymerisation, cells were treated 24 hours after transfection with 10 µM of nocodazole, and incubated for 1 or 4 hours before being fixed. Control cells were incubated with the same volume of DMSO as that used to dissolve nocodazole (maximum 0.1% v/v).

To analyse the effects of calcium concentration on peroxisome motility, cells were treated with the calcium ionophore calcimycin (A23187). Prior to live-cell imaging, cells were treated with 10 µM of calcimycin and incubated for 10 minutes. Control cells were incubated with the same volume of DMSO as that used to dissolve nocodazole (maximum 0.1% v/v).

2.5. Immunofluorescence (IMF)

Cells grown on glass coverslips were processed for IMF 24/48 hours after seeding or transfection, and 72h after silencing. Cells were routinely fixed for 20 minutes with 4% paraformaldehyde (PFA), permeabilized with 0.2% triton X-100 for 10 minutes and blocked with 1% BSA for 10 minutes. To visualise the microtubule network, cells were fixed for 10 minutes with 4% PFA followed by 5 minutes with ice-cold methanol. In conditions where the protein of interest was extracted from the peroxisomal membrane by triton X-100, cells were permeabilized using a digitonin solution for 5 minutes. After blocking, cells were incubated with the primary antibody for 1 hour in a humid chamber (Table 2.8). This step was repeated for the secondary antibody, protected from light. Coverslips were washed with ddH_2O to remove PBS and mounted with Mowiol medium on glass slides. All immunofluorescence steps were performed at room temperature and cells were washed three times with PBS between each individual step.

Table 2.8 – Primary and secondary antibodies.

Antibodies	Type	Dilution		Source
		IMF	WB	
ACBD5 (HPA012145)	mc ms	1:100	1:250	Sigma-Aldrich, Schnelldorf, Germany
ATP synthase	mc ms	-	1:1000	Abcam, Cambridge, England
BCL2 (PSI-3335)	mc rb	1:100	1:1000	ProSci, San Diego, USA
CATALASE	pc ms	1:200	-	Abcam, Cambridge, England
CYCLOPHILLIN	pc rb	-	1:1000	Abcam, Cambridge, England
FLAG	mc ms	1:500	-	Sigma-Aldrich, Schnelldorf, Germany
FLAG	pc rb	1:750	1:1000	Sigma-Aldrich, Schnelldorf, Germany
GAPDH	mc rb	-	1:5000	ProSci, San Diego, USA
GFP (A11122)	pc rb	1:200	1:1000	Molecular Probes (ThermoFisher Scientific, Waltan, USA)
HA	mc ms	-	1:1000	BioLegend, San Diego, USA
MIRO1 (HPA010687)	pc rb	1:100	1:250	Sigma-Aldrich, Schnelldorf, Germany
MIRO1 (PSI-8027)	pc rb	1:100	1:1000	ProSci, San Diego, USA
Myc (Ab9106)	mc rb	1:200	1:1000	Abcam, Cambridge, England
Myc 9E10	mc ms	1:200	1:1000	Santa Cruz Biotechonology, Santa Cruz, USA
PEX14	pc rb	1:1400	1:4000	Kind gift from D.Crane Griffith University, Australia
PDI	mc ms	1:100	-	Thermo Scientific, Waltham, USA
PMP70	mc ms	1:500	1:5000	Sigma-Aldrich, Schnelldorf, Germany
TOM20 (612278)	mc ms	1:200	-	BD Transduction Laboratories, San Diego, USA
γ-TUBULIN	mc ms	1:100	-	Sigma-Aldrich, Schnelldorf, Germany
AlexaFluor 488 IgG	dk anti-rb	1:400	-	Molecular Probes (ThermoFisher Scientific, Waltan, USA)
AlexaFluor 488 IgG	dk anti-ms	1:400	-	Molecular Probes (ThermoFisher Scientific, Waltan, USA)
AlexaFluor 594 IgG	dk anti-rb	1:1000	-	Molecular Probes (ThermoFisher Scientific, Waltan, USA)
AlexaFluor 594 IgG	dk anti-ms	1:1000	-	Molecular Probes (ThermoFisher Scientific, Waltan, USA)
TRITC IgG	dk anti-ms	1:100	-	Dianova, Hamburg, Germany
TRITC IgG	dk anti-rb	1:400	-	Dianova, Hamburg, Germany
HRP IgG	gt anti-ms	-	1:5000	Bio-Rad, Munich, Germany
HRP IgG	gt anti-rb	-	1:5000	Bio-Rad, Munich, Germany
Hoechst dye	-	1:2000	-	Polysciences, Inc., Eppelheim, Germany

Abbreviations: IMF, immunofluorescence; WB, western blot; mc, monoclonal; pc, polyclonal; ms, mouse; rb, rabbit; gt, goat; dk, donkey; HRP, horseradish peroxidase.

2.6. Microscopy

2.6.1. Epifluorescence and confocal microscopy

Routine cell imaging was performed using an Olympus IX81 microscope equipped with an UPlanSApo 100x/1.40 oil objective (Olympus Optical, Hamburg, Germany). Digital images were taken with a CoolSNAP HQ2 CCD and adjusted for contrast and brightness using the Olympus Soft Imaging Viewer software (Olympus Soft Imaging Solutions GmbH) and MetaMorph 7 (Molecular Devices, USA).

Confocal images were obtained using a Zeiss LSM 510 inverted microscope equipped with a Plan Apochromat 63x/1.4 NA (oil/dic) objective (Carl Zeiss, Oberkochen, Germany), using the Argon 488nm and He 543nm laser lines. Digital images were adjusted for contrast and brightness using the Zeiss LSM Image Browser software (Carl Zeiss MircroImaging GmbH).

Live-cell imaging data was collected using an Olympus IX81 microscope equipped with a Yokogawa CSUX1 spinning disk head, CoolSNAP HQ2 CCD camera, 60x/1.35 oil objective, and outfitted with a controlled temperature chamber and objective warmer. Digital images were taken and processed using VisiView software (Visitron Systems, Germany).

2.6.2. Live-cell imaging

For live-cell imaging, COS-7 cells and human fibroblasts were plated in 3,5ø cm glass bottom dishes (Cellvis, USA and MatTek, USA). Prior to image acquisition, a controlled-temperature chamber was set-up on the microscope stage at 37ºC, as well as an objective warmer. During image acquisition, cells were kept at 37ºC and in CO_2–independent medium (HEPES buffered). For COS-7 cells, 500 stacks of 5 planes (0.5 µm thickness, 100ms exposure) were taken in a continuous stream. For human fibroblasts, 250 stacks of 9 planes (0.5 µm thickness, 100ms exposure) were taken in a continuous stream. All conditions and laser intensities were kept between experiments. For each condition analysed, a representative cell was selected and the acquired images were converted into a movie at 10x the original speed. Cells that moved during

the acquision process were removed from the datasets as these would affect the peroxisome motility measurements.

2.7. Protein assays

2.7.1. Cell lysis for protein assays

Cell lysates were prepared for silencing experiments and immunoprecipitations. Routinely, cells were transfected in 6ø cm dishes and collected after 48/72 hours. All lysis steps were performed at 4ºC or on ice, and all buffers were prepared fresh. For lysis, cells were washed with PBS, and 0.1-1 ml of lysis buffer was added to the plates. To remove all cells, a scraper was used and the cells were collected in an eppendorf tube. To improve lysis efficiency, cells were incubated in a rotating shaker for 15 minutes. Lysed cells were centrifuged at 15,000 g for 15 minutes to remove debris and the supernatant was kept. Protein concentration was determined by Bradford assay (Bradford, 1976).

2.7.2. Co-immunoprecipitation

GFP, Myc or FLAG-tagged proteins and HA-tagged PEX19 were expressed in COS-7 cells. After 48 hours, cells were washed with PBS and incubated with 5 ml of DSP cross-linker solution for 30 minutes, followed by quenching for 10 minutes with 100 mM Tris (pH 7.4). After crosslinking, cells were lysed as described above and the supernatant was mixed with GFP-TRAP (ChromoTek) or Myc/FLAG-antibody coupled agarose beads, and incubated for 2 hours at 4ºC. Beads were subsequently washed extensively with lysis buffer by quick centrifugations at 12,000 g and by incubating in a rotating shaker for 15 minutes at 4ºC. Bound protein was eluted with Laemmli buffer (GFP-TRAP) or 50 mM NaOH (agarose beads), and the eluted protein was denatured in Laemmli buffer for 10 minutes at 95ºC. Samples of lysate supernatant (before incubation with beads) were kept as “input”.

The cross-linker DSP (dithiobis (succinimidyl propionate)) was used for PEX19 interaction analysis due to the transient nature of the PEX19-TA protein interaction. This cross-linker was selected due to its short spacer (12.0 Å) and

cleavability. DSP has two identical reactive groups (activated esters) at each end of an 8-carbon spacer. These groups react with primary amines of proteins that are in very close proximity. The spacer is cleavable and the cross-link can be removed by reducing agents as those contained in SDS loading buffer.

2.7.3. Subcellular fractionation (performed by Markus Islinger)

Peroxisome purification from rat liver was performed as described (Islinger et al., 2012a). In brief, liver tissue was homogenized in homogenization buffer (HB; 250 mM sucrose, 5 mM MOPS, 1 mM EDTA, 2 mM PMSF, 1 mM DTT, 1 mM ε-aminocaproic acid, 0.1% ethanol, pH 7.4) using an ice-cooled Potter-Elvehjem tissue grinder (1 stroke/120 s). All further separation steps were performed at 4°C. The homogenate was cleared from cell debris and nuclei in an initial centrifugation step at 600 g_{av}, 10 min. The resulting pellet was re-homogenized and re-centrifuged applying the same conditions; both supernatants were pooled and comprise the initial post nuclear supernatant (PNS). Subsequently, PNS was centrifuged at 1,900 g_{av}, 15 min to yield the pellet of heavy mitochondria (HM). The resulting supernatant was again centrifuged at 25,500 g_{av}, 20 min resulting in the light mitochondrial pellet (LM). The corresponding supernatant was centrifuged an additional time at 100,000 g_{av}, 30 min to separate the microsomal pellet (MIC) from cytosol (CYT). To increase purity of the fractions, each pellet recovered was washed in 5 ml HB/g liver tissue and centrifuged using the same parameters. Highly purified peroxisomes were obtained from LM applying a sigmoidal Optiprep-gradient from 1.26 – 1.12 g/ml in a vertical type rotor at an integrated force of 1,256 $\times$ 10^6 g min. In such a gradient highly purified peroxisomes form a distinct band at 1.20 g/ml.

2.7.4. Electrophoresis and Immunoblotting

Standard 1D-SDS PolyAcrylamide Gel-Electrophoresis (SDS-PAGE) was performed with 10-12.5% separating and 4% stacking gels (Table 2.9). To mark protein size a pre-stained molecular weight marker (Precision Plus) was used and the sample running front was visualized by bromophenol blue added to the

loading buffer. Gels were conducted for 30 minutes at 80 V until the proteins entered the separating gel, and at 130 V for approximately 90 minutes, in chambers containing SDS running buffer.

Protein transfer to nitrocellulose membranes was performed by semi-dry western blotting for 60 minutes at 14 V. After protein transfer, membranes were blocked with 5% low fat powdered milk in TBS-T for 1 hour. Membranes were incubated with the primary antibody diluted in TBS-T, overnight at 4°C on a shaker. After incubation, membranes were washed three times for 10 minutes with TBS-T. Incubation with the secondary antibody was performed for 90 minutes at room temperature, after which membranes were washed three times for 10 minutes with TBS-T. For protein detection, membranes were incubated for 2 minutes with ECL and exposed to photographic film for 1 to 10 minutes in a light protected environment, and developed using a OPTIMAX film processor.

Table 2.9 – Recipe for acrylamide gels

	Separating Gel		**Stacking Gel**
	10%	12.5%	4%
30% Polyacrylamide	3.33 ml	4.17 ml	0.83 ml
2 M Tris pH 8.8	1.86 ml	1.86 ml	-
1 M Tris pH 6.8	-	-	0.63 ml
20% SDS (0.1%)	50 µl	50 µl	25 µl
dH_2O	4.73 ml	3.89 ml	3.43 ml
10% APS	30 µl	30 µl	40 µl
TEMED	5 µl	5 µl	5 µl
Total volume	10 ml	10 ml	5 ml

2.8. Computational analysis

2.8.1. Bioinformatics

Data on human TA proteins was sourced from the literature. SNARE proteins were omitted as they have been previously shown to differ significantly from other ER TA proteins (Kalbfleisch et al., 2007). Protein sequences were obtained from the NCBI database (www.ncbi.nlm.nih.gov), all isoforms were analysed and those that lacked a C-terminal TMD were removed. Yeast TA

proteins were sourced from literature and by homology with human proteins. For each protein, the TMD and tail were predicted using the TMHMM server v. 2.0 (Krogh et al., 2001). When no TMD was predicted but the protein had been characterized as a TA protein, the TMPred server (www.ch.embnet.org) was used, with a threshold score of 1500. As a measure for hydrophobicity, the Grand Average of Hydropathicity (GRAVY) of membrane spanning helices was calculated according to (Kyte and Doolittle, 1982), using the ProtParam server (Gasteiger et al., 2005) from ExPASy. Tail charge was calculated using the Protein Calculator v3.4 (Putnam Lab at The Scripps Research Institute, La Jolla, CA, USA), at pH7.0. PEX19-binding sites were analysed using the BLOCKS algorithm found at the PeroxisomeDB 2.0 (Schlüter et al., 2010). It should be noted that, due to the low number of know mPTS sequences, the reliability of the PEX19 predictor is low and this tool should be used with caution.

2.8.2. TA protein classifier (performed by Doug McNeall)

For the support vector machine (SVM) classifier (Cortes and Vapnik, 1995), we trained a SVM classifier with the [protein data] using the SVM application in package e1071 (Meyer et al., 2014), of the R statistical programming environment [R Core team, 2014] utilizing the LIBSVM library of Chang et al. (Chang and Lin, 2011). The SVM takes the training set of [Tail Charge, GRAVY and location in cell], and builds a statistical model to predict the probability of [location in cell], given any combination of [Tail Charge, GRAVY]. Initially, we restrict the training data to three unique classes, corresponding to [location in cell] – mitochondria (MITO), peroxisomes (PO) and endoplasmic reticulum (ER). This was used to calculate the targeting probability of a set of predicted human TA proteins previously published (Kalbfleisch et al., 2007). A fourth class – MITO and PO – was later added to calculate protein localisation probabilities.

2.8.3. Peroxisome motility measurements (performed with Jeremy Metz)

Peroxisomes were automatically detected and tracked using a customised in-house algorithm. Briefly, each image was filtered using a scale-space Laplace

of Gaussian filtering approach (Lindeberg, 1998, 2013) over scales corresponding to the size range of peroxisomes. After filtering, a threshold was determined using the median absolute deviation as a robust estimator of the background level (Murtagh and Starck, 2000), and applied to the filter response to determine peroxisome positions. Once detected, peroxisomes were tracked using a global optimization subroutine (using a modified version of the Jonker-Volgenant algorithm (Jonker and Volgenant, 1987)). For each peroxisome, each individual displacement between frames was tracked, giving instantaneous speeds. Tracking results were manually verified for accuracy. Whole cell peroxisome motility is represented by cumulative distribution functions (CDF) created from the total number of tracked movements. In a CDF plot, each individual point of the curve represents a peroxisome movement (instantaneous speed). These movements are organized by growing speed, generating an overview of the whole cell motility. For example, to quickly know the percentage of movements up to 0.1 µm/s, a line parallel to the Y axes can be drawn and the the value at which it intersects the graph is the % of movements. CDF plots presented in the results represent the total number of movements of all cells analysed for each group. Trajectories for the tracked peroxisomes were analysed by splitting their instantaneous speeds into two groups, using a cut-off for linear motion speed of 0.24 µm/s (Bonekamp et al., 2012). The relative populations of the two groups of peroxisome speeds was used as an indication of the amount of linear motion for each dataset, and compared against all trajectories to obtain a percentage of microtubule-dependent motility per cell.

2.8.4. Quantification of peroxisome number

The number of peroxisomes per cell was obtained from the motility analysis output, and determined by the detected peroxisomes from the first stack of each analysed cell.

2.8.5. Peroxisome elongation measurements

Peroxisome elongation lengths were obtained from live-cell imaging data and manually measured using MetaMorph 7. Each observed elongation was

measured at the longest point of extension. Kymographs were generated using ImageJ.

2.9. Statistical analysis

For the analysis of GRAVY, charge, tail length and PEX19 binding, scatter plots were created with GraphPad Prism 5 (GraphPad software Inc., USA). A one-way ANOVA with post hoc Tukey test was used to determine statistical differences between groups. *p<0.05, **p<0.01, ***p<0.001.

For quantitative analysis of the effect of MIRO1 expression on peroxisome distribution, motility and number, at least 3 independent experiments were carried out. Statistical analyses were performed using Microsoft Excel and GraphPad Prism 5 software. Data are presented as means ± SEM. Two-tailed unpaired t-tests and one-way ANOVA with post hoc Tukey tests were used to determine statistical differences against control values. * p<0.05, ** p<0.01, *** p<0.001.

Chapter 3 – Results

Predicting the targeting of tail-anchored proteins to subcellular compartments in mammalian cells

3.1. Introduction

TA proteins are a set of topologically grouped membrane proteins that possess a single TMD and a short tail at the C-terminus (Borgese et al., 2003). The TMD anchors the protein to the cytosolic side of several organelles, and allows the functional domains to exert their function in a semi-compartmentalized manner. These proteins can be targeted to mitochondria, peroxisomes, ER and intracellular compartments that are connected to the secretory pathway (Borgese et al., 2007), and are known to mediate essential biochemical processes such as protein import, apoptosis, signal transduction and antiviral signalling (Wattenberg and Lithgow, 2001). Furthermore, several TA proteins have a promiscuous targeting that allows them to go to more than one cellular membrane, meaning they are prone to affect several organelles when mutated (Schrader et al., 2014).

Due to the proximity of the TMD to the C-terminus, this domain can only be recognised by cytosolic chaperones after leaving the ribosome, leading to the post-translational insertion of these proteins (Borgese and Fasana, 2011; Kutay et al., 1993). As a result, specific sorting machineries are required to recognize and target TA proteins. This is the case for the GET/TRC40 pathway (yeast and mammalian, respectively), which has been identified and extensively characterised in recent years (reviewed in Hegde and Keenan, 2011), and is responsible for the targeting and insertion of several ER TA proteins. In addition, some studies have proposed a role for PEX19 and PEX3 in the sorting and insertion of the peroxisomal TA protein Pex15/PEX26 (yeast and mammalian, respectively) (Chen et al., 2014a; Halbach et al., 2006; Yagita et al., 2013). Lastly, less is known about sorting and insertion of mitochondrial TA proteins, with conflicting reports exploring the role of the TOM complex and the existence of an unassisted membrane insertion (Bellot et al., 2007; Kemper et al., 2008; Setoguchi et al., 2006), leaving open the possibility of an as yet unidentified molecular pathway.

Targeting of TA proteins to cellular membranes has been strongly debated due to the absence of a consensus targeting signal (Beilharz et al., 2003; Borgese and Fasana, 2011; Marty et al., 2014). Several biochemical parameters, such as the TMD hydrophobicity and the charge of the amino acids flanking the TMD have been proposed to play a role (Borgese et al., 2007), but little information is

available on how these and other factors contribute to organelle targeting, in particular to peroxisomes.

Peroxisomes are essential organelles for human health and development that play major roles in lipid and ROS metabolism. In the past few years, a growing number of proteins and functions have been identified in this organelle, showcasing their importance for cellular homeostasis (Smith and Aitchison, 2013). Amongst these proteins are several TA proteins shared between mitochondria and peroxisomes (e.g. FIS1, MFF, GDAP1 and MAVS) (Dixit et al., 2010; Gandre-Babbe and van der Bliek, 2008; Huber et al., 2013; Koch et al., 2005), some of which have been associated with new disorders with combined defects in both peroxisomes and mitochondria (Huber et al., 2013; Shamseldin et al., 2012).

In order to understand the targeting nuances of TA proteins, we started by re-assessing the localisation of several known TA proteins in mammalian cells and found additional proteins that are targeted to multiple organelles. With the identification of new peroxisomal TA proteins we were able, for the first time, to distinguish these from other TA proteins and analyse the importance of tail charge for membrane targeting and PEX19 binding. We have found that peroxisomal targeting requires a highly positive charged tail, which can counteract strongly hydrophobic TMDs, and that this is directly related to the affinity of the proteins to the peroxisomal chaperone PEX19. Finally, we developed a prediction tool that allowed us to test the targeting of TA proteins, leading to the characterization of new proteins and the identification of a previously unknown peroxisomal TA protein.

3.2. Results

3.2.1. TA proteins have promiscuous targeting in mammalian cells

In the past few years several TA proteins have been shown to target more than one organelle and exert similar but differently regulated functions depending on their target membrane (Dixit et al., 2010; Huber et al., 2013). This multiple targeting is not dependent on the expression of different isoforms from the same protein, indicating that the same sequence enables the targeting of a

protein to different membranes. To assess how extensive sharing of TA proteins between organelles is and to identify additional proteins at peroxisomes, we examined the localisation of a cohort of TA proteins (Figure 3.1). Expression of myc or GFP tagged proteins in COS-7 cells and colocalization with the peroxisomal marker PEX14 revealed that a subset of mitochondrial TA proteins had the ability to target both mitochondria and peroxisomes (Figure 3.1, Table 3.1). These included the anti-apoptotic proteins BCL-XL and BCL2, the motor protein-adaptors MIRO1 and MIRO2, and OMP25 (Figure 3.1A, B). BCL2 and MIRO2 were additionally found at the ER, which had already been reported for BCL2 (Krajewski et al., 1993). Other members of the BCL2 family, the pro-apoptotic proteins BAK and BAX, were only found at mitochondria when expressed in COS-7 cells (Figure 3.1C), and the ER TA proteins SEC61β, VAPB and FALDH isoform 2 (FALDH-ER in this study) were exclusively targeted to the ER (Figure 3.1D). Additionally, ACBD5 and FALDH isoform 1 (FALDH-PO in this study) were targeted to peroxisomes (Figure 3.1E). Of note, these two proteins have been recently characterised as TA proteins by our group (data not shown), and add to the number of exclusively peroxisomal TA proteins. Interestingly, the two isoforms of FALDH expressed only differ in their C-terminal tail, pointing to a role of this sequence in the targeting to either peroxisomes or the ER (Figure 3.1D, E, Table 3.3) (Ashibe et al., 2007).

To confirm the targeting of some of the tested proteins, antibodies were purchased to analyse endogenous localisation by IMF and WB of rat liver cell fractions. Of these, only a few were able to recognize the target protein in the conditions tested. To confirm our triple localisation of BCL2, an antibody against BCL2 was tested in COS-7 and HepG2 cells. To our surprise, this antibody showed a strong peroxisomal staining, some cytosolic staining, and no clear mitochondrial or ER localisation (Figure 3.2A). When tested on cells expressing GPF-BCL2, the antibody partially co-localised with the expressed protein. Despite the lack of a complete co-localisation, the BCL2 antibody was only able to recognise mitochondria when GFP-BCL2 was expressed. To test if the antibody was correctly recognizing BCL2, we stained cells expressing the GFP-tagged protein and a clear co-localisation of both signals was observed (Figure 3.2B). Additionally, this antibody recognized a band of 26 kDa in the cytosolic and the highly purified peroxisomal fractions of rat liver, which is the predicted size for BCL2 (Figure 3.2C). This could indicate that this antibody has a high

affinity for a specific isoform of BCL2 that is present in the cytosol and at peroxisomes in these cells.

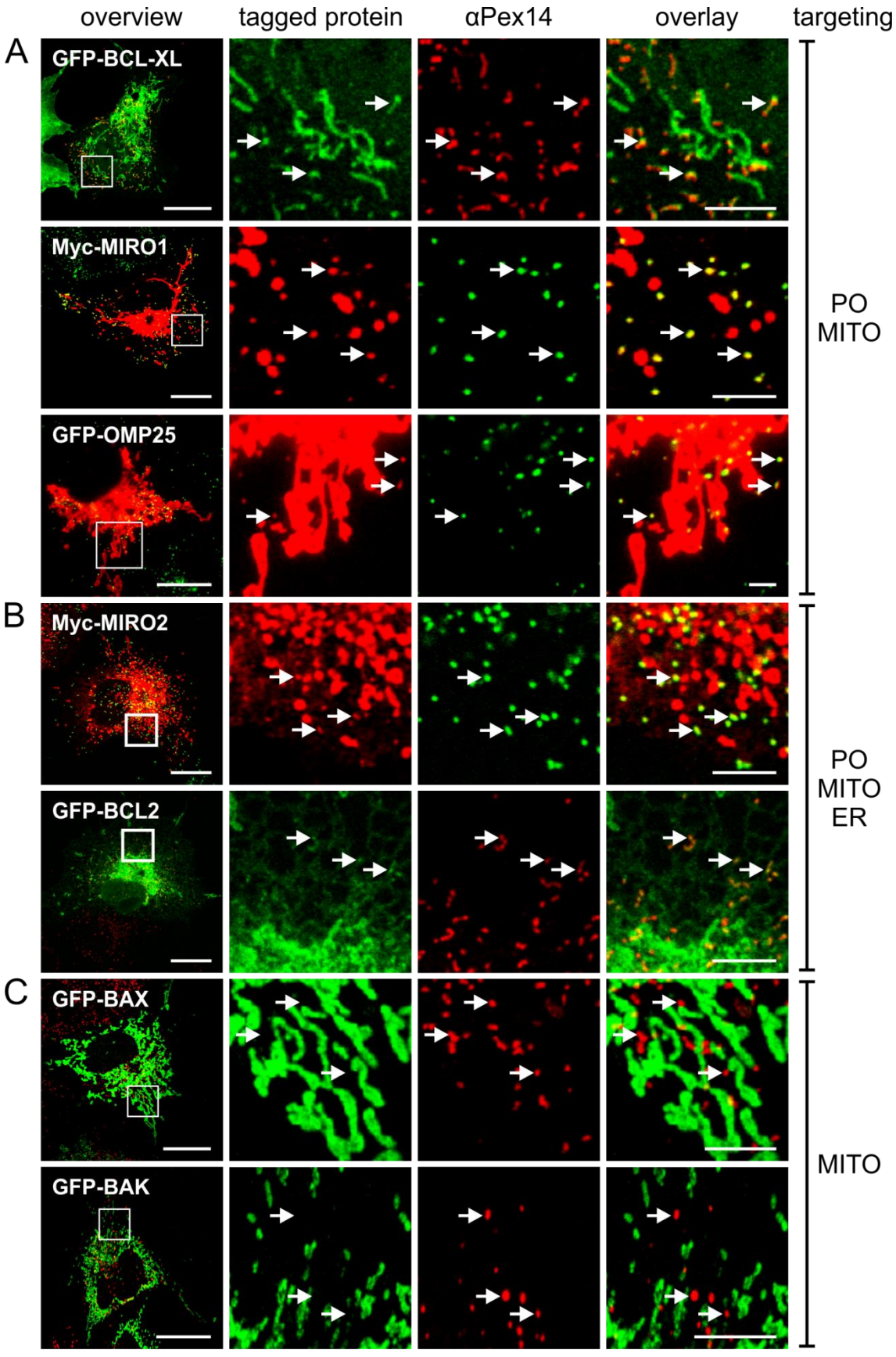

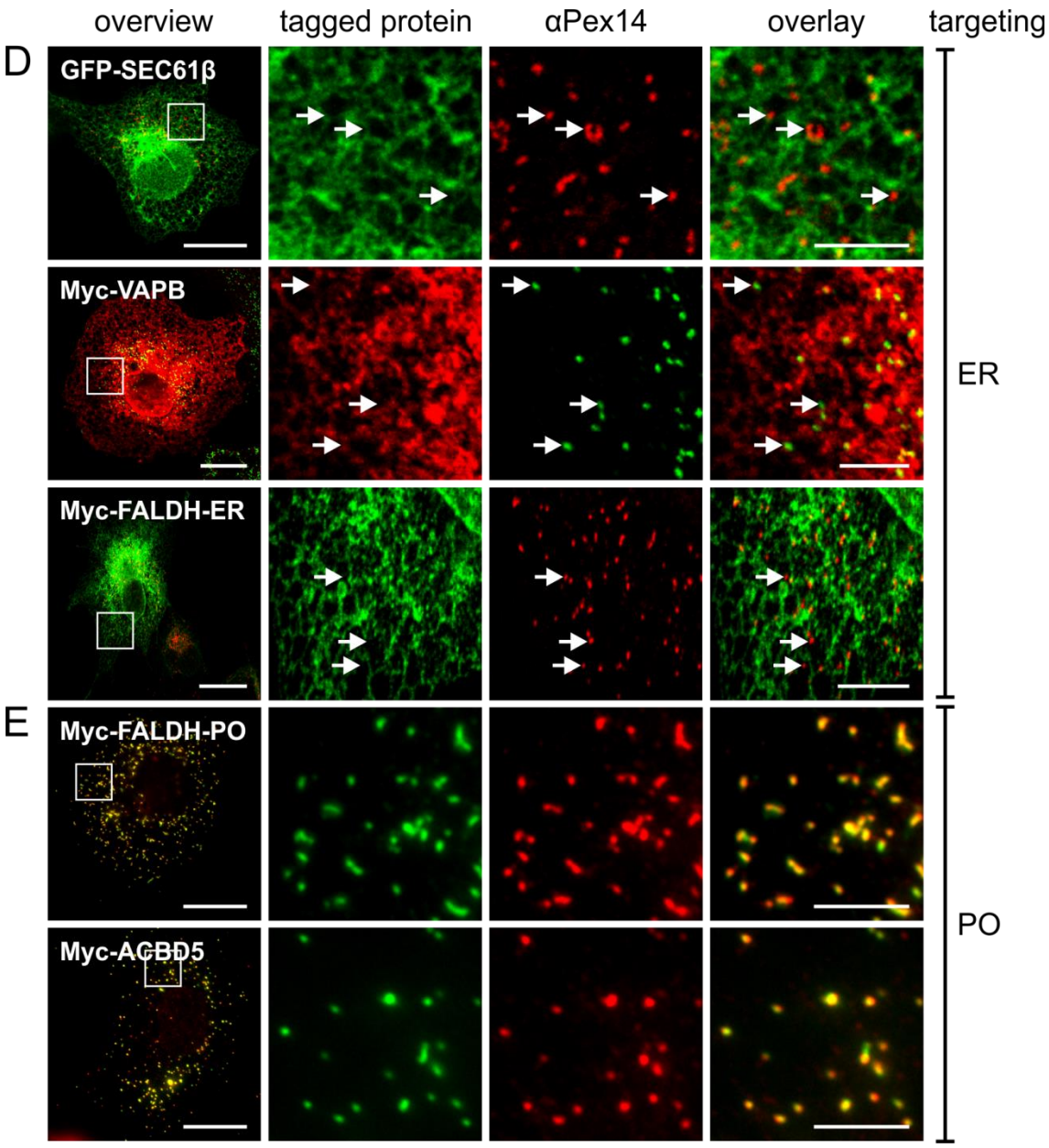

Fig. 3.1 – Targeting survey of TA proteins in mammalian cells. Tagged TA proteins were expressed in COS-7 and processed for immunofluorescence using antibodies against myc and PEX14 (peroxisomal marker). Several of the tested proteins showed targeting to two (A) or three (B) organelles. In particular, GFP-BCL-XL, Myc-MIRO1 and GFP-OMP25, which have been previously identified in mitochondria, were also localised to peroxisomes (A), and Myc-MIRO2 and GFP-BCL2 are additionally targeted to peroxisomes and the ER (B). Other proteins are exclusively targeted to (C) mitochondria (GFP-BAX, GFP-BAK), (D) ER (GFP-SEC61β, Myc-VAPB, Myc-FALDH-ER), and (E) peroxisomes (Myc-FALDH-PO, Myc-ACBD5). Arrows highlight regions of colocalization (A, B) or lack of colocalization (C, D) with peroxisomes. Higher magnification view of boxed regions (see overview) is shown. Bars, 20 µm (overview), 5 µm (overlay).

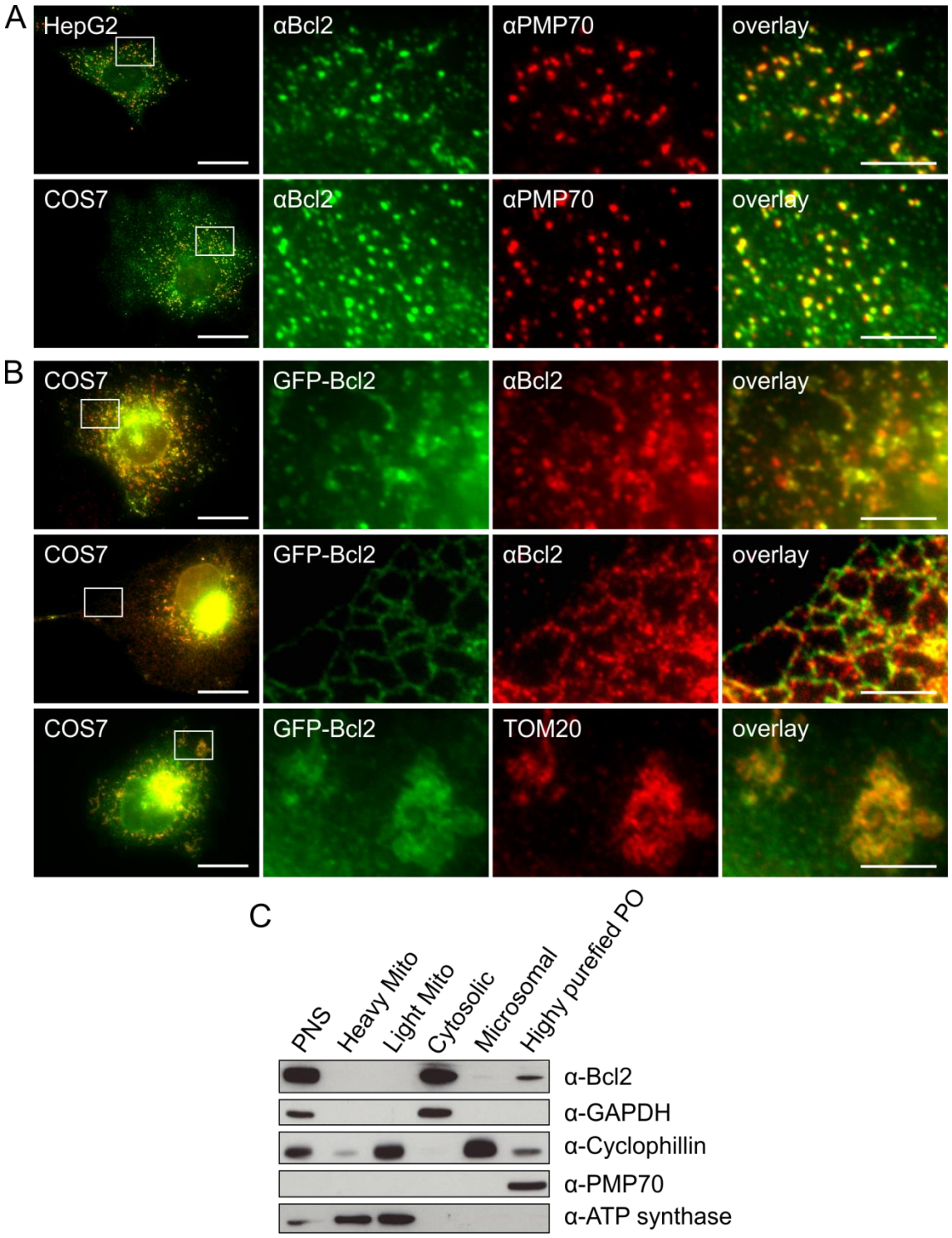

Fig. 3.2 – Endogenous BCL2 is peroxisomal and cytosolic. (A) Subcellular localization of endogenous BCL2 in HepG2 and COS-7 cells labelled with antibodies against BCL2 and PMP70 (peroxisomal marker). The recognised protein is present in peroxisomes and the cytosol. (B) GFP-BCL2 expressed in COS-7 cells and co-stained with antibodies against BCL2 and TOM20 (mitochondrial marker). The anti-BCL2 antibody partially recognises the expressed protein in these cells. Higher magnification view of boxed regions (see overview) is shown. Bars, 20 µm (overview), 5 µm (overlay). (C) Detection of endogenous BCL2 in subcellular fractions isolated from rat liver. Equal amounts of protein were separated by SDS-PAGE and immunoblotted using

anti-ATP synthase α (mitochondrial marker), anti-GAPDH (cytosolic marker), anti-Cyclophilin (ER marker) and anti-PMP70 (peroxisomal marker) antibodies. Note that BCL2 is associated with the cytosolic fraction and the highly purified peroxisomal fraction. PNS – post nuclear supernatant.

3.2.2. Targeting of TA proteins is strongly influenced by TMD hydrophobicity and tail charge

As previously mentioned, the targeting information for sorting TA proteins to each organelle is generally localised to the C-terminus, in particular to the TMD and flanking amino acids (Borgese and Fasana, 2011). Additionally, instead of consisting of a conserved amino acid sequence, TA protein targeting seems to rely on physicochemical parameters such as TMD hydrophobicity and sequence charge (Beilharz et al., 2003; Borgese et al., 2007). To characterise the parameters that affect TA protein targeting, we started by assembling a list of known proteins from the literature and our own experimental findings (Table 3.1). The final list contains a total of 50 proteins, distributed between the ER, mitochondria and peroxisomes, with some of them targeted to more than one organelle. Using this list, we searched the NCBI database for updated sequences and known isoforms. All isoforms were analysed for the presence of a TMD using TMHMM and TMpred, and the sequence and length of the TMD and tail of all proteins was annotated (Table 3.2). Any isoforms that did not fit the selected parameters were removed (see 2.8.1). Furthermore, we also selected the 10 and 20 amino acids before the TMD for analysis as these could potently affect chaperone binding (Table 3.3). For the obtained sequences we calculated the hydrophobicity of the TMD by using the grand average of hydropathy (GRAVY), and the tail charge (Table 3.4). Information on yeast TA proteins was also assembled in order to compare TMD hydrophobicity to human proteins (Table 3.5).

Table 3.1 – Human TA proteins used in this study.

Location	Name	Function	Reference
MITO	MAOA	Amine neurotransmitter metabolism	(Kalbfleisch et al., 2007)
	MAOB	Amine neurotransmitter metabolism	(Kalbfleisch et al., 2007)
	CYB5B	Electron carrier	(Kalbfleisch et al., 2007)
	BAX*	Apoptosis	(Kalbfleisch et al., 2007)
	MTX1	Protein import	(Kalbfleisch et al., 2007)
	TOMM5	Protein import	(Kato and Mihara, 2008)

Location	Name	Function	Reference
MITO	TOMM6	Protein import	(Kato and Mihara, 2008)
	TOMM7	Protein import	(Kalbfleisch et al., 2007)
	TOMM22	Protein import	(Saeki et al., 2000)
	BAK1*	Apoptosis	(Youle and Strasser, 2008)
	MCL1	Apoptosis	(Youle and Strasser, 2008)
	BCL2L13	Apoptosis	(Youle and Strasser, 2008)
	BCL2L10	Apoptosis	(Ke et al., 2001)
	BCL2L2	Apoptosis	(Youle and Strasser, 2008)
	HRK	Apoptosis	(Youle and Strasser, 2008)
	GDAP1L1	Unknown	(Niemann et al., 2014)
PO	ACBD5*	Acyl-CoA binding	(Islinger et al., 2007)
	PEX26	Protein important (probable)	(Halbach et al., 2006)
	FALDH*	Fatty aldehyde degradation	-
	FAR1	Plasmalogen biosynthesis	(Honsho et al., 2013)
MITO/PO	MIRO1*	Organelle motility	(Kalbfleisch et al., 2007)
	GDAP1	Organelle fission	(Kalbfleisch et al., 2007)
	FIS1	Organelle fission	(Kalbfleisch et al., 2007)
	MAVS	Antiviral signalling	(Kalbfleisch et al., 2007)
	MFF	Organelle fission	(Gandre-Babbe and van der Bliek, 2008)
	OMP25*	Unknown	(Kalbfleisch et al., 2007)
	BCL-XL*	Apoptosis	(Youle and Strasser, 2008)
MITO/PO/ER	MIRO2*	Organelle motility	(Kalbfleisch et al., 2007)
	BCL2*	Apoptosis	(Youle and Strasser, 2008)
MITO/ER	BNIP3	Apoptosis	(Yasuda et al., 1998)
ER	BIK	Apoptosis	(Youle and Strasser, 2008)
	CYB5A	Electron carrier	(Kalbfleisch et al., 2007)
	HMOX1	Heme catabolism	(Kalbfleisch et al., 2007)
	SEC61B*	Protein import	(Kalbfleisch et al., 2007)
	SEC61G	Protein import	(Kalbfleisch et al., 2007)
	FALDH*	Fatty aldehyde degradation	(Kalbfleisch et al., 2007)
	UBE2J1	Ubiquitination	(Lenk et al., 2002)
	UBE2J2	Ubiquitination	(Kalbfleisch et al., 2007)
	PTPN1	Cell signalling	(Kalbfleisch et al., 2007)
	VAPA	Vesicle trafficking (probable)	(Kalbfleisch et al., 2007)
	VAPB*	Vesicle trafficking (probable)	(Borgese et al., 2007)
	SERP1	Protein interaction/regulation	(Kalbfleisch et al., 2007)
	SLMAP	Unknown	(Kalbfleisch et al., 2007)
	PARP16	Unfolded protein response regulator	(Jwa and Chang, 2012)
	CDKAL1	tRNA processing	(Brambillasca et al., 2012)
	SMPD4	Sphingomyelin hydrolysis	(Krut et al., 2006)
	USP19	Deubiquitination	(Hassink et al., 2009)
	JPH1	ER/PM interaction	(Takeshima et al., 2000)
	JPH2	ER/PM interaction	(Takeshima et al., 2000)
	JPH3	ER/PM interaction	(Takeshima et al., 2000)
	JPH4	ER/PM interaction	(Takeshima et al., 2000)

Note: references refer to the literature mined to acquire a comprehensive list of human TA proteins. * Proteins tested in this study.

Table 3.2 – Identification of TA protein isoforms and TMD prediction.

Location	Name	Isoforms	Accession	Size (aa)	TMD	TMD length	Tail length	Predictor
MITO	MAOA	isoform1	NP_000231.1	527	504-519	16	8	TMPred
		isoform2	NP_001257387.1	394	371-386	16	8	
	MAOB	-	NP_000889.3	520	490-512	23	8	TMHMM
	CYB5B	-	NP_085056.2	150	122-144	23	6	TMHMM
	BAX	zeta	NP_001278360.1	114	88-110	23	4	TMHMM
		sigma	NP_620199.2	179	156-175	20	4	
		alpha	NP_620116.1	192	169-188	20	4	
		delta	NP_620118.1	143	120-139	20	4	
	MTX1	isoform 1	NP_002446.3	466	421-443	23	23	TMHMM
		isoform 2	NP_942584.2	435	390-412	23	23	
	TOMM5	isoform 1	NP_001001790.1	51	28-45	18	6	TMPred
	TOMM6	-	NP_001127965.1	74	44-62	19	12	TMPred
	TOMM7	-	NP_061932.1	55	21-36	16	19	TMHMM
	TOMM22	-	NP_064628.1	142	84-101	18	41	TMHMM
	BAK1	-	NP_001179.1	211	183-205	23	6	TMHMM
	MCL	isoform 1	NP_068779.1	350	327-349	23	1	TMHMM
		isoform 3	NP_001184249.1	197	174-196	23	1	
	BCL2L13	isoform a	NP_056182.2	485	460-482	23	3	TMHMM
		isoform b	NP_001257655.1	509	484-506	23	3	
		isoform c	NP_001257656.1	461	436-458	23	3	
		isoform e	NP_001257658.1	323	298-320	23	3	
		isoform g	NP_001257662.1	205	180-202	23	3	
	BCL2L10	-	NP_065129.1	204	183-200	18	4	TMHMM
	BCL2L2	-	NP_001186768.1	193	169-191	23	2	TMHMM
	HRK	-	NP_003797.1	91	65-87	23	4	TMHMM

Location	Name	Isoforms	Accession	Size (aa)	TMD	TMD length	Tail length	Predictor
MITO	GDAP1L1	isoform 1	NP_001243666.1	386	359-381	23	5	TMHMM
		isoform 2	NP_076939.3	367	340-362	23	5	
		isoform 3	NP_001243667.1	278	251-273	23	5	
		isoform 4	NP_001243668.1	309	282-304	23	5	
		isoform 5	NP_001243669.1	296	269-291	23	5	
PO	ACBD5	isoform 1	NP_663736.2	525	495-517	23	8	TMHMM
		isoform 2	NP_001035938.1	490	460-482	23	8	
		isoform 3	NP_001258441.1	523	493-515	23	8	
		isoform 4	NP_001288180.1	416	386-408	23	8	
		isoform 5	NP_001288183.1	348	318-340	23	8	
	PEX26	isoform a	NP_001121121.1	305	252-269	18	36	TMPred
	FALDH	isoform 1	NP_001026976.1	508	463-480	18	28	TMHMM
	FAR1	-	NP_115604.1	515	466-483	18	32	TMHMM
MITO/PO	MIRO1	isoform 1	NP_001028740.1	691	666-688	23	3	TMHMM
		isoform 2	NP_001028738.1	659	634-656	23	3	
		isoform 3	NP_060777.3	618	593-615	23	3	
		isoform 4	NP_001028739.2	491	466-488	23	3	
		isoform 5	NP_001275683.1	650	625-647	23	3	
		isoform 6	NP_001275684.1	597	572-594	23	3	
		isoform 7	NP_001275687.1	523	498-520	23	3	
	GDAP1	isoform a	NP_061845.2	358	319-340	22	18	TMPred
		isoform b	NP_001035808.1	290	251-272	22	18	
	FIS1	-	NP_057152.2	152	122-144	23	8	TMHMM
	MAVS	isoform 1	NP_065797.2	540	513-535	23	5	TMHMM
		isoform 2	NP_001193420.1	399	372-394	23	5	
	MFF	isoform a	NP_001263990.1	342	323-340	18	2	TMHMM
		isoform b	NP_001263991.1	291	272-289	18	2	

Location	Name	Isoforms	Accession	Size (aa)	TMD	TMD length	Tail length	Predictor
MITO/PO	MFF	isoform c	NP_001263992.1	243	224-241	18	2	TMHMM
		isoform d	NP_001263993.1	238	219-236	18	2	
		isoform e	NP_001263994.1	218	199-216	18	2	
		isoform f	NP_001263996.1	221	202-219	18	2	
		isoform g	NP_001263997.1	252	233-250	18	2	
	OMP25 SYNJ2BP	-	NP_060843.2	145	117-139	23	6	TMHMM
	BCL-XL	isoform 1	NP_612815.1	233	213-230	18	3	TMHMM
		isoform 2	NP_001182.1	170	150-167	18	3	
MITO/PO/ER	MIRO2	-	NP_620124.1	618	593-615	23	3	TMHMM
	Bcl2	alpha	NP_000624.2	239	214-236	23	3	TMHMM
MITO/ER	BNIP3	-	NP_004043.2	194	161-183	23	11	TMHMM
ER	BIK	-	NP_001188.1	160	136-158	23	2	TMHMM
	CYB5A	isoform 1	NP_683725.1	134	109-131	23	3	TMHMM
		isoform 3	NP_001177736.1	124	99-121	23	3	
	HMOX-1	-	NP_002124.1	288	265-287	23	1	TMHMM
	SEC61B	beta	NP_006799.1	96	68-90	23	6	TMHMM
	SEC61G	gamma	NP_001012474	68	36-58	23	10	TMHMM
	FALDH	isoform 2	NP_000373.1	485	464-482	19	3	TMHMM
	UBE2J1	-	NP_057105.2	318	286-308	23	10	TMHMM
	UBE2J2	isoform 1	NP_919296.1	275	243-265	23	10	TMHMM
		isoform 2	NP_477515.2	259	227-249	23	10	
		isoform 3	NP_919439.1	207	175-197	23	10	
	PTPN1	isoform 1	NP_002818.1	435	409-431	23	4	TMHMM
		isoform 2	NP_001265547.1	362	336-358	23	4	
	VAPA	isoform 1	NP_003565.4	294	271-293	23	1	TMHMM
		isoform 2	NP_919415.2	249	226-248	23	1	
	VAPB	isoform 1	NP_004729.1	243	220-242	23	1	TMHMM

Location	Name	Isoforms	Accession	Size (aa)	TMD	TMD length	Tail length	Predictor
ER	SERP1	-	NP_055260.1	66	37-59	23	7	TMHMM
	SLMAP	-	NP_009090.2	811	784-806	23	5	TMHMM
	PARP16	-	NP_060321.3	323	292-314	23	9	TMHMM
	CDKAL1	-	NP_060244.2	579	556-578	23	1	TMHMM
	SMPD4	isoform 1	NP_060221.2	837	799-821	23	16	TMHMM
		isoform 2	NP_060421.2	866	828-850	23	16	
		isoform 3	NP_001164554.1	764	726-748	23	16	
	USP19	isoform 1	NP_001186089.1	1419	1392-1414	23	5	TMHMM
		isoform 4	NP_006668.1	1318	1291-1313	23	5	
	JPH1	-	NP_065698.1	661	638-660	23	1	TMHMM
	JPH2	isoform 1	NP_065166.2	696	673-695	23	1	TMHMM
	JPH3	isoform 1	NP_065706.2	748	725-747	23	1	TMHMM
	JPH4	-	NP_001139500.1	628	608-624	4	17	TMPred

Table 3.3 – TMD, tail and pre-TMD sequences

Location	Name	Isoforms	TMD sequence	Tail sequence	-10 AA	-20 AA
MITO	MAOA	isoform1 isoform2	IIGFSTSVTALGFVLY	KYKLLPRS	NLPSVSGLLK	VEITHTFWERNLPSVSGLLK
	MAOB	-	PGLLRLIGLTTIFSATALGFLAH	KRGLLVRV	TFLERHLPSV	VDVPAQPITTTFLERHLPSV
	CYB5B	-	CWAYWILPIIGAVLLGFLYRYYT	SESKSS	DPSKNDTCKS	SDLKPESGSKDPSKNDTCKS
	BAX	zeta	GTPTWQTVTIFVAGVLTASLTIW	KKMG	GGWDGLLSYF	ERLLGWIQDQGGWDGLLSYF
		sigma	GGWTVTIFVAGVLTASLTIW	KKMG	ERLLGWIQDQ	IMGWTLDFLRERLLGWIQDQ
		alpha delta	TWQTVTIFVAGVLTASLTIW	KKMG	DGLLSYFGTP	LGWIQDQGGWDGLLSYFGTP
	MTX1	isoform 1 isoform 2	ILSVLAGLAAMVGYALLSGIVSI	QRATPARAPGTRTLGMAEEDEEE	EEEPYRRRNQ	QRQTPAGPETEEEPYRRRNQ
	TOMM5	isoform 1	IRNFLIYVALLRVTPFIL	KKLDSI	RKMREDVISS	APKLDPEEMKRKMREDVISS
	TOMM6	-	NLILNLGLFAAGVWLARNL	SDIDLMAPQPGV	FATDRNDFRR	VGDWLRGVYRFATDRNDFRR
	TOMM7	-	FAIRWGFIPLVIYLGF	KRGADPGMPEPTVLSLLWG	RLQQLFKGSQ	MVKLSKEAKQRLQQLFKGSQ
	TOMM22	-	ALWIGTTSFMILVLPVVF	ETEKLQMEQQQQLQQRQILLGPNTGLS GGMPGALPSLPGKI	AQKMYRFSRA	GATFDLSLFVAQKMYRFSRA
	BAK1	-	LGNGPILNVLVVLGVVLLGQFVV	RRFFKS	QRGGWVAALN	LHHCIARWIAQRGGWVAALN
	MCL1	isoform 1 isoform 3	GIRNVLLAFAGVAGVGAGLAYLI	R	EFFHVEDLEG	VKQRGWDGFVEFFHVEDLEG
	BCL2L13	isoform a isoform b isoform c isoform e isoform g	ILLFGGAAAVAILAVAIGVALAL	RKK	KPMPLSEGKS	KSRLSPAGEMKPMPLSEGKS
	BCL2L10	-	LVQAFLSCLLTTAFIYLW	TRLL	PFPLAFWRKQ	WDGFCHFFRTPFPLAFWRKQ
	BCL2L2	-	SVRTVLTGAVALGALVTVGAFFA	SK	ARRLREGNWA	ALYGDGALEEARRLREGNWA
	HRK	-	LPTYWPWLCAAAQVAALAAWLLG	RRNL	RSRRAPAPGA	HQRTMWRRRARSRRAPAPGA

Location	Name	Isoforms	TMD sequence	Tail sequence	-10 AA	-20 AA
MITO	GDAP1L1	isoform 1 isoform 2 isoform 3 isoform 4 isoform 5	SFFGASFLMGSLGGMGYFAYWYL	KKKYI	AFRLVKRKPP	TTLLSAVIPNAFRLVKRKPP
PO	ACBD5	isoform 1 isoform 2 isoform 3 isoform 4 isoform 5	SPGVLTFAIIWPFIAQWLVYLYY	QRRRRKLN	QRPSWWPFEM	TLQTAPQPTSQRPSWWPFEM
	PEX26	isoform a	FKKSLLAALILCLLVVRF	DPASPSSLHFLYKLAQLFRWIRKAAFSRLYQLRIRD	SAVSHFFSLP	LPMLVRQLWDSAVSHFFSLP
	FALDH	isoform 1	KLGLLLLTFLGIVAAVLV	KKYQAVLRRKALLIFLVVHRLRWSSKQR	FFLLKRFNKE	NSQSKVDWGKFFLLKRFNKE
	FAR1	-	IRYGFNTILVILIWRIFI	ARSQMARNIWYFVVSLCYKFLSYFRASSTMRY	ARKHLNKLRN	LNEEMSGLPAARKHLNKLRN
MITO/PO	MIRO1	isoform 1	WLRASFGATVFAVLGFAMYKALL	KQR	TQADLKSSTF	IFTAVLNRHVTQADLKSSTF
		isoform 2				
		isoform 3				LTTMAMYPHVTQADLKSSTF
		isoform 4				
		isoform 5				WVFLKTALHVTQADLKSSTF
		isoform 6				LTTMAMYPHVTQADLKSSTF
		isoform 7				WVFLKTALHVTQADLKSSTF
	GDAP1	isoform a isoform b	VLGTTLVVGLLAGVGYFAFMLF	RKRLGSMILAFRPRPNYF	FRVAKKRAPK	ILISAVLPTAFRVAKKRAPK
	FIS1	-	GLVGMAIVGGMALGVAGLAGLIG	LAVSKSKS	RLIDKAMKKD	PQNNQAKELERLIDKAMKKD
	MAVS	isoform 1 isoform 2	PGALWLQVAVTGVLVVTLLVVLY	RRRLH	EREVPCHRPS	PRPQADRKFQEREVPCHRPS

Location	Name	Isoforms	TMD sequence	Tail sequence	-10 AA	-20 AA
MITO/PO	MFF	isoform a isoform b isoform c isoform d isoform e isoform f isoform g	VMYSITVAFWLLNSWLWF	RR	ENKERAKREM	LNRRLQLLEEENKERAKREM
	OMP25	-	GIPIFMVLVPVFALTMVAAWAFM	RYRQQL	IGHRGEGDPS	QHRLQVQNGPIGHRGEGDPS
	BCL-XL	isoform 1 isoform 2	WFLTGMTVAGVVLLGSLF	SRK	SRKGQERFNR	ELYGNNAAAESRKGQERFNR
MITO/PO/ER	MIRO2	-	GLLGVVGAAVAAVLSFSLYRVLV	KSQ	ELHPSSFWLR	MAAFPHLVHAELHPSSFWLR
	Bcl2	alpha	WLSLKTLLSLALVGACITLGAYL	GHK	PSMRPLFDFS	GWDAFVELYGPSMRPLFDFS
MITO/ER	BNIP3	-	FLKVFLPSLLLSHLLAIGLGIYI	GRRLTTSTSTF	MKKGGIFSAE	ATLSMRNTSVMKKGGIFSAE
ER	BIK	-	VLLALLLLLALLLPLLSGGLHLL	LK	NPGSWVSCEQ	ENIMRFWRSPNPGSWVSCEQ
	CYB5A	isoform 1 isoform 3	WWTNWVIPAISAVAVALMYRLYM	AED	LITTIDSSSS	RPKLNKPPETLITTIDSSSS FIIGELHPETLITTIDSSSS
	HMOX-1	-	APLLRWVLTLSFLVATVAVGLYA	M	GKPPLNTRSQ	QDSAPVETPRGKPPLNTRSQ
	SEC61B	beta	VGPVPVLVMSLLFIASVFMLHIW	GKYTRS	FYTEDSPGLK	TSAGTGGMWRFYTEDSPGLK
	SEC61G	gamma	IAMATAIGFAIMGFIGFFVKLIH	IPINNIIVGG	TKPDRKEFQK	KDSIRLVKRCTKPDRKEFQK
	FALDH	isoform 2	LGLLLLTFLGIVAAVLVKA	EYY	FLLKRFNKEK	SQSKVDWGKFFLLKRFNKEK
	UBE2J1	-	GSAVLIVILTLALAALIFRRIYL	ANEYIFDFEL	QPRDNHTDHG	STSPDVIQGHQPRDNHTDHG
	UBE2J2	isoform 1 isoform 2 isoform 3	GLLGGALANLFVIVGFAAFAYTV	KYVLRSIAQE	AGLQQANRHH	GHAPGAVPNLAGLQQANRHH
	PTPN1	isoform 1 isoform 2	FLVNMCVATVLTAGAYLCYRFLF	NSNT	EDHALSYWKP	KGEPSLPEKDEDHALSYWKP

Location	Name	Isoforms	TMD sequence	Tail sequence	-10 AA	-20 AA
ER	VAPA	isoform 1 isoform 2	SPLPSLLVVIAAIFIGFFLGKFI	L	STASFRDNVT	VAHSDKPGSTSTASFRDNVT
	VAPB	isoform 1	LSTRLLALVVLFFIVGVIIGKIA	L	ALAPTGKEEG	KTVQSNSPISALAPTGKEEG
	SERP1	-	SVGPWLLALFIFVVCGSAIFQII	QSIRMGM	TSRNAPEEKA	NITQRGNVAKTSRNAPEEKA
	SLMAP	-	WPWMPMLAALVAVTAIVLYVPGL	ARASP	LLREKGNNKP	ELKQCKNNLKLLREKGNNKP
	PARP16	-	FTVMISLYLLLLLIVSVINSSAF	QHFWNRAKR	SQLSWFSSHW	SQKPPKSRASSQLSWFSSHW
	CDKAL1	-	CALRMSVGLALLGLLFAFFVKVY	N	VLPMPRLHQD	SQCDSASSRMVLPMPRLHQD
	SMPD4	isoform 1 isoform 2 isoform 3	VASLFCVGPLPCTLLLTLGYVLY	ASAMTLLTERGKLHQP	TLVSLLLAFF	LSLRFLGSYRTLVSLLLAFF
	USP19	isoform 1 isoform 4	YFVLGTVAALVALVLNVFYPLVS	QSRWR	PTTPDEGCLR	QDWVGPLPRGPTTPDEGCLR
	JPH1	-	NSIMIVLVMLLNIGLAILFVHFL	T	ALEKEANSGP	KNPASNDSCPALEKEANSGP
	JPH2	isoform 1	NTILICMVILLNIGLAILFVHLL	T	EAEVEVEEVP	KARKEAALAAEAEVEVEEVP
	JPH3	isoform 1	APILVVMVILLNIGVAILFINFF	I	GDELKSSTGS	PVALESDEENGDELKSSTGS
	JPH4	-	VVGAVALLDLSLAFLFS	QLLT	PAQPGAANPL	ELGEPAATERPAQPGAANPL

Table 3.4 – GRAVY and charge prediction

Location	Name	Isoforms	Tail length	TMD	Tail	-10 AA		-20 AA		Pex19 binding
				GRAVY	Charge	GRAVY	Charge	GRAVY	Charge	
MITO	MAOA	isoform1	8	1.706	2.9	0.46	0.9	-0.045	0.2	0.72
		isoform2	8							0.54
	MAOB	-	8	1.278	2.9	0.03	0.2	0.17	-0.8	0.39
	CYB5B	-	6	1.183	-0.1	-1.97	-0.1	-1.755	-0.1	0.22
	BAX	zeta	4	0.996	1.9	0.27	-1.1	-0.25	-2.1	0.22
		sigma	4	1.450	1.9	-0.77	-1.1	-0.045	-1.1	0.33
		alpha	4	1.280	1.9	0.17	-1.1	-0.175	-2.1	0.35
		delta	4							0.27
	MTX1	isoform 1	23	2.143	-3.1	-3.39	-0.1	-2.605	-0.1	0.39
		isoform 2	23							0.37
	TOMM5	isoform 1	6	1.578	0.9	-1.09	0.9	-1.245	-0.1	0.23
	TOMM6	-	12	1.211	-2.1	-1.73	0.9	-1.03	1.9	0.056
	TOMM7	-	19	1.650	-0.1	-0.97	1.9	-0.875	3.9	0.08
	TOMM22	-	41	2.067	-0.1	-1.02	2.9	0.18	1.9	0.75
	BAK1	-	6	1.991	2.9	-0.16	0.9	0.275	2.4	0.52
	MCL1	isoform 1	1	1.622	0.9	-0.4	-3.8	-0.495	-2.8	2.9
		isoform 3	1							1.7
	BCL2L13	isoform a	3	2.657	2.9	-1.08	0.9	-0.94	1.9	0.33
		isoform b	3							0.34
		isoform c	3							6.6
		isoform e	3							6.2
		isoform g	3							4
	BCL2L10	-	4	1.750	0.9	-0.48	1.9	-0.355	2.1	0.069
	BCL2L2	-	2	1.670	0.9	-1.44	1.9	-0.79	-1.1	0.8
	HRK	-	4	1.152	1.9	-1.25	2.9	-1.755	7.1	1.8

Location	Name	Isoforms	Tail length	TMD	Tail	-10 AA		-20 AA		Pex19 binding
				GRAVY	Charge	GRAVY	Charge	GRAVY	Charge	
MITO	GDAP1L1	isoform 1	5	0.904	2.9	-0.74	3.9	0.17	3.9	0.35
		isoform 2	5							0.33
		isoform 3	5							0.25
		isoform 4	5							0.28
		isoform 5	5							0.27
PO	ACBD5	isoform 1	8	1.226	4.9	-1.26	-0.1	-1.005	-0.1	0.3
		isoform 2	8							0.28
		isoform 3	8							0.3
		isoform 4	8							0.24
		isoform 5	8							0.2
	PEX26	isoform a	36	1.906	5.2	0.82	0.1	0.585	0.2	0.057
	FALDH	isoform 1	28	2.483	9.1	-0.33	1.9	-1.015	2.9	0.058
	FAR1	-	32	1.589	4.9	-1.76	4.1	-0.98	2.2	0.41
MITO/PO	MIRO1	isoform 1	3	1.304	1.9	-0.55	-0.1	0.195	1.2	0.14
		isoform 2	3							0.14
		isoform 3	3					0.03	0.1	0.13
		isoform 4	3							0.1
		isoform 5	3					0.32	1.1	0.14
		isoform 6	3					0.03	0.1	0.13
		isoform 7	3					0.32	1.1	0.11
	GDAP1	isoform a	18	2.064	4.9	-1.17	4.9	0.48	4.9	0.24
		isoform b	18							0.2
	FIS1	-	8	1.939	1.9	-1.12	1.9	-1.605	0.9	3.2
	MAVS	isoform 1	5	2.013	3.1	-1.65	0.1	-1.925	2.1	0.36
		isoform 2	5							0.27

Location	Name	Isoforms	Tail length	TMD	Tail	-10 AA		-20 AA		Pex19 binding
				GRAVY	Charge	GRAVY	Charge	GRAVY	Charge	
MITO/PO	MFF	isoform a	2	1.322	1.9	-2.71	0.9	-1.745	0.9	0.014
		isoform b	2							0.012
		isoform c	2							0.01
		isoform d	2							0.01
		isoform e	2							0.0093
		isoform f	2							0.0094
		isoform g	2							0.011
	OMP25	-	6	2.152	1.9	-1.38	-0.8	-1.475	0.4	0.28
	BCL-XL	isoform 1	3	1.822	1.9	-2.63	2.9	-1.64	0.9	3.4
		isoform 2	3							2.5
MITO/PO/ER	MIRO2	-	3	1.983	0.9	-0.49	0.2	0.26	0.6	0.98
	BCL2	alpha	3	1.613	1.1	-0.15	-0.1	0.055	-2.1	0.67
MITO/ER	BNIP3	-	11	1.874	1.9	-0.19	0.9	-0.06	1.9	0.058
ER	BIK	-	2	2.539	0.9	-0.83	-1.1	-0.92	-0.1	0.0055
	CYB5A	isoform 1	3	1.035	-2.1	0.47	-1.1	-0.815	0.9	3.6
		isoform 3	3					0.37	-2.8	3.3
	HMOX-1	-	1	1.683	-0.1	-1.67	1.9	-1.52	0.9	0.29
	SEC61B	beta	6	2.048	1.9	-0.91	-1.1	-0.71	-0.1	0.21
	SEC61G	gamma	10	1.900	-0.1	-2.62	1.9	-1.615	4.9	0.073
	FALDH	isoform 2	3	2.447	-1.1	-1	2.9	-1.035	3.9	0.14
	UBE2J1	-	10	2.043	-3.1	-2.76	-0.6	-1.67	-1.4	0.27
	UBE2J2	isoform 1	10	1.852	0.9	-1.44	1.4	-0.675	1.6	1.4
		isoform 2	10							1.3
		isoform 3	10							1.1
	PTPN1	isoform 1	4	1.570	-0.1	-1.31	-0.8	-1.6	-1.8	1.2
		isoform 2	4							1

Location	Name	Isoforms	Tail length	TMD	Tail	-10 AA		-20 AA		Pex19 binding
				GRAVY	Charge	GRAVY	Charge	GRAVY	Charge	
ER	VAPA	isoform 1	1	2.039	-0.1	-0.57	-0.1	-0.73	0.2	0.61
		isoform 2	1							0.52
	VAPB	isoform 1	1	2.274	-0.1	-0.66	-1.1	-0.675	-0.1	0.1
	SERP1	-	7	2.091	0.9	-1.84	-0.1	-1.395	1.9	0.0029
	SLMAP	-	5	1.674	0.9	-1.72	1.9	-1.64	3.9	1.5
	PARP16	-	9	2.152	3.1	-0.51	0.1	-1.235	3.1	0.078
	CDKAL1	-	1	1.839	-0.1	-0.42	0.2	-0.635	0.1	0.57
	SMPD4	isoform 1	16	1.739	1.2	2.53	-0.1	1.36	1.9	0.29
		isoform 2	16							0.3
		isoform 3	16							0.27
	USP19	isoform 1	5	1.983	1.9	-1.02	-1.1	-0.93	-1.1	1.3
		isoform 4	5							1.2
	JPH1	-	1	2.313	-0.1	-0.98	-1.1	-1.235	-1.1	2.9
	JPH2	isoform 1	1	2.400	-0.1	-0.47	-5.1	-0.385	-3.1	0.021
	JPH3	isoform 1	1	2.583	-0.1	-1.1	-1.1	-1.055	-5.1	0.5
	JPH4	-	17	2.182	-0.1	-0.3	-0.1	-0.665	-2.1	1.4

Table 3.5 – Yeast TA proteins

Location	Name	Accession	Tail length	TMD	TMD length	Predictor	TMD sequence	Tail sequence	GRAVY TMD	Tail Charge
MITO	FMP32	NP_116608.1	1	184-206	23	TMHMM	VMQWLIGVCTGTFALVLAYMRLL	T	1,583	-0,1
	TOM5	NP_015459.1	5	28-45	18	TMHMM	AAYVAAFLWVSPMIWHLV	KKQWK	1.550	2,9
	TOM6	NP_014688.1	7	32-54	23	TMHMM	LYTIALNGAFFVAGVAFIQSPLM	DMLAPQL	1.483	-1,1
	TOM7	NP_014329.1	15	20-45	26	TMPred	ILTLTHNVAHYGWIPFVLYLGWAHTS	NRPNFLNLLSPLPSV	0.623	0,9
	TOM22	NP_014268.1	33	98-119	22	TMPred	LAWTLTTTALLLGVPLSLSILA	EQQLIEMEKTFDLQSDA NNILAQGEKDAAATAN	1.691	-5,1
	GEM1	NP_009351.1	7	633-655	23	TMHMM	TALIFGSTVGFVALCSFTLMKLF	KSSKFSK	1.691	2,9
MITO/PO	FIS1	NP_012199.3	5	131-150	20	TMHMM	GVVVAGGVLAGAVAVASFFL	RNKRR	2.250	3,9
PO	PEX15	NP_014598.1	31	332-352	21	TMPred	VLNKNGLLLTGLLLLLCLKKY	KSLMAIFKHVPAAFHTV YPQIVGLLKLLASI	1.105	3,4
ER	HLJ1	NP_013884.1	1	206-223	18	TMHMM	LVLFIIFIVLPMIKDYLF	S	2.311	-0,1
	CSM4	NP_015124.1	2	132-154	23	TMHMM	VIAELNSLIIVFFISLVFLWVSI	EV	2.365	-1,1
	YBL100c	AAT93377.1	8	77-96	20	TMHMM	IAAVRANIIICACFFYLFCY	CSCDSYES	1.925	-2,1
	USE1	NP_011417.1	6	217-239	23	TMHMM	SYLFYITVFIFMILGLVFTFIII	QLFPAL	2.500	-0,1
	CYB5	NP_014288.3	3	98-117	20	TMHMM	GSGTLVVILAILMLGVAYYL	LNE	2.040	-1,1
	VPS64	NP_010486.3	5	579-599	21	TMPred	VSKGMLFGVVAISFGLVATAV	KQLPQ	1.838	0,9
	HMX1	NP_013306.2	7	288-310	23	TMHMM	RALHTVMLLVLSIIAIWVLYFLV	KSFLSIV	2.174	0,9
	SBH2	NP_010936.1	7	59-81	23	TMHMM	VDSLVVLFLSVGFIFSVIALHLL	TKFTHII	2.326	1,1
	SBH1	NP_011011.3	8	55-74	20	TMHMM	LVVLFLAVGFIFSVVALHVI	SKVAGKLF	2.850	1,9
	SSS1	NP_010371.1	5	53-75	23	TMHMM	AVGIGFIAVGIIGYAIKLIHIPI	RYVIV	1.948	0,9
	UBC6	NP_011026.3	1	231-249	19	TMHMM	SSMVYIGIAIFLFLVGLFM	K	2.295	0,9
	SCS2	NP_011046.3	1	226-243	18	TMPred	MGIFILVALLILVLGWFY	R	2.622	0,9
	SCS22	NP_009461.2	1	155-174	20	TMHMM	LSSRALLIITVIALLVGWIY	Y	1.980	-0,1

TMD hydrophobicity has been previously shown to correlate with TA protein targeting, particularly in yeast (Beilharz et al., 2003). In this system, ER proteins have highly hydrophobic TMDs (GRAVY > 1.75) in comparison with exclusively mitochondrial or peroxisomal proteins (Figure 3.3A). In humans, whereas a significant difference can still be found between ER and mitochondrial proteins, both sets show a much broader distribution of TMD hydrophobicity (Figure 3.3B, C). While this points to a role of TMD hydrophobicity in ER and mitochondrial protein targeting, no statistical differences were found between these groups and peroxisomes (Figure 3.3C). However, it should be noted that the number of analysed peroxisomal TA proteins is much lower than mitochondrial/ER proteins, and therefore small differences in TMD hydrophobicity might not be discernible.

Another factor which has been proposed to regulate protein targeting is the tail charge (Borgese et al., 2007). As shown in figure 3.3D, peroxisomal TA proteins have a significantly higher positive tail charge than those targeted to the ER, mitochondria, or those shared by peroxisomes and mitochondria. Moreover, no significant differences were found in tail charge between mitochondrial and ER proteins.

Other factors were also considered such as tail length, PEX19 binding, and charge and hydrophobicity of the residues prior to the TMD (Figure 3.3E-J). Although there was a significant difference between the mean peroxisomal tail length and that of other organelle specific TA proteins, a long tail does not seem to be a requirement for peroxisomal targeting, as shown by the case of ACBD5, which has a tail length comparable to the average of other groups. Additionally, as we now identified four TA proteins targeted to peroxisomes, we decided to look at the targeting prediction for binding of the peroxisomal chaperone PEX19 (Schlüter et al., 2010). As a control, all the proteins in the list were also tested in the predictor. As shown in figure 3.3F, not all peroxisomal TA proteins have a predicted PEX19 binding site, and several non-peroxisomal proteins are predicted to have PEX19 binding sites, suggesting that the use of these tools alone is not sufficient to predict targeting. Finally, we analysed the residues prior to the TMD for both charge and hydrophobicity, but no significant differences were found between any of the groups (Figure 3.4G-J).

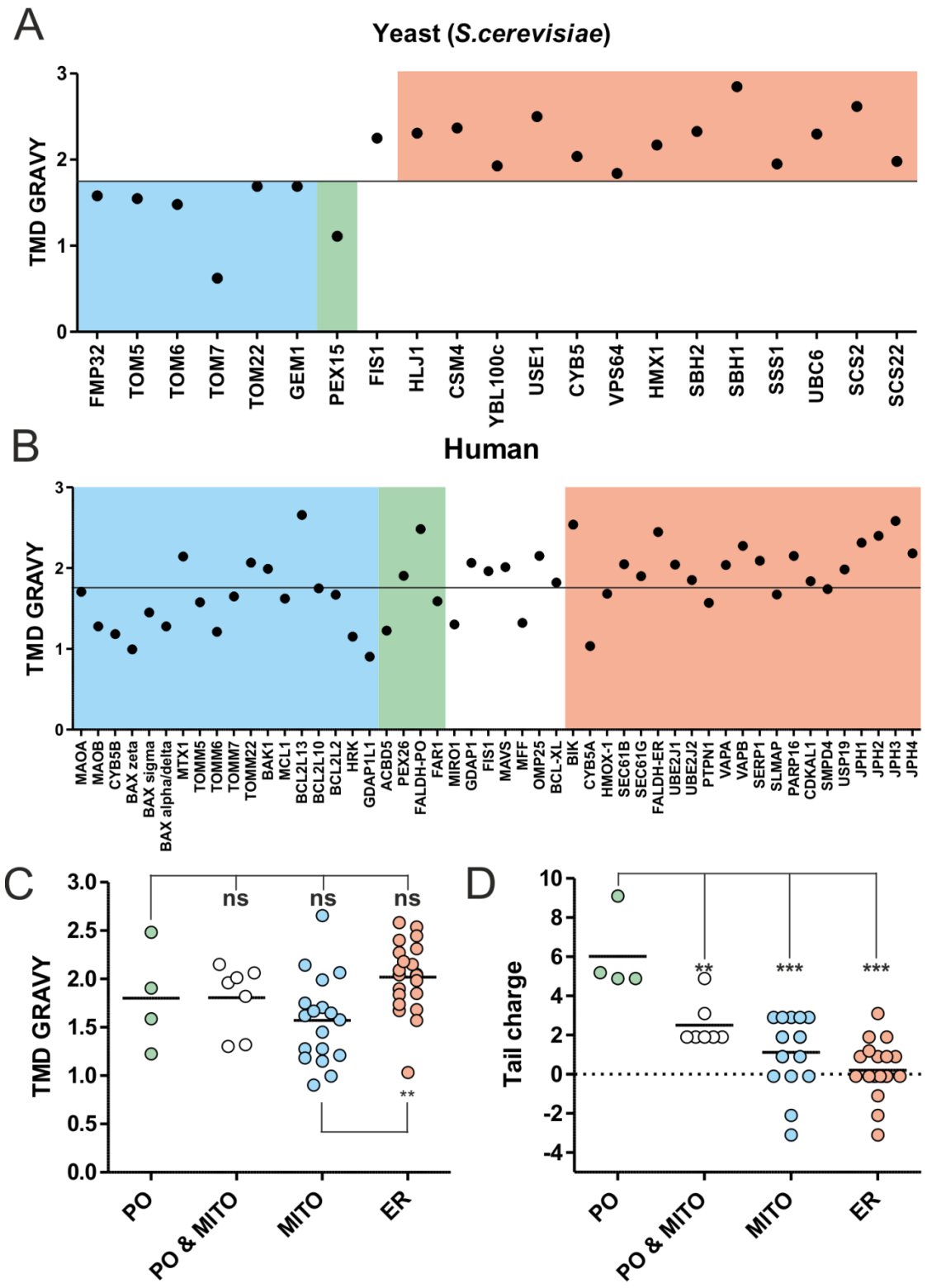
A
Yeast (S.cerevisiae)
TMD GRAVY
FMP32
TOM5
TOM6
TOM7
TOM22
GEM1
PEX15
FIS1
HLJ1
CSM4
YBL100c
USE1
CYB5
VPS64
HMX1
SBH2
SBH1
SSS1
UBC6
SCS2
SCS22
B
Human
TMD GRAVY
MAOA
MAOB
CYB5B
BAX zeta
BAX sigma
BAX alpha/delta
MTX1
TOMM5
TOMM6
TOMM7
TOMM22
BAK1
MCL1
BCL2L13
BCL2L10
BCL2L2
HRK
GDAP1L1
ACBD5
PEX26
FALDH-PO
FAR1
MIRO1
GDAP1
FIS1
MAVS
MFF
OMP25
BCL-XL
BIK
CYB5A
HMOX-1
SEC61B
SEC61G
FALDH-ER
UBE2J1
UBE2J2
PTPN1
VAPA
VAPB
SERP1
SLMAP
PARP16
CDKAL1
SMPD4
USP19
JPH1
JPH2
JPH3
JPH4
C
TMD GRAVY
ns
ns
ns
**
PO
PO & MITO
MITO
ER
D
Tail charge
**
***
***
PO
PO & MITO
MITO
ER

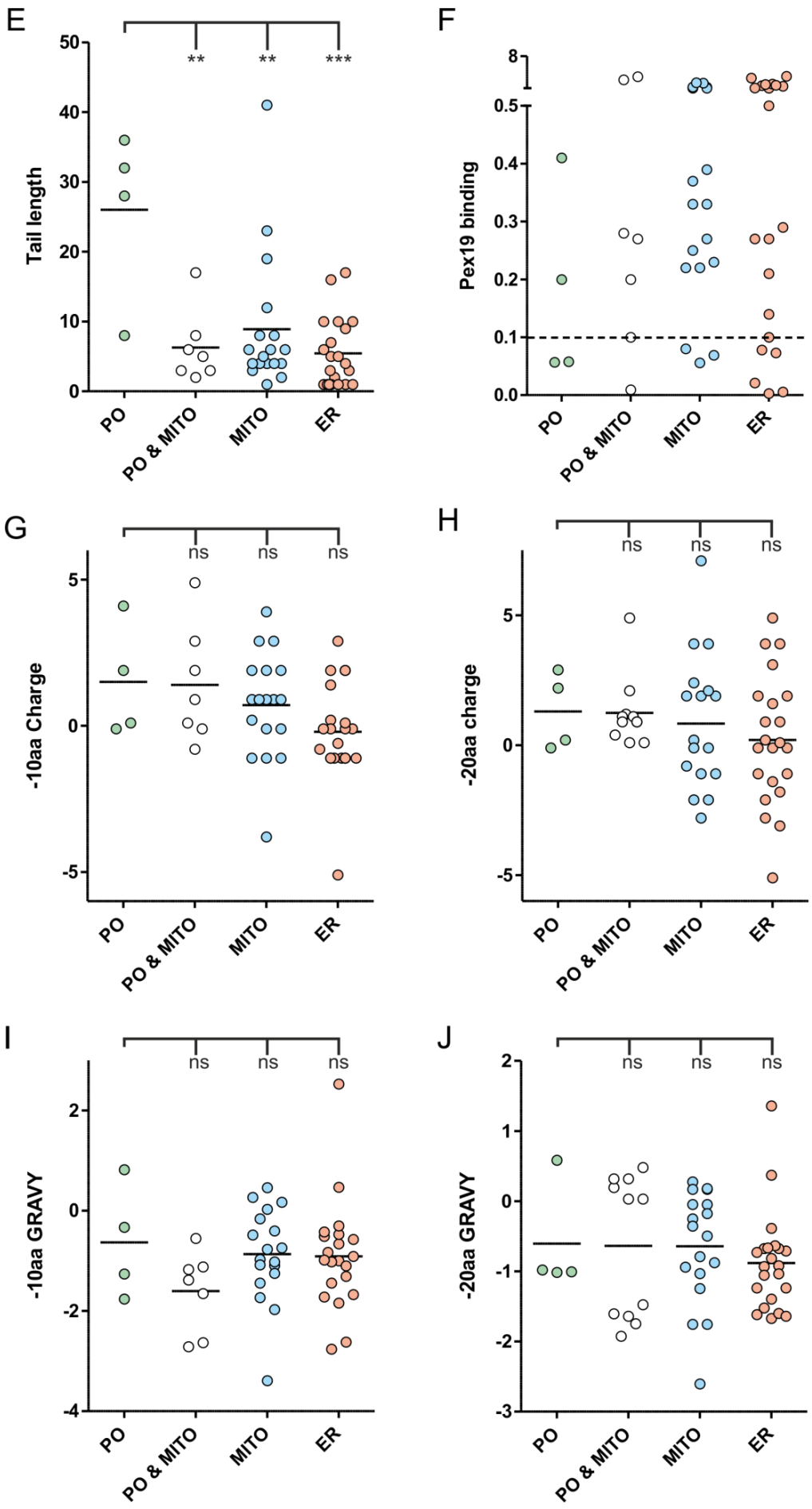
E
Tail length
50
40
30
20
10
0
**
**
***
PO
PO & MITO
MITO
ER
F
Pex19 binding
8
0.5
0.4
0.3
0.2
0.1
0.0
PO
PO & MITO
MITO
ER
G
-10aa Charge
5
0
-5
ns
ns
ns
PO
PO & MITO
MITO
ER
H
-20aa charge
5
0
-5
ns
ns
ns
PO
PO & MITO
MITO
ER
I
-10aa GRAVY
2
0
-2
-4
ns
ns
ns
PO
PO & MITO
MITO
ER
J
-20aa GRAVY
2
1
0
-1
-2
-3
ns
ns
ns
PO
PO & MITO
MITO
ER

Fig. 3.3 – Comparison of the physicochemical parameters of TA proteins between different organelles. (A-B) Scatter plots depicting the TMD GRAVY plotted for each TA protein of known localization in yeast (*S.cerevisiae*) (A) and humans (B). Partition line at 1.75 GRAVY in yeast was defined has the intermediate value between the highest mitochondrial GRAVY and the lowest ER GRAVY. This line was overlapped with human plot to compare distribution of TMD hydrophobicity. Coloured regions represent: blue – mitochondria, green – peroxisomes, white – mitochondria and peroxisomes, salmon pink – ER. (C-J) Scatter plots of tail charge (C), TMD GRAVY (D), tail length (E), PEX19 binding (F), total charge within the 10 (G) and 20 (H) amino acids preceding the tail-region, GRAVY within the 10 (I) and 20 (J) amino acids preceding the tail-region. Whole samples range is shown, with mean values represented as horizontal lines in each sample. Dotted line in (F) indicates the cut-off value used to predict PEX19 binding (0.1) (Schlüter et al., 2007). Samples were compared using one-way ANOVA with post hoc Tukey test (** $p < 0.01$, *** $p < 0.001$, ns - not significant). For all plots, mitochondrial TA proteins (MITO) are depicted in blue, peroxisomal (PO) are in green, shared (PO & MITO) are in white, and ER-TA proteins in salmon-pink.

3.2.3. Alterations in tail charge and TMD hydrophobicity shift targeting between peroxisomes, mitochondria and the ER

To analyse the effect of tail charge and TMD hydrophobicity on protein sorting, a GFP fusion protein was created by adding the TMD and tail of ACBD5 to the C-terminus of a GFP tag (Figure 3.4A). This construct, GFP-ACBD5^{TMD-T}, was then mutated to have increasingly lower tail charge (Mut1 and Mut2) or a more hydrophobic TMD (Mut3). The wild type construct, with a TMD GRAVY of 1.2 and a tail charge of 4.9 was strongly targeted to peroxisomes (Figure 3.4B), with some cells showing a dual targeting to peroxisomes and mitochondria (but never mitochondria alone). Mutation of two tail residues from arginine to alanine, decreasing the tail charge to 2.9 (Mut1), resulted in a re-targeting of the protein to mitochondria (Figure 3.4B). In these conditions, a significant number of cells also showed dual targeting to peroxisomes and mitochondria (Figure 3.4B, C), but never peroxisomes only. Further lowering of the charge to 0.9 shifted the targeting to the ER (Figure 3.4B), with some cells presenting a shared mitochondrial and ER targeting (Figure 3.4C). These results demonstrate that this region of the protein is sufficient for membrane insertion and specific organelle targeting, and that subtle changes in tail charge can easily shift targeting between organelles, in this case from peroxisomes to

mitochondria and finally to the ER. As the full ACBD5 protein is exclusively peroxisomal, other factors are likely at play to target some TA proteins to only one organelle, or to degrade mistargeted proteins. Following a similar approach, we tested the targeting of Flag-FIS1WT against a mutated version with a highly positive charged tail (Flag-FIS1SR) (Figure 3.5A) (Onoue et al., 2013). Flag-FIS1WT (charge 1.9) was localised to both mitochondria and peroxisomes, whereas Flag-FIS1SR (charge 4.9) was predominantly targeted to peroxisomes, further strengthening the hypotheses that a high positive tail charge strongly promotes peroxisomal targeting. Although the Flag-FIS1WT construct had been previously described to localise to mitochondria only, in our experimental set up this protein was targeted to both mitochondria and peroxisomes. This is in agreement with previously published data on this protein (Koch et al., 2005).

Since a high TMD hydrophobicity seems to promote ER targeting, we tested if peroxisomal proteins could be rerouted to this organelle by increasing TMD hydrophobicity but maintaining the high positive tail charge. For this, we mutated the TMD of GFP-ACBD5$^{TMD\text{-}T}$ and increased its GRAVY from 1.2 to 2.8 (Figure 3.4A). This approach successfully shifted the targeting of this protein to the ER (Figure 3.4B), with some low levels of dual targeting to the ER and peroxisomes, suggesting that a balance between TMD hydrophobicity and tail charge is required for peroxisomal targeting. These results are in line with our observations of the targeting of both FALDH isoforms (Figure 3.1D, E). The two isoforms have a very hydrophobic TMD (2.5) and are identical with the exception of the tail sequence (Ashibe et al., 2007). The ER isoform possesses a negative charge whereas the peroxisomal isoform has a very high positive tail charge of 9.1 (Table 3.4), which in this case appears to override the TMD hydrophobicity, and promote peroxisome targeting.

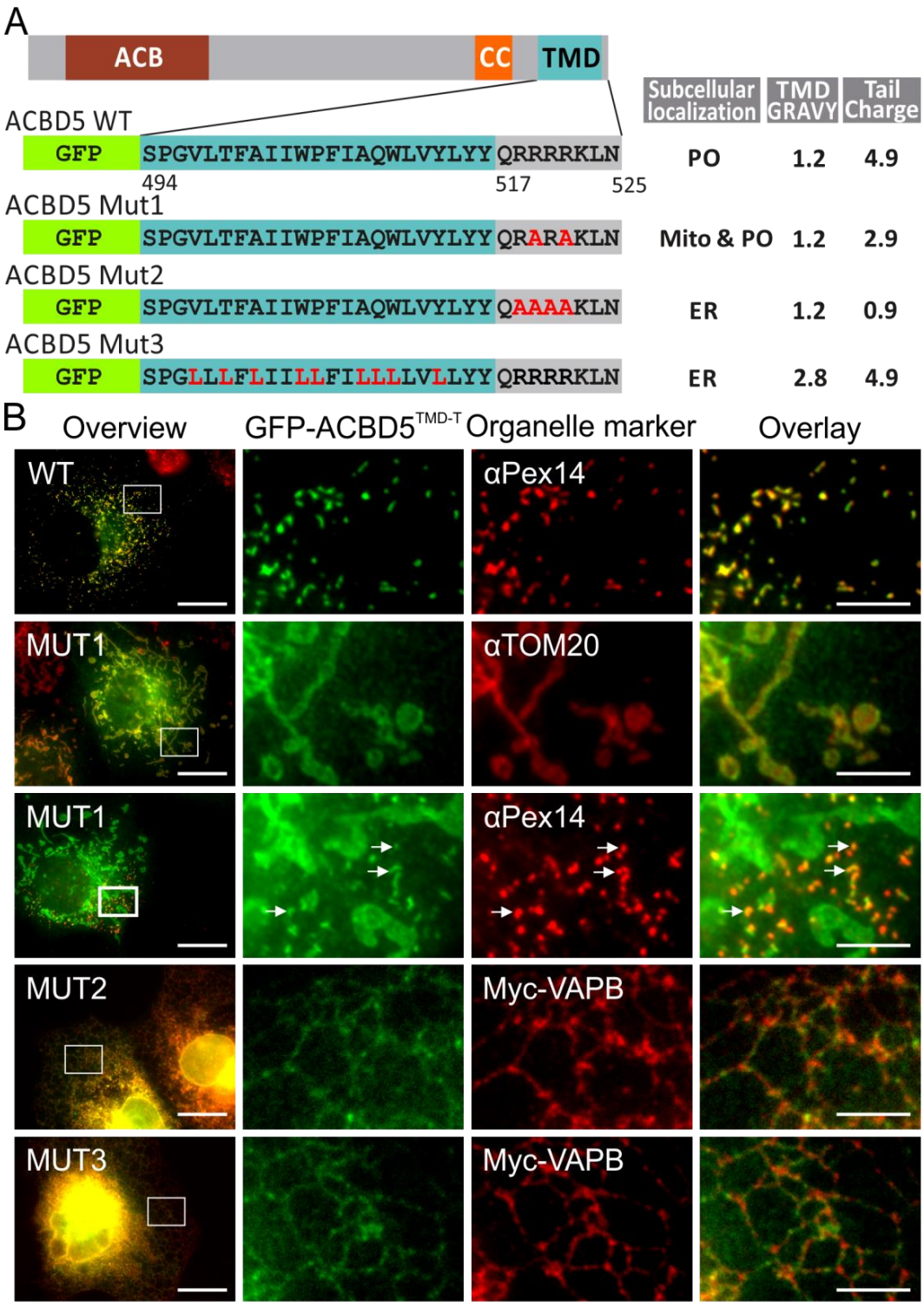
A
ACB
CC
TMD
Subcellular localization
TMD GRAVY
Tail Charge
ACBD5 WT
GFP SPGVLTFAIIWPFIAQWLVYLYY QRRRRKLN
494
517
525
PO 1.2 4.9
ACBD5 Mut1
GFP SPGVLTFAIIWPFIAQWLVYLYY QRARAKLN
Mito & PO 1.2 2.9
ACBD5 Mut2
GFP SPGVLTFAIIWPFIAQWLVYLYY QAAAAKLN
ER 1.2 0.9
ACBD5 Mut3
GFP SPGLLLFLIILLFILLLLVLLYY QRRRRKLN
ER 2.8 4.9
B
Overview
GFP-ACBD5TMD-T
Organelle marker
Overlay
WT
αPex14
MUT1
αTOM20
MUT1
αPex14
MUT2
Myc-VAPB
MUT3
Myc-VAPB
C
GFP-ACBD5TMD-T
%subcellular localization
100
80
60
40
20
0
WT
MUT1
MUT2
MUT3
PO
MITO
ER
SHARED

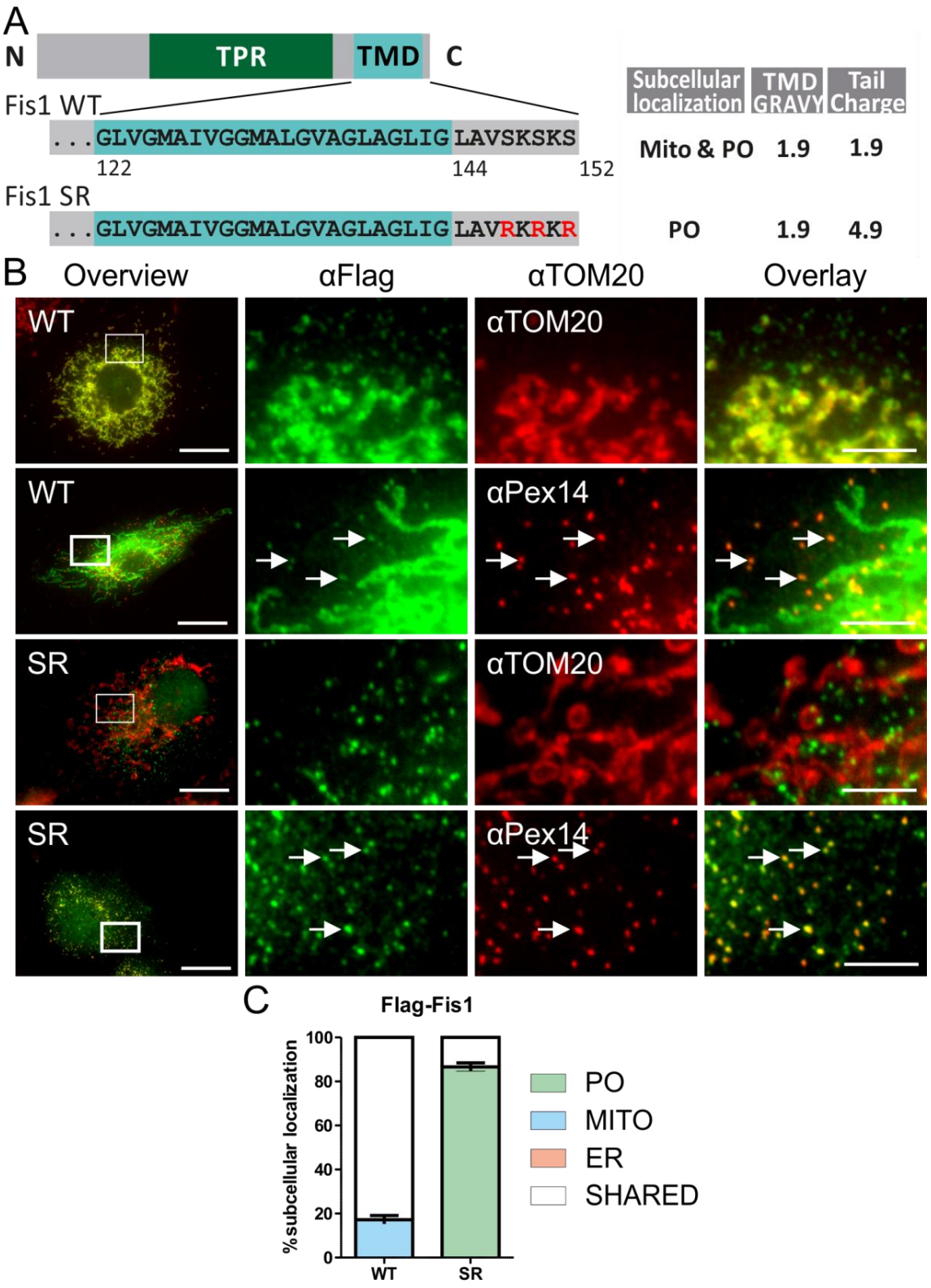
A
N
TPR
TMD
C
Fis1 WT
...GLVGMAIVGGMALGVAGLAGLIG LAVSKSKS
122
144
152
Fis1 SR
...GLVGMAIVGGMALGVAGLAGLIG LAVRKRKR
Subcellular localization
TMD GRAVY
Tail Charge
Mito & PO
1.9
1.9
PO
1.9
4.9
B
Overview
αFlag
αTOM20
Overlay
WT
αTOM20
WT
αPex14
SR
αTOM20
SR
αPex14
C
Flag-Fis1
%subcellular localization
100
80
60
40
20
0
WT
SR
PO
MITO
ER
SHARED

Fig. 3.4 – Alterations in tail charge and TMD GRAVY redistribute GFP-ACBD5^{TMD-TT} to other organelles. (A) Overview of the domain structure of ACBD5 and ACBD5 GFP-TMD-Tail mutants (GFP-ACBD5^{TMD-T}), their subcellular localisation, TMD GRAVY and tail charge. ACB, Acyl CoA binding domain; CC, predicted coiled coil region. (B) COS-7 cells were transfected with GFP-ACBD5^{TMD-T} WT or GFP-ACBD5^{TMD-T} tail mutants (Mut 1-3), and, where indicated, Myc-VAPB (ER marker). Fixed cells were labeled with antibodies against PEX14 (peroxisomal marker), TOM20 (mitochondrial marker), and Myc. GFP-ACBD5^{TMD-T} WT was exclusively targeted to peroxisomes in most cells, whereas Mut1 was strongly targeted to mitochondria. In some cells, dual localisation of Mut1 to peroxisomes was observed (white arrows). GFP-ACBD5^{TMD-T} Mut2 and 3 were targeted to the ER and rarely showed dual targeting. Higher magnification view of boxed regions (see overview) is shown. Bars: 20 µm (overview), 5 µm (overlay). (C) Quantitative analysis of the subcellular localization of GFP-ACBD5^{TMD-T} fusion proteins. The percentage of cells with peroxisomal (PO), mitochondrial (MITO), ER or shared localization is shown. Shared localization is as follows: WT/MUT1 – PO and MITO; MUT2 – MITO and ER; MUT3 – ER and PO. Values represent mean ± SEM of at least three independent experiments.

Fig. 3.5 – Alterations in tail charge redirect FLAG-FIS1 to other organelles. (A) Overview of the domain structure of FIS1 and FLAG-FIS1 proteins (WT and SR), their subcellular localisation, TMD GRAVY and tail charge. TPR, Tetratricopeptide repeat domain. (D) COS-7 cells were transfected with FLAG-FIS1 WT and SR. Fixed cells were labelled with antibodies against TOM20 (mitochondrial marker) and FLAG. FLAG-FIS1 WT was dually targeted to peroxisomes and mitochondria in most cells. This targeting was shifted to peroxisomes in the SR mutant. Arrows point to peroxisome colocalization. Higher magnification view of boxed regions (see overview) is shown. Bars: 20 µm (overview), 5 µm (overlay). (C) Quantitative analysis of the subcellular localization of FLAG-FIS1 WT and SR proteins. The percentage of cells with peroxisomal (PO), mitochondrial (MITO), ER or shared localization is shown. Shared localization is between mitochondria and peroxisomes. Values represent mean ± SEM of at least three independent experiments.

3.2.4. TA proteins are targeted to peroxisomes via PEX19

The peroxisomal chaperone PEX19 and the membrane protein PEX3 have been previously shown to interact with PEX26 and regulate its targeting and insertion in peroxisomes (Chen et al., 2014a; Halbach et al., 2006; Yagita et al., 2013). Additionally, other TA proteins such as FIS1 and GDAP1 have also been shown to interact with PEX19 (Delille and Schrader, 2008; Huber et al., 2013).

To verify if ACBD5 and FALDH-PO also interact with PEX19, we co-expressed GFP-tagged versions of these proteins with HA-PEX19 in COS-7 cells, and performed co-immunoprecipitation experiments. As shown in figure 3.6A, HA-PEX19 was co-immunoprecipitated with GPF-ACBD5 and GFP-FALDH-PO, supporting a role for this protein in the targeting of peroxisomal TA proteins. It should be noted that endogenous ACBD5 (60 kDa) and FALDH (55 kDa) generally run at a higher band size than expected, possibly due to post-translational modifications Additionally, no interaction between FALDH-ER and PEX19 was found, pointing to the presence of a PEX19 binding site in the C-terminal tail of FALDH-PO. Next, we investigated the interaction of PEX19 with the GFP-ACBD5^{TMD-T} fusion proteins, as altering the charge and hydrophobicity

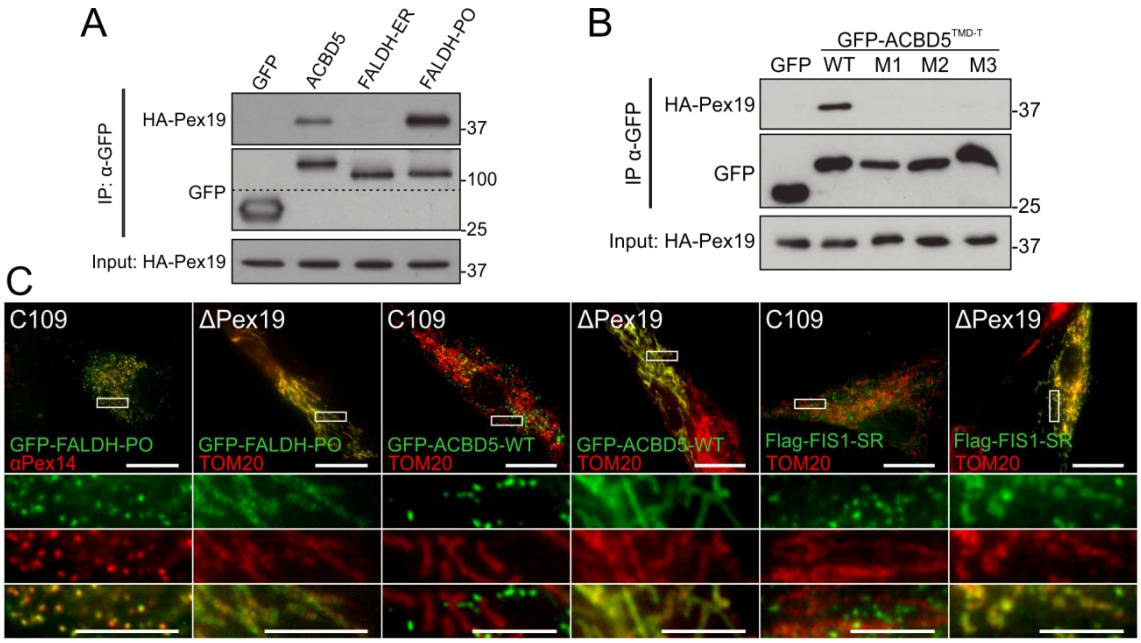

Fig. 3.6 – PEX19 affinity is a key determinant in targeting to the peroxisomal membrane. (A-B) Immunoblots (IB) of coimmunoprecipations from COS-7 cell lysates, expressing HA-PEX19 and various GFP fusions as indicated, using GFP-Trap. Cytosolic GFP was used as a control. (A) HA-PEX19 was coimmunoprecipitated by GFP-ACBD5 and GFP-FALDH-PO, but not by GFP-FALDH-ER. (B) HA-PEX19 was coimmunoprecipitated with GFP-ACBD5^{TMD-T} WT but not by Mut1, Mut2 and Mut3. Input, 1% of total cell lysates; IP, immunoprecipitation. (C) Control and ΔPEX19 fibroblasts were transfected with GFP and FLAG fusions as indicated, fixed and labelled with antibodies against PEX14 (peroxisomal marker), TOM20 (mitochondril marker) and FLAG. In the absence of peroxisomes, all peroxisomal proteins were targeted to mitochondria. Higher magnification view of boxed regions (see top panel) is shown. Bars, 20 µm (top panel), 5 µm (lower panels).

of the tail and TMD should influence their binding. Our results show that whereas GFP-ACBD5^{TMD-T} WT is bound by HA-PEX19, none of the mutant constructs is significantly associated with this chaperone (Figure 3.6B). We also analysed the targeting of GFP-FALDH-PO, GFP-ACBD5 and Flag-FIS1SR in cells lacking PEX19 (ΔPEX19 patient fibroblasts) (Figure 3.6C). Whereas in control fibroblasts the three proteins were targeted to peroxisomes, in ΔPEX19 cells, which lack peroxisomes, all the tested proteins were targeted to mitochondria, suggesting that this might be the default pathway for peroxisomal TA proteins. Remarkably, even FALDH-PO was targeted to mitochondria instead of the ER, despite its high TMD hydrophobicity.

3.2.5. Prediction of TA protein localisation in mammalian cells

Having established the importance of tail charge and TMD hydrophobicity for protein targeting, we set out to create a targeting tool that would allow us to predict *in silico* the localisation of uncharacterized TA proteins. For this, a SVM classifier was trained using the TMD GRAVY, tail charge and cellular location of 43 proteins from our dataset (Table 3.1). This classifier builds a statistical model that is able to predict the probability of a protein to be targeted to each organelle, using the TMD GRAVY and tail charge of that protein (Figure 3.7A). Three clusters (or regions of high class probability) of peroxisomal, mitochondrial and ER proteins can be clearly observed, with very few exceptions (i.e. mitochondrial TOMM22 clusters with ER). When using the highest probability class, the SVM misclassifies 9 of the 43 data points (21%) when used in an in-sample fashion. A more rigorous leave-one-out cross validation misclassifies 14 of the 43 data points (33%). Using this classifier, we tested a previously published list of TA proteins predicted in the human proteome (Kalbfleisch et al., 2007). For each entry, a probability of peroxisomal, mitochondrial and ER targeting was obtained (Appendix 1).The predicted localisation of three proteins was experimentally verified (Figure 3.7B). Of the tested proteins, ACBD4 was predicted and verified as a new peroxisomal protein (Figure 3.7B). This protein contains an acyl-CoA binding domain and belongs to the family of acyl-CoA binding proteins. Another protein which was also predicted to target peroxisomes is ATP5J2, a subunit of the mitochondrial ATP synthase complex. When expressed in COS-7 cells this protein shows a

dual targeting to peroxisomes and mitochondria (Figure 3.7B), and can induce some mitochondrial swelling. Finally we analysed the targeting of the predicted ER protein PPP1R3F, which is a regulatory subunit of protein phosphatase type-1 complexes. This was confirmed by expressing the myc-tagged protein in COS-7 cells. In the future, the localisation of these proteins should also be confirmed by analysing the localisation of the endogenous protein using antibodies.

3.3. Discussion

Regulated sorting of membrane proteins is a process that allows cells to strictly control the function of each individual compartment, whilst inhibiting the accumulation of hydrophobic and potently aggregated proteins in the cytosol (Mannini et al., 2014). A clear understanding of the basic signals that modulate this sorting would allow us, in principle, to predict the targeting of any given protein, and facilitate the understanding of protein function. TA proteins lack any identifiable consensus sequence that would allow their recognition by a targeting complex or chaperone, and have therefore been the object of intense research in the past few years (reviewed in Borgese and Fasana, 2011). Here, we have extended the existing information on TA protein localisation and characterized the targeting signals of peroxisomal TA proteins. Additionally, by taking advantage of the growing number of known TA proteins, we created a bioinformatic tool that allows us to predict membrane localisation.

3.3.1. Where are TA proteins targeted too?

TA proteins are targeted to several eukaryotic membranes, such as the ER and exocytic pathway, outer mitochondrial and chloroplast membrane, and peroxisomes (Borgese et al., 2007). While some proteins are exclusively targeted to one organelle, several have the ability to target two organelles, as exemplified by MFF, FIS1, GDAP1 and MAVS (Dixit et al., 2010; Gandre-Babbe and van der Bliek, 2008; Huber et al., 2013; Koch et al., 2005). Our results show that more TA proteins have dual or even triple targeting (Figure 3.1, Table 3.1), demonstrating that a thorough characterisation of these proteins is still

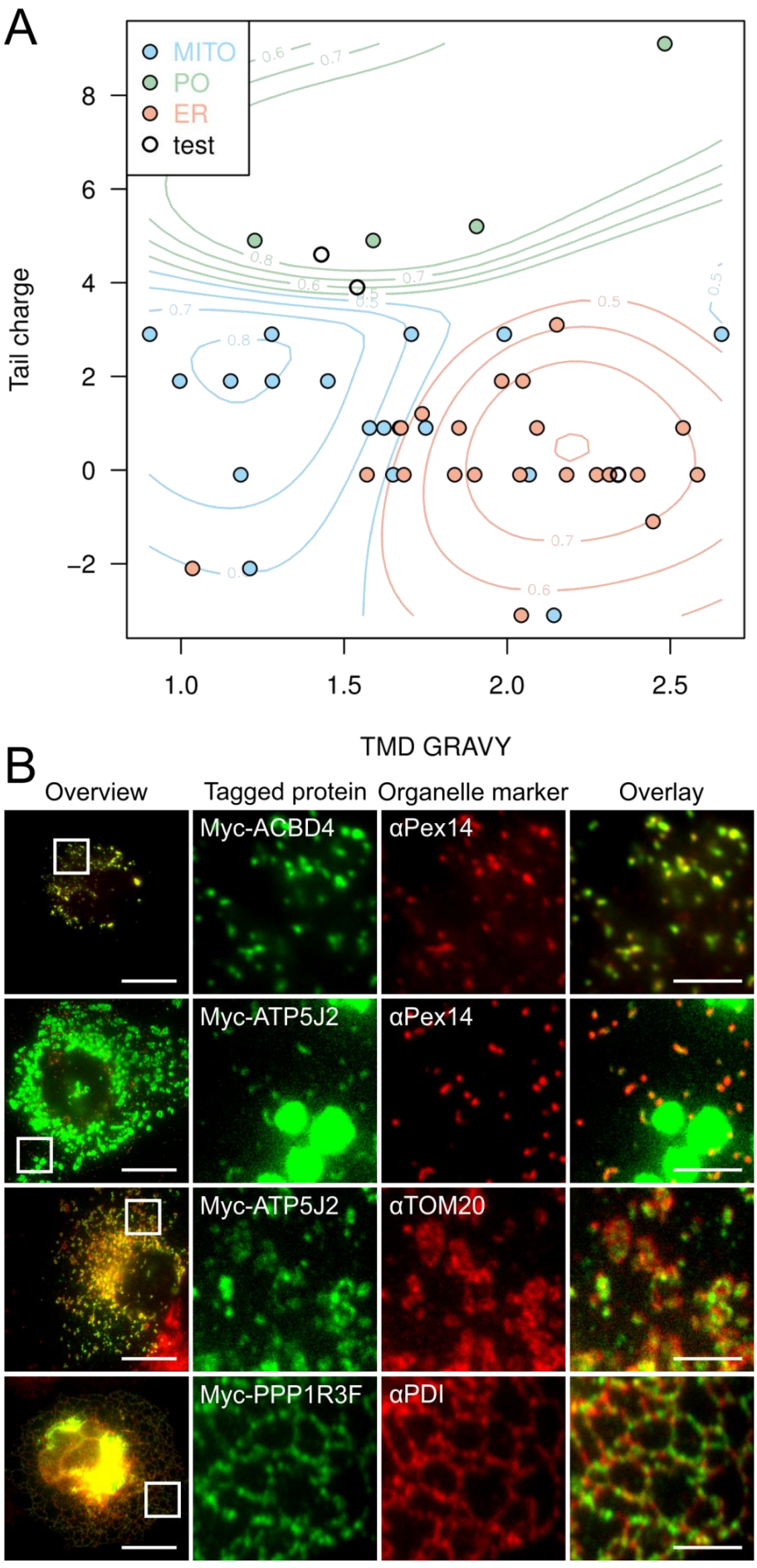
A
MITO
PO
ER
test
Tail charge
TMD GRAVY
B
Overview
Tagged protein
Organelle marker
Overlay
Myc-ACBD4
αPex14
Myc-ATP5J2
αPex14
Myc-ATP5J2
αTOM20
Myc-PPP1R3F
αPDI

Fig. 3.7 – A combination of tail charge and TMD GRAVY allows prediction of organelle targeting for mammalian TA proteins. (A) SVM classifier plot showing clustering of TA proteins to different organelle locations based on TMD GRAVY and tail charge. Probability contours are as indicated. MITO, mitochondria; PO, peroxisomes; ER, endoplasmic reticulum; test – selected TA proteins (see B). (B) COS-7 cells were transfected with Myc fusions of ACBD4, ATP5J2, and PPP1R3F. Fixed cells were labelled with antibodies against PEX14 (peroxisomal marker), TOM20 (mitochondrial marker), PDI (ER marker) and Myc. Higher magnification view of boxed regions (see overview) is shown. Bars, 20 µm (overview), 5 µm (overlay).

lacking. Discovery of a new cellular localisation for a protein could not only reveal new functions for an organelle, but uncover new layers of complexity for the regulation of that protein, with implications in pathological conditions. For example, the presence of BCL2-family proteins at peroxisomes could point to a previously unknown role of this organelle in apoptosis. Moreover, as the dually targeted proteins are both anti-apoptotic (BCL-XL and BCL2), this could point to a role of peroxisomes as signalling platforms during apoptotic stress.

Yet, some caution should be taken when considering the results from our localisation experiments. As some of these proteins might have cell-type specific expression, their localisation in COS-7 might not be representative of their endogenous localisation. Additionally, as all of the proteins were overexpressed, some of the dual or triple targeting results could represent mistargeting to unspecific cellular membranes. For example, overexpression of ACBD5 (and FALDH-PO) led to mitochondrial targeting in some cells, even though endogenous ACBD5 has only been detected on peroxisomes (not shown). This could be overcome by analysing the localisation of the endogenous protein by IMF or WB of subcellular fractions. However, antibodies against the target proteins are not always available or working effectively. Despite our attempts to analyse several of these proteins, only a few of the available antibodies were functional in our set up. Interestingly, the antibody used against BCL2 showed a clear co-localisation with the peroxisomal marker PEX14 in IMF, as well as cytosolic staining, instead of the expected mitochondrial and ER staining (Figure 3.2). Similar results were obtained when analysing subcellular fractions of rat liver, where bands were found in the peroxisomal and cytosolic fractions. This could indicate that the antibody is

recognizing a protein isoform that is cytosolic and targeted to peroxisomes (or possibly two isoforms).

3.3.2. How do TA proteins know where to go?

Several studies have shown that targeting of TA proteins depends on several physicochemical parameters of their C-terminus, rather than a defined consensus sequence (Beilharz et al., 2003; Borgese et al., 2007; Kuroda et al., 1998; Marty et al., 2014). Particularly, the hydrophobicity and length of the TMD, as well as the charge of the tail, seem to play key roles in targeting to the ER, mitochondria and peroxisomes (Horie et al., 2002; Mariappan et al., 2010; Yagita et al., 2013). While most of these studies use model proteins to test the effects of several mutations, additional biological input can be obtained by analysing larger groups of TA proteins (Borgese et al., 2007). Building on previous studies and taking advantage of the growing number of known TA proteins, we collected data on 50 proteins and re-analysed their physicochemical characteristics. In accordance with previous publications, the most relevant parameters for TA protein targeting were TMD hydrophobicity and tail charge (Figure 3.3). These two factors alone allowed us to cluster ER, mitochondrial and peroxisomal proteins, as show in our SVM classifier (Figure 3.7).

Our results show that exclusively peroxisomal TA proteins have a highly positive charged tail sequence when compared with proteins targeted to other organelles (Figure 3.3D). This characteristic was experimentally tested by gradually decreasing the tail charge in the GFP-ACBD5$^{TMD\text{-}T}$ fusion proteins (Figure 3.4), or increasing it as had been previously shown with Flag-FIS1SR (Figure 3.5) (Onoue et al., 2013). The initial shift in targeting to mitochondria and secondly to the ER is in agreement with previous data suggesting that a positively charged tail could significantly differentiate between mitochondrial and ER proteins (Borgese et al., 2007; Horie et al., 2002; Kuroda et al., 1998). Interestingly, while we do see this with the expressed proteins, our bioinformatics analysis doesn't show any statistical differences between mitochondria and ER (Figure 3.3D), suggesting tail charge alone cannot be used to distinguish targeting to these two organelles.

TMD hydrophobicity has been previously shown to strongly correlate with TA protein targeting. Studies in yeast have shown a clear distinction between mitochondrial and ER proteins, with the former having a lower GRAVY than the latter (Figure 3.3A) (Beilharz et al., 2003). These results are frequently compared to TA proteins in humans, and are confirmed by our analysis (Figure 3.3C). However, whereas a clear cut difference between mitochondrial and ER TMD hydrophobicity is seen in yeast (Figure 3.3A), an overlap between ER and mitochondrial TA proteins is observed with the human proteins (Figure 3.3B). This strongly suggests that this factor alone is also not sufficient to regulate targeting between these organelles. This is clearly exemplified by the two FALDH isoforms which have the same TMD GRAVY, and yet are targeted to distinct organelles, as a result of tail charge differences (Table 3.4). Curiously, peroxisomal TA proteins have a wide range of TMD hydrophobicity, leading to the assumption that this factor does not have a major role in peroxisomal targeting. However, when the GRAVY of GFP-ACBD5^{TMD-T} was increased (Mut3), this protein was targeted to the ER (Figure 3.4A, B). Similar results have been shown in *Neurospora crassa*, where an increase in TMD hydrophobicity can shift the targeting of this protein to the ER (Chen et al., 2014a). These results suggest that a balance exists between TMD hydrophobicity and tail charge that determines the targeting of TA proteins.

Finally, peroxisomal TA proteins also appear to have longer C-terminal tails (Figure 3.3E). Despite the significance of this result, we should note that only 4 proteins were used for this analysis, and that this is not a pre-requisite for targeting since ACBD5, and the newly identified ACBD4, have short tails. Nonetheless, further testing could be performed by taking advantage of the FALDH isoforms. As these proteins have the same amino acid sequence apart from the tail segment, we could follow two approaches. On the one hand, we could mutate FALDH-ER to have the same charge as FALDH-PO, to understand if the long tail of FALDH-PO is necessary for peroxisomal targeting. On the other hand, we could gradually decrease the charge of FALDH-PO and see if a tail as long as 28 amino acids could be inserted in the ER. These approaches have recently been tested with PEX26 (Yagita et al., 2013). Using this model, the authors have shown that decreasing the tail charge or decreasing tail size while maintaining charge has the same effect, with PEX26 being dually targeted to peroxisomes and mitochondria.

3.3.3. How are TA proteins targeted to peroxisomes?

Previous studies have shown a role for import receptor/chaperone PEX19 in the targeting and insertion of peroxisomal TA proteins PEX26 (Pex15 in yeast) (Chen et al., 2014a; Halbach et al., 2006; Yagita et al., 2013) and FAR1 (Honsho et al., 2013). This protein recognizes several peroxisomal membrane proteins (PMPs) through PEX19-binding sites, which contain several basic and hydrophobic residues near the TMD (Rottensteiner et al., 2004). Here, we show that ACBD5 and FALDH-PO interact with PEX19 (Figure 3.6A), strengthening the hypothesis that PEX19 is responsible for the targeting of TA proteins to peroxisomes. Additionally, PEX19 was able to bind GFP-ACBD5^{TMD-T} WT, indicating that the targeting information of ACBD5 is located at its C-terminus. However, this interaction was lost when PEX19 was co-expressed with GFP-ACBD5^{TMD-T} mutants with altered TMD hydrophobicity or tail charge, implying that PEX19 loses affinity or is out-competed by other chaperones (e.g. TRC40) (Figure 3.6B). To test this, *in vitro* experiments were performed by collaborators using purified PEX19 and fluorescently labelled peptides for WT, Mut1 and Mut2 (unpublished data). These show similar affinities of PEX19 to WT and Mut1 fragments, and loss of affinity for Mut2, suggesting that the lack of interaction between PEX19 and Mut1 seen by co-immunoprecipitation could be due to competition with a yet unidentified mitochondrial chaperone, or differences in PEX19-Mut1 interaction stability between *in vitro* and *in vivo* experiments. Similar experiments should be performed using a recombinant version of the ER receptor TRC40, testing the binding of the protein to Mut2 and Mut3.

Interestingly, in the absence of PEX19, and subsequently peroxisomes, ACBD5, FALDH-PO and FIS1-SR were targeted to mitochondria (Figure 3.6C). Whereas ACBD5 has a low TMD GRAVY, which is suitable for mitochondrial targeting, FALDH-PO has the same TMD GRAVY as its ER counterpart, suggesting that either the tail charge or the tail length of this protein inhibit binding by TRC40, and targeting to the ER. This supports a model where the mitochondrial pathway represents the default route for TA proteins, either by unassisted insertion (Pedrazzini et al., 1996) or by using a specific mitochondrial chaperone that is yet to be identified (Kemper et al., 2008). In favour of this, the recent identification on mitochondria of a degradation

pathway for mislocalised TA proteins, could represent an evolutionary mechanism to inhibit accumulation of peroxisomal (or other) TA proteins at this organelle (Chen et al., 2014b; Okreglak and Walter, 2014). As the protein responsible for this pathway (ATAD1) is also localised to peroxisomes, it would be interesting to see if it performs a similar function at this organelle.

3.3.4. Can we predict TA protein targeting?

TA proteins are present in all domains of life, including Archae and Bacteria (Borgese and Righi, 2010) and several bioinformatics studies have uncovered hundreds of potential new proteins in yeast, plants and mammals (Beilharz et al., 2003; Kalbfleisch et al., 2007; Kriechbaumer et al., 2009). Several of these proteins have been characterized and are linked to essential cellular processes. As there are still numerous uncharacterised proteins, a systematic analysis of their localisation would be a good starting point to find new functions.

We started by looking at several biochemical parameters that could influence the targeting of these proteins (Figure 3.3) and using several approaches identified the TMD GRAVY and tail charge as the most relevant factors affecting targeting. Using this information we created a prediction tool that provides us with the probability of any given mammalian TA protein to be either mitochondrial, peroxisomal or ER (Figure 3.7A). For these three major organelles, we were able to predict with up to 80% accuracy the targeting of TA proteins. Furthermore, using this prediction tool, we tested the targeting of several uncharacterised proteins (Figure 3.7B). Two of them, ACBD4 and PPP1R3F were targeted as predicted to peroxisomes and ER, respectively. A third one, ATP5J2, was targeted to peroxisomes and mitochondria but strongly predicted as peroxisomal (91.4% vs 5.9% to mitochondria) (Appendix 1). This result illustrates some of the weaknesses of a prediction based analyses, since ATP5J2 is part of the ATP synthase complex which is localised to the inner mitochondrial membrane (IMM). It is possible that, since so far no other proteins have been identified in the IMM, our predictor lacks information to compute this possibility, and fails to predict it. However, it remains to be shown if this protein is targeted and stable on peroxisomes at endogenous levels, and if so, what is its role on this organelle.

Prediction based approaches should be employed with caution. In this case, it should be noted that the data used to create this classifier was itself obtained through indirect approaches. Furthermore, the diversity of parameters that can influence such a complex process as protein targeting cannot be computed by a simple two variable analysis. Other factors such as targeting information present at the N-terminus could also affect the localisation of these proteins. Although TA proteins lack any known targeting sequences, it is still possible that some proteins possess yet unidentified targeting sequences, or are bound by other proteins during translation, which could affect their targeting. Nevertheless, this predictor was able to classify correctly the tested proteins (since ATP5J2 was found on peroxisomes), and these and other proteins can be added to it to further improve its power. Moreover, if other variables such as tail length are proven to affect targeting, these could be included, adding an extra dimension to the classifier. Finally, creating a similar predicting tool for yeast and plants, or integrating data from these organisms in the existing predictor, could in principle enable the analysis of other databases.

Chapter 4 – Results

MIRO1 is a regulator of peroxisome motility and dynamics in mammalian cells

4.1. Introduction

The regulation of organelle positioning within eukaryotic cells is crucial for the maintenance of cellular homeostasis, allowing cellular movement and polarisation, and facilitating metabolic and physical interactions between organelles (Jongsma et al., 2015; Knoblach and Rachubinski, 2016). Conversely, defects in organelle motility are associated with the development of severe neurodegenerative disorders such as Alzheimer's and Parkinson's disease (Devine et al., 2016; Mattson et al., 2008).

In mammalian cells, peroxisomes are found associated with the microtubule cytoskeleton and move bidirectionally by associating with kinesin and dynein motors (reviewed in Neuhaus et al., 2016). Compared with other organelles, only a small proportion of peroxisomes (5-15%) show fast directional movement (Rapp et al., 1996; Schrader et al., 2000; Wiemer et al., 1997), which helps maintain a uniform distribution at optimal energy expenditure (Bonekamp et al., 2012). However, little information is known on the molecular complexes regulating peroxisome motility. Recent studies have focused on identifying the protein linkers between peroxisomes and molecular motors. Dietrich and colleagues have shown a direct interaction between PEX1 and the minus-end directed motor KIFC3, proposing a role for these proteins in peroxisome tethering to microtubules and motility regulation (Dietrich et al., 2013). Additionally, PEX14 has been shown to interact directly with tubulin, revealing a possible role for this peroxin in the anchoring of peroxisomes to microtubules (Bharti et al., 2011).

As established in chapter 3, several TA proteins are targeted to more than one organelle (Figure 3.1), and are particularly prone to be dually targeted to mitochondria and peroxisomes. Interestingly, MIRO1 and MIRO2, which were initially identified on the outer mitochondrial membrane (Fransson et al., 2003), are also targeted to peroxisomes when expressed in COS-7 cells (Figure 3.1A, B). Miro proteins form a family of Ras GTPases highly conserved throughout eukaryotes, known to play key roles in mitochondrial motility, homeostasis, inheritance and ER tethering (reviewed in Yamaoka and Hara-Nishimura, 2014). Mammalian MIRO1 and MIRO2 share 60% similarity and an analogous structure containing two GTPase domains intercalated by two calcium binding EF hand motifs. Studies on mammalian MIRO proteins have focused mainly on

MIRO1 due its clear role in mitochondrial motility, particularly in neurons (MacAskill et al., 2009b; Wang and Schwarz, 2009). Here we show that endogenous and myc-tagged MIRO1 is localised to both mitochondria and peroxisomes, and that dual targeting depends on the C-terminal tail. Overexpression of wild-type and mutated MIRO1 alters peroxisome distribution either to the cell periphery or to the perinuclear area, and this effect is inhibited by microtubule depolymerising drugs. Live-cell imaging of peroxisomes in cells expressing an exclusively peroxisomal MIRO1 fusion protein revealed an increase in microtubule-dependent peroxisome motility, and suggests a role for motor forces on the formation of new peroxisomes. These findings support a mechanism in which MIRO1 bridges the interaction between peroxisomes and kinesin (plus-end) motors, and provides us with a tool to further analyse peroxisome dynamics in different cell types.

4.2. Results

4.2.1. MIRO1 is targeted to peroxisomes and interacts with the peroxisomal chaperone PEX19

As shown in chapter 3, expressed myc-tagged MIRO1 is targeted to both peroxisomes and mitochondria in COS-7 cells (Figure 3.1A). To confirm these results, we analysed the endogenous localisation of MIRO1 in different cell types by IMF and immunoblotting using two antibodies. Interestingly, each antibody recognized different organelles in HepG2 cells. As shown in Figure 4.1A, MIRO1 is recognized on mitochondria when using the HPA010687 antibody, and on peroxisomes when using the PSI-8027 antibody. Both antibodies show some unspecific background staining in HepG2 cells. Although endogenous MIRO1 had been previously identified on mitochondria (Fransson et al., 2003; Saotome et al., 2008), no prior studies have shown its presence on peroxisomes, raising the possibility that our second antibody could be recognizing an unspecific protein on peroxisomes. While both antibodies are raised against N-terminal peptides of MIRO1, the immunogen sequence for PSI-8027 is not available, and therefore we do not know if both immunogens have sequence overlap. Furthermore, MIRO1 and MIRO2 share 69% sequence similarity at the N-terminus, raising the possibility that these antibodies could

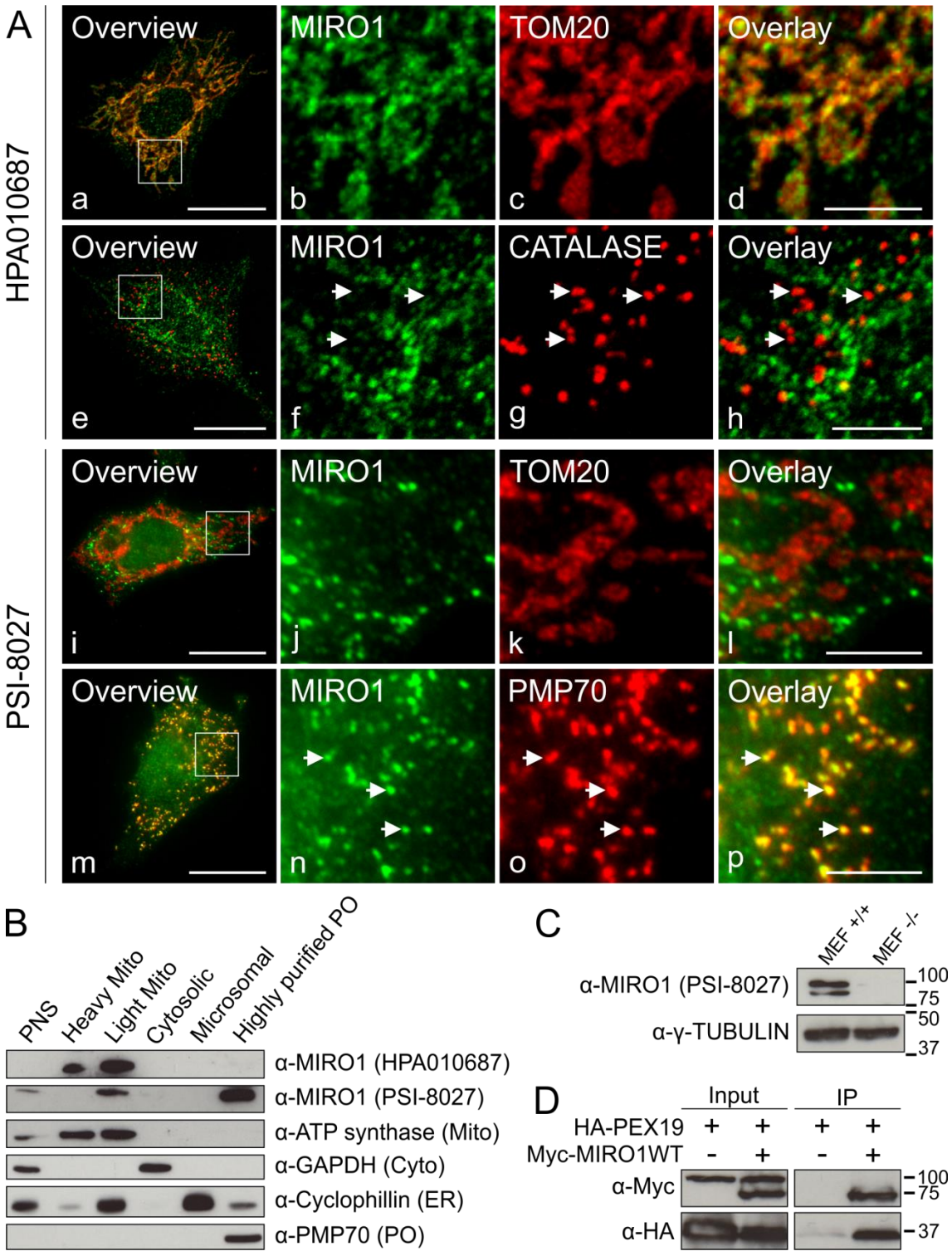

Figure 4.1 – MIRO1 is targeted to peroxisomes and mitochondria in mammalian cells. (A) HepG2 cells were fixed and stained using two different antibodies against MIRO1 – HPA010687 (Sigma-Aldrich) and PSI-8027 (ProSci), as well as antibodies against TOM20 (mitochondrial marker), PMP70 and catalase (peroxisomal markers). Arrows point to the presence (n-p) or absence (f-h) of signal co-localisation with peroxisomes. (a-h) are confocal and (i-p) are epifluorescence microscopy. Scale bar: overview 20 µm, overlay 5 µm. (B) Detection of endogenous MIRO1 in subcellular fractions isolated from rat liver. Equal amounts of protein were separated by SDS-PAGE and

immunoblotted using both anti-MIRO1 antibodies, anti-ATP synthase α (mitochondrial marker), anti-GAPDH (cytosolic marker), anti-Cyclophilin (ER marker) and anti-PMP70 (peroxisomal marker). In accordance with (A), MIRO1 was detected in the mitochondrial fractions (heavy and light) by the HPA010687 antibody, and in the peroxisomal fraction (as well as light mitochondrial fraction) by PSI-8027. (C) Immunoblot of cell lysates from MIRO1 KO and control MEFs stained against MIRO1 (PSI-8027) and γ-tubulin. The PSI-8027 antibody specifically recognises MIRO1 in these cells. (D) Co-immunoprecipation from COS-7 cell lysates expressing HA-PEX19 and myc-MIRO1WT, using myc-tagged agarose beads. HA-PEX19 was only co-immunoprecipitated in the presence of myc-MIRO1WT. Higher band in α-myc blot is unspecific and characteristic for this antibody. Input – 10% of total cell lysates. PNS – post nuclear supernatant, Mito – mitochondria, PO – peroxisome, IP – immunoprecipitation.

recognise both proteins. To complement our observations, we tested both antibodies in subcellular fractions of rat liver (Figure 4.1B). While the HPA010687 antibody recognizes a protein in the heavy and light mitochondrial fractions, the PSI-8027 antibody recognizes a protein in the light mitochondrial and the highly purified peroxisome fractions. Both proteins have similar sizes around 80 kDa, suggesting that each antibody could be recognizing different isoforms of MIRO1. Additionally, the PSI-8027 antibody recognizes two bands between 75 and 100 kDa in cell lysates from WT mouse embryonic fibroblasts (MEFs) but none in MIRO1 knockout (KO) MEFs (Figure 4.1C), demonstrating that this antibody is recognizing MIRO1, and that endogenous MIRO1 is targeted to peroxisomes. Further experients should be performed to strengthen these observations, such as testing the HPA010687 antibody on similar MEF WT and MIRO1 KO cell lysates, and performing depletion studies, to confirm that the antibodies are recognising MIRO1.

Several TA proteins require PEX19 binding for targeting and insertion into the peroxisomal membrane, making it likely that MIRO1 is also bound and delivered to peroxisomes by this pathway. Evidence of this interaction was initially found by searching the BioGRID database (Stark et al., 2006), an interaction repository that compiles data from published literature. In particular, PEX19's interaction with MIRO1 was identified in a high-throughput interaction study with PEX19 as bait (Huttlin et al., 2015). To confirm this, myc-MIRO1WT was co-expressed with HA-PEX19 in COS-7 cells, and processed for co-

immunoprecipitation using myc-tagged agarose beads. Similarly to other shared TA proteins (e.g. FIS1, GDAP1), PEX19 was bound to MIRO1 (Figure 4.1D), suggesting a role for this protein in the targeting of MIRO1 to peroxisomes.

4.2.2. MIRO1 expression alters peroxisomal distribution in COS-7 cells

MIRO1 has been shown to play a key role on mitochondrial motility in mammalian cells (MacAskill et al., 2009b; Saotome et al., 2008; Wang and Schwarz, 2009). To assess its role on peroxisomes we expressed WT and four mutated versions of myc-tagged MIRO1 in COS-7 cells, and analysed their effect on peroxisome dynamics (Figure 4.2). As previously described (Fransson et al., 2003, 2006), the expression of myc-MIRO1WT and mutants resulted in several mitochondrial phenotypes such as formation of perinuclear aggregates (Figure 4.2B i, m), highly elongated networks (Figure 4.2B e) and fragmented organelles (Figure 4.2B k). Conversely, expression of myc-MIRO1WT and mutants did not induce peroxisome elongation or network formation. Instead, depending on the expressed protein, peroxisomes accumulated at the cell periphery (Figure 4.2B a-d, i-j) or in intracellular inclusions (Figure 4.2B k-n), suggesting an effect on organelle motility. Expression of myc-Miro1WT induced the formation of peroxisome accumulations at the cell periphery in ~25% of transfected cells (Figure 4.2B, C), as shown at higher magnification (Figure 4.2B b-d). Expression of the V13 mutant, which is constitutively active at the first GTPase domain, also induced the accumulation of peroxisomes at the cell periphery but to a lower extend than the WT protein (Figure 4.2B i-j, C). Additionally, expression of this mutant, as well as of myc-MIRO1N18 (dominant negative for the first GTPase domain) and myc-MIRO1KK (unable to bind calcium) led to the formation of peroxisome aggregates scattered through the cell (Figure 4.2B k-n, C). Finally, cells expressing myc-MIRO1ΔTM (lacking the TMD and tail sequence) showed a cytoplasmic distribution of this protein and had no visible effects on the peroxisomal network (Figure 4.2B o-p, C).

As the expression of these constructs had severe effects on the mitochondrial network and, as result, on cellular homeostasis, we created an exclusively peroxisomal set of MIRO1 proteins. For this, two different strategies were developed by exchanging the TMD and tail of MIRO1 for new targeting

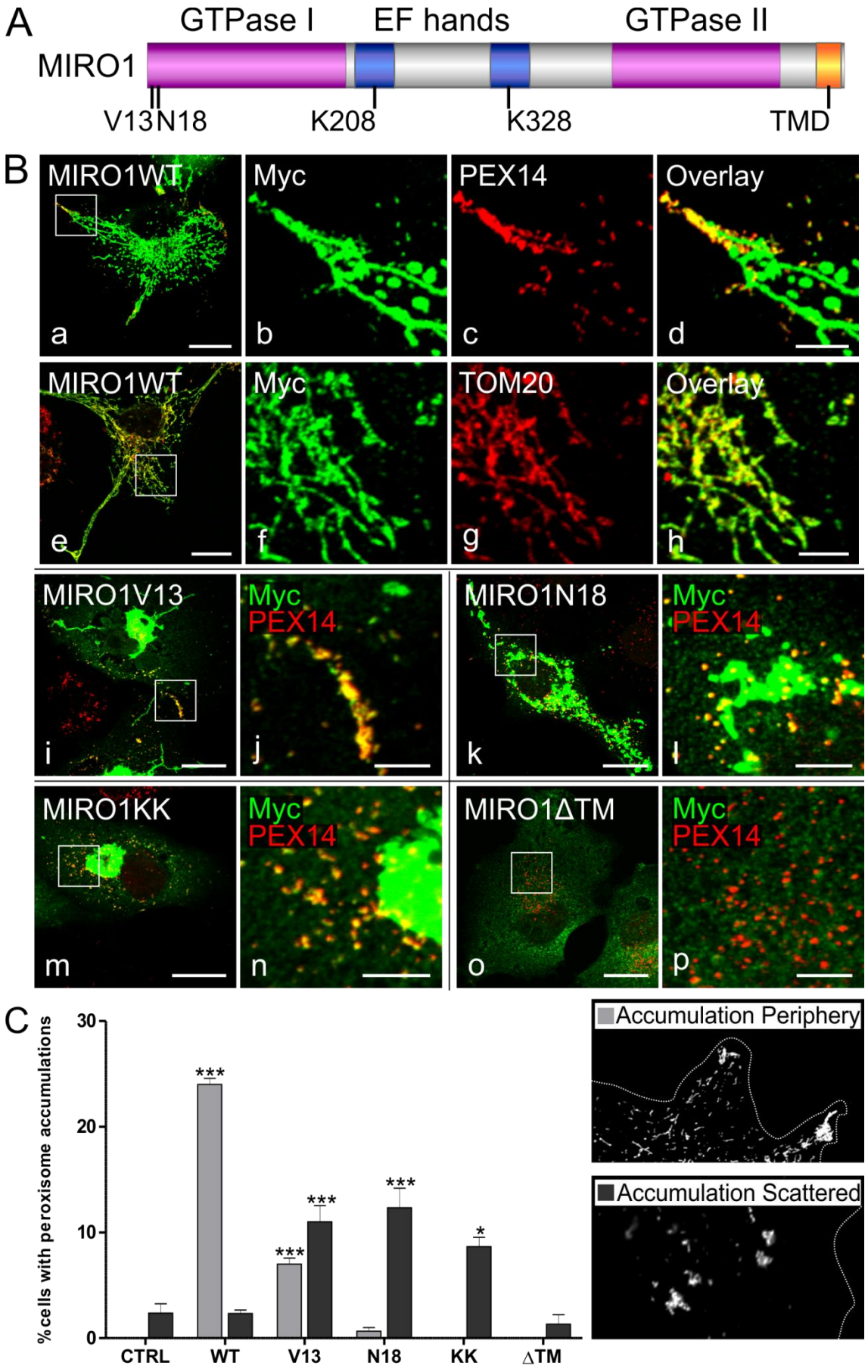
A
GTPase I
EF hands
GTPase II
MIRO1
V13N18
K208
K328
TMD
B
MIRO1WT
Myc
PEX14
Overlay
a
b
c
d
MIRO1WT
Myc
TOM20
Overlay
e
f
g
h
MIRO1V13
Myc
PEX14
i
j
MIRO1N18
Myc
PEX14
k
l
MIRO1KK
Myc
PEX14
m
n
MIRO1ΔTM
Myc
PEX14
o
p
C
% cells with peroxisome accumulations
30
20
10
0
***
***
***
***
*
CTRL
WT
V13
N18
KK
ΔTM
Accumulation Periphery
Accumulation Scattered

Figure 4.2 – Myc-MIRO1 is targeted to peroxisomes and alters their distribution. (A) Schematic view of MIRO1 domains and mutation sites. (B) COS-7 cells were transfected by turbofect with myc-MIRO1WT (a-h), myc-MIRO1V13 (i-j), myc-MIRO1N18 (k-l), myc-MIRO1KK (m-n) and myc-MIRO1ΔTM (o-p). Fixed cells were labelled with anti-myc, anti-PEX14 (peroxisomes) and anti-TOM20 (mitochondria). Expressed myc-MIRO1WT localizes to peroxisomes and mitochondria, and alters their distribution (a-h). All of the expressed mutants show peroxisomal (and mitochondrial) localisation, except for the myc-MIRO1ΔTM which shows a cytosolic staining. All images are confocal. Scale bars: overview 20 µm, magnification 5 µm. (C) Quantitative analysis of peroxisomal distribution in control cells (no plasmid) and cells expressing different myc-MIRO1 plasmids. Cells with peroxisome accumulations in the periphery or scattered were counted. Values represent mean ± SEM of three independent experiments (100 replicates per experiment – total 300 cells per condition; ** $p<0.01$; *** $p<0.001$; one-way ANOVA with post hoc Tukey test against control cells).

information (Figure 4.3A). Our first strategy was to insert MIRO1 into the GFP-ACBD5^{TMD-T} plasmid (see chapter 3), creating a GFP-tagged MIRO1 (GFP-MIRO1WT-PO). Additionally, we exchanged the GFP-tag with the myc-MIRO1 protein, creating myc-MIRO1WT-PO. Expression of both proteins led to a re-distribution of peroxisomes to the cell periphery, confirming our previous results (Figure 4.3B). However, dual targeting to mitochondria and peroxisomes was still observed in several cells, particularly in cells with higher expression. Additionally, an increase in elongated peroxisomes was observed with the expression of GFP-MIRO1WT-PO, suggesting that the N-terminal tag could be affecting peroxisome membrane dynamics (Figure 4.3B).

To overcome these issues, a second strategy was employed using a previously described PEX26/ALDP construct (Halbach et al., 2006). This fusion protein contains two PEX19 binding domains and two TMDs, and it has been shown to target GFP exclusively to peroxisomes (Figure 4.3A). Expression of the resulting myc-MIRO1WT-Pex protein in COS-7 cells revealed an exclusively peroxisomal targeting, with no effects on mitochondrial morphology and distribution (Figure 4.3C). In agreement with the dually targeted versions, expression of the myc-MIRO1WT-Pex and myc-MIRO1V13-Pex induced the accumulation of peroxisomes in the cell periphery, and expression of myc-MIRO1N18-Pex and myc-MIRO1KK-Pex led to the formation of scattered

aggregates in the cell (Figure 4.3D, E). This effect was much more pronounced with the myc-MIRO1-Pex proteins than with the dually targeted myc-MIRO1 (Figure 4.2C and Figure 4.3E). Additionally, peroxisomal proliferation was observed in some cells expressing myc-MIRO1WT-Pex and myc-MIRO1V13-Pex, whereas others expressing myc-MIRO1N18-Pex and myc-MIRO1KK-Pex had lower number of peroxisomes. Organelle quantification was hindered by the overlap of peroxisomes at the periphery and in intracellular aggregates, but examples of these can be seen in figure 4.3D (e.g. myc-MIRO1V13-Pex and myc-MIRO1N18-Pex). These effects suggest that, similarly to the role on mitochondria, MIRO1 could be affecting peroxisome motility and as a result the position of this organelle in the cell.

4.2.3. MIRO1 expression regulates peroxisome distribution in a microtubule-dependent manner

MIRO1 is part of a protein complex that includes both kinesin and dynein motors and promotes mitochondrial movement through the microtubule cytoskeleton (reviewed in Devine et al., 2016). To test if the effect of MIRO1 expression on peroxisome distribution is due to microtubule-dependent motility, COS-7 cells were transfected with myc-MIRO1WT-Pex and treated with the microtubule-depolymerizing drug nocodazole. After a 1 hour treatment, the majority of cells expressing myc-MIRO1WT-Pex no longer presented peroxisome accumulations at the cell periphery. After 4 hours no cells could be found with these accumulations (Figure 4.4A), suggesting that microtubule stability is necessary for the formation and maintenance of peroxisome accumulations at the cell periphery. Additionally, microtubule depolymerisation induced peroxisome elongation in several cells, as exemplified in the control cells (Figure 4.4A) and as previously described (Schrader et al., 1996).

To quantify the effect of MIRO1 expression on peroxisome motility, live-cell imaging experiments were performed to track peroxisome movement over time. For this, COS-7 cells were dually transfected with myc-MIRO1V13-Pex and GFP-SKL (peroxisome marker) and imaged using a spinning disc microscope. This system allowed us to improve time resolution compared with previous studies. To analyse this data systematically, a tracking algorithm was developed

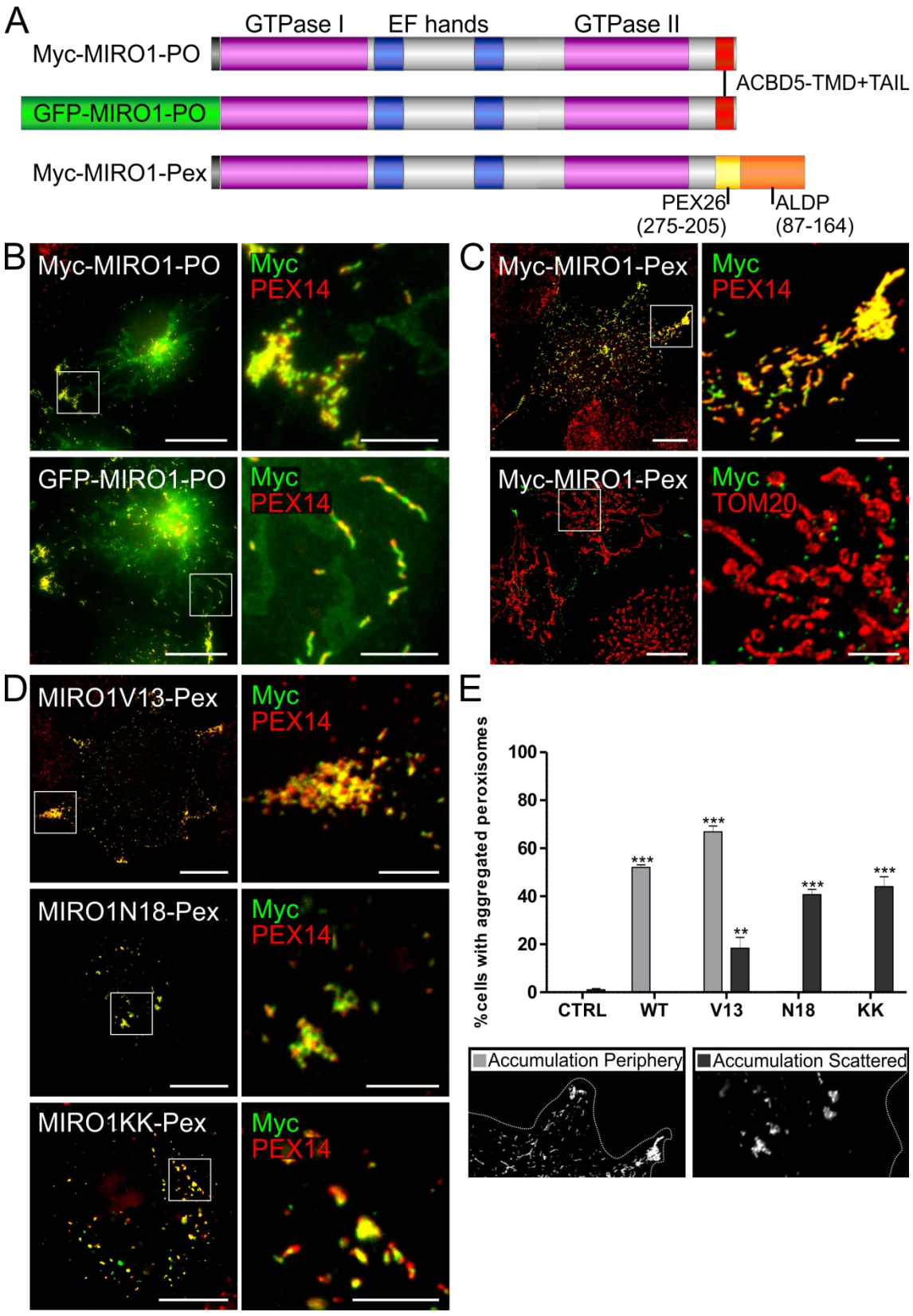

Figure 4.3 – Myc-MIRO1-Pex is exclusively targeted to peroxisomes and alters their distribution in COS-7 cells. (A) Cloning strategies to target MIRO1 exclusively to peroxisomes. The TMD and tail region of MIRO1 was substituted by i) the TMD and tail of the peroxisomal TA protein ACBD5, or ii) a PEX2626/ALDP fusion domain which has been previously shown to target GTP to peroxisomes (Halbach et al., 2006). (B-D) COS-7 cells were transfected with

GFP- or myc-tagged MIRO1 using turbofect and fixed after 24h. Cells were stained against myc, PEX14 and TOM20. (B) GFP- and myc-MIRO1WT-PO were targeted to peroxisomes in all cells and altered peroxisome distribution. However, weak mitochondrial staining was present in several cells, and increased peroxisome elongation was observed with the expression of GFP-MIRO1-PO. (C) Myc-MIRO1WT-PEX was exclusively targeted to peroxisomes and induced their re-distribution to the cell periphery without affecting mitochondrial morphology and distribution. (D) Mutated myc-MIRO1-Pex proteins were exclusively targeted to peroxisomes and induced the formation of peroxisomes accumulations in the cell periphery (V13) or scattered (V13, N18 and KK). (B) is epifluorescence and (C-D) are confocal microscopy. Scale bars: overview 20 µm, magnification 5 µm (E) Quantitative analysis of peroxisomal distribution in cells expressing different myc-MIRO1-Pex plasmids. Cells with peroxisome accumulations in the periphery or scattered were counted. Values represent mean ± SEM of three independent experiments (100 replicates per experiment – total 300 cells per condition; * $p<0.05$; ** $p<0.01$; *** $p<0.001$; one-way ANOVA with post hoc Tukey test against control cells).

by Jeremy Metz (Biomedical informatics hub analyst) to identify and follow individual peroxisomes, providing us with information on the speed of motile organelles. The myc-MIRO1V13-Pex plasmid was used due to its strong induction of peroxisome accumulations in the cell periphery. Figure 4.4 B shows the cumulative distribution function (CDF) for each group of cells. This function shows the distribution of the total population of peroxisomes (1.0), and each value of the curve corresponds to a single organelle movement. The total number of movements is aligned by increasing speeds to give the CDF. For this analysis, all speed values above 0.24 µm/s were considered microtubule dependent-movements as previously described (Bonekamp et al., 2012). A clear increase in the number of fast moving peroxisomes can be observed in cells expressing myc-MIRO1V13-Pex (Supp. Movie S1 and S2). Whereas in control cells the mean number of peroxisomes moving via microtubules was 5.23 ± 0.66 %, in cells expressing myc-MIRO1V13-Pex this number increased to 13.99 ± 2.04 % (Figure 4.4C). The variation observed between cells expressing MIRO1 is likely a result of different levels of protein expression. Additionally, a close analysis of the peroxisomes accumulated at the cell periphery revealed that while the organelles seem to be confined to a relatively restricted area of the cell, peroxisomes regularly move within these structures, revealing very dynamic interactions (Supp. Movie S3).

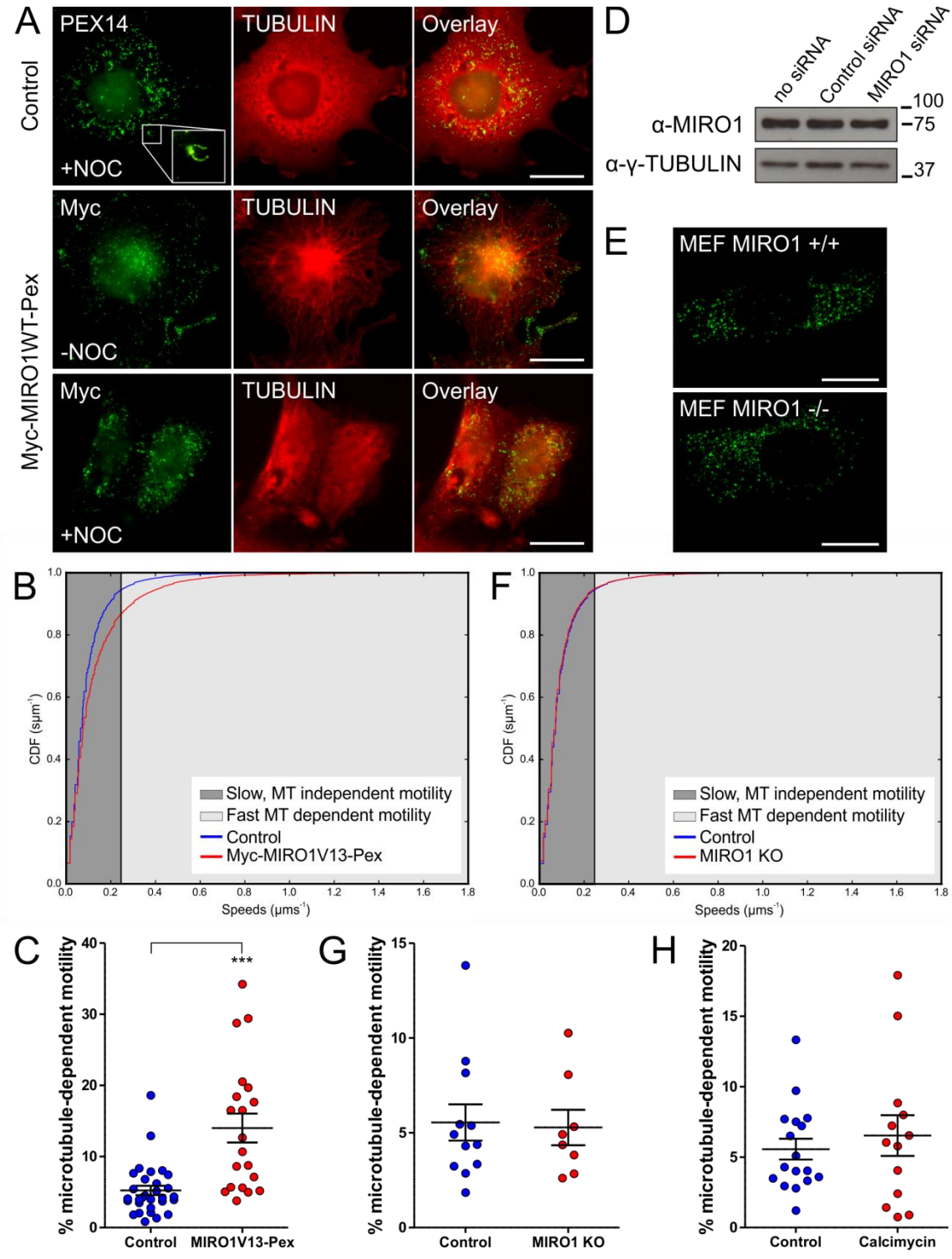

Figure 4.4 – MIRO1 expression increases microtubule-dependent peroxisome motility in COS-7 cells. (A) COS-7 cells were transfected with myc-MIRO1WT-Pex and, after 24 hours, treated with 10 μM nocodazole or DMSO (control), for 4 hours. Fixed cells were stained against myc (green) and TUBULIN (red). Cells expressing myc-Miro1WT-Pex no longer showed aggregates at the cell periphery after treatment with nocodazole. (B-C) COS-7 cells were transfected with myc-Miro1V13-Pex and GFP-SKL and seeded in glass-bottom dishes prior to imaging. For each cell analysed, 500 stacks of 5 planes were obtained over time, and peroxisomes were detected and tracked

using an automated algorithm and manually checked. (B) Cumulative distribution function (CDF) of control (blue line) and myc-MIRO1V13-Pex expressing cells (red line), plotted against peroxisome speed. A threshold of 0.24 µm/s was defined for microtubule dependent-motility (Bonekamp et al., 2012). There is a clear increase in the number of peroxisomes moving in a fast directed motion, suggestive of microtubule-dependent motility. (C) Percentage of fast moving peroxisomes per cell in control (5.23 ± 0.66) and myc-MIRO1V13-Pex cells (13.99 ± 2.04). Values represent mean ± SEM of 20 to 30 cells obtained in three independent experiments (*** $p<0.001$; two-tailed unpaired t-test against control cells). (D) Silencing of MIRO1 in HepG2 cells after 72 hours transfection with lipofectamine 3000. (E) Control and MIRO KO MEFs were transfected by microporation with GFP-SKL and fixed after 24 hours. No differences in peroxisome morphology and distribution were observed. (F-G) Control and MIRO1 KO MEFs were transfected with GFP-SKL and seeded in glass-bottom dishes prior to imaging. For each cell analysed, 250 stacks of 9 planes were obtained over time. (F) CDFs of control (blue line) and MIRO1 KO cells (red line), plotted against peroxisome speed. No changes in peroxisome motility were observed in the absence of MIRO1. (G) Percentage of fast moving peroxisomes per cell in control (5.54 ± 0.95) and MIRO1 KO cells (5.28 ± 0.93). Values represent mean ± SEM of 8 to 12 cells obtained in 1 experiment. (H) Percentage of fast moving peroxisomes per cell in control (5.57 ± 0.74) and calcimycin treated cells (6.54 ± 1.44). Values represent mean ± SEM of 13 to 17 cells obtained in 2 experiments (A-E) All images are from epifluorescence microscopy. Scale bars: 20 µm.

To further analyse the effects of MIRO1 on peroxisome motility, we aimed to silence this protein in HepG2 cells (Figure 4.4D). However, after several attempts using two different pools of MIRO1 siRNA (see table 2.7) and different concentrations, we were unable to silence this protein. As a control for the silencing procedure, additional proteins were successfully silenced using the same procedure (not shown). To overcome this issue, we examined peroxisome distribution and motility in MIRO1 KO MEFs (Figure 4.4E-G). These cells, which were initially described by the Nguyen et al., have an altered mitochondrial distribution but no alterations of peroxisome morphology and distribution (Nguyen et al., 2014). In agreement, we did not find any alterations in peroxisome distribution (Figure 4.4E) nor motility (Figure 4.4F-G) (Supp. Movie S4 and S5). Finally, as MIRO1 has been described as a calcium sensing protein, inhibiting mitochondrial motility in conditions of high cytosolic Ca^{2+} concentrations, we tried to verify if the same was true for peroxisomes. To test this, we treated COS-7 cells with the calcium ionophore calcimycin for 10

minutes prior to imaging, which should lead to an influx of calcium from the growing medium to the cells (Huber et al., 1997; Wang and Schwarz, 2009). However, we were unable to see any changes of peroxisome motility in COS-7 cells using this method (Figure 4.4H). Furthermore, treatment with this ionophore, even at low concentrations, increased cell death, as observed during live-cell imaging.

4.2.4. MIRO1 expression in fibroblasts induces organelle proliferation

Protein expression and regulation can vary between different cell types, stressing the need to test different conditions when characterising protein function. For example, whereas early studies on MIRO1 in COS-7 cells suggested a role for it in apoptosis (Fransson et al., 2003), later studies identified its role in mitochondrial motility in cardiomyocytes and neuronal cells (MacAskill et al., 2009b; Saotome et al., 2008; Wang and Schwarz, 2009). To further analyse MIRO1 and its function at peroxisomes, we expressed myc-MIRO1WT-Pex in primary human skin fibroblasts (C109) and looked at its effect after 24 hours (Figure 4.5A). Surprisingly, in these cells peroxisomes did not accumulate at the cell periphery but instead proliferated, presenting a significantly higher number of peroxisomes when compared with control cells (Figure 4.5A, B). Additionally, peroxisome motility was also significantly higher (Figure 4.5C, D) (Supp. Movie S6 and S7), suggesting that organelle proliferation could be a result of increased motility. As the mean peroxisome motility in control fibroblasts is lower than in control COS-7 cells (4.51 ± 0.43 vs 5.23 ± 0.66 %), this could also point to the presence of stronger peroxisomal tethers in fibroblasts or differences in motility regulation. To further analyse this, we expressed myc-MIRO1WT-Pex in two patient cell lines with altered peroxisome number, size and motility. ΔPEX5 and ΔPEX14 fibroblasts lack matrix protein import, and have less and larger peroxisomes. Additionally, ΔPEX14 patient fibroblasts have been described as lacking peroxisome motility (Bharti et al., 2011). Expression of myc-MIRO1WT-Pex in both ΔPEX5 and ΔPEX14 cells induced peroxisome proliferation (Figure 4.5B, E, F), creating a mixed population of large and small peroxisomes. Similarly to C109 cells, MIRO1 expression also significantly increased organelle motility (Figure 4.5D) (Supp. Movie S8-11), most prominently in the smaller peroxisomes. It should be

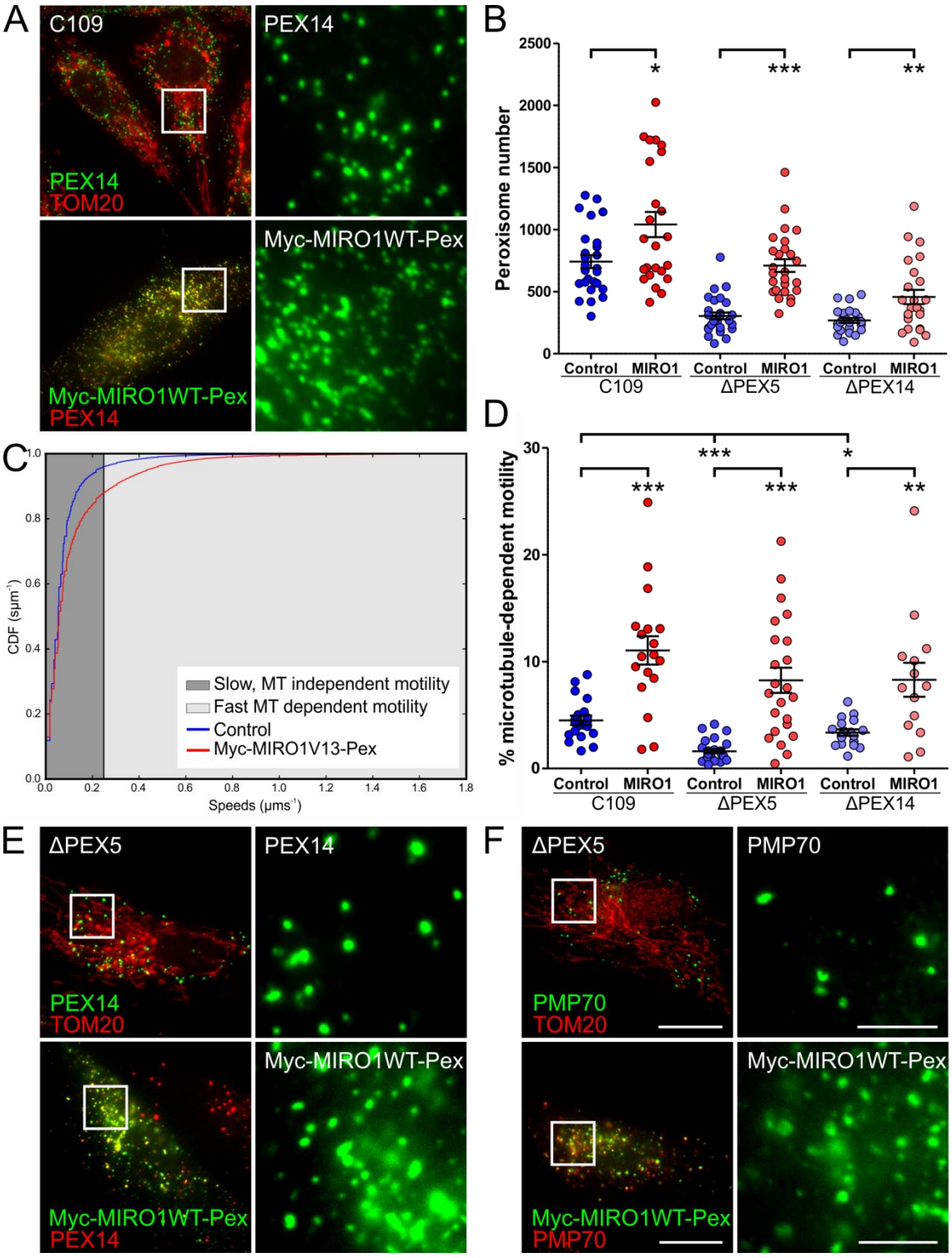

Figure 4.5 – MIRO1 expression induces peroxisome proliferation in human skin fibroblasts. (A) C109 cells were transfected with myc-MIRO1WT-Pex by microporation and fixed after 24 hours. Cells were stained against PEX14, TOM20 and myc. Expression of myc-MIRO1WT-Pex significantly increased the number of peroxisomes. (B) Quantitative analysis of peroxisome number in C109, ΔPEX5 and ΔPEX14 cells. In all tested fibroblast cell lines, expression of myc-MIRO1WT-Pex significantly increased peroxisome number: C109 – 741 ± 53 vs 1040 ± 101, ΔPEX5 – 304 ± 27 vs 710 ± 51, and ΔPEX14 – 268 ± 18 vs 457 ± 58. Values represent mean ± SEM of 24 to 29 cells obtained from three

independent experiments. (C-D) Human skin fibroblasts were transfected with GFP-ACBD5^{TMD-T} (peroxisome membrane marker) on its own, or co-transfected with myc-MIRO1WT-Pex, and seeded in glass-bottom dishes prior to imaging. For each cell analysed, 250 stacks of 9 planes were obtained over time, and peroxisomes were detected and tracked using an automated algorithm and manually checked. (C) Cumulative distribution function (CDF) of control (blue line) and myc-MIRO1WT-Pex expressing (red line) C109 cells, plotted against peroxisome speed. Microtubule dependent-motility was defined above 0.24 µm/s (Bonekamp et al., 2012). There is a clear increase in the number of peroxisomes moving in a fast directed motion, suggestive of microtubule-dependent motility. (D) Percentage of fast moving peroxisomes per cell in control and myc-MIRO1WT-Pex expressing fibroblasts. In all tested cell lines, peroxisome motility was significantly increased upon MIRO1 expression: C109 – 4.51 ± 0.43 vs 11.05 ± 1.32, ΔPEX5 – 1.61 ± 0.20 vs 8.25 ± 1.17, ΔPEX14 – 3.36 ± 0.30 vs 8.30 ± 1.59. Values represent mean ± SEM of 14 to 26 cells obtained in three independent experiments. (E-F) ΔPEX5 and ΔPEX14 cells were transfected with myc-MIRO1WT-Pex by microporation and fixed after 24 hours. Cells were stained against PEX14, PMP70, TOM20 and myc. Expression of myc-MIRO1WT-Pex significantly increased the number of peroxisomes. All images are from epifluorescence microscopy. Scale bars: overview 20 µm, magnification 5 µm. (B-D) * $p<0.05$; ** $p<0.01$; *** $p<0.001$; one-way ANOVA with post hoc Tukey test against control cells.

noted that, since these fibroblasts have defects in matrix protein import, a different organelle marker was used to observe peroxisomes by live-cell imaging. For these experiments we expressed GFP-ACBD5^{TMD-T} in both patient and control fibroblasts. Although expression of this membrane marker had no effects on peroxisome motility when compared to GFP-SKL in C109 fibroblasts (not shown), some peroxisomal proliferation was observed, particularly in ΔPEX5 and ΔPEX14 patient fibroblasts.

4.2.5. MIRO1 expression in patient fibroblasts induces the formation of organelle elongations

In addition to its effect on peroxisome number and motility, MIRO1 expression in patient fibroblasts induced the formation of peroxisome elongations (Figure 4.6). As shown in figure 4.6A, expression of myc-MIRO1WT-Pex in ΔPEX5 cells induced the formation of long peroxisomal structures, usually following straight lines with sporadic bends, suggestive of an organelle following one or several

microtubules. To test this hypothesis, ΔPEX5 cells expressing myc-MIRO1WT-Pex were fixed with methanol and paraformaldehyde, and co-stained with tubulin to mark microtubules (Figure 4.6B). In these conditions, several of the observed elongations were co-localising with microtubules, suggesting that their formation could be a result of a motor force pulling peroxisomes by moving through microtubules. Furthermore, whereas myc-MIRO1WT-Pex appears homogeneously distributed over the length of the elongation, PEX14 is more strongly accumulated at one of the extremities, suggesting that these elongations extend from a large peroxisome, and might give rise to new organelles (Figure 4.6A). To verify this, we re-analysed the data obtained for the motility analysis and examined the formation of these structures. A time-lapse analysis of this motility showed that peroxisome elongations originate from large peroxisomes, can grow at varying speeds and generally form relatively straight lines in a single direction (Figure 4.6C, D) (Supp. Movie S12 and S13). These elongations can sometimes quickly retract, suggesting that the peroxisomal membrane has elastic properties (Figure 4.6C, D). A meticulous analysis of all the videos previously acquired showed that these elongations are formed both in ΔPEX5 and ΔPEX14 patient fibroblasts, albeit more frequently in ΔPEX5 (Figure 4.6E). Additionally, expression of myc-MIRO1WT-Pex significantly increased the length of these elongations in ΔPEX5 cells but not in ΔPEX14 cells, suggesting that the PEX14 absence could be interfering with the stability of elongated peroxisomal structures.

4.3. Discussion

Organelles move within (and between (Ahmad et al., 2014)) cells in order to perform localised functions, communicate with other organelles, and to enable segregation during cell division (Jongsma et al., 2015; Sheng and Cai, 2012). Whereas peroxisome motility is a well described process in yeast, showing its importance for organelle inheritance, little is known about its function and regulation in mammalian cells (Knoblach and Rachubinski, 2016; Neuhaus et al., 2016). Having a clear picture of how peroxisome motility is regulated in mammalian cells would not only contribute to our understanding of this organelle, but also provide us with tools to further analyse peroxisomes and their role in the cellular environment. Here we show that the Ras GTPase

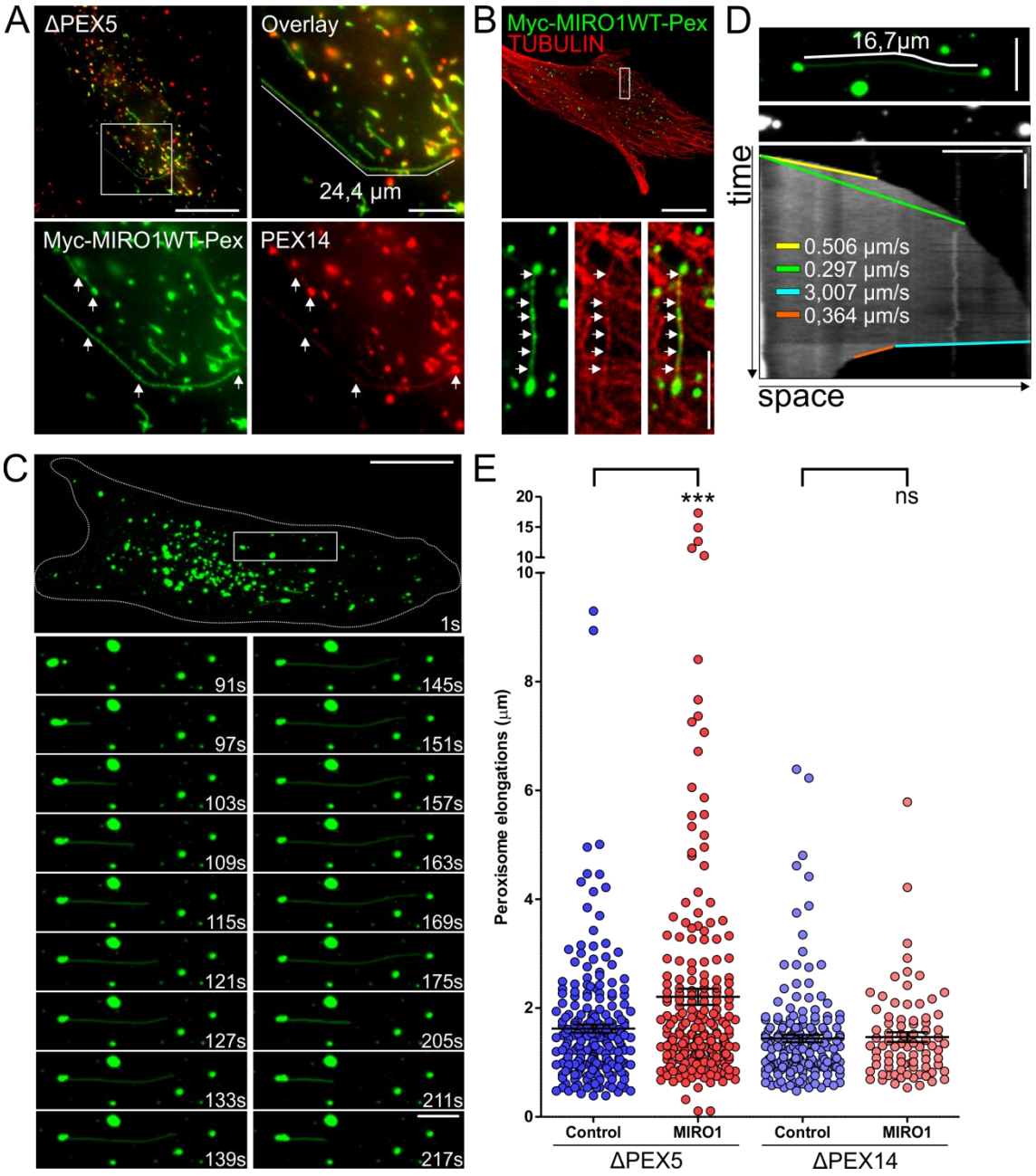

Figure 4.6 – Expression of MIRO1 increases the length of peroxisomal elongations in ΔPEX5 patient fibroblasts. (A-B) ΔPEX5 patient fibroblasts were microporated with myc-MIRO1WT-Pex and fixed after 24 hours. (A) Cells were stained against myc and PEX14. The majority of observed elongations in fixed cells show an evenly distributed myc-MIRO1 signal, likely originating from a large peroxisome as shown by the strong PEX14 staining at one of the extremities. (B) ΔPEX5 cells were fixed using methanol (see 2.5) and stained against PEX14 and TUBULIN. Elongated peroxisomal structures were usually found overlaying microtubules. (C-D) ΔPEX5 patient fibroblasts were transfected with GFP-ACBD5^{TMD-T} (peroxisome membrane marker) and myc-MIRO1WT-Pex, and seeded in glass-bottom dishes prior to imaging. (C) Time lapse of peroxisome elongation forming and retracting in a ΔPEX5 cell expressing GFP-ACBD5^{TMD-T} and myc-MIRO1WT-Pex. (D) Kymograph of peroxisome elongation observed in (C). Scale bars: 20 seconds (vertical), 5 µm

(horizontal). (E) Quantitative analysis of peroxisome elongation length in ΔPEX5 and ΔPEX14 cells. Expression of myc-MIRO1WT-Pex significantly increased the length of peroxisomal elongations in ΔPEX5 cells (1.62 ± 0.08 vs 2.21 ± 0.15), but not in ΔPEX14 cells (1.44 ± 0.07 vs 1.47 ± 0.09). Values represent mean ± SEM of measurements made in 22 to 29 cells obtained from three independent experiments (*** $p<0.001$; two-tailed unpaired t-test against control cells). (A) is epifluorescence, (B) confocal and (C) spinning disc microscopy. Scale bars: overview 20 µm, magnification 5 µm.

MIRO1 is a peroxisomal TA protein, and that it plays a role in peroxisome microtubule-dependent motility. Furthermore, we propose that peroxisome motility contributes to the formation of new peroxisomes, likely playing an important role in peroxisome inheritance in mammalian cells.

4.3.1. Where is MIRO1 targeted to?

Reports have shown that Miro proteins are targeted to mitochondria in several organisms from yeast, to plants and mammals, and play key roles in this organelle's motility and homeostasis (reviewed in Yamaoka and Hara-Nishimura, 2014). Due to its topological grouping within the TA proteins, we expressed and analysed the localisation of MIRO1. Interestingly, expressed myc-MIRO1 was not only targeted to mitochondria but also to peroxisomes (see Figure 3.1). Analysis of the localisation of the endogenous protein in both HepG2 cells and highly purified peroxisome fractions from rat liver confirmed these results (Figure 4.1). Strangely, the two antibodies used in these experiments recognised difference subcellular structures in HepG2 cells. This could be due to the existence of two (or more) protein isoforms localised to different organelles, each of which is recognized by one antibody. However, both antibodies recognize partly overlapping sequences at the N-terminus, and should be able to recognize all of the currently identified MIRO1 isoforms (not shown). Another hypothesis could be that one of the antibodies is specifically recognizing a post-translationally modified isoform specific to one of the organelles. It would be interesting to clone and express different isoforms of MIRO1 to test if all are dually targeted to peroxisomes and mitochondria, and if they are differently recognised by each antibody. Furthermore, MIRO1 was found to interact with the peroxisomal chaperone PEX19 by co-

immunoprecipitation. It should be noted that, similarly to previous PEX19-TA protein co-IP experiments (Delille and Schrader, 2008), a cross-linking reagent was used to stabilise the PEX19-MIRO1 interaction. Further experiments to confirm this interaction should be performed, in particular in the absence of cross-linker. Nevertheless, this result further strengthens the hypothesis that endogenous MIRO1 is targeted to peroxisomes, and that peroxisomal TA proteins are targeted to this organelle by the same pathway as several other peroxisomal membrane proteins (Giannopoulou et al., 2016). It would be interesting to further investigate the biochemical interaction of PEX19 and MIRO1, and to see if the same domains that are responsible for the recognition and targeting of PMPs also interact with MIRO1.

4.3.2. What is MIRO1's role at peroxisomes?

Several studies have characterised the role of MIRO1 on mitochondrial motility in mammalian cells (reviewed in Devine et al., 2016). However, other roles in mitochondrial homeostasis and calcium regulation have also been suggested (Chang et al., 2011; Frederick et al., 2004). Furthermore, MIRO1 has been shown to interact with several proteins such as MFN1, MFN2 and ARMC3, without clear functions associated with these interactions (López-Doménech et al., 2012; Misko et al., 2010). As shown in figures 4.2 and 4.3, expression of myc-tagged MIRO1 in COS-7 cells had a clear effect on peroxisome distribution, leading to peroxisome accumulations both at the cell periphery and within the cell, depending on which version of the protein was expressed. Since the expression of myc-MIRO1 had strong effects on mitochondrial morphology and cellular homeostasis, we created an exclusively peroxisomal version of MIRO1 (myc-MIRO1-Pex), which enabled us to clearly analyse the effects of MIRO1 expression on peroxisomes. This was done by substituting the TMD and tail of MIRO1 by a PEX26/ALDP construct, with two TMDs and two PEX19 binding sites. This strategy altered the topology of MIRO1, which could have an effect on the protein's function or ability to interact with other proteins. Furthermore, despite the effects observed on peroxisome motility, which are in agreement with a cytosolic orientation of MIRO1 in the Pex constructs, an analysis of protein topology should be performed to confirm the localisation of the N and C terminus of this protein.

Our attempt to maintain MIRO1 as a TA protein by changing its C-terminus to that of the peroxisomal ACBD5 led to a high number of cells with mitochondrial targeting. This could be due to: 1) the presence of additional targeting information in MIRO1 that enables some of the expressed protein to target mitochondria; 2) ambiguity in the targeting information present at ACBD5's TMD and tail fragment, as observed by the expression of GFP-ACBD5^{TMD-T}, which is dually targeted to peroxisomes and mitochondria in ~15% of cells (see Figure 3.4); 3) an overload of the targeting system due to protein overexpression, which could allow mistargeting to other organelles. As a mechanism for the degradation of mistargeted TA proteins at mitochondria has been described (see 1.2.2) (Chen et al., 2014b; Okreglak and Walter, 2014), it would be interesting to test if expression of ATAD1 in these cells would induce the degradation of myc/GFP-MIRO1WT-PO at mitochondria.

Since expression of myc-MIRO1WT-Pex led to the accumulation of peroxisomes at the cell periphery, this would suggest that MIRO1 plays a similar role at peroxisomes as that of mitochondria, increasing microtubule plus-end directed motility. In agreement with this, similar peroxisome accumulations have been previously observed using an inducible cargo assay where kinesin motors are artificially tagged to peroxisomes in a regulated and inducible manner (Kapitein et al., 2010). Expression of a mutated MIRO1 protein, which is constitutively active at the first GTPase domain (myc-MIRO1V13-Pex), further increased the number of cells with peroxisome accumulations at the cell periphery (Figure 4.3E). Although still poorly understood, as MIRO1's first GTPase domain enables its interaction with TRAK proteins (Fransson et al., 2006), expression of WT and a constitutively active protein might favour the activity of the motility complex.

Concurrently, expression of a dominant negative mutant for the first GTPase domain (myc-MIRO1N18-Pex) led to the formation of peroxisome accumulations within the cell, and at times closer to the nucleus. This could point to either a defect/loss of motility, or an increase in minus-end directed motility (dynein-dependent), which has also been previously shown to depend on the MIRO1/TRAK complex (Morlino et al., 2014; van Spronsen et al., 2013). Since several cells expressing this protein also appeared to have less peroxisomes, it might be that an inactive MIRO1 at the first GTPase inhibits

peroxisome motility, which could either prevent peroxisome growth and division, or signal for peroxisome degradation. This can to some extent mimic the phenotypes present in some peroxisome patient fibroblasts, where a reduced number of peroxisomes and altered distribution has been associated with motility defects (Nguyen et al., 2006).

Lastly, expression of myc-MIRO1KK-Pex, a mutant for both calcium binding EF-hands, had a very similar phenotype to myc-MIRO1N18-Pex, suggesting that the proteins inability to bind calcium could also inhibit organelle motility. These two mutants were also previously shown to induce similar phenotypes on mitochondria in COS-7 cells (Fransson et al., 2006). Further studies should be performed to analyse the effect of these mutants on peroxisomes in neuronal cells. In these, expression of the WT and dominant negative mutant induces a similar phenotypes on mitochondrial motility and distribution in these cells, whereas the expression of constitutively active MIRO1 appears to decrease the number of moving mitochondria in axonal processes (MacAskill et al., 2009a).

To confirm that the changes observed on peroxisome distribution were due to microtubule-dependent motility, we treated cells expressing myc-MIRO1WT-Pex with nocodazole (Figure 4.4). In these cells, peroxisomes were no longer accumulated at the cell periphery, confirming that this effect in dependent on the microtubule cytoskeleton. Similar experiments should be performed using myc-MIRO1N18-Pex and KK-Pex, to test if the peroxisome accumulations observed in these cells start to disperse after a few hours or if, for example, peroxisomes proliferate. Furthermore, a live-cell imaging approach was used to track the movement of individual peroxisomes. Expression of myc-MIRO1-V13-Pex in COS-7 cells induced a significant increase in the number of fast-moving peroxisomes, strengthening the view that organelle accumulation at the periphery is due to an increase in anterograde transport. To complement these observations, we tried to knockdown MIRO1 in HepG2 cells and analyse if there were any changes in peroxisome distribution and motility. Unfortunately, despite our attempts (using two different pools of MIRO1 siRNA and different concentrations), we were unable to decrease the levels of this protein (Figure 4.4D). To overcome this issue, we obtained MEFs of MIRO1 KO mice and analysed both peroxisome distribution and motility in these cells (Figure 4.4E-G). As previously reported, despite the changes in mitochondrial distribution

observed in MIRO1 KO MEFs, no alterations of peroxisome distribution were observed (Figure 4.4E) (Nguyen et al., 2014). Furthermore, we did not detect any changes of peroxisome motility by live-cell imaging. Although unexpected, and to some degree conflicting with our previous results, it should be noted that only a small proportion of peroxisomes present microtubule-dependent motility. If other motility complexes are present at peroxisomes, these could be sufficient to compensate for the absence of MIRO1. For example, MIRO2 also localises to peroxisomes when expressed in COS-7 cells (see Figure 3.1), and might play a similar role on peroxisome motility. Additionally, alternative motility complexes yet unidentified might also contribute to peroxisome motility. An alternative way to analyse the effect of endogenous MIRO1 on peroxisome motility might be to overexpress PEX19. If this protein is the *de facto* chaperone responsible for MIRO1 targeting to peroxisomes, an increase in its availability might shift a higher pool of MIRO1 to peroxisomes and, similarly to the results obtained with myc-MIRO1WT expression, increase plus end directed motility.

MIRO1 has also been described as a calcium sensing protein, inhibiting mitochondrial motility in response to increases in intracellular Ca^{2+} concentration (MacAskill et al., 2009b; Wang and Schwarz, 2009). Additionally, peroxisome motility has been previously shown to cease upon treatment with calcium ionophores, which induce an increase in intracellular calcium (Huber et al., 1997). As this could be due to Ca^{2+} binding by MIRO1, we tried an experimental set up to test the effects of calcium on peroxisome motility in COS-7 cells. Unfortunately, after several tries, we were unable to replicate the previously published results. Further experiments should be performed testing different calcium ionophores, as well as calcium indicator dyes for microscopy.

4.3.3. How does peroxisome motility regulate organelle dynamics?

As previously established, peroxisomes are highly dynamic organelles responding to changes in the cellular environment by adapting their shape, number, localisation and size (Schrader et al., 2016). However, the role of motility in several processes such as peroxisome proliferation, degradation and inheritance is still poorly understood in mammalian cells (Neuhaus et al., 2016). In yeast, motility plays an essential role in peroxisome segregation to the

budding cell, with the inheritance of peroxisomes proteins 1 and 2 (Inp1 and Inp2) playing crucial roles in the maintenance of peroxisomes in the mother cell (Inp1), and the myosin-dependent transport of peroxisomes to the daughter cell (Inp2) (Fagarasanu et al., 2010). Although no homologs for the Inp proteins have been found in mammalian cells, it is likely that peroxisome partitioning during the cell cycle also relies on a cytoskeleton-dependent reorganization of the peroxisomal network, as suggested by observations of peroxisome clusters at spindle poles during metaphase (Knoblach and Rachubinski, 2016; Kredel et al., 2009). However, unlike in yeast, this distribution likely relies on microtubules and associated motor proteins. In line with this, Kanfer et al. have recently described a role for MIRO1 in mitochondrial distribution during the cell cycle, by interacting with the microtubule growing tip associated protein CENP-F (Kanfer et al., 2015). It would be interesting to see if a similar mechanism is regulating peroxisome distribution during the cell cycle.

Another likely role for peroxisome motility is in the formation of new peroxisomes. Although peroxisomes are still able to elongate and divide in the absence of microtubules, as observed when cells are treated with microtubule depolymerising drugs, they are unable to uniformly disperse, forming clusters (Schrader et al., 1996; Wiemer et al., 1997). The peroxisome proliferation observed after myc-MIRO1-Pex expression in human fibroblasts, and to a lesser extent in COS-7 cells, points to a likely role for peroxisome motility in organelle growth and division (Figure 4.5). In these cells, the increase in peroxisomal linkers (i.e. myc-MIRO1WT-Pex) for motor proteins, likely increases the pulling forces exerted on the peroxisomal membrane, leading to its bending and likely facilitating division (Zimmerberg and Kozlov, 2006). This is further strengthened by the observation of peroxisome elongations in ΔPEX5 and ΔPEX14 fibroblasts, which could facilitate peroxisome division by forming narrow tubules for DLP1-dependent division. In these cells, peroxisomes are usually larger and less frequently, likely due to changes in metabolism that alter membrane composition, and peroxisomes ability to divide (Itoyama et al., 2012). This process would explain how these patient fibroblasts can be maintained for several generations while keeping a low but constant pool of peroxisomes. It should be noted that similar peroxisomal elongations have also been observed in plant cells, known as peroxules (Barton et al., 2014). These can form in response to hydroxyl ROS and exposure to UV light (Sinclair et al., 2009), and

have been suggested to play a role in organelle growth and division (Jedd and Chua, 2002), as well as organelle tethering, since peroxule formation allows two organelles to keep interacting despite opposing pulling forces (Gao et al., 2016).

Another interesting observation is the lack of peroxisome accumulations at the cell periphery in human fibroblasts in comparison with COS-7 cells. This suggests that peroxisome motility is differently regulated between cell types. In this case, since peroxisome motility in control fibroblasts appears to be lower than in COS-7 cells, it is possible that peroxisomes are more tethered to microtubules or other organelles in fibroblasts. One such tether could be PEX14 due to its ability to directly interact with TUBULIN (Bharti et al., 2011). In line with this, we saw less elongations in ΔPEX14 cells in comparison to ΔPEX5, suggesting that in the absence of this protein peroxisomes might be less attached to microtubules and consequently less likely to be pulled. When MIRO1 was expressed in these cells, we also did not see an increase in the length of elongations, suggesting that a strong tether is necessary for an opposing motor force to enable the formation of an elongation. Further experiments should be performed with fixed cells to test if elongated peroxisomes in ΔPEX14 cells are also co-localising with microtubules (as performed for ΔPEX5 cells). Nevertheless, expression of MIRO1 still increased peroxisome motility in ΔPEX14 cells, most significantly in small peroxisomes, showing that these organelles are still able to move and their motility can be increased by higher motor recruitment to the organelle.

Chapter 5 – Results

Investigating the role of TRAK1 in peroxisome motility in mammalian cells

5.1. Introduction

As previously described, MIRO proteins are part of a protein complex that regulates mitochondrial (and peroxisomal) motility in mammalian cells. TRAK1 and/or TRAK2 are essential elements of this complex which enable MIRO's interaction with kinesin and dynein motors (van Spronsen et al., 2013), and regulate motility in response to cellular cues, such as an increase in intracellular glucose (Pekkurnaz et al., 2014).

Both TRAK1 and TRAK2 are cytoplasmic proteins which lack any obvious domain structure apart from an N-terminal coiled-coil region homologous to the huntingtin-associated protein 1 (HAP1) domain (Stowers et al., 2002), which can be found in several motor-interacting proteins. These proteins interact directly with the kinesin heavy chain (KHC) to enable cargo transport (Brickley et al., 2005). In addition to mitochondria, TRAK proteins have also been shown to regulate the endocytic traffic of γ-aminobutyric acid type A (GABAA) receptors in mice (Gilbert et al., 2006) and early endosomes (Kirk et al., 2006). Both proteins also interact with β O-linked N-acetylglucosamine transferase, which post-translationally modifies TRAK proteins by glycosylation (Pekkurnaz et al., 2014).

TRAK proteins were initially described in *Drosophila*, where the deletion of their orthologue, dMilton, strongly affects neuronal development by altering mitochondrial motility, with mitochondria accumulating in neuronal cell bodies and being absent from axons and synapses (Glater et al., 2006; Stowers et al., 2002). Additionally, TRAK1 silencing in hippocampal mouse neurons also led to a decrease in mitochondrial motility in the axons (Brickley and Stephenson, 2011). This effect was not observed for TRAK2, pointing to differences in motility regulation between these proteins.

In chapter 4, we showed that MIRO1 is targeted to peroxisomes and plays a role in this organelle's motility. Since TRAK1 forms a complex with MIRO proteins and regulates mitochondrial motility, we looked at its localisation in COS-7 cells and its possible role in peroxisome motility.

5.2. Results

5.2.1. TRAK proteins are targeted to peroxisomes in cells expressing MIRO1

The adaptor protein TRAK1 interacts with KHC, enabling the transport of several cargoes such as mitochondria and endosomes (Brickley and Stephenson, 2011; Kirk et al., 2006). Due to its role in MIRO1-dependent mitochondrial motility, we decided to examine its subcellular localisation in mammalian cells and possible role in peroxisome motility. To do this, GFP-TRAK1 was expressed in COS-7 cells on its own or co-expressed with myc-MIRO1WT and myc-MIRO1WT-Pex (Figure 5.1). As previously described, expression of TRAK1 proteins induced the formation of bulbous and thread-like mitochondria, as well as perinuclear mitochondrial clusters in COS-7 cells (Figure 5.1) (Fransson et al., 2006). When expressed on its own, GFP-TRAK1 was not detected on peroxisomes (Figure 5.1 a-e) and had no effect on peroxisome morphology and distribution. However, when co-expressed with myc-Miro1WT and myc-MIRO1WT-Pex, TRAK1 was targeted to both mitochondria and peroxisomes (Figure 5.1 f-j and p-t). In these cells peroxisome morphology and distribution was identical to that of cells expressing MIRO1 alone, making it difficult to discern any TRAK1-dependent phenotype on peroxisomes. Similar results were obtained upon expression of GFP-TRAK2 in these cells (not shown).

5.2.2. TRAK1 patient fibroblasts have an altered mitochondrial distribution but no effect on peroxisome distribution/motility

TRAK1 appears to play an essential role in mitochondrial motility and, as a result, in neuronal health. Both TRAK1 knockout in *Drosophila* and knockdown in mouse hippocampal neurons had severe effects on mitochondrial distribution and impaired synaptic activity (Brickley and Stephenson, 2011; Stowers et al., 2002). Recently, a patient with a TRAK1 mutation has been identified, who presents severe neurodevelopmental defects (unpublished data). As part of a collaboration with Dr. Yair Anikster (Sheba Medical Center, Israel), we received primary skin fibroblasts from this patient for analysis. Control and patient fibroblasts were fixed and stained using antibodies against PEX14 (peroxisomal

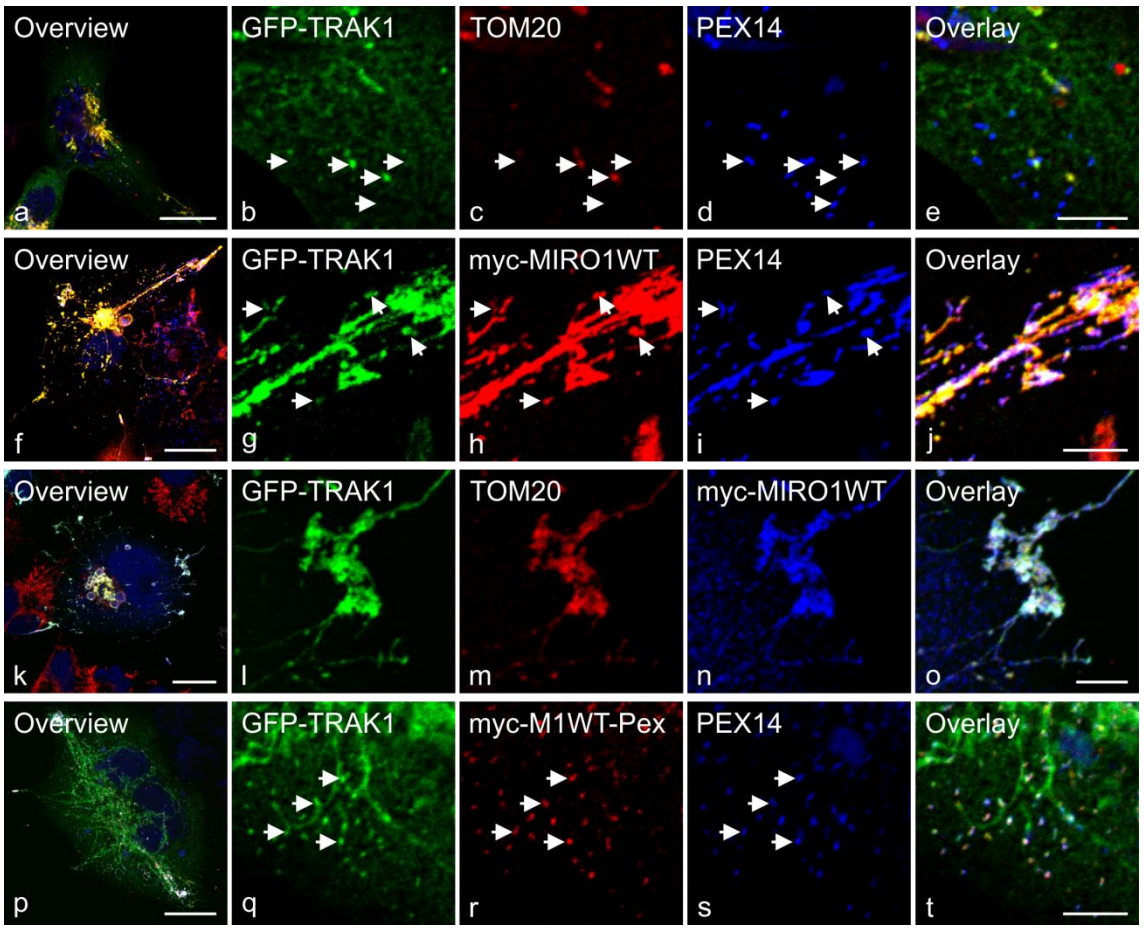

Figure 5.1 – TRAK1 is targeted to peroxisomes when co-expressed with MIRO1. COS-7 cells were transfected by turbofect with GFP-TRAK1 (all), myc-MIRO1WT (f-o) or myc-MIRO1WT-Pex (p-t), and stained with antibodies against myc, TOM20 (mitochondrial marker) and PEX14 (peroxisomal marker). Arrows point to the presence (g-l, q-s) or absence (b-d) of signal co-localisation with peroxisomes. Expressed GFP-TRAK1 is targeted to mitochondria and induces the formation of elongated, globular or clustered networks. GFP-TRAK1 is targeted to peroxisomes in the presence of MIRO1. All images are confocal microscopy. Scale bar: overview 20 µm, overlay 5 µm.

marker) and TOM20 (mitochondrial marker). As shown in figure 5.2A, peroxisomes from patient fibroblasts had a normal morphology and distribution when compared with control cells. Furthermore, no changes in peroxisome number were observed (Figure 5.2B). In contrast, the majority of cells presented an altered mitochondrial distribution, with clustered mitochondria around the nucleus, resembling the phenotype of MIRO1 KO MEFs (Nguyen et al., 2014).

To analyse peroxisome motility, control and patient fibroblasts were microporated with GFP-SKL and imaged using a spinning disc microscope.

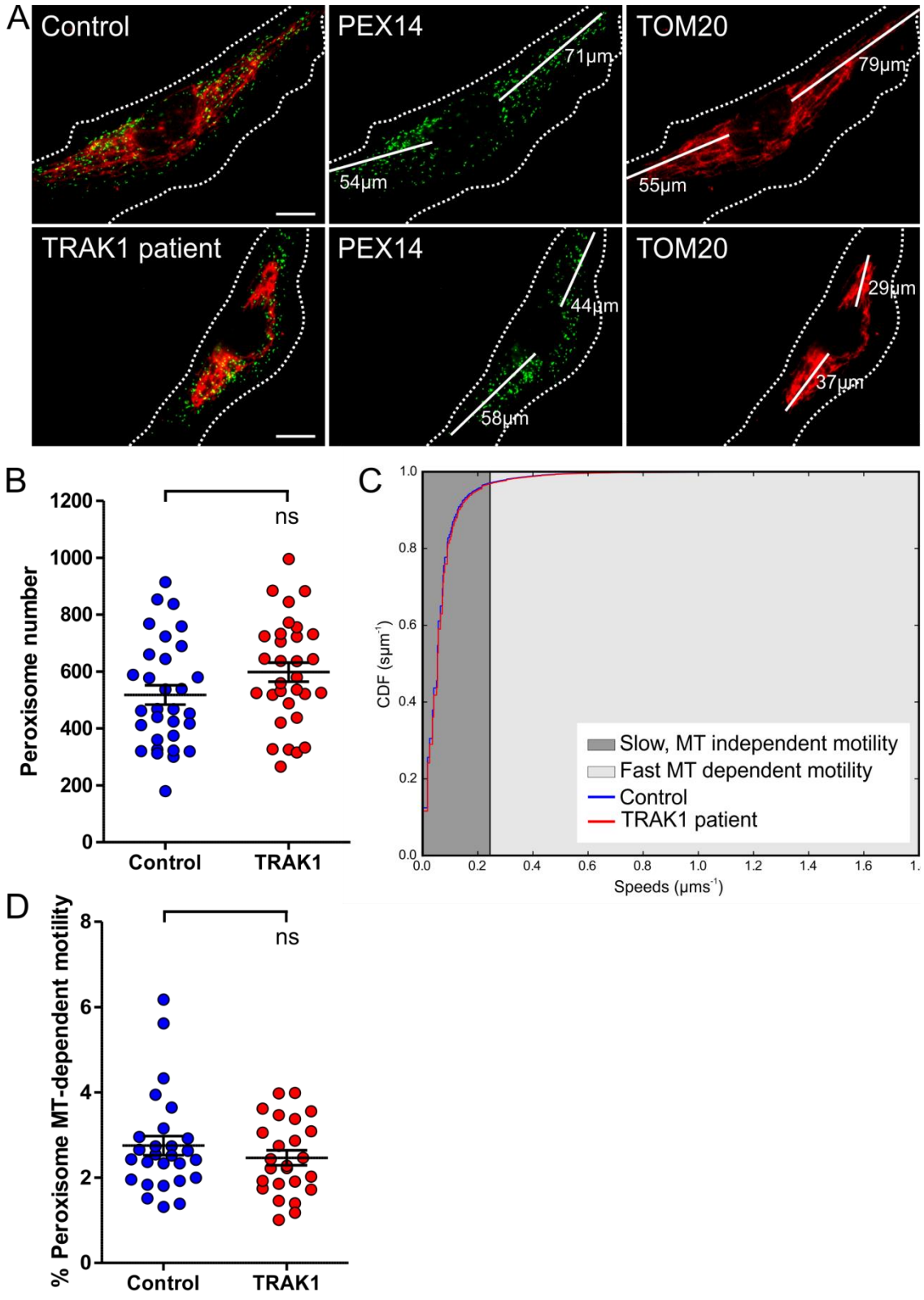

Figure 5.2 – TRAK1 patient fibroblasts maintain normal peroxisome distribution and motility. (A) Control and TRAK1 patient fibroblasts were fixed and stained with antibodies against PEX14 and TOM20. Peroxisomes are uniformly distributed in control and patient cells, reaching the periphery, whereas mitochondria cluster near the nucleus. Representative images depicting organelle distance from the nucleus to the cell periphery. All images are epifluorescence microscopy. Scale bar: 20 µm. (B) Quantitative analysis of

peroxisome number in control and patient fibroblasts. No changes in peroxisome number were observed in patient fibroblasts (518 ± 34 vs 598 ± 33). Values represent mean ± SEM of 31 cells obtained from three independent experiments (C-D) Analysis of peroxisome motility in control and patient cells expressing GFP-SKL. (C) Cumulative distribution function (CDF) of control (blue line) and patient cells (red line), plotted against peroxisome speed. A threshold of 0.24 µm/s was defined for microtubule dependent-motility (Bonekamp et al., 2012). No changes in peroxisome motility were observed between control and patient fibroblasts. (D) Percentage of fast moving peroxisomes per cell in control (2.75 ± 0.22) and patient cells (2.47 ± 0.17). Values represent mean ± SEM of 25 to 27 cells obtained in three independent experiments (ns: not significant; two-tailed unpaired t-test).

Analysis of peroxisome motility revealed no differences in long range, microtubule-dependent motions between controls and patient fibroblasts, in agreement with the immunofluorescence results (Figure 5.2C-D). These observations reveal that a loss of TRAK1 function appears to specifically affect mitochondrial distribution and motility in fibroblasts.

5.3. Discussion

Several proteins have been shown to bind and regulate MIRO function. The most prominent of these, TRAK1 and TRAK2, form a complex with MIRO proteins and molecular motors to enable organelle motility (reviewed in Devine et al., 2016). Due to MIRO1's newly discovered role in peroxisome motility, we decided to analyse if TRAK proteins are also targeted to peroxisomes and a possible role for TRAK1 in peroxisome motility. Expression of either TRAK1 or TRAK2 revealed a mitochondrial localization as previously described (Fransson et al., 2006; MacAskill et al., 2009a). In these cells, no clear co-localization was seen with peroxisomes. This could be due to either a complete absence of TRAK proteins from peroxisomes, or a low abundance of MIRO binding partners at peroxisomes, which would limit the detection of this protein. Since COS-7 have been shown to express low levels of MIRO1 (Fransson et al., 2003), additional studies could be perform using HepG2 cells which have a higher level of endogenous MIRO1. However, a clear peroxisomal localization was seen when GFP-TRAK1 was co-expressed with myc-MIRO1WT and myc-

MIRO1WT-Pex. Co-expression of either MIRO1 plasmids induced the formation of peroxisome accumulations at the cell periphery, without any further observable changes on peroxisome morphology and distribution. Although these results show us that TRAK proteins can be targeted to peroxisomes in the presence of high levels of MIRO1, further studies should be performed to determine if these proteins are *de facto* peroxisomal proteins, or if additional proteins are regulating the MIRO1 motility complex at peroxisomes.

Furthermore, we looked at peroxisome morphology, distribution and motility in TRAK1 patient fibroblasts. In contrast to mitochondria, all peroxisomal parameters analysed were similar to control cells. Although these results further point to the absence of endogenous TRAK1 at peroxisomes, it should be noted that no peroxisomal alterations were observed in MIRO1 KO MEFs. As previously suggested, it is possible that TRAK1 is present at peroxisomes but its role can be compensated for by either TRAK2, or a different motility complex.

Chapter 6 – General discussion

Peroxisomes were initially identified and characterised by Rhodin and De Duve more than 50 years ago (De Duve and Baudhuin, 1966; Rhodin, 1954), and over the past few decades numerous groups have strived to understand their functions and dynamics, regularly identifying new proteins and mechanisms associated with this essential organelle. Nevertheless, and as several recent studies have shown, there are still huge gaps in our understanding of basic peroxisome function. In this thesis, we set out to further characterise peroxisomes by investigating two specific questions: the targeting of TA proteins to this organelle and the regulation of peroxisome motility in mammalian cells.

In chapter 3, using *in vivo* and *in silico* techniques, we were able to identify the biochemical parameters that direct the targeting of peroxisomal TA proteins, and to develop a tool to predict targeting of these proteins to peroxisomes, mitochondria and the ER. In chapter 4, we analysed one specific TA protein – MIRO1, which was found to be dually targeted to peroxisomes and mitochondria, and to play a key role in peroxisome motility and dynamics.

One of the prevailing themes that we regularly came across was the close connection between peroxisomes and mitochondria. As seen in chapter 3, several TA proteins are shared between peroxisomes and mitochondria, and in the absence of peroxisomes, several of this organelle's proteins are re-directed to mitochondria, pointing to a very permissible targeting system between these two organelles. Additionally, these shared proteins are responsible for several processes such as organelle division, antiviral signalling and organelle motility, implicating a synchronised response of both organelles to maintain cellular homeostasis.

In this discussion we aim to integrate our results from an evolutionary point of view, highlighting the close interaction between peroxisomes and mitochondria.

6.1. TA protein promiscuity and its role in organelle evolution

Protein targeting is generally considered to be a tightly regulated process that enables any given protein to find its destination in order to perform its function. In line with this, cells have developed several mechanisms in order to regulate

gene expression, RNA localisation, protein import, amongst others, controlling every step of the way. Concurrently, defects in any of these steps or mutations on the protein itself which induce its mistargeting are associated with deleterious effects. However, when looking at the targeting of TA proteins, it appears that not all proteins in the cell follow these rules so strictly.

Several TA proteins have been show to target more than one organelle, taking advantage of less stringent targeting information. Previous studies have found that TA protein targeting is not dependent on a conserved sequence or structural conformation, but on several physicochemical parameters (reviewed in Borgese and Fasana, 2011). Our own results support this by showing that a balance between high positive C-terminal charge and moderate TMD hydrophobicity enables peroxisomal targeting of TA proteins. But how does this bend the rules? In a hypothetical scenario of a shift in protein targeting from organelle A to B, it would take several localised and specific mutations to delete/create a targeting signal in order to change the proteins cellular localisation. In the case of TA proteins, a single mutation in the TMD or tail sequence could increase/decrease either TMD hydrophobicity or tail charge and slightly shift the targeting from one organelle to another, without completely depleting the original organelle of its necessary protein. This situation can be observed in our own results. As shown in figure 3.4, GFP-ACBD5$^{TMD\text{-}T}$ WT is targeted exclusively to peroxisomes in the majority of cells, with some cells presenting dual targeting to mitochondria and peroxisomes (~15%). Just two point mutations in the tail region, that replace charged residues for uncharged, were able to change this balance to ~35% of shared peroxisomal and mitochondrial targeting, and the majority of cells with exclusively mitochondrial targeting. This gradual change in protein localisation shows that, in the case of TA proteins, one single mutation is unlikely to completely inhibit targeting to the original organelle, therefore maintaining its function. Furthermore, the targeting to a new organelle is likely to be gradual, with lower levels of the protein being recognised by the new system's chaperone, and possibly having minor deleterious effects. This could both promote a gain of function for the new organelle, but at the same time give it time to adapt to a new protein, offering the cell an evolutionary advantage.

One of the main advantages of such a system would be the organelle's gain of function. If a single mutation is capable of transferring the basic component of, for example, a signalling process to a new organelle, this would likely strongly affect the homeostatic outcome of a cell. For example, MAVS is one of the core members of an antiviral signalling pathway (Dixit et al., 2010), and its dual targeting to mitochondria and peroxisomes effectively recruits cytosolic elements of this pathway to both organelles, but it also enables the existence of two signalling nixes that can play different roles in antiviral response, evolving additional levels of regulation.

From a different point of view, we could question why would it be advantageous for a protein to be targeted to more than one organelle when, by definition, protein compartmentalization is considered an advantage to separate and regulate different cellular processes? One way to look at it would be to consider the advantage of sharing the division machinery, in particular MFF, FIS1, GDAP1 and DLP1. Taking into account the previously suggested hypotheses that 1) mitochondria appeared before peroxisomes in eukaryotic cells and 2) peroxisomes are derived from the ER (Bolte et al., 2015), we could reasonably suggest that this pathway originated to divide mitochondria that couldn't otherwise form *de novo* to regenerate the organelle population. If so, the later acquisition of these proteins by peroxisomes would allow them to further distance themselves from the ER, enabling them to independently regenerate and become self-sustained. Whereas an obvious disadvantage would be that the loss of function of one protein would affect both organelles, we should consider that, so far, several TA proteins play essential roles in cellular viability (Schrader et al., 2014), so there shouldn't be any selection against their sharing. Also, depending on the membrane to which they are targeted, each protein can be further regulated by organelle specific factors (e.g. MID49/MID51 at mitochondria and PEX11 at peroxisomes) (Koch and Brocard, 2012; Palmer et al., 2011).

6.2. MIRO1 and the evolution of motility pathways for peroxisomes

As mentioned above, peroxisomes and mitochondria have a very close connection (Schrader et al., 2015a). Both organelles have long been shown to

share some metabolic functions, such as fatty acid β-oxidation and ROS degradation, and have more recently been shown to share components of their division, antiviral and motility machineries.

As shown in chapter 4, the TA protein MIRO1 regulates peroxisome motility in mammalian cells. This protein has been previously shown to form a complex with TRAK proteins and KIF5 (also known as kinesin 1 and KHC) and dynein motors, enabling mitochondrial motility through microtubules (reviewed in Devine et al., 2016). Concurrently, peroxisome motility in mammalian cells has also been shown to rely on the microtubule network (Schrader et al., 1996; Wiemer et al., 1997), but until now no clear link between the organelle and motors had been identified.

It is interesting to notice that, unlike the division machinery, which is partly conserved between yeast and mammals, the same does not appear to occur for the motility complex. In the budding yeast *Saccharomyces cerevisiae*, although both mitochondria and peroxisomes rely on the same myosin, Myo2, for actin-dependent motility, they use different organelle-motor connectors: Mmr1 and Ypt11 for mitochondria, and Inp2 for peroxisomes (reviewed in Knoblach and Rachubinski, 2015). One clear difference between mammalian cells and budding yeast is the reliance on the microtubule cytoskeleton for the former and on actin filaments for the latter. This on itself justifies the existence of a different motility complex. Interestingly, additional forms of peroxisomal transport have been identified in other microorganisms. In the fission yeast *Schizosaccharomyces pombe*, peroxisomes exhibit a mix of slow erratic movements and fast directed motility, resembling microtubule-dependent motility. However, depolymerisation of the microtubule or actin cytoskeleton has no effect on peroxisome motility in these cells (Jourdain et al., 2008). Instead, peroxisome motility appears to rely on a close association of this organelle with the surface of mitochondria. Another interesting example of peroxisome motility occurs in the filamentous fungus *Ustilago maydis*. In this organism, peroxisomal motility relies on the microtubule cytoskeleton. However, instead of having a motility complex that interacts directly with microtubules, peroxisomes have been suggested to hitchhike on moving endosomes (Guimaraes et al., 2015; Salogiannis et al., 2016). How these different motility pathways have evolved is still unknown.

Furthermore, it would be interesting to investigating the targeting of MIRO1 in some of the organisms mentioned above. The yeast homolog of MIRO1, Gem1, is targeted to mitochondria and has been suggested to interact and regulate the mitochondria-ER tethering complex ERMES (Kornmann et al., 2011). If found on peroxisomes, this protein could likewise play a role on a peroxisome-ER tethering complex. Additionally, as both *S. pombe* and *U. maydis* rely on microtubule-dependent motility to move several organelles, it would be interesting to look for a MIRO1 homolog, analyse its localisation and possible role in these organisms. Concurrently, it would be interesting to investigate if peroxisome motility in mammalian cells is always dependent on a direct interaction with microtubules, or if they are also capable of hitchhiking with other organelles.

6.3. Future work

In this thesis we significantly improved the current knowledge on the targeting of TA proteins to cellular membranes and the regulation of peroxisome motility in mammalian cells. Nevertheless, several questions still remain regarding these two processes, such as:

- Which additional factors regulate TA protein targeting to each organelle? Is it possible that posttranslational modification can favour/inhibit dual targeting of TA proteins to each organelle?
- How are TA proteins recognised and targeted to mitochondria?
- Which proteins regulate MIRO1 function on peroxisomes?

Regarding TA proteins, it would be interesting to analyse the function and targeting of the several still uncharacterised TA proteins. This would potentially shed some light on additional factors regulating the targeting of these proteins. Furthermore, an extensive analysis of known mitochondrial chaperones and their affinity for mitochondrial TA proteins could further improve our knowledge of the mechanisms that regulate the targeting to this organelle. Finally, the identification of new TA proteins would allow us to further strengthen our current predictor, as well as improve it by adding additional physicochemical parameters.

Concerning peroxisome motility, the identification of MIRO1's regulators at peroxisomes would improve our understanding of peroxisome motility and its function on peroxisomal homeostasis. To compliment this, the use of recently developed optogenetic techniques to regulate peroxisome motility in mammalian cells would facilitate the analysis of peroxisome positioning on organelle function. Optogenetics enables the regulation of protein dimerization using a light beam, allowing, for example, a tight temporal control of peroxisome motility by inducing the binding of a kinesin motor to a membrane anchor (Bergeijk et al., 2015). Despite the many advantages of this technique, the experimental set up necessary for its implementation hamper its general use. Additionally, it would be interesting to analyse MIRO2 and its role at peroxisomes and the ER.

Appendix 1

Accession	TMD	TAIL	GRAVY	CHARGE	MITO	PO	ER	Target Probability
NP_057105.2	GSAVLIVILTLALAALIFRRIYL	ANEYIFDFEL	2.04	-3.1	0.385	0.031	0.584	ER
NP_004453.3	YSPIYLSFVMLLAALSWQYL	TTLSQVTEDYVQTGEH	1.19	-2.8	0.381	0.037	0.582	ER
NP_000108.1	LWGQLLLFLVFVIVLFFIYHFMQ	AEEGNPF	2.07	-2.1	0.326	0.022	0.652	ER
NP_068802.1	YLAYGSITPISAFVFVVFFSVFF	PSFYEDFCCWI	1.84	-2.1	0.344	0.021	0.635	ER
NP_683725.1	WWTNWVIPAISAVAVALMYRLYM	AED	1.04	-2.1	0.385	0.035	0.580	ER
NP_001005210.1	LFIAFVGFVVSIASVATNFLLGI	TANCCHRWSKASEEEEI	2.25	-1.9	0.316	0.027	0.658	ER
NP_940683.1	LGFWRVLLLIFVIALLSLGIAYY	VSGVLPFVENQPELVH	2.09	-1.8	0.307	0.020	0.673	ER
NP_006625.1	VGLVVVGVLLIILIVLLVVFLPQ	SSDSSSAPRTQDAGIASGPGN	3.07	-1.1	0.378	0.129	0.493	ER
NP_071430.2	PLNICVFILLLVFIVVKCF	TSE	2.63	-1.1	0.312	0.052	0.637	ER
NP_000373.1	LGLLLLTFLGIVAAVLVKA	EYY	2.45	-1.1	0.283	0.032	0.685	ER
NP_057465.1	LLAPLGLLAILTLAVATLYGLSL	ATPGE	2.09	-1.1	0.266	0.016	0.719	ER
NP_338599.1	LLAPLGLLAILTLAVATLYGLSL	ATPGE	2.09	-1.1	0.266	0.016	0.719	ER
NP_073579.4	IFSLPLVGLVVISALLWCWW	AETSS	2.07	-1.1	0.268	0.015	0.717	ER
NP_001129158.2	FVRLGLAAVIVVIMGAFLVEAWY	SRNVSPGESEAFKPE	1.96	-1.1	0.285	0.014	0.701	ER
NP_056446.4	GVFSQKCSVSPILILCLLLLGVL	NLETM	1.90	-1.1	0.299	0.014	0.686	ER
NP_001078898.1	YGWIAAAVGWSLWFLTLILL	CVDKLMKLTPDEPKDLQA	1.71	-1.1	0.365	0.016	0.620	ER
NP_149047.2	ATSQELVICLALLAFLILHYIW	SQIQCLIFTLMDWI	1.70	-1.1	0.369	0.016	0.616	ER
NP_058626.1	GFRVWILFFLVMCSFSLLFLDWY	DS	1.62	-1.1	0.401	0.016	0.583	ER
NP_001018881.1	LILSIVCLMITQLAGFSGPNF	QDGCILRSE	1.57	-1.1	0.420	0.017	0.563	ER
NP_694540.3	YYLISVCGVVVVVFAWYI	THDVN	2.17	-0.8	0.247	0.015	0.738	ER
NP_570115.1	SWRLGLALLLGGALLFWVLL	HRRWSEAVAEVGPD	1.83	-0.8	0.317	0.013	0.669	ER
NP_005104.3	PIARVFVIIYMALLHLWVMIVLL	TYTPEMHHDQPYGK	2.28	-0.6	0.241	0.018	0.741	ER
NP_055561.2	VVGIFAGFGLLLLVASPFLLLAT	PFVLCCKCKCSKGDDDPLPT	2.31	-0.2	0.229	0.016	0.756	ER
NP_003752.2	IVLICVIVFIIILFIVLFATGAF	S	3.30	-0.1	0.409	0.156	0.435	ER
NP_005810.1	WCAIAILFAVLLVVLILFLV	L	3.29	-0.1	0.408	0.155	0.437	ER
NP_002658.1	FINFCLILICLLLICIIVML	L	3.28	-0.1	0.408	0.153	0.439	ER
NP_001971.2	LMFIIICVIVLLVILGIILATTL	S	3.22	-0.1	0.404	0.144	0.452	ER
NP_004772.1	WAIGITVLVIFIIIIIVWVV	SS	3.13	-0.1	0.396	0.129	0.475	ER
NP_004595.2	VLIAICVSITVVLLAVIIGVTVV	G	3.09	-0.1	0.392	0.121	0.486	ER

Accession	TMD	TAIL	GRAVY	CHARGE	MITO	PO	ER	Target Probability
NP_055046.1	MIMLGAICAIIVVVIVIYFF	T	3.07	-0.1	0.390	0.117	0.493	ER
NP_003756.1	WCAIAVLVGVLLLVLILLFS	L	2.96	-0.1	0.374	0.095	0.531	ER
NP_055047.1	LKMMIILGVICAIILIIIIVYFS	T	2.82	-0.1	0.345	0.068	0.587	ER
NP_004594.1	IMIIICCVILGIVIASTVGGIF	A	2.78	-0.1	0.335	0.062	0.603	ER
NP_064564.1	ITTVVLPTLAVVVLLIVVFVYVA	TRPTITE	2.76	-0.1	0.330	0.058	0.612	ER
NP_004844.1	SASCGMIMVILLLLVAIVVVAVW	PTN	2.73	-0.1	0.322	0.054	0.624	ER
NP_079504.2	WLPVLMVVIAAALAVFLA	NKDNLMI	2.65	-0.1	0.300	0.042	0.657	ER
NP_997274.2	LAAILFGAVLLAAVALAVCVAKL	S	2.59	-0.1	0.284	0.035	0.681	ER
NP_065706.2	APILVVMVILLNIGVAILFINFF	I	2.58	-0.1	0.281	0.034	0.684	ER
NP_079010.2	MMYFILFLWLLVYCLLLF	PQLDVSRL	2.58	-0.1	0.281	0.034	0.684	ER
NP_689613.1	WVMLWFLGLQALGLVAVLCLVII	YVQQ	2.48	-0.1	0.256	0.025	0.718	ER
NP_511043.1	AITYLLIFILLMIIALQNIV	ML	2.48	-0.1	0.256	0.025	0.718	ER
NP_443106.1	IMIIICCVVLGVVLASSIGGTLG	L	2.41	-0.1	0.242	0.021	0.738	ER
NP_001002294.1	CFFFHWLKLFAIPILLIAVFLVL	T	2.40	-0.1	0.240	0.020	0.740	ER
NP_008825.4	CFFFHWLKLFAIPILLIAVFLVL	T	2.40	-0.1	0.240	0.020	0.740	ER
NP_065166.2	NTILICMVILLNIGLAILFVHLL	T	2.40	-0.1	0.240	0.020	0.740	ER
NP_149992.3	VLAGLVVVPVALNSGVSLLVLAL	CLSLAWFS	2.34	-0.1	0.230	0.017	0.752	ER
NP_065698.1	NSIMIVLVMLLNIGLAILFVHFL	T	2.31	-0.1	0.226	0.015	0.759	ER
NP_004729.1	LSTRLLALVVLFFIVGVIIGKIA	L	2.27	-0.1	0.223	0.014	0.763	ER
NP_006287.2	VYYYRIIIPVLLMLVFLALF	FL	2.22	-0.1	0.221	0.013	0.767	ER
NP_612502.1	MLLSVAIFILLTLVYAYW	TM	2.21	-0.1	0.221	0.013	0.767	ER
NP_004278.2	FMIGGMLLTCVVMFLVVQYL	T	2.20	-0.1	0.221	0.012	0.767	ER
NP_001017440.1	SLICAFAMAFIISVMLIAANQIL	RSGME	2.19	-0.1	0.221	0.012	0.767	ER
NP_113656.2	SLICAFAMAFIISVMLIAANQIL	RSGME	2.19	-0.1	0.221	0.012	0.767	ER
NP_001170.2	LLLPQFGMVIILISVSAINLFVA	L	2.18	-0.1	0.221	0.012	0.767	ER
NP_004478.3	VPLLAAIYFLMIHVLLILCFTGH	L	2.08	-0.1	0.231	0.011	0.758	ER
NP_149076.1	LIIAVLVSASIANLWLWM	NQ	2.08	-0.1	0.231	0.011	0.758	ER
NP_115828.1	VVGAVALLDLSLAFLFSQLL	T	2.06	-0.1	0.235	0.011	0.754	ER
NP_003565.4	SPLPSLLVVIAAIFIGFFLGKFI	L	2.04	-0.1	0.239	0.011	0.750	ER

Accession	TMD	TAIL	GRAVY	CHARGE	MITO	PO	ER	Target Probability
NP_919415.2	SPLPSLLVVIAAIFIGFFLGKFI	L	2.04	-0.1	0.239	0.011	0.750	ER
NP_114410.1	FLNTFTVSLIVTVIPLL	QNVPVPLGNNVGKMQVYE	2.02	-0.1	0.244	0.011	0.745	ER
NP_001001701.2	SYWLDLWLFILFDVVVFLFVYFL	P	2.00	-0.1	0.250	0.011	0.740	ER
NP_660320.3	VPLSSATLLAPLLSGLFVLWLCI	Q	1.94	-0.1	0.270	0.011	0.719	ER
NP_973733.1	VPLSSATLLAPLLSGLFVLWLCI	Q	1.94	-0.1	0.270	0.011	0.719	ER
NP_998817.1	VPLSSATLLAPLLSGLFVLWLCI	Q	1.94	-0.1	0.270	0.011	0.719	ER
NP_001012474.1	IAMATAIGFAIMGFIGFFVKLIH	IPINNIIVGG	1.90	-0.1	0.287	0.011	0.702	ER
NP_055117.1	IAMATAIGFAIMGFIGFFVKLIH	IPINNIIVGG	1.90	-0.1	0.287	0.011	0.702	ER
NP_001181915.1	LLPAIATTIAVCFLLHSLG	PS	1.87	-0.1	0.301	0.011	0.688	ER
NP_060244.2	CALRMSVGLALLGLLFAFFVKVY	N	1.84	-0.1	0.317	0.011	0.672	ER
NP_055931.1	IGFCLVHILFIVLVYITYHWNAL	SA	1.79	-0.1	0.346	0.012	0.642	ER
NP_848029.2	WVSIALALAGPGAILILELSWFL	G	1.79	-0.1	0.346	0.012	0.642	ER
NP_001006623.1	TGFLFSFMINNVYTLFLFIIYCV	RQEYFIPNKEFSL	1.72	-0.1	0.391	0.013	0.596	ER
NP_002124.1	APLLRWVLTLSFLVATVAVGLYA	M	1.68	-0.1	0.419	0.013	0.568	ER
NP_002125.3	LQFILAAGVALAAGLLAWYY	M	1.68	-0.1	0.419	0.013	0.568	ER
NP_001452.2	MTSTMTIGKFMLALAFFAIIIAY	F	1.67	-0.1	0.425	0.013	0.561	ER
NP_004883.3	STYAKLAAVAVFFIMLIVYVRFW	WL	1.63	-0.1	0.453	0.014	0.533	ER
NP_689794.1	WFQQLLLSLTMLLLAFVTSFFYL	LYS	1.62	-0.1	0.459	0.014	0.527	ER
NP_079095.3	FGVLTGLAAIASLLYLLTHYLLP	YA	1.60	-0.1	0.472	0.014	0.513	ER
NP_001004312.1	LSLRWCLFWASLCLLVVYLQFSF	LSPAFF	1.60	-0.1	0.472	0.014	0.513	ER
NP_002818.1	FLVNMCVATVLTAGAYLCYRFLF	NSNT	1.57	-0.1	0.492	0.015	0.494	ER
NP_872379.2	ALQVLALLLPVLLLVGLSA	-	2.42	0.0	0.242	0.021	0.737	ER
NP_776155.1	IVISSGFVGGFLLGLAS	-	1.89	0.0	0.292	0.011	0.697	ER
NP_149095.2	TTLPLLFLLAMLTMFAW	-	1.84	0.0	0.319	0.011	0.670	ER
NP_060428.1	MLAGAATGMALGSLFWVF	-	1.59	0.0	0.487	0.015	0.498	ER
NP_003560.2	TLCIIILILVIGVAIISLIIWGL	NH	3.00	0.1	0.387	0.100	0.513	ER
NP_653289.3	PLIPAPVLGLLLLLLLSVLLL	GPSPPPTWPHLQLCYLQPPPV	2.59	0.1	0.285	0.034	0.682	ER
NP_060854.2	HYEIFVFLLLCSILFFIIFLFIF	HYI	2.57	0.1	0.279	0.032	0.690	ER
NP_001007025.1	SLILGGVIGICTILLLLYAF	H	2.41	0.1	0.239	0.020	0.742	ER

Accession	TMD	TAIL	GRAVY	CHARGE	MITO	PO	ER	Target Probability
NP_001007026.1	SLILGGVIGICTILLLLYAF	H	2.41	0.1	0.239	0.020	0.742	ER
NP_004862.1	SLILGGVIGICTILLLLYAF	H	2.41	0.1	0.239	0.020	0.742	ER
NP_001012660.1	VFFVLICFLVMSSSYLAF	RISRLEQQLCSLSWDDPVPGHR	2.34	0.1	0.226	0.015	0.759	ER
NP_004853.2	CGSLCLLGCIAGCCFIPFCV	DALQDVDHYCPNCRALLGTYKRL	2.17	0.1	0.218	0.011	0.771	ER
NP_001027454.1	IPVWIKILLFVVVAVFLFLV	YQAMETNQVNPFSNFLHVDPRKSN	2.89	0.2	0.370	0.077	0.553	ER
NP_001027455.1	IPVWIKILLFVVVAVFLFLV	YQAMETNQVNPFSNFLHVDPRKSN	2.89	0.2	0.370	0.077	0.553	ER
NP_922945.1	WRLIAVILGILCLVILVIAVVLG	TMAGFKAVEFKG	2.88	0.9	0.398	0.069	0.532	ER
NP_919337.1	WIIIAVSVVLVAIIALIIGLSVG	K	2.87	0.9	0.396	0.067	0.537	ER
NP_055738.3	AVILVLFAFFSILIAFIIQYFVI	K	2.82	0.9	0.383	0.059	0.558	ER
NP_056021.1	IAALIAAAACTVILVIVVPICTM	KS	2.68	0.9	0.337	0.038	0.625	ER
NP_001003712.1	YFIIFLLILLQVIINFMF	K	2.59	0.9	0.303	0.029	0.668	ER
NP_065892.1	YFIIFLLILLQVIINFMF	K	2.59	0.9	0.303	0.029	0.668	ER
NP_001188.1	VLLALLLLLALLLPLLSGGLHLL	LK	2.54	0.9	0.285	0.024	0.690	ER
NP_003054.1	ELFLNFTIVLITVILMWLLV	RSYQY	2.36	0.9	0.232	0.014	0.754	ER
NP_659488.2	IFAYLMAVILSVTLLLIFSIFWT	KQFLWGVG	2.35	0.9	0.230	0.013	0.756	ER
NP_073600.3	FAAIIVLGFATLSILFAFILQYF	LMK	2.26	0.9	0.218	0.011	0.770	ER
NP_055260.1	SVGPWLLALFIFVVCGSAIFQII	QSIRMGM	2.09	0.9	0.230	0.010	0.760	ER
NP_036313.3	WLFGATAVALGGVALSVVIA	ARN	2.05	0.9	0.241	0.010	0.749	ER
NP_001010897.1	PVGPWLLALFVFVVCGSAIFQII	QSIRMGM	2.04	0.9	0.244	0.010	0.746	ER
NP_065947.1	WFLLCVFLACQLFINHIL	K	2.02	0.9	0.251	0.010	0.739	ER
NP_663613.1	WFLLCVFLACQLFINHIL	K	2.02	0.9	0.251	0.010	0.739	ER
NP_620124.1	GLLGVVGAAVAAVLSFSLYRVLV	KSQ	1.98	0.9	0.267	0.011	0.722	ER
NP_776182.2	FWIWVSMTVCVFWLMCMC	RLNPGIYPQQV	1.97	0.9	0.272	0.011	0.718	ER
NP_058439.1	WWKNCKMMIMLGAICAIIVVVIV	RRD	1.91	0.9	0.305	0.012	0.684	ER
NP_477515.2	GLLGGALANLFVIVGFAAFAYTV	KYVLRSIAQE	1.85	0.9	0.346	0.013	0.642	ER
NP_919296.1	GLLGGALANLFVIVGFAAFAYTV	KYVLRSIAQE	1.85	0.9	0.346	0.013	0.642	ER
NP_919439.1	GLLGGALANLFVIVGFAAFAYTV	KYVLRSIAQE	1.85	0.9	0.346	0.013	0.642	ER
NP_919440.1	GLLGGALANLFVIVGFAAFAYTV	KYVLRSIAQE	1.85	0.9	0.346	0.013	0.642	ER
NP_065129.1	LVQAFLSCLLTTAFIYLW	TRLL	1.75	0.9	0.428	0.015	0.557	ER

Accession	TMD	TAIL	GRAVY	CHARGE	MITO	PO	ER	Target Probability
NP_060331.3	SLVCSVTLLITILCSTLILVAVF	KYGHFSL	2.53	1.1	0.290	0.023	0.687	ER
NP_660349.1	LLLFLLMMLGVRGLLLVGLVYLV	SHLSQR	2.53	1.1	0.290	0.023	0.687	ER
NP_001103129.1	GLFHHILVGLLVVAFFFLLFQFC	THINFQKGA	2.19	1.1	0.222	0.011	0.768	ER
NP_006361.1	LLLSIIILLELAILGGLVYYKFF	RSH	2.10	1.1	0.233	0.010	0.757	ER
NP_001035189.1	NTILLTIIAMVVYTAYVFIPIHI	RLAWEFFSKICGYHSTISN	1.85	1.1	0.356	0.014	0.629	ER
NP_001003806.1	YYMYLLLLLKSVVYFAIITCCLL	RRTAFCCNGEKS	1.95	1.8	0.329	0.021	0.651	ER
NP_004793.2	LLLLLLLLLLLALFLYSVPGYLV	KKILGA	2.64	1.9	0.383	0.033	0.584	ER
NP_919224.1	LLLLLLLLLLLALFLYSVPGYLV	KKILGA	2.64	1.9	0.383	0.033	0.584	ER
NP_919303.1	LLLLLLLLLLLALFLYSVPGYLV	KKILGA	2.64	1.9	0.383	0.033	0.584	ER
NP_060937.1	WLLWAMLIIVCFIFISMILFIRI	MPKLK	2.62	1.9	0.374	0.031	0.594	ER
NP_005629.1	TIIIIIVSIVFIYIIVSPLCGGF	TWPSCVKK	2.57	1.9	0.353	0.027	0.620	ER
NP_659440.2	FLSAGVTALLVIIIIIATSV	RK	2.57	1.9	0.353	0.027	0.620	ER
NP_005859.1	LLCYMMLFSLFVFFIIYWII	KLR	2.53	1.9	0.336	0.024	0.640	ER
NP_001192209.1	IGLLAAGILGAGALIAGMCFIII	QSLRTDRQRIGICS	2.45	1.9	0.304	0.020	0.676	ER
NP_919304.1	WLIIKIVLALLGLLMLGLFLYSL	PGYMVKKLLGA	2.37	1.9	0.278	0.016	0.706	ER
NP_878250.2	VDGAVGILVHIWLFPIIVLISIL	SPRR	2.30	1.9	0.263	0.015	0.722	ER
NP_872333.1	SLICAFAIAFIISVMLIAANQVL	RSGMK	2.29	1.9	0.261	0.015	0.724	ER
NP_060843.1	GIPIFMVLVPVFALTMVAAWAFM	RYRQQL	2.15	1.9	0.261	0.016	0.723	ER
NP_071884.1	IAAVVFSYIATLLYVVHAV	FSLIRWKSS	2.12	1.9	0.266	0.016	0.718	ER
NP_071885.1	LLFIFEFVFSYIATLLYVVHAVF	SLIRWKSS	2.08	1.9	0.276	0.017	0.707	ER
NP_006799.1	VGPVPVLVMSLLFIASVFMLHIW	GKYTRS	2.05	1.9	0.286	0.018	0.696	ER
NP_006668.1	YFVLGTVAALVALVLNVFYPLVS	QSRWR	1.98	1.9	0.318	0.021	0.661	ER
NP_057152.2	GLVGMAIVGGMALGVAGLAGLIG	LAVSKSKS	1.94	1.9	0.341	0.024	0.635	ER
NP_003837.1	GIVGLCGLVSSILSILTLIYPWL	RLKP	1.90	1.9	0.369	0.026	0.605	ER
NP_004043.3	FLKVFLPSLLLSHLLAIGLGIYI	GRRLTTSTSTF	1.87	1.9	0.392	0.029	0.580	ER
NP_004322.1	FLKVFIPSLFLSHVLALGLGIYI	GKRLSTPSASTY	1.85	1.9	0.408	0.030	0.562	ER
NP_001182.1	WFLTGMTVAGVVLLGSLF	SRK	1.82	1.9	0.433	0.033	0.534	ER
NP_612815.1	WFLTGMTVAGVVLLGSLF	SRK	1.82	1.9	0.433	0.033	0.534	ER
NP_009086.4	VVLLGVGLAVVVSLTLTAVILVL	TRRCRTASHPVSASE	2.84	2.1	0.465	0.059	0.476	ER

Accession	TMD	TAIL	GRAVY	CHARGE	MITO	PO	ER	Target Probability
NP_775828.1	TWSGVCTVILVACVLVFLLGIVL	HNMSCISKRFTVISCG	2.56	2.1	0.363	0.028	0.609	ER
NP_056182.2	ILLFGGAAAVAILAVAIGVALAL	RKK	2.66	2.9	0.459	0.047	0.494	ER
NP_057648.2	PLLVAGGVAVAAIALILGVAFLV	RKK	2.60	2.9	0.436	0.042	0.521	ER
NP_997293.2	VIYAAMCMTVTCGILLLVMV	KLRTSRISSKARDPSSIQIPGEL	2.42	2.9	0.366	0.034	0.600	ER
NP_060348.1	AVTTVGVAAGLLAAASLVGILLA	RSKRERQ	2.15	2.9	0.331	0.046	0.623	ER
NP_001557.1	IPLLALSPNLLIVWLFLSIAYLV	TKLRCK	2.10	2.9	0.340	0.053	0.607	ER
NP_001179.1	LGNGPILNVLVVLGVVLLGQFVV	RRFFKS	1.99	2.9	0.381	0.075	0.544	ER
NP_004400.4	LLLFAVVLSRAAALGCIGLVA	HAGQLTAVWRRPGAARAP	2.29	3.1	0.348	0.045	0.608	ER
NP_060321.3	FTVMISLYLLLLLIVSVINSSAF	QHFWNRAKR	2.15	3.1	0.345	0.060	0.595	ER
NP_065797.2	PGALWLQVAVTGVLVVTLLVVLY	RRRLH	2.01	3.1	0.384	0.095	0.521	ER
NP_689807.1	FCLRWLALVALSFIVPCMCC	YVPLRMCHRCGEACGCCGGKHKAAG	2.07	3.2	0.369	0.089	0.542	ER
NP_036393.1	TLPLILGLILGLVIMVTLAIYHV	HHKMTANQVQIPRDRSQYKHMG	2.29	3.6	0.379	0.082	0.538	ER
NP_612145.2	TVFNSMLVSIVGMALYTGYVF	MPQHIMAILHYFEIVQ	1.44	-0.6	0.507	0.017	0.476	MITO
NP_001156910.1	KNFFYFYILASVILNVHLQVY	I	1.00	-0.1	0.572	0.033	0.395	MITO
NP_003155.2	KYFQSVTSNRWLMVKIFLIL	IVFFIIFVVFLA	0.63	-0.1	0.475	0.076	0.449	MITO
NP_004168.1	LIIIIVLVVVLLGILALIIGLSV	GLN	3.45	-0.1	0.413	0.174	0.413	MITO
NP_067023.1	LAMGMLAGAATGAALGSLM	WSPCWF	1.51	-0.1	0.527	0.016	0.458	MITO
NP_115788.1	TCLTACWTALCCCCLWDML	T	1.49	-0.1	0.537	0.016	0.447	MITO
NP_002819.2	LTKMGFMSVILVGAFVGWTLFFQ	QNAL	1.46	-0.1	0.551	0.017	0.432	MITO
NP_071770.1	LFYLKILYKSGIIWLSWYSFILL	VL	1.31	-0.1	0.598	0.020	0.383	MITO
NP_001026883.1	YLAGSIFTCLTVALGFYRLW	I	1.23	-0.1	0.604	0.022	0.373	MITO
NP_085056.2	CWAYWILPIIGAVLLGFLYRYYT	SESKSS	1.18	-0.1	0.603	0.024	0.373	MITO
NP_113670.1	SWLSIVGPVVGLNLPLSYA	KATSQDERNVP	1.16	-0.1	0.602	0.025	0.374	MITO
NP_954652.1	SNGAFSGPCASACLLFLCWLLQP	QMGS	1.01	-0.1	0.575	0.032	0.393	MITO
NP_872347.2	LSFFILLVLLLLLFIIVFILIFF	-	3.53	0.0	0.415	0.181	0.404	MITO
NP_115615.2	VTVGYLVQFTYLFIYFQFI	-	1.46	0.0	0.562	0.017	0.421	MITO
NP_061323.2	LNLSASCLMYLFSAAASWLY	HY	1.16	0.1	0.627	0.025	0.348	MITO
NP_689711.2	ALFIPSTSQCLFSLLLLSYLFIHHSL	NHHLLTMNILFV	1.33	0.4	0.652	0.021	0.327	MITO
NP_113628.1	LSIFCCCVILIVIVVIVV	KTAI	3.60	0.9	0.423	0.183	0.394	MITO

Accession	TMD	TAIL	GRAVY	CHARGE	MITO	PO	ER	Target Probability
NP_009090.2	WPWMPMLAALVAVTAIVLYVPGL	ARASP	1.67	0.9	0.499	0.017	0.483	MITO
NP_004041.1	SVRTVLTGAVALGALVTVGAFFA	SK	1.67	0.9	0.499	0.017	0.483	MITO
NP_001098018.1	AAATTVAAAAAAAAAAAAA	RVTLT	1.66	0.9	0.508	0.018	0.474	MITO
NP_714919.2	GWNFCSIPWCLFWATVLLLIIYL	QFSFRSSV	1.66	0.9	0.508	0.018	0.474	MITO
NP_068779.1	GIRNVLLAFAGVAGVGAGLAYLI	R	1.62	0.9	0.543	0.019	0.439	MITO
NP_689909.2	VSAMGYCLLFGPCTVVTF	WRTLLLAGC	1.59	0.9	0.567	0.020	0.413	MITO
NP_001014301.1	ILRVGFAAFSVLWACCSRI	CGAKQP	1.53	0.9	0.611	0.021	0.367	MITO
NP_803182.1	ASLTATLTFGLFAGLGGAGA	STSGSSGACGFSYK	1.25	0.9	0.711	0.030	0.259	MITO
NP_957516.1	ASLTATLTFGLFAGLGGAGA	STSGSSGACGFSYK	1.25	0.9	0.711	0.030	0.259	MITO
NP_733764.1	PAGALQSWGLWLGCPLLVLM	AKLLW	1.23	0.9	0.712	0.030	0.257	MITO
NP_001020128.1	LRVCPARLLWCCWALPLHLALAW	TPPLPSSRPAQLWPWS	1.19	0.9	0.712	0.032	0.256	MITO
NP_055414.2	GASLTATLTFGLFAGLGGAG	ASTSGSSGACGFSYK	1.14	0.9	0.708	0.034	0.257	MITO
NP_000624.2	WLSLKTLLSLALVGACITLGAYL	GHK	1.61	1.1	0.567	0.022	0.411	MITO
NP_060678.2	FALASHFFWALWALIQNQYSTI	DFDFLRYAVIRFNQYFKVKPQASALEMPK	0.77	1.9	0.666	0.075	0.259	MITO
NP_001001433.1	LVILILFVIIIVLIVVLVGV	KSR	3.89	1.9	0.418	0.195	0.387	MITO
NP_003754.2	LVILILFVIIIVLIVVLVGV	KSR	3.89	1.9	0.418	0.195	0.387	MITO
NP_003753.2	AIMALVAAILLLVIIILIVM	KYRT	3.48	1.9	0.442	0.170	0.388	MITO
NP_003485.1	WAIILFIILFILLLFLAIFIYAF	PNYAAMKLVKPFS	3.11	1.9	0.475	0.110	0.415	MITO
NP_803173.1	MCILVLVLSVIILILGLIIWLVY	KTK	3.10	1.9	0.475	0.108	0.417	MITO
NP_001140156.1	LLLITLIAVVAVVAAILPWVLLV	RKQA	3.01	1.9	0.475	0.090	0.435	MITO
NP_001034201.1	YIIIAFILIILIIFLVLFIYTLP	GAISRRIVVGS	3.00	1.9	0.475	0.088	0.437	MITO
NP_954740.1	MMIMLGAICAIIVVVIVS	KYR	2.98	1.9	0.474	0.084	0.443	MITO
NP_038479.1	WVIIGLLFLLILLLFVAVLLYSL	PNYLSMKIVKPNV	2.96	1.9	0.472	0.080	0.448	MITO
NP_579899.1	WVIIGLLFLLILLLFVAVLLYSL	PNYLSMKIVKPNV	2.96	1.9	0.472	0.080	0.448	MITO
NP_620119.2	GGWTVTIFVAGVLTASLTIW	KKMG	1.45	1.9	0.720	0.054	0.226	MITO
NP_848032.1	VNVFGAIINMAASVSGVIGGLKF	SRTYYVKGI	1.43	1.9	0.729	0.054	0.217	MITO
NP_064579.3	VMYSITVAFWLLNSWLWF	RR	1.32	1.9	0.763	0.054	0.184	MITO
NP_001028738.1	WLRASFGATVFAVLGFAMYKALL	KQR	1.30	1.9	0.766	0.053	0.180	MITO
NP_001028740.1	WLRASFGATVFAVLGFAMYKALL	KQR	1.30	1.9	0.766	0.053	0.180	MITO

Accession	TMD	TAIL	GRAVY	CHARGE	MITO	PO	ER	Target Probability
NP_060777.3	WLRASFGATVFAVLGFAMYKALL	KQR	1.30	1.9	0.766	0.053	0.180	MITO
NP_620116.1	TWQTVTIFVAGVLTASLTIW	KKMG	1.28	1.9	0.769	0.053	0.177	MITO
NP_620118.1	TWQTVTIFVAGVLTASLTIW	KKMG	1.28	1.9	0.769	0.053	0.177	MITO
NP_004709.2	LYRTTMALTVGGTIYCLIALYMA	SQPKNK	1.22	1.9	0.774	0.053	0.173	MITO
NP_003797.1	LPTYWPWLCAAAQVAALAAWLLG	RRNL	1.15	1.9	0.772	0.054	0.174	MITO
NP_071928.2	FWLYVIITSSLPHICSFVMYL	TGTRQMMSSKHGVRIDV	1.52	2.2	0.696	0.071	0.233	MITO
NP_076939.3	SFFGASFLMGSLGGMGYFAYWYL	KKKYI	0.90	2.9	0.728	0.096	0.176	MITO
NP_001196.2	LLIFLALALFLATVLYIV	KKRLFPFL	2.94	2.9	0.516	0.084	0.400	MITO
NP_053581.2	LLIFLALALFLATVLYIV	KKRLFPFL	2.94	2.9	0.516	0.084	0.400	MITO
NP_053582.2	LLIFLALALFLATVLYIV	KKRLFPFL	2.94	2.9	0.516	0.084	0.400	MITO
NP_053583.2	LLIFLALALFLATVLYIV	KKRLFPFL	2.94	2.9	0.516	0.084	0.400	MITO
NP_001006625.1	TLVGIIVGVLLAIGFIGAIIVVV	MRKMSGRYSP	2.94	2.9	0.516	0.084	0.400	MITO
NP_001006626.1	TLVGIIVGVLLAIGFIGAIIVVV	MRKMSGRP	2.94	2.9	0.516	0.084	0.400	MITO
NP_003838.1	GIIGLGGLVSSIAGMITVAY	PQMKLKTR	1.70	2.9	0.583	0.150	0.267	MITO
NP_065119.2	AISTVEFVTAAVGVFSFLGLFP	KGQRAKYY	1.66	2.9	0.609	0.155	0.236	MITO
NP_000231.1	LLKIIGFSTSVTALGFVLY	KYKLLPRS	1.63	2.9	0.628	0.157	0.215	MITO
NP_000889.3	PGLLRLIGLTTIFSATALGFLAH	KRGLLVRV	1.28	2.9	0.751	0.130	0.119	MITO
NP_620580.1	LVIGVISGIAVFVVILFIGILFIIL	RKRQGSRGAMGHYVLAERE	3.22	3.2	0.495	0.137	0.368	MITO
NP_001182188.1	VVALVLAAFVLGAALAAGLGLVC	AHSAPHAPGPPARASPSGPQPRRSQ	2.63	3.4	0.473	0.059	0.468	MITO
NP_056194.1	GIFLAIILFPFGFICCFAL	RKRRCPNCGATFA	2.61	3.8	0.477	0.079	0.444	MITO
NP_009000.1	VIIAASVAGMGLAAMSLIGVMFS	RNKRQKQ	2.07	3.9	0.374	0.253	0.372	MITO
NP_004576.2	EVGVATALGILVVAGCSFAI	RRYQKKATA	1.99	3.9	0.369	0.332	0.299	MITO
NP_057169.2	FSLLMFFGILGATTLSVSILLWA	TQRRKAKTS	1.93	3.9	0.358	0.398	0.244	PO
NP_542159.3	FSLLMFFGILGATTLSVSILLWA	TQRRKAKTS	1.93	3.9	0.358	0.398	0.244	PO
NP_001671.2	TVRNGGLIFAGLAFIVGLLILLS	RRFRCGGNKKRRQINEDEP	1.86	3.9	0.329	0.484	0.187	PO
NP_067614.1	TVRNGGLIFAGLAFIVGLLILLS	RRFRCGGNKKRRQINEDEP	1.86	3.9	0.329	0.484	0.187	PO
NP_078998.1	PLGLPGPALLFFLLWPFVVQWLF	RMFRTQKR	1.54	3.9	0.233	0.703	0.064	PO
NP_851800.1	AAALDLTNSIITAVFLSVVAILA	MQEKKRRHLLYVGGR	1.95	4.1	0.301	0.485	0.214	PO
NP_057410.1	VKMLRLVFALVTAVCCLADGALI	YRKLLFNPSGPYQKKPVHEKKEVL	1.92	4.1	0.285	0.525	0.190	PO

Accession	TMD	TAIL	GRAVY	CHARGE	MITO	PO	ER	Target Probability
NP_002957.1	VGFQSFFSLIAGLTIACNDYFVV	HMKQKGKK	1.37	4.1	0.193	0.759	0.048	PO
NP_056230.1	WSLFAVNFFVGAAGASQLF	RIWRYNQELKAKAHK	1.27	4.1	0.257	0.684	0.059	PO
NP_861449.2	RWMALIALSFLAPCMCCYL	PLRACYHCGVMCRCCGGKHKAAA	1.58	4.2	0.121	0.834	0.045	PO
NP_001003713.1	ISGITMVLACYVLFSYSFSY	KHLKHERLRKYH	1.43	4.6	0.059	0.914	0.027	PO
NP_004880.1	ISGITMVLACYVLFSYSFSY	KHLKHERLRKYH	1.43	4.6	0.059	0.914	0.027	PO
NP_061845.2	VLGTTLVVGLLAGVGYFAFMLF	RKRLGSMILAFRPRPNYF	2.06	4.9	0.153	0.701	0.146	PO
NP_116136.1	TLTGRMNCVLATYGSIALIVLYF	KLRSKKTPAVKAT	1.27	4.9	0.067	0.899	0.035	PO
NP_663736.1	SPGVLTFAIIWPFIAQWLVYLYY	QRRRRKLN	1.23	4.9	0.082	0.877	0.041	PO
NP_877434.2	LGIIALVTSPLLLLASPCIICCV	CKSCRGKKKKHDPSTT	2.37	5.1	0.318	0.394	0.288	PO
NP_005463.1	SYMYILFVMFLFAVTVGSLILGY	TRSRKVDKRSDPYHVYIKNRVSMI	1.90	5.1	0.055	0.888	0.057	PO
NP_000560.5	YQVSFCLVMVLLFAVDTGLYFSV	KTNIRSSTRDWKDHKFKWRKDPQDK	1.67	5.2	0.022	0.955	0.022	PO
NP_000646.2	PLFIPVAVMVTAFSGLAFIIWLA	RRLKKGKKSKRSMNDPY	2.13	6.9	0.045	0.897	0.058	PO

Bibliography

Agrawal G, Joshi S and Subramani S (2011) Cell-free sorting of peroxisomal membrane proteins from the endoplasmic reticulum. *Proc. Natl. Acad. Sci. U. S. A.* 108(22): 9113–9118.

Agrawal G and Subramani S (2013) Emerging role of the endoplasmic reticulum in peroxisome biogenesis. *Front. Physiol.* 4(October): 286.

Agrawal G and Subramani S (2016) De novo peroxisome biogenesis: Evolving concepts and conundrums. *Biochim. Biophys. Acta - Mol. Cell Res.* 1863(5): 892–901.

Ahmad T, Mukherjee S, Pattnaik B, Kumar M, Singh S, Rehman R, Tiwari BK, Jha KA, Barhanpurkar AP, Wani MR, Roy SS, Mabalirajan U, Ghosh B and Agrawal A (2014) Miro 1 regulates intercellular mitochondrial transport & enhances mesenchymal stem cell rescue efficacy. *EMBO J.* 33(9): 994–1010.

Antonenkov VD, Grunau S, Ohlmeier S and Hiltunen JK (2010) Peroxisomes are oxidative organelles. *Antioxid Redox Signal* 13(4): 525–537.

Ashibe B, Hirai T, Higashi K, Sekimizu K and Motojima K (2007) Dual subcellular localization in the endoplasmic reticulum and peroxisomes and a vital role in protecting against oxidative stress of fatty aldehyde dehydrogenase are achieved by alternative splicing. *J. Biol. Chem.* 282(28): 20763–20773.

Bagattin A, Hugendubler L and Mueller E (2010) Transcriptional coactivator PGC-1alpha promotes peroxisomal remodeling and biogenesis. *Proc. Natl. Acad. Sci. U. S. A.* 107(47): 20376–20381.

Barton KA, Jaipargas E-A, Griffiths N and Mathur J (2014) Live imaging of peroxisomes and peroxules in plants. In *Molecular Machines Involved in Peroxisome Biogenesis and Maintenance*. Springer, 233–253.

Baudhuin P, Beaufay H, Rahman-Li Y, Sellinger OZ, Wattiaux R, Jacques P and De Duve C (1964) Tissue fractionation studies. 17. Intracellular distribution of monoamine oxidase, aspartate aminotransferase, alanine aminotransferase, D-amino acid oxidase and catalase in rat-liver tissue. *Biochem. J.* 92(1): 179–184.

Behrends C and Fulda S (2012) Receptor proteins in selective autophagy. *Int. J. Cell Biol.* 2012: 673290.

Beilharz T, Egan B, Silver P a, Hofmann K and Lithgow T (2003) Bipartite signals mediate subcellular targeting of tail-anchored membrane proteins in

Saccharomyces cerevisiae. *J. Biol. Chem.* 278(10): 8219–8223.

Bellot G, Cartron P-F, Er E, Oliver L, Juin P, Armstrong LC, Bornstein P, Mihara K, Manon S and Vallette FM (2007) TOM22, a core component of the mitochondria outer membrane protein translocation pore, is a mitochondrial receptor for the proapoptotic protein Bax. *Cell Death Differ.* 14(4): 785–794.

Bender S, Reuter A, Eberle F, Einhorn E, Binder M and Bartenschlager R (2015) Activation of Type I and III Interferon Response by Mitochondrial and Peroxisomal MAVS and Inhibition by Hepatitis C Virus. *PLoS Pathog.* 11(11): e1005264.

Bergeijk P Van, Adrian M, Hoogenraad CC and Kapitein LC (2015) Optogenetic control of organelle transport and positioning. *Nature*(518): 111–114.

Berger J, Dorninger F, Forss-petter S and Kunze M (2016) Peroxisomes in brain development and function. *BBA - Mol. Cell Res.* 1863(5): 934–955.

Bharti P, Schliebs W, Schievelbusch T, Neuhaus A, David C, Kock K, Herrmann C, Meyer HE, Wiese S, Warscheid B, Theiss C and Erdmann R (2011) PEX14 is required for microtubule-based peroxisome motility in human cells. *J. Cell Sci.* 124(Pt 10): 1759–1768.

Birsa N, Norkett R, Wauer T, Mevissen TET, Wu H-C, Foltynie T, Bhatia K, Hirst WD, Komander D, Plun-Favreau H and Kittler JT (2014) Lysine 27 ubiquitination of the mitochondrial transport protein miro is dependent on serine 65 of the Parkin ubiquitin ligase. *J. Biol. Chem.* 289(21): 14569–14582.

Birschmann I, Stroobants AK, van der Berg M, Schafer A, Rosenkranz K, Kunau W-H and Tabak HF (2003) Pex15p of Saccharomyces cerevisiae provides a molecular basis for recruitment of the AAA peroxin Pex6p to peroxisomal membranes. *Mol. Biol. Cell* 14(February): 2226–2236.

Boldogh IR, Nowkowski DW, Yang H-C, Chung H, Karmon S, Royes P and Pon LA (2004) A protein complex containing Mdm10p, Mdm12p, and Mmm1p links mitochondrial membranes and DNA to the cytoskeleton-based segragation machinery. *Mol. Biol. Cell* 14: 4618–4627.

Boldogh IR and Pon LA (2007) Mitochondria on the move. *Trends Cell Biol.* 17(10): 502–510.

Bolte K, Rensing S a. and Maier U-G (2015) The evolution of eukaryotic cells from the perspective of peroxisomes. *BioEssays* 37(2): 195–203.

Boname JM, Bloor S, Wandel MP, Nathan JA, Antrobus R, Dingwell KS, Thurston TL, Smith DL, Smith JC, Randow F and Lehner PJ (2014) Cleavage by signal peptide peptidase is required for the degradation of selected tail-anchored proteins. *J. Cell Biol.* 205(6): 847–862.

Bonekamp N a, Sampaio P, de Abreu FV, Lüers GH and Schrader M (2012)

Transient complex interactions of mammalian peroxisomes without exchange of matrix or membrane marker proteins. *Traffic* 13(7): 960–978.

Bonekamp NA, Fahimi HD, Völkl A and Schrader M (2009) Reactive oxygen species and peroxisomes: struggling for balance. *BioFactors* 35(4): 346–355.

Borgese N, Brambillasca S and Colombo S (2007) How tails guide tail-anchored proteins to their destinations. *Curr. Opin. Cell Biol.* 19(4): 368–375.

Borgese N, Colombo S and Pedrazzini E (2003) The tale of tail-anchored proteins: coming from the cytosol and looking for a membrane. *J. Cell Biol.* 161(6): 1013–1019.

Borgese N and Fasana E (2011) Targeting pathways of C-tail-anchored proteins. *Biochim. Biophys. Acta* 1808(3): 937–946.

Borgese N, Gazzoni I, Barberi M, Colombo S and Pedrazzini E (2001) Targeting of a tail-anchored protein to endoplasmic reticulum and mitochondrial outer membrane by independent but competing pathways. *Mol Biol Cell* 12(8): 2482–2496.

Borgese N and Righi M (2010) Remote origins of tail-anchored proteins. *Traffic* 11(7): 877–885.

Bradford MM (1976) A rapid and sensitive method for the quantitation of microgram quantities of protein utilizing the principle of protein-dye binding. *Anal. Biochem.* 72(1-2): 248–254.

Brambillasca S, Altkrueger A, Colombo SF, Friederich A, Eickelmann P, Mark M, Borgese N and Solimena M (2012) CDK5 regulatory subunit-associated protein 1-like 1 (CDKAL1) is a tail-anchored protein in the endoplasmic reticulum (ER) of insulinoma cells. *J. Biol. Chem.* 287(50): 41808–41819.

Brambillasca S, Yabal M, Soffientini P, Stefanovic S, Makarow M, Hegde RS and Borgese N (2005) Transmembrane topogenesis of a tail-anchored protein is modulated by membrane lipid composition. *EMBO J.* 24(14): 2533–2542.

Braverman N, Dodt G, Gould SJ and Valle D (1998) An isoform of pex5p, the human PTS1 receptor, is required for the import of PTS2 proteins into peroxisomes. *Hum. Mol. Genet.* 7(8): 1195–1205.

Braverman NE, Agostino MDD and Maclean GE (2013) Peroxisomes biogenesis disorders: biological, clinical and pathophysiological perspectives. *Dev. Disabil. Res. Rev.* 17: 187–196.

Brickley K, Pozo KKBK and Stephenson FA (2011) N-acetylglucosamine transferase is an integral component of a kinesin-directed mitochondrial trafficking complex. *Biochim. Biophys. Acta* 1813(1): 269–281.

Brickley K, Smith MJ, Beck M and Stephenson FA (2005) GRIF-1 and OIP106, members of a novel gene family of coiled-coil domain proteins: association in vivo and in vitro with kinesin. *J. Biol. Chem.* 280(15): 14723–14732.

Brickley K and Stephenson FA (2011) Trafficking kinesin protein (TRAK)-mediated transport of mitochondria in axons of hippocampal neurons. *J. Biol. Chem.* 286(20): 18079–18092.

Brodsky JL (2010) The special delivery of a tail-anchored protein: why it pays to use a dedicated courier. *Mol. Cell* 40(1): 5–7.

Buentzel J, Vilardi F, Lotz-Havla A, Gärtner J and Thoms S (2015) Conserved targeting information in mammalian and fungal peroxisomal tail-anchored proteins. *Sci. Rep.* 5: 17420.

Bui HT and Shaw JM (2013) Dynamin Assembly Strategies and Adaptor Proteins in Mitochondrial Fission. *Curr. Biol.* 23(19): R891–R899.

Chang C and Lin C (2011) LIBSVM : A Library for Support Vector Machines. *ACM Trans. Intell. Syst. Technol.* 2: 1–39.

Chang J, Mast FD, Fagarasanu A, Rachubinski D a, Eitzen G a, Dacks JB and Rachubinski R a (2009) Pex3 peroxisome biogenesis proteins function in peroxisome inheritance as class V myosin receptors. *J. Cell Biol.* 187(2): 233–246.

Chang KT, Niescier RF and Min KT (2011) Mitochondrial matrix Ca2+ as an intrinsic signal regulating mitochondrial motility in axons. *Proc. Natl. Acad. Sci.* 108(37): 15456–15461.

Chartron JW, Clemons WM and Suloway CJM (2012) The complex process of GETting tail-anchored membrane proteins to the ER. *Curr. Opin. Struct. Biol.* 22(2): 217–224.

Chen Y, Pieuchot L, Loh RA, Yang J, Kari TMA, Wong JY and Jedd G (2014) (a) Hydrophobic handoff for direct delivery of peroxisome tail-anchored proteins. *Nat. Commun.* 5: 5790.

Chen Y-C, Umanah GKE, Dephoure N, Andrabi SA, Gygi SP, Dawson TM, Dawson VL and Rutter J (2014) (b) Msp 1 / ATAD1 maintains mitochondrial function by facilitating the degradation of mislocalized tail-anchored proteins. 33(14)

Colombo SF, Longhi R and Borgese N (2009) The role of cytosolic proteins in the insertion of tail-anchored proteins into phospholipid bilayers. *J. Cell Sci.* 122(Pt 14): 2383–2392.

Cortes C and Vapnik V (1995) Support-vector networks. *Mach. Learn.* 20(3): 273–297.

Daumke O, Roux A and Haucke V (2014) BAR domain scaffolds in dynamin-mediated membrane fission. *Cell* 156(5): 882–892.

de Brito OM and Scorrano L (2008) Mitofusin 2 tethers endoplasmic reticulum to mitochondria. *Nature* 456(7222): 605–610.

De Duve C and Baudhuin P (1966) Peroxisomes (microbodies and related particles). *Physiol. Rev.* 46(2): 323–357.

Deas E, Wood NW and Plun-Favreau H (2011) Mitophagy and Parkinson's disease: The PINK1-parkin link. *Biochim. Biophys. Acta - Mol. Cell Res.* 1813(4): 623–633.

Delille HK and Schrader M (2008) Targeting of hFis1 to peroxisomes is mediated by Pex19p. *J. Biol. Chem.* 283(45): 31107–31115.

Delmaghani S, Defourny J, Aghaie A, Beurg M, Dulon D, Thelen N, Perfettini I, Zelles T, Aller M, Meyer A, Emptoz A, Giraudet F, Leibovici M, Dartevelle S, Soubigou G, Thiry M, Vizi ES, Safieddine S, Hardelin JP, Avan P and Petit C (2015) Hypervulnerability to Sound Exposure through Impaired Adaptive Proliferation of Peroxisomes. *Cell* 163(4): 894–906.

Denic V, Dötsch V and Sinning I (2013) Endoplasmic reticulum targeting and insertion of tail-anchored membrane proteins by the GET pathway. *Cold Spring Harb. Perspect. Biol.* 5(8)

Deosaran E, Larsen KB, Hua R, Sargent G, Wang Y, Kim S, Lamark T, Jauregui M, Law K, Lippincott-Schwartz J, Brech A, Johansen T and Kim PK (2013) NBR1 acts as an autophagy receptor for peroxisomes. *J. Cell Sci.* 126(Pt 4): 939–952.

Devine MJ, Birsa N and Kittler JT (2016) Miro sculpts mitochondrial dynamics in neuronal health and disease. *Neurobiol. Dis.* 90: 27–34.

Diano S, Liu Z-W, Jeong JK, Dietrich MO, Ruan H-B, Kim E, Suyama S, Kelly K, Gyengesi E, Arbiser JL, Belsham DD, Sarruf D a, Schwartz MW, Bennett AM, Shanabrough M, Mobbs C V, Yang X, Gao X-B and Horvath TL (2011) Peroxisome proliferation–associated control of reactive oxygen species sets melanocortin tone and feeding in diet-induced obesity. *Nat. Med.* 17(9): 1121–1127.

Dietrich D, Seiler F, Essmann F and Dodt G (2013) Identification of the kinesin KifC3 as a new player for positioning of peroxisomes and other organelles in mammalian cells. *Biochim. Biophys. Acta - Mol. Cell Res.* 1833(12): 3013–3024.

Dimitrov L, Lam SK and Schekman R (2013) The Role of the Endoplasmic Reticulum in Peroxisome Biogenesis Lazar. *Cold Spring Harb. Perspect. Biol.* 5(5): a013243.

Dixit E, Boulant S, Zhang Y, Lee ASY, Odendall C, Shum B, Hacohen N, Chen

ZJ, Whelan SP, Fransen M, Nibert ML, Superti-Furga G and Kagan JC (2010) Peroxisomes are signaling platforms for antiviral innate immunity. *Cell* 141(4): 668–681.

Dodt G, Braverman N, Wong C, Moser A, Moser HW, Watkins P, Valle D and Gould SJ (1995) Mutations in the PTS1 receptor gene, PXR1, define complementation group 2 of the peroxisome biogenesis disorders. *Nat. Genet.* 9(2): 115–125.

Dodt G and Gould SJ (1996) Multiple PEX genes are required for proper subcellular distribution and stability of Pex5p, the PTS1 receptor: Evidence that PTS1 protein import is mediated by a cycling receptor. *J. Cell Biol.* 135(6 II): 1763–1774.Ebberink MS, Csanyi B, Chong WK, Denis S, Sharp P, Mooijer PAW, Dekker CJM, Spooner C, Ngu LH, de Sousa C, Wanders RJA, Fietz MJ, Clayton PT, Waterham HR and Ferdinandusse S (2010) Identification of an unusual variant peroxisome biogenesis disorder caused by mutations in the PEX16 gene. *J. Med. Genet.* 47(9): 608–615.

Elgersma Y, Kwast L, Van Den Berg M, Snyder WB, Distel B, Subramani S and Tabak HF (1997) Overexpression of Pex15p, a phosphorylated peroxisomal integral membrane protein required for peroxisome assembly in S. cerevisiae, causes proliferation of the endoplasmic reticulum membrane. *EMBO J.* 16(24): 7326–7341.

Emmanouilidis L, Gopalswamy M, Passon DM, Wilmanns M and Sattler M (2016) Structural biology of the import pathways of peroxisomal matrix proteins. *Biochim. Biophys. Acta - Mol. Cell Res.* 1863(5): 804–813.

Erdmann R and Schliebs W (2005) Peroxisomal matrix protein import: the transient pore model. *Nat. Rev. Mol. Cell Biol.* 6: 738–742.

Fagarasanu A, Mast FD, Knoblach B and Rachubinski R a (2010) Molecular mechanisms of organelle inheritance: lessons from peroxisomes in yeast. *Nat. Rev. Mol. Cell Biol.* 11(9): 644–654.

Fahimi HD, Baumgart E and Völkl A (1993) Ultrastructural aspects of the biogenesis of peroxisomes in rat liver. *Biochimie* 75(3-4): 201–208.

Fang Y, Morrell JC, Jones JM and Gould SJ (2004) PEX3 functions as a PEX19 docking factor in the import of class I peroxisomal membrane proteins. *J Cell Biol* 164(6): 863–875.

Favaloro V, Spasic M, Schwappach B and Dobberstein B (2008) Distinct targeting pathways for the membrane insertion of tail-anchored (TA) proteins. *J. Cell Sci.* 121(Pt 11): 1832–1840.

Francisco T, Rodrigues TA, Pinto MP, Carvalho AF, Azevedo JE and Grou CP (2014) Ubiquitin in the peroxisomal protein import pathway. *Biochimie* 98(1): 29–35.

Fransen M, Nordgren M, Wang B and Apanasets O (2012) Role of peroxisomes

in ROS/RNS-metabolism: Implications for human disease. *Biochim. Biophys. Acta* 1822(9): 1363–1373.

Fransen M, Nordgren M, Wang B, Apanasets O and Van Veldhoven PP (2013) Aging, age-related diseases and peroxisomes. In *Peroxisomes and Their Key Role in Cellular Signaling and Metabolism*. Springer, 45–65.

Fransson A, Ruusala A and Aspenström P (2003) Atypical Rho GTPases have roles in mitochondrial homeostasis and apoptosis. *J. Biol. Chem.* 278(8): 6495–6502.

Fransson A, Ruusala A and Aspenström P (2006) The atypical Rho GTPases Miro-1 and Miro-2 have essential roles in mitochondrial trafficking. *Biochem. Biophys. Res. Commun.* 344(2): 500–510.

Frederick RL, McCaffery JM, Cunningham KW, Okamoto K and Shaw JM (2004) Yeast Miro GTPase, Gem1p, regulates mitochondrial morphology via a novel pathway. *J. Cell Biol.* 167(1): 87–98.

Frederick RL, Okamoto K and Shaw JM (2008) Multiple pathways influence mitochondrial inheritance in budding yeast. *Genetics* 178(2): 825–837.

Fujiki Y, Matsuzono Y, Matsuzaki T and Fransen M (2006) Import of peroxisomal membrane proteins: The interplay of Pex3p- and Pex19p-mediated interactions. *Biochim. Biophys. Acta - Mol. Cell Res.* 1763(12): 1639–1646.

Fujiki Y, Okumoto K, Mukai S, Honsho M and Tamura S (2014) Peroxisome biogenesis in mammalian cells. *Front. Physiol.* 5(August): 307.

Fukuda S, Shimozawa N, Suzuki Y, Zhang Z, Tomatsu S, Tsukamoto T, Hashiguchi N, Osumi T, Masuno M, Imaizumi K, Kuroki Y, Fujiki Y, Orii T and Kondo N (1996) Human peroxisome assembly factor-2 (PAF-2): a gene responsible for group C peroxisome biogenesis disorder in humans. *Am. J. Hum. Genet.* 59(6): 1210–1220.

Gandre-Babbe S and van der Bliek AM (2008) The novel tail-anchored membrane protein Mff controls mitochondrial and peroxisomal fission in mammalian cells. *Mol. Biol. Cell* 19: 2402–2412.

Gao H, Metz J, Teanby NA, Ward AD, Botchway SW, Coles B, Pollard MR and Sparkes I (2016) In Vivo Quantification of Peroxisome Tethering to Chloroplasts in Tobacco Epidermal Cells Using Optical Tweezers. *Plant Physiol.* 170(1): 263–272.

Gasteiger E, Hoogland C, Gattiker A, Duvaud S, Wilkins MR, Appel RD and Bairoch A (2005) Protein Identification and Analysis Tools on the ExPASy Server. *Proteomics Protoc. Handb.*: 571–607.

Ghaedi K, Honsho M, Shimozawa N, Suzuki Y, Kondo N and Fujiki Y (2000)

PEX3 is the causal gene responsible for peroxisome membrane assembly-defective Zellweger syndrome of complementation group G. *Am. J. Hum. Genet.* 67(4): 976–981.

Giannopoulou EA, Emmanouilidis L, Sattler M, Dodt G and Wilmanns M (2016) Towards the molecular mechanism of the integration of peroxisomal membrane proteins. *Biochim. Biophys. Acta - Mol. Cell Res.* 1863(5): 863–869.

Gilbert SL, Zhang L, Forster ML, Anderson JR, Iwase T, Soliven B, Donahue LR, Sweet HO, Bronson RT, Davisson MT, Wollmann RL and Lahn BT (2006) Trak1 mutation disrupts GABA(A) receptor homeostasis in hypertonic mice. *Nat. Genet.* 38(2): 245–250.

Glater EE, Megeath LJ, Stowers RS and Schwarz TL (2006) Axonal transport of mitochondria requires milton to recruit kinesin heavy chain and is light chain independent. *J. Cell Biol.* 173(4): 545–557.

Goitre L, Trapani E, Trabalzini L and Retta SF (2014) The Ras superfamily of small GTPases: the unlocked secrets. *Ras Signal. Methods Protoc.* 1120: 1–18.

Golde TE, Wolfe MS and Greenbaum DC (2009) Signal peptide peptidases: A family of intramembrane-cleaving proteases that cleave type 2 transmembrane proteins. *Semin. Cell Dev. Biol.* 20(2): 225–230.

Gondcaille C, Depreter M, Fourcade S, Lecca MR, Leclercq S, Martin PGP, Pineau T, Cadepond F, Eletr M, Bertrand N, Beley A, Duclos S, De Craemer D, Roels F, Savary S and Bugaut M (2005) Phenylbutyrate up-regulates the adrenoleukodystrophy-related gene as a nonclassical peroxisome proliferator. *J. Cell Biol.* 169(1): 93–104.

Gould SJ, Kalish JE, Morrell JC, Bjorkman J, Urquhart AJ and Crane DI (1996) Pex13p is an SH3 protein of the peroxisome membrane and a docking factor for the predominantly cytoplasmic PTS1 receptor. *J. Cell Biol.* 135(1): 85–95.

Guimaraes SC, Schuster M, Bielska E, Dagdas G, Kilaru S, Meadows BRA, Schrader M and Steinberg G (2015) Peroxisomes, lipid droplets, and endoplasmic reticulum ‘hitchhike’ on motile early endosomes. *J. Cell Biol.* 211(5): 945–954.

Guo X, Macleod GT, Wellington A, Hu F, Panchumarthi S, Schoenfield M, Marin L, Charlton MP, Atwood HL and Zinsmaier KE (2005) The GTPase dMiro is required for axonal transport of mitochondria to Drosophila synapses. *Neuron* 47(3): 379–393.

Gurvitz A and Rottensteiner H (2006) The biochemistry of oleate induction: Transcriptional upregulation and peroxisome proliferation. *Biochim.*

Biophys. Acta - Mol. Cell Res. 1763(12): 1392–1402.

Halbach A, Landgraf C, Lorenzen S, Rosenkranz K, Volkmer-Engert R, Erdmann R and Rottensteiner H (2006) Targeting of the tail-anchored peroxisomal membrane proteins PEX26 and PEX15 occurs through C-terminal PEX19-binding sites. *J. Cell Sci.* 119(Pt 12): 2508–2517.

Hancock WO (2014) Bidirectional cargo transport: moving beyond tug of war. *Nat. Rev. Mol. Cell Biol.* 15(9): 615–628.

Hassink GC, Zhao B, Sompallae R, Altun M, Gastaldello S, Zinin N V, Masucci MG and Lindsten K (2009) The ER-resident ubiquitin-specific protease 19 participates in the UPR and rescues ERAD substrates. *EMBO Rep.* 10(7): 755–761.

Hegde RS and Keenan RJ (2011) Tail-anchored membrane protein insertion into the endoplasmic reticulum. *Nat. Rev. Mol. Cell Biol.* 12(12): 787–798.

Hendricks AG, Perlson E, Ross JL, Schroeder HW, Tokito M and Holzbaur ELF (2010) Motor coordination via a tug-of-war mechanism drives bidirectional vesicle transport. *Curr. Biol.* 20(8): 697–702.

Hettema EH, Erdmann R, van der Klei IJ and Veenhuis M (2014) Evolving models for peroxisome biogenesis. *Curr. Opin. Cell Biol.* 29: 25–30.

Honsho M, Asaoku S, Fukumoto K and Fujiki Y (2013) Topogenesis and homeostasis of fatty acyl-CoA reductase 1. *J. Biol. Chem.* 288(48): 34588–34598.

Honsho M, Tamura S, Shimozawa N, Suzuki Y, Kondo N and Fujiki Y (1998) Mutation in PEX16 is causal in the peroxisome-deficient Zellweger syndrome of complementation group D. *Am J Hum Genet* 63(6): 1622–1630.

Honsho M, Yamashita S ichi and Fujiki Y (2016) Peroxisome homeostasis: Mechanisms of division and selective degradation of peroxisomes in mammals. *Biochim. Biophys. Acta - Mol. Cell Res.* 1863(5): 984–991.

Horie C, Suzuki H, Sakaguchi M and Mihara K (2002) Characterization of Signal That Directs C-Tail–anchored Proteins to Mammalian Mitochondrial Outer Membrane. *Mol. Biol. Cell* 13(5): 1615–1625.

Hu J, Baker A, Bartel B, Linka N, Mullen RT, Reumann S and Zolman BK (2012) Plant Peroxisomes: Biogenesis and Function. *Plant Cell* 24(6): 2279–2303.

Hua R and Kim PK (2016) Multiple paths to peroxisomes: Mechanism of peroxisome maintenance in mammals. *Biochim. Biophys. Acta - Mol. Cell Res.* 1863(5): 881–891.

Huber C, Saffrich R, Anton M, Passreiter M, Ansorge W, Gorgas K and Just W

(1997) A heterotrimeric G protein-phospholipase A2 signaling cascade is involved in the regulation of peroxisomal motility in CHO cells. *J. Cell Sci.* 110 (Pt 23: 2955–2968.

Huber N, Guimaraes SC, Schrader M, Suter U and Niemann A (2013) Charcot-Marie-Tooth disease-associated mutants of GDAP1 dissociate its roles in peroxisomal and mitochondrial fission. *EMBO Rep.* 14(6): 545–552.

Huttlin EL, Ting L, Bruckner RJ, Gebreab F, Gygi MP, Szpyt J, Tam S, Zarraga G, Colby G, Baltier K, Dong R, Guarani V, Vaites LP, Ordureau A, Rad R, Erickson BK, W??hr M, Chick J, Zhai B, Kolippakkam D, Mintseris J, Obar RA, Harris T, Artavanis-Tsakonas S, Sowa ME, De Camilli P, Paulo JA, Harper JW and Gygi SP (2015) The BioPlex Network: A Systematic Exploration of the Human Interactome. *Cell* 162(2): 425–440.

Islinger M, Abdolzade-bavil A, Liebler S, Weber G and Völkl A (2012) (a) Assessing heterogeneity of peroxisomes: isolation of two subpopulations from rat liver. In Josic D and Hixson DC (eds) *Liver Proteomics: Methods and Protocols*. Totowa, NJ: Humana Press, 83–96.

Islinger M, Cardoso MJR and Schrader M (2010) Be different--the diversity of peroxisomes in the animal kingdom. *Biochim. Biophys. Acta* 1803(8): 881–897.

Islinger M, Grille S, Fahimi HD and Schrader M (2012) (b) The peroxisome: an update on mysteries. *Histochem. Cell Biol.* 137(5): 547–574.

Islinger M, Lüers GH, Li KW, Loos M and Völkl A (2007) Rat liver peroxisomes after fibrate treatment. A survey using quantitative mass spectrometry. *J. Biol. Chem.* 282(32): 23055–23069.

Itoyama A, Honsho M, Abe Y, Moser A, Yoshida Y and Fujiki Y (2012) Docosahexaenoic acid mediates peroxisomal elongation, a prerequisite for peroxisome division. *J. Cell Sci.* 125(Pt 3): 589–602.

Ivashchenko O, Van Veldhoven PP, Brees C, Ho Y-S, Terlecky SR and Fransen M (2011) Intraperoxisomal redox balance in mammalian cells: oxidative stress and interorganellar cross-talk. *Mol. Biol. Cell* 22(9): 1440–1451.

Iwata JI, Ezaki J, Komatsu M, Yokota S, Ueno T, Tanida I, Chiba T, Tanaka K and Kominami E (2006) Excess peroxisomes are degraded by autophagic machinery in mammals. *J. Biol. Chem.* 281(7): 4035–4041.

Iyer SPN, Akimoto Y and Hart GW (2003) Identification and cloning of a novel family of coiled-coil domain proteins that interact with O-GlcNac transferase. *J. Biol. Chem.* 278(7): 5399–5409.

Jedd G and Chua N-H (2002) Visualization of peroxisomes in living plant cells reveals acto-myosin-dependent cytoplasmic streaming and peroxisome

budding. *Plant Cell Physiol.* 43(4): 384–392.

Jones JM, Morrell JC and Gould SJ (2001) Multiple distinct targeting signals in integral peroxisomal membrane proteins. *J. Cell Biol.* 153(6): 1141–1149.

Jones JM, Morrell JC and Gould SJ (2004) PEX19 is a predominantly cytosolic chaperone and import receptor for class 1 peroxisomal membrane proteins. *J. Cell Biol.* 164(1): 57–67.

Jongsma MLM, Berlin I and Neefjes J (2015) On the move: Organelle dynamics during mitosis. *Trends Cell Biol.* 25(3): 112–124.

Jonker R and Volgenant A (1987) A shortest augmenting path algorithm for dense and sparse linear assignment problems. *Computing* 38(4): 325–340.

Jourdain I, Sontam D, Johnson C, Dillies C and Hyams JS (2008) Dynamin-dependent biogenesis, cell cycle regulation and mitochondrial association of peroxisomes in fission yeast. *Traffic* 9(3): 353–365.

Just W and Kunau W-H (2014) History and Discovery of Peroxins. In *Molecular Machines Involved in Peroxisome Biogenesis and Maintenance*. Springer, 3–15.

Jwa M and Chang P (2012) PARP16 is a tail-anchored endoplasmic reticulum protein required for the PERK- and IRE1α-mediated unfolded protein response. *Nat. Cell Biol.* 14(11): 1223–1230.

Kalbfleisch T, Cambon A and Wattenberg BW (2007) A bioinformatics approach to identifying tail-anchored proteins in the human genome. *Traffic* 8(12): 1687–1694.

Kanfer G, Courthéoux T, Peterka M, Meier S, Soste M, Melnik A, Reis K, Aspenström P, Peter M, Picotti P and Kornmann B (2015) Mitotic redistribution of the mitochondrial network by Miro and Cenp-F. *Nat. Commun.* 6: 8015.

Kapitein LC, Schlager M a, van der Zwan W a, Wulf PS, Keijzer N and Hoogenraad CC (2010) Probing intracellular motor protein activity using an inducible cargo trafficking assay. *Biophys. J.* 99(7): 2143–2152.

Kato H and Mihara K (2008) Identification of Tom5 and Tom6 in the preprotein translocase complex of human mitochondrial outer membrane. *Biochem. Biophys. Res. Commun.* 369(3): 958–963.

Kaur N and Hu J (2009) Dynamics of peroxisome abundance: a tale of division and proliferation. *Curr. Opin. Plant Biol.* 12(6): 781–788.

Kawahara H, Minami R and Yokota N (2013) BAG6/BAT3: Emerging roles in quality control for nascent polypeptides. *J. Biochem.* 153(2): 147–160.

Ke N, Godzik A and Reed JC (2001) Bcl-B, a novel Bcl-2 family member that

differentially binds and regulates Bax and Bak. *J. Biol. Chem.* 276(16): 12481–12484.

Kemper C, Habib SJ, Engl G, Heckmeyer P, Dimmer KS and Rapaport D (2008) Integration of tail-anchored proteins into the mitochondrial outer membrane does not require any known import components. *J. Cell Sci.* 121(Pt 12): 1990–1998.

Kim PK, Hailey DW, Mullen RT and Lippincott-Schwartz J (2008) Ubiquitin signals autophagic degradation of cytosolic proteins and peroxisomes. *Proc. Natl. Acad. Sci. U. S. A.* 105(52): 20567–20574.

Kim PK and Mullen RT (2013) PEX16: a multifaceted regulator of peroxisome biogenesis. *Front. Physiol.* 4(September): 241.

Kim PK, Mullen RT, Schumann U and Lippincott-Schwartz J (2006) The origin and maintenance of mammalian peroxisomes involves a de novo PEX16-dependent pathway from the ER. *J. Cell Biol.* 173(4): 521–532.

Kirk E, Chin L-S and Li L (2006) GRIF1 binds Hrs and is a new regulator of endosomal trafficking. *J. Cell Sci.* 119(Pt 22): 4689–4701.

Kliewer S a, Umesono K, Noonan DJ, Heyman R a and Evans RM (1992) Convergence of 9-cis retinoic acid and peroxisome proliferator signalling pathways through heterodimer formation of their receptors. *Nature* 358(6389): 771–774.

Klosowiak JL, Focia PJ, Chakravarthy S, Landahl EC, Freymann DM and Rice SE (2013) Structural coupling of the EF hand and C-terminal GTPase domains in the mitochondrial protein Miro. *EMBO Rep.* 14(11): 968–974.

Klouwer FCC, Berendse K, Ferdinandusse S, Wanders RJA, Engelen M and Poll-The BT (2015) Zellweger spectrum disorders: clinical overview and management approach. *Orphanet J. Rare Dis.* 10(1): 151.

Knoblach B and Rachubinski R a. (2015) Sharing the cell’s bounty - organelle inheritance in yeast. *J. Cell Sci.* 128: 621–630.

Knoblach B and Rachubinski RA (2016) How peroxisomes partition between cells. A story of yeast, mammals and filamentous fungi. *Curr. Opin. Cell Biol.* 41: 73–80.

Kobayashi S, Tanaka A and Fujiki Y (2007) Fis1, DLP1, and Pex11p coordinately regulate peroxisome morphogenesis. *Exp. Cell Res.* 313(8): 1675–1686.

Koch A, Thiemann M, Grabenbauer M, Yoon Y, McNiven M a and Schrader M (2003) Dynamin-like protein 1 is involved in peroxisomal fission. *J. Biol. Chem.* 278(10): 8597–8605.

Koch A, Yoon Y, Bonekamp NA, Mcniven MA and Schrader M (2005) A Role for

Fis1 in Both Mitochondrial and Peroxisomal Fission in Mammalian Cells. *Mol. Biol. Cell* 16: 5077–5086.

Koch J and Brocard C (2012) PEX11 proteins attract Mff and hFis1 to coordinate peroxisomal fission. *J. Cell Sci.* 125: 3813–3826.

Koch J, Feichtinger RG, Freisinger P, Pies M, Schrödl F, Iuso A, Sperl W, Mayr J a, Prokisch H and Haack TB (2016) Disturbed mitochondrial and peroxisomal dynamics due to loss of MFF causes Leigh-like encephalopathy, optic atrophy and peripheral neuropathy. *J. Med. Genet.* 53(4): 270–278.

Koch J, Pranjic K, Huber A, Ellinger A, Hartig A, Kragler F and Brocard C (2010) PEX11 family members are membrane elongation factors that coordinate peroxisome proliferation and maintenance. *J. Cell Sci.* 123: 3389–3400.

Kornmann B, Currie E, Collins SR, Schuldiner M, Nunnari J, Weissman JS and Walter P (2009) An ER-mitochondria tethering complex revealed by a synthetic biology screen. *Science* 325(5939): 477–481.

Kornmann B, Osman C and Walter P (2011) The conserved GTPase Gem1 regulates endoplasmic reticulum-mitochondria connections. *Proc. Natl. Acad. Sci.* 108(34): 14151–14156.

Koshiba T, Holman H a, Kubara K, Yasukawa K, Kawabata S, Okamoto K, MacFarlane J and Shaw JM (2011) Structure-function analysis of the yeast mitochondrial Rho GTPase, Gem1p: implications for mitochondrial inheritance. *J. Biol. Chem.* 286(1): 354–362.

Koutsopoulos OS, Laine D, Osellame L, Chudakov DM, Parton RG, Frazier AE and Ryan MT (2010) Human Miltons associate with mitochondria and induce microtubule-dependent remodeling of mitochondrial networks. *Biochim. Biophys. Acta* 1803(5): 564–574.

Krajewski S, Tanaka S, Takayama S, Schibler MJ, Fenton W and Reed JC (1993) Investigation of the Subcellular Distribution of the bcl-2 Oncoprotein : Residence in the Nuclear Envelope , Endoplasmic Reticulum , and Outer Mitochondrial Membranes. *Cancer Res.* 53(19): 4701–4714.

Kredel S, Oswald F, Nienhaus K, Deuschle K, Röcker C, Wolff M, Heilker R, Nienhaus GU and Wiedenmann J (2009) mRuby, a bright monomeric red fluorescent protein for labeling of subcellular structures. *PLoS One* 4(2): e4391.

Kriechbaumer V, Shaw R, Mukherjee J, Bowsher CG, Harrison A-M and Abell BM (2009) Subcellular distribution of tail-anchored proteins in Arabidopsis. *Traffic* 10(12): 1753–1764.

Krogh a, Larsson B, von Heijne G and Sonnhammer EL (2001) Predicting transmembrane protein topology with a hidden Markov model: application

to complete genomes. *J. Mol. Biol.* 305(3): 567–580.

Krumpe K, Frumkin I, Herzig Y, Rimon N, Özbalci C, Brügger B, Rapaport D and Schuldiner M (2012) Ergosterol content specifies targeting of tail-anchored proteins to mitochondrial outer membranes. *Mol. Biol. Cell* 23(20): 3927–3935.

Krut O, Wiegmann K, Kashkar H, Yazdanpanah B and Krönke M (2006) Novel tumor necrosis factor-responsive mammalian neutral sphingomyelinase-3 is a C-tail-anchored protein. *J. Biol. Chem.* 281(19): 13784–13793.

Kural C, Kim H, Syed S, Goshima G, Gelfand VI and Selvin PR (2005) Kinesin and dynein move a peroxisome in vivo: a tug-of-war or coordinated movement? *Science (80-.).* 308(5727): 1469–1472.

Kuroda R, Ikenoue T, Honsho M, Tsujimoto S, Mitoma JY and Ito A (1998) Charged amine acids at the carboxyl-terminal portions determine the intracellular locations of two isoforms of cytochrome b5. *J. Biol. Chem.* 273(47): 31097–31102.

Kutay U, Hartmann E and Rapoport T a (1993) A class of membrane proteins with a C-terminal anchor. *Trends Cell Biol.* 3(3): 72–75.

Kyte J and Doolittle RF (1982) A simple method for displaying the hydropathic character of a protein. *J. Mol. Biol.* 157(1): 105–132.

Laurenti G, Benedetti E, D'Angelo B, Cristiano L, Cinque B, Raysi S, Alecci M, Cer?? MP, Cifone MG, Galzio R, Giordano A and Cimini A (2011) Hypoxia induces peroxisome proliferator-activated receptor ?? (PPAR??) and lipid metabolism peroxisomal enzymes in human glioblastoma cells. *J. Cell. Biochem.* 112(12): 3891–3901.

Lawrence EJ, Boucher E and Mandato CA (2016) Mitochondria-cytoskeleton associations in mammalian cytokinesis. *Cell Div.* 11(1): 3.

Lenk U, Yu H, Walter J, Gelman MS, Hartmann E, Kopito RR and Sommer T (2002) A role for mammalian Ubc6 homologues in ER-associated protein degradation. *J. Cell Sci.* 115(Pt 14): 3007–3014.

Léon S, Goodman JM and Subramani S (2006) Uniqueness of the mechanism of protein import into the peroxisome matrix: Transport of folded, co-factor-bound and oligomeric proteins by shuttling receptors. *Biochim. Biophys. Acta - Mol. Cell Res.* 1763(12): 1552–1564.

Leznicki P, Clancy A, Schwappach B and High S (2010) Bat3 promotes the membrane integration of tail-anchored proteins. *J. Cell Sci.* 123(Pt 13): 2170–2178.

Li X and Gould SJ (2002) PEX11 promotes peroxisome division independently of peroxisome metabolism. *J. Cell Biol.* 156(4): 643–651.

Li X and Gould SJ (2003) The dynamin-like GTPase DLP1 is essential for peroxisome division and is recruited to peroxisomes in part by PEX11. *J. Biol. Chem.* 278(19): 17012–17020.

Li Y, Lim S, Hoffman D, Aspenstrom P, Federoff HJ and Rempe D a (2009) HUMMR, a hypoxia- and HIF-1alpha-inducible protein, alters mitochondrial distribution and transport. *J. Cell Biol.* 185(6): 1065–1081.

Lindeberg T (1998) Feature detection with automatic scale selection. *Int. J. Comput. Vis.* 30(2): 79–116.

Lindeberg T (2013) *Scale-space theory in computer vision*. Springer Science & Business Media.

Liu S, Sawada T, Lee S, Yu W, Silverio G, Alapatt P, Millan I, Shen A, Saxton W, Kanao T, Ryosuke T, Hattori N, Imai Y and Lu B (2012) Parkinson's Disease–Associated Kinase PINK1 Regulates Miro Protein Level and Axonal Transport of Mitochondria. *PLoS Genet.* 8(3): e1002537.

Lizard G, Rouaud O, Demarquoy J, Cherkaoui-Malki M and Iuliano L (2012) Potential Roles of Peroxisomes in Alzheimer's Disease and in Dementia of the Alzheimer's Type. *J. Alzheimer's Dis.* 29: 241–254.

Lodhi IJ and Semenkovich CF (2014) Peroxisomes: A Nexus for Lipid Metabolism and Cellular Signaling. *Cell Metab.* 19(3): 380–392.

López-Doménech G, Serrat R, Mirra S, D'Aniello S, Somorjai I, Abad A, Vitureira N, García-Arumí E, Alonso MT, Rodriguez-Prados M, Burgaya F, Andreu AL, García-Sancho J, Trullas R, Garcia-Fernàndez J and Soriano E (2012) The Eutherian Armcx genes regulate mitochondrial trafficking in neurons and interact with Miro and Trak2. *Nat. Commun.* 3: 814.

López-Erauskin J, Galino J, Ruiz M, Cuezva JM, Fabregat I, Cacabelos D, Boada J, Martínez J, Ferrer I, Pamplona R, Villarroya F, Portero-Otín M, Fourcadeand S and Pujol A (2013) Impaired mitochondrial oxidative phosphorylation in the peroxisomal disease X-linked adrenoleukodystrophy. *Hum. Mol. Genet.* 22(16): 3296–3305.

Loureiro J, Lilley BN, Spooner E, Noriega V, Tortorella D and Ploegh HL (2006) Signal peptide peptidase is required for dislocation from the endoplasmic reticulum. *Nature* 441(7095): 894–897.

MacAskill AF, Brickley K, Stephenson FA and Kittler JT (2009) (a) GTPase dependent recruitment of Grif-1 by Miro1 regulates mitochondrial trafficking in hippocampal neurons. *Mol. Cell. Neurosci.* 40(3): 301–312.

MacAskill AF, Rinholm JE, Twelvetrees AE, Arancibia-Carcamo IL, Muir J, Fransson A, Aspenstrom P, Attwell D and Kittler JT (2009) (b) Miro1 is a calcium sensor for glutamate receptor-dependent localization of mitochondria at synapses. *Neuron* 61(4): 541–555.

Mannini B, Mulvihill E, Sgromo C, Cascella R, Khodarahmi R, Ramazzotti M, Dobson CM, Cecchi C and Chiti F (2014) Toxicity of protein oligomers is rationalized by a function combining size and surface hydrophobicity. *ACS Chem. Biol.* 9(10): 2309–2317.

Mariappan M, Li X, Stefanovic S, Sharma A, Mateja A, Keenan RJ and Hegde RS (2010) A ribosome-associating factor chaperones tail-anchored membrane proteins. *Nature* 466(7310): 1120–1124.

Mariappan M, Mateja A, Dobosz M, Bove E, Hegde RS and Keenan RJ (2011) The mechanism of membrane-associated steps in tail-anchored protein insertion. *Nature* 477(7362): 61–66.

Marty NJ, Teresinski HJ, Hwang YT, Clendening E a., Gidda SK, Sliwinska E, Zhang D, Miernyk J a., Brito GC, Andrews DW, Dyer JM and Mullen RT (2014) New insights into the targeting of a subset of tail-anchored proteins to the outer mitochondrial membrane. *Front. Plant Sci.* 5(September): 426.

Mast FD, Rachubinski RA and Aitchison JD (2015) Signaling dynamics and peroxisomes. *Curr. Opin. Cell Biol.* 35: 131–136.

Mateja A, Szlachcic A, Downing ME, Dobosz M, Mariappan M, Hegde RS and Keenan RJ (2009) The structural basis of tail-anchored membrane protein recognition by Get3. *Nature* 461(7262): 361–366.

Matsumoto N, Tamura S and Fujiki Y (2003) The pathogenic peroxin Pex26p recruits the Pex1p-Pex6p AAA ATPase complexes to peroxisomes. *Nat. Cell Biol.* 5(5): 454–460.

Matsuzaki T and Fujiki Y (2008) The peroxisomal membrane protein import receptor Pex3p is directly transported to peroxisomes by a novel Pex19p- and Pex16p-dependent pathway. *J. Cell Biol.* 183(7): 1275–1286.

Matsuzono Y, Kinoshita N, Tamura S, Shimozawa N, Hamasaki M, Ghaedi K, Wanders RJ, Suzuki Y, Kondo N and Fujiki Y (1999) Human PEX19: cDNA cloning by functional complementation, mutation analysis in a patient with Zellweger syndrome, and potential role in peroxisomal membrane assembly. *Proc. Natl. Acad. Sci. U. S. A.* 96(5): 2116–2121.

Mattson MP, Gleichmann M and Cheng A (2008) Mitochondria in neuroplasticity and neurological disorders. *Neuron* 60(5): 748–766.

Mayerhofer PU (2016) Targeting and insertion of peroxisomal membrane proteins: ER trafficking versus direct delivery to peroxisomes. *Biochim. Biophys. Acta - Mol. Cell Res.* 1863(5): 870–880.

McNew JA and Goodman JM (1994) An oligomeric protein is imported into peroxisomes in vivo. *J. Cell Biol.* 127(5): 1245–1257.

Mears J a, Lackner LL, Fang S, Ingerman E, Nunnari J and Hinshaw JE (2011)

Conformational changes in Dnm1 support a contractile mechanism for mitochondrial fission. *Nat. Struct. Mol. Biol.* 18(1): 20–26.

Meinecke M, Bartsch P and Wagner R (2016) Peroxisomal protein import pores. *Biochim. Biophys. Acta - Mol. Cell Res.* 1863(5): 821–827.

Meyer D, Dimitriadou E, Hornik K, Weingessel A and Leisch F (2014) *Misc functions of the Department of Statistics (e1071), TU Wien*.

Misko A, Jiang S, Wegorzewska I, Milbrandt J and Baloh RH (2010) Mitofusin 2 is necessary for transport of axonal mitochondria and interacts with the Miro/Milton complex. *J. Neurosci.* 30(12): 4232–4240.

Mizushima N and Komatsu M (2011) Autophagy: renovation of cells and tissues. *Cell* 147(4): 728–741.

Morlino G, Barreiro O, Baixauli F, Robles-Valero J, González-Granado JM, Villa-Bellosta R, Cuenca J, Sánchez-Sorzano CO, Veiga E, Martín-Cófreces NB and Sánchez-Madrid F (2014) Miro-1 links mitochondria and microtubule Dynein motors to control lymphocyte migration and polarity. *Mol. Cell. Biol.* 34(8): 1412–1426.

Mórotz GM, De Vos KJ, Vagnoni A, Ackerley S, Shaw CE and Miller CCJ (2012) Amyotrophic lateral sclerosis-associated mutant VAPBP56s perturbs calcium homeostasis to disrupt axonal transport of mitochondria. *Hum. Mol. Genet.* 21(9): 1979–1988.

Motz C, Martin H, Krimmer T and Rassow J (2002) Bcl-2 and porin follow different pathways of TOM-dependent insertion into the mitochondrial outer membrane. *J. Mol. Biol.* 323(4): 729–738.

Muntau a C, Mayerhofer PU, Paton BC, Kammerer S and Roscher a a (2000) Defective peroxisome membrane synthesis due to mutations in human PEX3 causes Zellweger syndrome, complementation group G. *Am. J. Hum. Genet.* 67(4): 967–975.

Murley A, Lackner LL, Osman C, West M, Voeltz GK, Walter P and Nunnari J (2013) ER-associated mitochondrial division links the distribution of mitochondria and mitochondrial DNA in yeast. *Elife* 2: e00422.

Murtagh F and Starck J-L (2000) Image processing through multiscale analysis and measurement noise modeling. *Stat. Comput.* 10(2): 95–103.

Nazarko TY, Ozeki K, Till A, Ramakrishnan G, Lotfi P, Yan M and Subramani S (2014) Peroxisomal Atg37 binds Atg30 or palmitoyl-CoA to regulate phagophore formation during pexophagy. *J. Cell Biol.* 204(4): 541–557.

Neuhaus A, Eggeling C, Erdmann R and Schliebs W (2016) Why do peroxisomes associate with the cytoskeleton? *Biochim. Biophys. Acta - Mol. Cell Res.* 1863(5): 1019–1026.

Neuspiel M, Schauss AC, Braschi E, Zunino R, Rippstein P, Rachubinski R a, Andrade-Navarro M a and McBride HM (2008) Cargo-selected transport from the mitochondria to peroxisomes is mediated by vesicular carriers. *Curr. Biol.* 18(2): 102–108.

Nguyen T, Bjorkman J, Paton BC and Crane DI (2006) Failure of microtubule-mediated peroxisome division and trafficking in disorders with reduced peroxisome abundance. *J. Cell Sci.* 119(Pt 4): 636–645.

Nguyen T, Lewandowska A, Choi J-Y, Markgraf DF, Junker M, Bilgin M, Ejsing CS, Voelker DR, Rapoport T a and Shaw JM (2012) Gem1 and ERMES do not directly affect phosphatidylserine transport from ER to mitochondria or mitochondrial inheritance. *Traffic* 13(6): 880–890.

Nguyen TT, Oh SS, Weaver D, Lewandowska A, Maxfield D, Schuler M-H, Smith NK, Macfarlane J, Saunders G, Palmer C a., Debattisti V, Koshiba T, Pulst S, Feldman EL, Hajnoczky G and Shaw JM (2014) Loss of Miro1-directed mitochondrial movement results in a novel murine model for neuron disease. *Proc. Natl. Acad. Sci.* 111(35): E3631–E3640.

Niemann A, Huber N, Wagner KM, Somandin C, Horn M, Lebrun-Julien F, Angst B, Pereira J a., Halfter H, Welzl H, Feltri ML, Wrabetz L, Young P, Wessig C, Toyka K V. and Suter U (2014) The Gdap1 knockout mouse mechanistically links redox control to Charcot-Marie-tooth disease. *Brain* 137(3): 668–682.

Nordgren M, Francisco T, Lismont C, Hennebel L, Brees C, Wang B, van Veldhoven PP, Azevedo JE and Fransen M (2015) Export-deficient monoubiquitinated PEX5 triggers peroxisome removal in SV40 large T antigen-transformed mouse embryonic fibroblasts. *Autophagy* 11(8): 1326–1340.

Nordgren M and Fransen M (2014) Peroxisomal metabolism and oxidative stress. *Biochimie* 98(1): 56–62.

Nordgren M, Wang B, Apanasets O and Fransen M (2013) Peroxisome degradation in mammals: mechanisms of action, recent advances, and perspectives. *Front. Physiol.* 4(June): 145.

Odendall C, Dixit E, Stavru F, Bierne H, Franz KM, Durbin AF, Boulant S, Gehrke L, Cossart P and Kagan JC (2014) Diverse intracellular pathogens activate type III interferon expression from peroxisomes. *Nat. Immunol.* 15(8): 717–728.

Okreglak V and Walter P (2014) The conserved AAA-ATPase Msp1 confers organelle specificity to tail-anchored proteins. *Proc. Natl. Acad. Sci. U. S. A.* 111(22): 8019–8024.

Onoue K, Jofuku A, Ban-Ishihara R, Ishihara T, Maeda M, Koshiba T, Itoh T,

Fukuda M, Otera H, Oka T, Takano H, Mizushima N, Mihara K and Ishihara N (2013) Fis1 acts as a mitochondrial recruitment factor for TBC1D15 that is involved in regulation of mitochondrial morphology. *J. Cell Sci.* 126(Pt 1): 176–185.

Opaliński L, Kiel JAKW, Williams C, Veenhuis M and van der Klei IJ (2011) Membrane curvature during peroxisome fission requires Pex11. *EMBO J.* 30: 5–16.

Otera H, Okumoto K, Tateishi K, Ikoma Y, Matsuda E, Nishimura M, Tsukamoto T, Osumi T, Ohashi K, Higuchi O and Fujiki Y (1998) Peroxisome Targeting Signal Type 1 (PTS1) Receptor Is Involved in Import of Both PTS1 and PTS2: Studies withPEX5-Defective CHO Cell Mutants. *Mol. Cell. Biol.* 18(1): 388–399.

Otera H, Wang C, Cleland MM, Setoguchi K, Yokota S, Youle RJ and Mihara K (2010) Mff is an essential factor for mitochondrial recruitment of Drp1 during mitochondrial fission in mammalian cells. *J. Cell Biol.* 191(6): 1141–1158.

Otzen M, Rucktäschel R, Thoms S, Emmrich K, Krikken AM, Erdmann R and van der Klei IJ (2012) Pex19p contributes to peroxisome inheritance in the association of peroxisomes to Myo2p. *Traffic* 13(7): 947–959.

Palmer CS, Osellame LD, Laine D, Koutsopoulos OS, Frazier AE and Ryan MT (2011) MiD49 and MiD51, new components of the mitochondrial fission machinery. *EMBO Rep.* 12(6): 565–573.

Pedrazzini E, Villa A and Borgese N (1996) A mutant cytochrome b5 with a lengthened membrane anchor escapes from the endoplasmic reticulum and reaches the plasma membrane. *Proc. Natl. Acad. Sci. U. S. A.* 93(9): 4207–4212.

Pekkurnaz G, Trinidad JC, Wang X, Kong D and Schwarz TL (2014) Glucose Regulates Mitochondrial Motility via Milton Modification by O-GlcNAc Transferase. *Cell* 158(1): 54–68.

Pieuchot L and Jedd G (2012) Peroxisome assembly and functional diversity in eukaryotic microorganisms. *Annu. Rev. Microbiol.* 66: 237–263.

Platta HW, Brinkmeier R, Reidick C, Galiani S, Clausen MP and Eggeling C (2016) Regulation of peroxisomal matrix protein import by ubiquitination. *Biochim. Biophys. Acta - Mol. Cell Res.* 1863(5): 838–849.

Rabu C, Schmid V, Schwappach B and High S (2009) Biogenesis of tail-anchored proteins: the beginning for the end? *J. Cell Sci.* 122: 3605–3612.

Rakhshandehroo M, Knoch B, Michael M and Kersten S (2010) Peroxisome Proliferator-Activated Receptor Alpha Target Genes. *PPAR Res.*: 612089.

Rapp S, Saffrich R, Anton M, Jäkle U, Ansorge W, Gorgas K and Just WW (1996) Microtubule-based peroxisome movement. *J. Cell Sci.* 109: 837–849.

Raychaudhuri S and Prinz WA (2008) Nonvesicular phospholipid transfer between peroxisomes and the endoplasmic reticulum. *Proc. Natl. Acad. Sci. U. S. A.* 105(41): 15785–15790.

Reddy JK, Goel SK, Nemali MR, Carrino JJ, Laffler TG, Reddy MK, Sperbeck SJ, Osumi T, Hashimoto T and Lalwani ND (1986) Transcription regulation of peroxisomal fatty acyl-CoA oxidase and enoyl-CoA hydratase/3-hydroxyacyl-CoA dehydrogenase in rat liver by peroxisome proliferators. *Proc. Natl. Acad. Sci. U. S. A.* 83(6): 1747–1751.

Rehling P, Marzioch M, Niesen F, Wittke E, Veenhuis M and Kunau WH (1996) The import receptor for the peroxisomal targeting signal 2 (PTS2) in Saccharomyces cerevisiae is encoded by the PAS7 gene. *EMBO J.* 15(12): 2901–2913.

Reis K, Fransson Å and Aspenström P (2009) The Miro GTPases : At the heart of the mitochondrial transport machinery. *FEBS Lett.* 583(9): 1391–1398.

Rhodin J (1954) *Correlation of ultrastructural organization and function in normal and experimentally changed proximal convoluted tubule cells of the mouse kidney*. Aktiebolaget Godvil.

Rottensteiner H, Kramer A, Lorenzen S, Stein K, Landgraf C, Volkmer-Engert R and Erdmann R (2004) Peroxisomal membrane proteins contain common Pex19p-binding sites that are an integral part of their targeting signals. *Mol. Biol. Cell* 15: 3406–3417.

Russo GJ, Louie K, Wellington A, Macleod GT, Hu F, Panchumarthi S and Zinsmaier KE (2009) Drosophila Miro Is Required for Both Anterograde and Retrograde Axonal Mitochondrial Transport. *J. Neurosci.* 29(17): 5443–5455.

Saeki K, Suzuki H, Tsuneoka M, Maeda M, Iwamoto R, Hasuwa H, Shida S, Takahashi T, Sakaguchi M, Endo T, Miura Y, Mekada E and Mihara K (2000) Identification of mammalian TOM22 as a subunit of the preprotein translocase of the mitochondrial outer membrane. *J. Biol. Chem.* 275(41): 31996–32002.

Salogiannis J, Egan MJ and Reck-Peterson SL (2016) Peroxisomes move by hitchhiking on early endosomes using the novel linker protein PxdA. *J. Cell Biol.* 212(3): 289–296.

Saotome M, Safiulina D, Szabadkai G, Das S, Fransson Å, Aspenström P, Rizzuto R, Hajnóczky G, Fransson A and Aspenstrom P (2008) Bidirectional Ca2+ -dependent control of mitochondrial dynamics by the

Miro GTPase. *Proc. Natl. Acad. Sci. U. S. A.* 105(52): 20728–20733.

Schliebs W, Saidowsky J, Agianian B, Dodt G, Herberg FW and Kunau W-H (1999) Recombinant Human Peroxisomal Targeting Signal Receptor PEX5: Structural basis for interaction of PEX5 with PEX14. *J. Biol. Chem.* 274(9): 5666–5673.

Schlüter A, Real-Chicharro A, Gabaldón T, Sánchez-Jiménez F and Pujol A (2010) PeroxisomeDB 2.0: an integrative view of the global peroxisomal metabolome. *Nucleic Acids Res.* 38(Database issue): D800–D805.

Schrader M, Almeida M and Grille S (2012) (a) Postfixation detergent treatment liberates the membrane modelling protein Pex11β from peroxisomal membranes. *Histochem. Cell Biol.* 138: 541–547.

Schrader M, Bonekamp NA and Islinger M (2012) (b) Fission and proliferation of peroxisomes. *Biochim. Biophys. Acta* 1822(9): 1343–1357.

Schrader M, Burkhardt JK, Baumgart E, Lüers GH, Spring H, Volkl A, Fahimi HD, Völkl A and Fahimi HD (1996) Interaction of microtubules with peroxisomes. Tubular and spherical peroxisomes in HepG2 cells and their alteractions induced by microtubule-active drugs. *Eur. J. Cell Biol.* 69: 24–35.

Schrader M, Castro I, Fahimi HD and Islinger M (2014) Peroxisome morphology in pathologies. In *Molecular Machines Involved in Peroxisome Biogenesis and Maintenance*. Springer, 125–151.

Schrader M, Costello J, Godinho LF and Islinger M (2015) (a) Peroxisome-mitochondria interplay and disease. *J. Inherit. Metab. Dis.* 38(4): 681–702.

Schrader M, Costello JL, Godinho LF, Azadi AS and Islinger M (2016) Proliferation and fission of peroxisomes - An update. *Biochim. Biophys. Acta - Mol. Cell Res.* 1863: 971–983.

Schrader M, Godinho LF, Costello JL and Islinger M (2015) (b) The different facets of organelle interplay—an overview of organelle interactions. *Front. Cell Dev. Biol.* 3: 56.

Schrader M, Grille S, Fahimi HD and Islinger M (2013) Peroxisome interactions and cross-talk with other subcellular compartments in animal cells. 69: 1–22.

Schrader M, King SJ, Stroh TA and Schroer TA (2000) Real time imaging reveals a peroxisomal reticulum in living cells. *J. Cell Sci.* 113: 3663–3671.

Schrader M, Krieglstein K and Dariush Fahimi H (1998) (a) Tubular peroxisomes in HepG2 cells: Selective induction by growth factors and arachidonic acid. *Eur. J. Cell Biol.* 75(2): 87–96.

Schrader M, Reuber BE, Morrell JC, Jimenez-sanchez G, Obie C, Stroh TA, Valle D, Schroer TA and Gould SJ (1998) (b) Expression of PEX11β mediates peroxisome proliferation in the absence of extracellular stimuli. *J. Biol. Chem.* 273(45): 29607–29614.

Schrader M, Thiemann M and Fahimi HD (2003) Peroxisomal Motility and Interaction With Microtubules. *Microsc. Res. Tech.* 61: 171–178.

Schuldiner M, Metz J, Schmid V, Denic V, Rakwalska M, Schmitt HD, Schwappach B and Weissman JS (2008) The GET Complex Mediates Insertion of Tail-Anchored Proteins into the ER Membrane. *Cell* 134: 634–645.

Serrat R, Mirra S, Figueiro-Silva J, Navas-Pérez E, Quevedo M, López-Doménech G, Podlesniy P, Ulloa F, Garcia-Fernàndez J, Trullas R and Soriano E (2014) The Armc10/SVH gene: genome context, regulation of mitochondrial dynamics and protection against Aβ-induced mitochondrial fragmentation. *Cell Death Dis.* 5: e1163.

Setoguchi K, Otera H and Mihara K (2006) Cytosolic factor- and TOM-independent import of C-tail-anchored mitochondrial outer membrane proteins. *EMBO J.* 25: 5635–5647.

Sexton JZ, He Q, Forsberg LJ and Brenman JE (2010) High content screening for non-classical peroxisome proliferators. *Int. J. High Throughput Screen.* 2010(1): 127–140.

Shai N, Schuldiner M and Zalckvar E (2015) No peroxisome is an island - Peroxisome contact sites. *Biochim. Biophys. Acta - Mol. Cell Res.* 1863(5): 1061–1069.

Shamseldin HE, Alshammari M, Al-Sheddi T, Salih M a, Alkhalidi H, Kentab A, Repetto GM, Hashem M and Alkuraya FS (2012) Genomic analysis of mitochondrial diseases in a consanguineous population reveals novel candidate disease genes. *J. Med. Genet.* 49(4): 234–241.

Sheng Z-H and Cai Q (2012) Mitochondrial transport in neurons: impact on synaptic homeostasis and neurodegeneration. *Nat. Rev. Neurosci.* 13(2): 77–93.

Shibata H, Kashiwayama Y, Imanaka T and Kato H (2004) Domain architecture and activity of human Pex19p, a chaperone-like protein for intracellular trafficking of peroxisomal membrane proteins. *J. Biol. Chem.* 279(37): 38486–38494.

Shimozawa N, Tsukamoto T, Nagase T, Takemoto Y, Koyama N, Suzuki Y, Komori M, Osumi T, Jeannette G, Wanders RJA and Kondo N (2004) Identification of a New Complementation Group of the Peroxisome Biogenesis Disorders and PEX14 as the Mutated Gene. *Hum. Mutat.* 23:

552–558.

Sinclair AM, Trobacher CP, Mathur N, Greenwood JS and Mathur J (2009) Peroxule extension over ER-defined paths constitutes a rapid subcellular response to hydroxyl stress. *Plant J.* 59(2): 231–242.

Smith JJ and Aitchison JD (2013) Peroxisomes take shape. *Nat. Rev. Mol. Cell Biol.* 14(12): 803–817.

Smith MJ, Pozo K, Brickley K and Stephenson FA (2006) Mapping the GRIF-1 Binding Domain of the Kinesin , KIF5C , Substantiates a Role for GRIF-1 as an Adaptor Protein in the Anterograde Trafficking of Cargoes. *J. Biol. Chem.* 281(37): 27216–27228.

Sparkes I and Gao H (2014) Plant Peroxisome Dynamics: Movement, Positioning and Connections. In *Molecular Machines Involved in Peroxisome Biogenesis and Maintenance*. Springer, 461–477.

Stark C, Breitkreutz B-J, Reguly T, Boucher L, Breitkreutz A and Tyers M (2006) BioGRID: a general repository for interaction datasets. *Nucl. Acids Res.* 34: D535–D539.

Stefanovic S and Hegde RS (2007) Identification of a Targeting Factor for Posttranslational Membrane Protein Insertion into the ER. *Cell* 128: 1147–1159.

Stolz A, Hilt W, Buchberger A and Wolf DH (2011) Cdc48: A power machine in protein degradation. *Trends Biochem. Sci.* 36(10): 515–523.

Stowers RS, Megeath LJ, Górska-Andrzejak J, Meinertzhagen I a and Schwarz TL (2002) Axonal transport of mitochondria to synapses depends on milton, a novel Drosophila protein. *Neuron* 36(6): 1063–1077.

Stroud DA, Oeljeklaus S, Wiese S, Bohnert M, Lewandrowski U, Sickmann A, Guiard B, Van Der Laan M, Warscheid B and Wiedemann N (2011) Composition and topology of the endoplasmic reticulum-mitochondria encounter structure. *J. Mol. Biol.* 413(4): 743–750.

Suzuki M, Danilchanka O and Mekalanos JJ (2014) Vibrio cholerae T3SS effector VopE modulates mitochondrial dynamics and innate immune signaling by targeting Miro GTPases. *Cell Host Microbe* 16(5): 581–591.

Takeshima H, Komazaki S, Nishi M, Iino M and Kangawa K (2000) Junctophilins: a novel family of junctional membrane complex proteins. *Mol. Cell* 6(1): 11–22.

Tanaka A, Cleland MM, Xu S, Narendra DP, Suen DF, Karbowski M and Youle RJ (2010) Proteasome and p97 mediate mitophagy and degradation of mitofusins induced by Parkin. *J. Cell Biol.* 191(7): 1367–1380.

Tanaka A, Okumoto K and Fujiki Y (2003) cDNA cloning and characterization of the third isoform of human peroxin Pex11p. *Biochem Biophys Res Commun* 300(4): 819–823.

Terlecky SR, Nuttley WM, McCollum D, Sock E and Subramani S (1995) The Pichia pastoris peroxisomal protein PAS8p is the receptor for the C-terminal tripeptide peroxisomal targeting signal. *EMBO J.* 14(15): 3627–3634.

Thoms S (2015) Import of proteins into peroxisomes: piggybacking to a new home away from home. Open Biol. 5(11): 150148.

Titorenko VI and Terlecky SR (2011) Peroxisome metabolism and cellular aging. *Traffic* 12(3): 252–259.

Toro AA, Araya CA, Córdova GJ, Arredondo CA, Cárdenas HG, Moreno RE, Venegas A, Koenig CS, Cancino J, Gonzalez A and Santos MJ (2009) Pex3p-dependent peroxisomal biogenesis initiates in the endoplasmic reticulum of human fibroblasts. *J. Cell. Biochem.* 107(6): 1083–1096.

Tripathi DN and Walker CL (2016) The peroxisome as a cell signaling organelle. *Curr. Opin. Cell Biol.* 39: 109–112.

van der Zand A, Braakman I and Tabak HF (2010) Peroxisomal membrane proteins insert into the endoplasmic reticulum. *Mol. Biol. Cell* 21: 2057–2065.

van der Zand A, Gent J, Braakman I and Tabak HF (2012) Biochemically distinct vesicles from the endoplasmic reticulum fuse to form peroxisomes. *Cell* 149(2): 397–409.

van Spronsen M, Mikhaylova M, Lipka J, Schlager MA, van den Heuvel DJ, Kuijpers M, Wulf PS, Keijzer N, Demmers J, Kapitein LC, Jaarsma D, Gerritsen HC, Akhmanova A and Hoogenraad CC (2013) TRAK/Milton Motor-Adaptor Proteins Steer Mitochondrial Trafficking to Axons and Dendrites. *Neuron* 77(3): 485–502.

Vilardi F and Lorenz H (2011) WRB is the receptor for TRC40/Asna1-mediated insertion of tail-anchored proteins into the ER membrane. *J. Cell Sci.* 40: 1301–1307.

Vlahou G, Eliáš M, von Kleist-Retzow J-C, Wiesner RJ and Rivero F (2011) The Ras related GTPase Miro is not required for mitochondrial transport in Dictyostelium discoideum. *Eur. J. Cell Biol.* 90(4): 342–355.

Walter KM, Schönenberger MJ, Trötzmüller M, Horn M, Elsässer H-P, Moser AB, Lucas MS, Schwarz T, Gerber PA, Faust PL, Moch H, Köfeler HC, Krek W and Kovacs WJ (2014) Hif-2α Promotes Degradation of Mammalian Peroxisomes by Selective Autophagy. *Cell Metab.* 20: 882–897.

Wanders RJA, Ferdinandusse S, Brites P and Kemp S (2010) Peroxisomes, lipid metabolism and lipotoxicity. *Biochim. Biophys. Acta* 1801(3): 272–280.

Wanders RJA and Waterham HR (2006) Biochemistry of Mammalian Peroxisomes Revisited. *Annu. Rev. Biochem.* 75: 295–332.

Wanders RJA, Waterham HR and Ferdinandusse S (2016) Metabolic Interplay between Peroxisomes and Other Subcellular Organelles Including Mitochondria and the Endoplasmic Reticulum. *Front. Cell Dev. Biol. Front. Cell Dev. Biol* 3(3): 833389–83.

Wang X and Schwarz TL (2009) The Mechanism of Ca2+ -Dependent Regulation of Kinesin-Mediated Mitochondrial Motility. *Cell* 136(1): 163–174.

Wang X, Winter D, Ashrafi G, Schlehe J, Wong YL, Selkoe D, Rice S, Steen J, Lavoie MJ and Schwarz TL (2011) PINK1 and Parkin Target Miro for Phosphorylation and Degradation to Arrest Mitochondrial Motility. *Cell* 147(4): 893–906.

Wang Y-X (2010) PPARs: diverse regulators in energy metabolism and metabolic diseases. *Cell Res.* 20(2): 124–137.

Waterham HR and Ebberink MS (2012) Genetics and molecular basis of human peroxisome biogenesis disorders. *Biochim. Biophys. Acta* 1822(9): 1430–1441.

Waterham HR, Ferdinandusse S and Wanders RJA (2016) Human disorders of peroxisome metabolism and biogenesis. *Biochim. Biophys. Acta - Mol. Cell Res.* 1863(5): 922–933.

Waterham HR, Koster J, van Roermund CWT, Mooyer PAW, Wanders RJA and Leonard JV (2007) A lethal defect of mitochondrial and peroxisomal fission. *N. Engl. J. Med.* 356(17): 1736–1741.

Wattenberg B and Lithgow T (2001) Targeting of C-Terminal (Tail) -Anchored Proteins : Understanding how Cytoplasmic Activities are Anchored to Intracellular Membranes. *Traffic* 2: 66–71.

Weihofen A, Thomas KJ, Ostaszewski BL, Cookson MR and Selkoe DJ (2009) Pink1 Forms a Multiprotein Complex with Miro and Milton , Linking Pink1 Function to Mitochondrial Trafficking. *Biochemistry* 48(9): 2045–2052.

Wennerberg K and Der CJ (2004) Rho-family GTPases: it's not only Rac and Rho (and I like it). *J. Cell Sci.* 117(Pt 8): 1301–1312.

Wiemer EAC, Wenzel T, Deerinck TJ, Ellisman MH and Subramani S (1997) Visualization of the peroxisomal compartment in living mammalian cells: dynamic behavior and association with microtubules. *J. Cell Biol.* 136(1): 71–80.

Williams C, Opalinski L, Landgraf C, Costello J, Schrader M, Krikken AM, Knoops K, Kram AM, Volkmer R and van der Klei IJ (2015) The membrane remodeling protein Pex11p activates the GTPase Dnm1p during peroxisomal fission. *Proc. Natl. Acad. Sci. U. S. A.* 112(20): 6377–6382.

Williams C and van der Klei IJ (2014) The Functions of Pex11 Family Proteins in Peroxisome Biology. In *Molecular Machines Involved in Peroxisome Biogenesis and Maintenance*. Springer, 425–437.

Yagita Y, Hiromasa T and Fujiki Y (2013) Tail-anchored PEX26 targets peroxisomes via a PEX19-dependent and TRC40-independent class I pathway. *J. Cell Biol.* 200(5): 651–666.

Yamamoto Y and Sakisaka T (2012) Molecular Machinery for Insertion of Tail-Anchored Membrane Proteins into the Endoplasmic Reticulum Membrane in Mammalian Cells. *Mol. Cell* 48(3): 1–11.

Yamaoka S and Hara-Nishimura I (2014) The mitochondrial Ras-related GTPase Miro: views from inside and outside the metazoan kingdom. *Front. Plant Sci.* 5(July): 350.

Yan M, Rayapuram N and Subramani S (2005) The control of peroxisome number and size during division and proliferation. *Curr. Opin. Cell Biol.* 17(4): 376–383.

Yasuda M, Theodorakis P, Subramanian T and Chinnadurai G (1998) Adenovirus E1B-19K/BCL-2 interacting protein BNIP3 contains a BH3 domain and a mitochondrial targeting sequence. *J. Biol. Chem.* 273(20): 12415–12421.

Yokota S, Haraguchi CM and Oda T (2008) Induction of peroxisomal Lon protease in rat liver after di-(2-ethylhexyl)phthalate treatment. *Histochem. Cell Biol.* 129(1): 73–83.

Yokota S, Oda T and Fahimi HD (2001) The role of 15-lipoxygenase in disruption of the peroxisomal membrane and in programmed degradation of peroxisomes in normal rat liver. *J. Histochem. Cytochem.* 49(5): 613–622.

Yoon Y, Krueger EW, Oswald BJ and Mcniven MA (2003) The mitochondrial protein hFis1 regulates mitochondrial fission in mammalian cells through an interaction with the dynamin-like protein DLP1. *Mol. Cell. Biol.* 23(15): 5409–5420.

Yoshida Y, Niwa H, Honsho M, Itoyama A and Fujiki Y (2015) Pex11 mediates peroxisomal proliferation by promoting deformation of the lipid membrane. *Biol. Open* 4(6): 710–721.

Youle RJ and Strasser A (2008) The BCL-2 protein family: opposing activities that mediate cell death. *Nat. Rev. Mol. Cell Biol.* 9(1): 47–59.

Youngman MJ, Hobbs AEA, Burgess SM, Srinivasan M and Jensen RE (2004) Mmm2p, a mitochondrial outer membrane protein required for yeast mitochondrial shape and maintenance of mtDNA nucleoids. *J. Cell Biol.* 164(5): 677–688.

Zhang F, Wang W, Siedlak SL, Liu Y, Liu J, Jiang K, Perry G, Zhu X and Wang X (2015) (a) Miro1 deficiency in amyotrophic lateral sclerosis. *Front. Aging Neurosci.* 7(May): 100.

Zhang J, Kim J, Alexander A, Cai S, Tripathi DN, Dere R, Tee AR, Tait-Mulder J, Di Nardo A, Han JM, Kwiatkowski E, Dunlop E a, Dodd KM, Folkerth RD, Faust PL, Kastan MB, Sahin M and Walker CL (2013) A tuberous sclerosis complex signalling node at the peroxisome regulates mTORC1 and autophagy in response to ROS. *Nat. Cell Biol.* 15(10): 1186–1196.

Zhang J, Tripathi DN, Jing J, Alexander A, Kim J, Powell RT, Dere R, Tait-Mulder J, Lee J-H, Paull TT, Pandita RK, Charaka VK, Pandita TK, Kastan MB and Walker CL (2015) (b) ATM functions at the peroxisome to induce pexophagy in response to ROS. *Nat Cell Biol* 17(10): 1259–1269.

Zimmerberg J and Kozlov MM (2006) How proteins produce cellular membrane curvature. *Nat. Rev. Mol. Cell Biol.* 7(1): 9–19.